Satellite-tracked Drifter Measurements in the Chukchi and Beaufort Seas

Principal Investigator
Thomas Weingartner[1]

Collaborators
Cayman Irvine[1], Elizabeth Dobbins[1], Seth Danielson[1]
Leandra DeSousa[2]*, Billy Adams[2]*, Robert Suydam[2]*, Willard Neatok[3]*

[1]University of Alaska Fairbanks, Institute of Marine Science
[2]North Slope Borough Department of Wildlife Management
[3]Village of Pt. Lay

*Under support from the North Slope Borough-Shell Baseline Studies Program

FINAL REPORT
April 2015
OCS Study BOEM 2015-022

BOEM
Bureau of Ocean Energy Management

UAF
University of Alaska Fairbanks

Contact Information:
email: CMI@alaska.edu
phone: 907.474.6782
fax: 907.474.7204

Coastal Marine Institute
School of Fisheries and Ocean Sciences
University of Alaska Fairbanks
P. O. Box 757220
Fairbanks, AK 99775-7220

This study was funded in part by the U.S. Department of the Interior, Bureau of Ocean Energy Management (BOEM) through Cooperative Agreement M11AC00001 between BOEM, Alaska Outer Continental Shelf Region, and the University of Alaska Fairbanks. This report, OCS Study BOEM 2015-022, is available through the Coastal Marine Institute, the Department of Interior library, and electronically from *http://www.boem.gov/BOEM-Newsroom/Library/Publications/Alaska-Scientific-and-Technical-Publications.aspx.*

Table of Contents

List of Figures

List of Tables

Abstract

In fall of 2011, 2012, and 2013, numerous satellite-tracked drifters were deployed in the northeast Chukchi Sea in conjunction with collaborators from the North Slope Borough. The drifters included non-drogued surface iSpheres, 1-m drogued Microstar (MS) drifters, and 10-m drogued Surface Velocity Profiler (SVP) drifters. Drifter deployments included sets of 12 – 20 drifters of mixed type, which were subsequently tracked until the drifters were beached, ceased operating, or were trapped in sea ice. There was considerable interannual variability in the resulting trajectories. In 2012, nearshore (within 10 miles of the Chukchi coast) drifters moved northeastward through Barrow Canyon. After exiting Barrow Canyon, these drifters moved eastward onto the Beaufort Sea shelf or the Beaufort slope, or northwestward along the Chukchi Sea slope. Drifters deployed further offshore in the northeast Chukchi Sea in 2011 and 2012 generally moved eastward toward the coast and eventually entered Barrow Canyon. After exiting Barrow Canyon they also moved eastward along the Beaufort shelfbreak (or shelf) or northwestward along the Chukchi shelfbreak. Many of the drifters that moved westward on the Chukchi shelfbreak turned southward and back onto the northeast Chukchi Sea shelf. All of the drogued drifters that returned to the northeastern Chukchi Sea shelf stopped transmitting in this region. However, many of the iSphere drifters continued southward over the shelf in September and October and eventually came ashore in Ledyard Bay, along the coast of the Lisburne Peninsula. One iSphere was caught in the ice south of Pt. Hope and was eventually crushed near the Siberian coast.

The SVP drifters deployed in 2012 had the greatest endurance and several drifted, trapped in sea ice, for several months before being crushed or losing battery life. The ice carried these drifters as far afield as the western Chukchi Sea (near Wrangel Island) and the Mackenzie Shelf in the eastern Beaufort Sea. Several SVPs continued transmitting through winter, while locked in the landfast ice zone of the Beaufort Sea, and then made broad zonal excursions over this shelf in early summer 2013 before they stopped transmitting.

Linear regressions were used to examine the statistical relationship between drifter velocities and the local surface winds over six regions, defined on an ad hoc basis, as the Chukchi shelf, the inner Chukchi Sea shelf (Alaskan Coastal Domain; water depths <30m and exclusive of Barrow Canyon), within Barrow Canyon, the Chukchi-Beaufort continental slope, the Beaufort Sea shelf, and the Canada Basin. The iSphere drifters consistently exhibited a strong statistical relationship with winds, often explaining more than 60% of the drifter velocity variance. For the MS drifters, winds explained more than 60% of the velocity variance only within the Alaskan Coastal Domain and the Beaufort Sea Shelf. Influence of winds explained less than 30% of the velocity variance of the SVP drifters in all regions. The spatial differences in response likely reflect dynamical differences over the region. These differences can be ascribed to stratification, mesoscale motions associated with unstable meltwater fronts, instabilities in shelfbreak currents, and/or time-varying geostrophic currents within the regions. Drifters that entered the Canada Basin were entrained in eddies most likely spawned by shelfbreak current instabilities. There were also seasonal differences in the wind-driven response within the same general area

of the shelf and we tentatively ascribe these differences to the absence/presence of fronts. Wind-current correlations among drifters far from fronts were substantially better than for those likely encountering fronts.

The 2013 trajectories were markedly different from those of 2012 as few escaped the northeastern Chukchi Sea. Instead, most drifters moved westward in response to strong northeasterly winds of August and September 2013. Approximately 60% of the zonal velocity variance for drifters deployed south of Hanna Shoal was due to the winds, while wind-current regressions north of Hanna Shoal were substantially poorer. Relative dispersion characteristics, based on clustered drifter deployments in 2012 and 2013, indicate anisotropic dispersion, with the zonal relative diffusivity being about twice that of the meridional diffusivity. Relative dispersion increases according to a $\text{time}^{2.5}$ power law after ~2 days, which is the Lagrangian decorrelation time scale.

I. Introduction and Background

There is strong industry interest in exploring the hydrocarbon potential of the Northeast Chukchi Sea Shelf. These activities require physical oceanographic data pertinent to the environmental and engineering concerns of both industry and the Bureau of Ocean Energy Management (BOEM). The measurements described herein provide information on upper-ocean and surface currents during the open water season (August through November) of 2011, 2012, and 2013.

The Chukchi and Beaufort Seas are the northernmost shelf seas bordering Alaska. Although properly a part of the western Arctic Ocean, both shelves are linked, atmospherically and oceanographically, to the Pacific Ocean. These connections profoundly influence the wind regime, the seasonal distribution of sea ice, the regional hydrologic cycle, and the water masses and circulation characteristics of the Chukchi Shelf. The atmospheric connection is primarily via the Aleutian Low, whose time-varying position and strength, and interactions with the anticyclonic Beaufort High (*Zhang et al.,* 2013) affect regional meteorological conditions. The oceanographic link is via the mean northward flow through Bering Strait, which draws water from the Bering Sea Shelf and Basin, and is sustained by a large-scale pressure gradient between the Pacific and Atlantic oceans (*Coachman et al.,* 1975; *Aagaard et al.*, 2006; **Figure 1**).

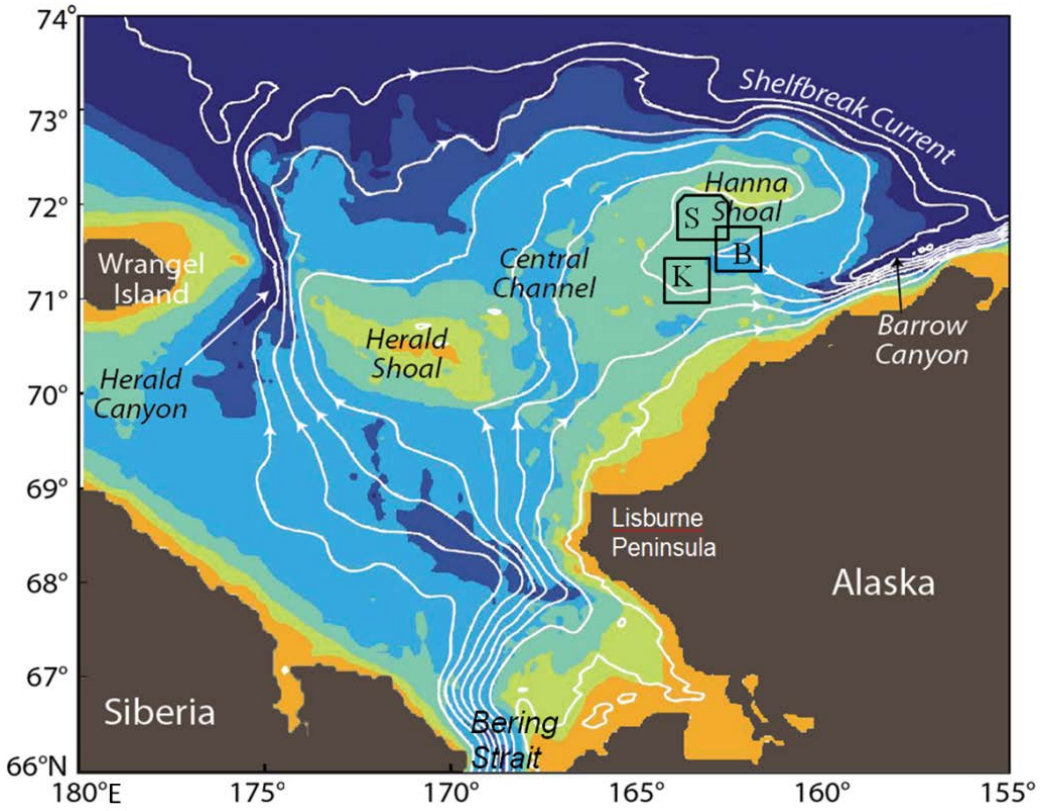

Figure 1. Mean depth-integrated streamlines (white lines) in the Chukchi Sea, after *Spall* (2007). The bathymetry is colored and major bathymetric features are labeled. The lettered boxes denote the approximate locations of the Klondike (K), Burger (B), and Statoil (S) exploration areas.

The northward flux of mass, heat, nutrients, carbon, and organisms through the strait bequeaths the Chukchi Shelf with physical and ecological characteristics that are unique among arctic shelves. For example, spring retreat occurs earlier, and fall onset of sea ice later, than most other arctic shelves because of the northward heat flux through the Strait. *Woodgate et al*. (2006) estimate that summer Pacific waters provide a heat source capable of melting nearly the entire (~640,000 km^2) 2-m thick ice cover of the Chukchi Sea and *Shimada et al.* (2006) contend that this flux may be an important source of interannual variability in the ice cover of the western Arctic Ocean. Similarly, the enormous biological productivity of this shelf (*Walsh et al.,* 1989; *Springer and McRoy,* 1993), including its ability to support large and diverse marine mammal populations, is due to the carbon and nutrient loads carried through Bering Strait.

The water properties of the Strait throughflow reflect the time-varying output of physical processes occurring over the Bering Shelf and northern North Pacific. These fluxes are a result of the net effects of upwelling from the deep Bering Sea basin and regionally-integrated heat and freshwater fluxes (*Aagaard et al.,* 2006), including the freezing and melting of sea ice (*Danielson et al.,* 2006), river runoff, atmospheric moisture and heat fluxes, and heat and freshwater contributions from the Gulf of Alaska (*Weingartner et al.,* 2005a). These factors all ultimately affect the heat and salt budgets of the Chukchi Sea Shelf (*Coachman et al*., 1975; *Woodgate et al.,* 2005a).

Ia. Mean Circulation and Water Masses

The shallow (~50m) Chukchi Sea Shelf extends ~800 km northward from Bering Strait to the shelfbreak at about the 200 m isobath. The mean flow over much of the shelf is northward due to the Pacific-Arctic pressure gradient and opposes the prevailing northeasterly winds. This pressure gradient propels the Bering Strait throughflow northward along three principal pathways that are associated with distinct bathymetric features (**Figure 1**); Herald Canyon, the Central Channel, and Barrow Canyon. Herald Shoal separates Herald Canyon from the Central Channel, and Hanna Shoal is between Barrow Canyon and the Central Channel. Regions of industrial interest with respect to hydrocarbon exploration are to the south of Hanna Shoal and east of the Central Channel and denoted by boxes in **Figure 1** as Klondike (K), Burger (B), and Statoil (S).

The mean circulation, as sketched in **Figure 1**, includes a western branch that flows northwestward from the Strait and exits the shelf through Herald Canyon. While most of this outflow probably descends through Herald Canyon, some of it may spread eastward across the central shelf. A second branch flows northward through the Central Channel and then splits; some water continues eastward toward the Alaskan coast along the south flank of Hanna Shoal (*Weingartner et al.,* 2005b; *Weingartner et al.,* 2013a) while the remainder flows northeastward toward the continental slope. The third branch flows northeastward along the Alaskan coast towards Barrow Canyon at the junction of the Chukchi and Beaufort shelves. In summer this flow includes the northward extension of the Alaskan Coastal Current (ACC) that originates

south of Bering Strait. At the head of Barrow Canyon the ACC is joined by waters flowing eastward from the central shelf, with the merged flow then continuing down-canyon as a narrow, but strong, coastal jet (*Weingartner et al.,* 2013b).

From summer through early fall, the Strait transport is northward on average and includes three major water masses, which following the nomenclature of *Coachman et al.* (1975) and *Walsh et al.* (1989) are: cold, salty, nutrient-rich Anadyr Water; warm, fresh, nutrient-poor Alaskan Coastal Water (ACW); and Bering Shelf Water. The latter has properties intermediate between, but nonetheless distinct from, the Anadyr and Alaskan Coastal water masses. *Coachman et al.* (1975) maintain that the Anadyr and Bering Shelf water masses mix to form Bering Sea Water (BSW) north of the Strait, whereas ACW maintains its properties on the Chukchi Shelf. In summer and fall, Chukchi bottom waters often include near-freezing, saline (dense) waters that formed in winter by freezing over both the Bering and Chukchi seas. In addition, shallow plumes of cool, dilute, surface waters, formed by ice melt, may also be present.

Bering Sea Water is transported to the northwest Chukchi, over the central shelf, and northward through the Central Channel (*Weingartner et al.,* 2005b; *Woodgate et al.,* 2005b). *Weingartner et al.* (2005b) and *Weingartner et al.* (2013a) suggest that, south of Hanna Shoal, some central-shelf waters flow eastward toward the coast, in agreement with the circulation models of *Winsor and Chapman* (2004) and *Spall* (2007). North of the Central Channel, where there are no long-term current measurements, both models suggest the average flow follows the bathymetry around the western and northern flanks of Hanna Shoal before turning southward along the eastern side of the Shoal and eventually entering Barrow Canyon. However, the models also predict that some of the water along the eastern flank of Hanna Shoal penetrates southwestward along the southern flank of the Shoal before turning eastward towards the coast. Hydrography suggests that this indeed does occur, at least episodically (*Weingartner et al.,* 2013a). The ACW flows northeastward within the Alaskan Coastal Current toward the head of Barrow Canyon. Here it merges with waters flowing eastward from the central shelf to form the canyon outflow. Hence in summer and fall, the canyon outflow contains a horizontally- and vertically-structured complex of water masses (*Pickart et al.,* 2005; *Shroyer and Plueddemann,* 2011) that include ACW, meltwater, dense winter waters, BSW, and mixtures of each.

Ib. Wind-Forced Variability

The mean circulation is due to the large scale pressure field between the Pacific and Arctic oceans and opposes the mean winds, which are from the northeast at ~4 m s^{-1} on average. The winds are the principal cause of flow variations, which can be substantial. Wind forcing varies seasonally with the largest variations being in fall and early winter and the smallest being in summer. *Weingartner et al.* (2005b) found that current fluctuations were coherent with wind velocity variations over the northeast shelf over spatial scales of at least 300 km. These adjustments reflect wind-induced modifications via coastal convergences and divergences to the shelf pressure field. Although the adjustment envelops a broad area, the magnitude of the current

response varies over the shelf. In particular, both wind-forced and mean currents are more vigorous in regions of steep topography (Central Channel and Barrow Canyon) than in areas of gentler bottom relief. On occasion, and most frequently in fall and winter, strong northeasterly storm winds can reverse the shelf flow field or even redistribute the flow from one of the main flow pathways to another.

The time-varying shelf pressure field may result in forces that oppose the surface wind stress, a dynamic with important implications. In particular, it suggests that the flow in a "thin" surface layer, which absorbs the bulk of the momentum imparted by the wind to the water column, may differ from deeper currents. The thickness of this wind-shear layer will vary due to wind velocity, bathymetry, and the stratification. Since moored current meters have difficulty measuring the uppermost ~5 m of the surface, understanding the surface circulation is critical for assessing potential pathways of drifting organisms and contaminants in the upper ocean. The purpose of this project was to assess the near-surface circulation in the northeast Chukchi Sea by means of satellite-tracked drifters.

Satellite-tracked drifters are quasi-Lagrangian, free-drifting instruments often used to study large oceanic regions. Their individual trajectories are largely unpredictable and often complex (and surprising). Consequently, the analytical methods applied are different than those for Eulerian measurements. The Lagrangian analytical approach is largely statistical in nature and meaningful analyses depend upon large numbers of drifters and/or trajectories. A substantial literature exists that discusses these techniques (e.g., *Davis*, 1991; *LaCasce*, 2008; and the references therein).

II. Project Objectives

The overall goal of this program was to evaluate the near-surface currents and their response to winds in the northeast Chukchi Sea where hydrocarbon exploration is underway and future development may take place. In particular, we sought to determine:

1. If the surface (upper 1 m) and near-surface (10 – 15 m) circulation field diverges and differs from the sub-surface circulation, as captured by current meter measurements, and
2. If the differences in the surface and sub-surface flows are related to seasonally-varying winds, bathymetry and hydrographic conditions.

These were the original goals of the Coastal Marine Institute (CMI) funded University of Alaska Fairbanks (UAF) project. As originally conceived, the one-year (2011) study would deploy 48 drifters, half drogued at 10 m and half at 1 m. The deployments were planned as clusters of 4 – 8 drifters (half at each depth) so differences in surface and subsurface circulation could be examined. Deployment was planned for areas with differing hydrographic conditions and within the regions of industry interest (e.g., Klondike, Burger, and Statoil). The North Slope Borough, Department of Wildlife Management (NSBW) undertook a companion program to deploy 24 1-m drogued drifters within 10 km of the coast in the Chukchi Sea. Unfortunately, construction

flaws by the manufacturer (Technocean, Inc. of Coral Gables, FL) resulted in a massive failure rate (>80%) of the deployed CMI project drifters, leaving only nine functioning drifters in 2011. Flaws in the Technocean drifters included the lack of functioning thermistors and, in our opinion, improper seals on the pressure canister that housed the electronics. As a consequence, many of the failed drifters presumably leaked within hours or days after deployment. We were also unable to decode the data string according to the manufacturer's instructions and technical advice. However, Dr. Danielson (UAF) eventually developed a successful decoding strategy. The NSBW experienced similar failure rates with their Technocean drifters and halted deployments shortly after beginning their program. The bulk of the drifter data discussed in this report thus derives from additional drifters deployed in BOEM and NSBW projects in 2012 and 2013. Only a few of these additional drifters were drogued at 10 m depth. Rather, most had 1-m drogues and some of the NSBW drifters deployed in 2012 were simply surface floats (undrogued). Due to the equipment failures and lack of 10-m drogued drifters, there were insufficient data sets to address all of our objectives in a statistically meaningful way. However, we applied statistical analyses where we felt that the data density allowed.

Quasi-Lagrangian measurements provide a unique description of the ocean circulation by yielding information on the pathways of water parcels and the various circulation structures in which they are embedded. To our knowledge, the drifter data assembled in this report represents, by far, the most comprehensive deployment activity in the open water season for any Arctic continental shelf. Consequently, we feel that the trajectory descriptions are an important aspect of the study, and that a sense of the complexity and diversity of the circulation field can only be attained through such an overview.

Nevertheless, the descriptive approach is limited by the enormous temporal and spatial variability of the ocean. As will become evident, two parcels or drifters deployed simultaneously at nearly identical positions often evolve along quite different pathways. Indeed, the drifters discussed herein executed a variety of complex and unique trajectories that crossed through dynamically different regimes (Chukchi Shelf, Chukchi-Beaufort shelfbreak, coastal currents, and the Canada Basin). Where the data density permitted, this variability is described statistically. Several of the deployments were made as "cluster" deployments and these allow us to examine relative dispersion (how particle pairs, initially deployed close to one another in time and space, move with respect to one another) and several kinematic properties of the flow field. We also explore wind-current relationships. In these analyses, we, *a priori*, regarded drifters in different dynamical regimes as providing statistics from a distinct "population", so that it would be inappropriate to group all the data into a single population. Consequently, we have examined the wind-current relationship separately for each area. Similarly, we have limited our analyses of relative dispersion and kinematic properties to the Chukchi Shelf because this region provided the largest number of data points for these estimates. We regard the results from the Chukchi Sea Shelf reported herein to be preliminary. In 2014, projects operated by the NSBW and the U.S. Department of Interior's Bureau of Safety and Environmental Enforcement (BSEE) deployed

about 100 more drifters on this shelf. Results of those exercises will be combined using the same analyses as described below. The intention is to produce a climatological description of relative dispersion on this shelf. The analyses are climatological in the sense that they cover deployments made over a number of years and at a number of locations on the shelf. This approach will lead to firmer confidence in the derived statistics.

III. Methods

IIIa. Drifters and Winds

The sampling approach used two different types of satellite-tracked drifters; the CODE-type and the SVP-type (**Figure 2**). Additional photographs showing deployed CODE drifters are shown in **Figures 3 and 4**. The NSBW used a combination of the CODE-type and iSphere drifters (**Figure 5**; manufactured by Metocean). CODE drifter performance characteristics (*Davis*, 1985) are that the drifter slippage is ~1 cm s^{-1} and thus small compared to the expected magnitudes of the 5 – 50 cm s^{-1} current velocities typical of the Chukchi Sea. CODE drifters (referred to herein as Microstar or MS) measure the upper 1 m of the water column and a SVP drifter drogue is at 10 m depth. These drogue depths were chosen to address our two goals and because these depths are the standard manufacturer designs. Each drifter also included a surface thermistor. Drifter positions were determined by satellite GPS fixes and recorded approximately hourly along with sea surface temperatures. The data were stored aboard the drifter and then transmitted via Service Argos (2011) twice per day or by Iridium link (2012 and 2013) hourly. All data were then interpolated to the top of the hour and checked for outliers in position data. Outliers were infrequent in 2012 and replaced with linearly interpolated positions. In contrast, the 2013 drifter deployments included periods of time when there is either no or only lower quality position data available. We believe that these periods coincide with rough seas when the surface float was periodically submerged and incapable of establishing sustained communications with the GPS satellites. As a consequence, drifter positions are determined by three different methods, derived from the quality flags in the raw data sets. The highest quality GPS fixes are calculated using signals from three GPS satellites, the lower quality positions are obtained from only two GPS satellites, and the poorest quality fixes are obtained from the Iridium satellite. Initially, we used only the highest quality data, as we had done in 2012. However, in 2013, this left hundreds of small gaps in the drifter positions; approximately 66 of the gaps were longer than one day, with the longest being four days. These longer gaps were distributed across all MS drifter deployments, but were concentrated during specific time periods (**Figure 6**).

To fill these gaps, a second data set was created that includes lower quality data. However, these data exhibit a variety of errors. The poorer quality data included positions that are duplicates of previous positions but at later times, repeated duplicate positions when the drifter was obviously not beached, sections offset from the track-line, and generally noisy data. Some of the offset sections were corrected using time adjustments provided by the drifter manufacturer, Pacific

Gyre. Most of the gaps were filled on this pass of editing. The remaining erroneous positions were replaced with error codes (NaNs) manually. Velocities calculated using the poor quality data are somewhat noisier than those using higher quality data. Some gaps remained (**Figure 7**) especially in the BOEM drifters deployed northeast or northwest of Hanna Shoal; the only gap greater than one day in the NSBW drifter positions occurred at the end of the NSBW-I-30 deployment. All remaining gaps were filled with a linear interpolation of positions. Velocities based on interpolated positions are highlighted in the time series for each drifter. The final data file has the position data flagged as follows: 0 for good quality, 1 for questionable positions that passed quality control, 2 for positions that failed quality control, 3 for when there was no original data at all, and 4 for interpolated values across gaps of three or more hours.

In all years the drifters were deployed from research vessels operating south, east, or north of Hanna Shoal in approximately 40 m water depth. In 2011, drifter deployments were made by research vessels under charter to Shell, Conoco-Phillips, and Statoil as part of their Chukchi Sea Environmental Studies Program (CSESP). In 2012, the drifter deployments were made from the USCG Healy and from the Norseman II. The NSBW drifters were deployed within 10 miles of the coast in water depths of <20 m offshore of Icy Cape, Wainwright, and Barrow. Unlike either the SVP or CODE drifter, the iSphere is analogous to a partially submerged basketball sitting half in and half out of the water, making them subject to considerable wind drag.

Regional wind data used in the analyses were obtained from the National Oceanic and Atmospheric Administration's WaveWatch forecast model and/or from the National Center for Environmental Prediction, North American Regional Re-analysis (NCEP-NARR; *Mesinger et al.,* 2006). Both wind data sets are available at three-hourly intervals on a 32 km grid. Comparisons were made using either wind product and the winds measured at meteorological buoys in the northeast Chukchi Sea, specifically those at Pt. Lay, Klondike, Burger, and Hanna SE for the period August – October 2012 (**Figure 8**). Our analyses indicate that the skill exceeds 0.9 and that the root mean square error differences are ~2.5 m s^{-1} for both wind components in all cases. **Figure 9** shows a comparison of the NARR and Burger observed winds for the same period and **Figure 10** shows a comparison between the WaveWatch model wind components and those recorded at the Pt. Lay buoy.

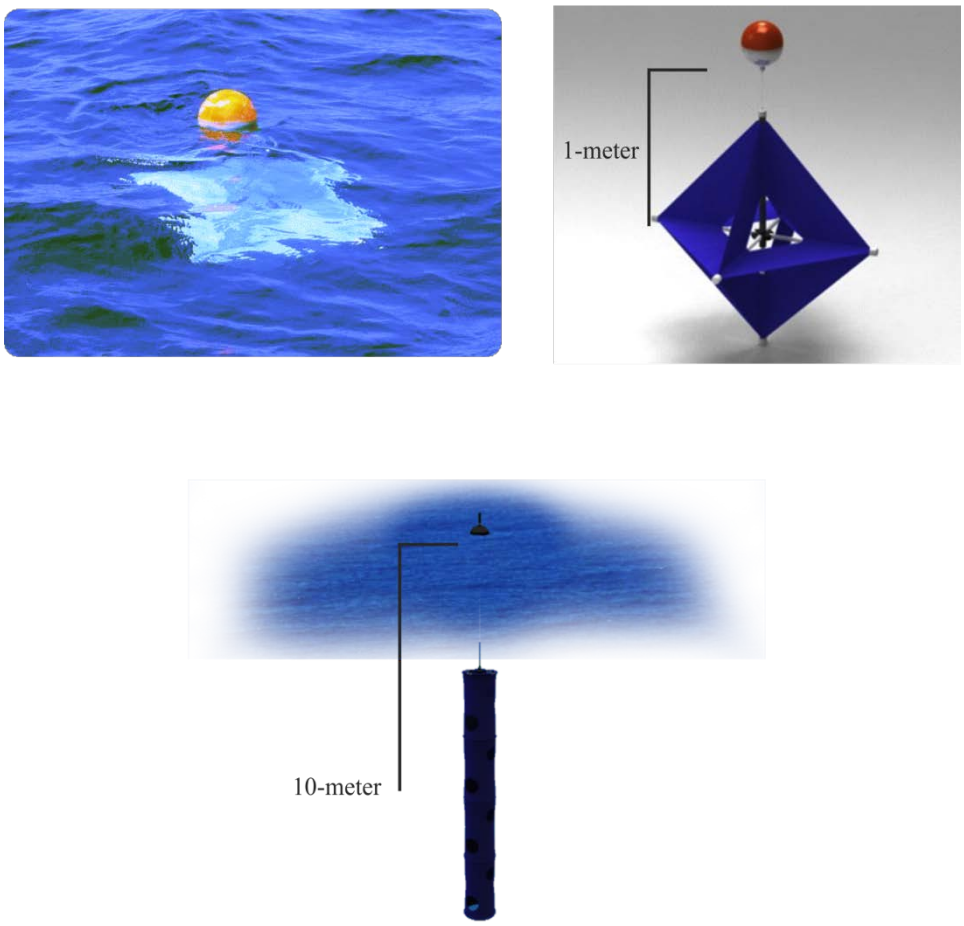

Figure 2. Schematics of the CODE-type 1-m drogued Microstar drifter (top) and the SVP-type 10-m drifter (bottom). Both drifter types shown are manufactured by Pacific Gyre, Inc.

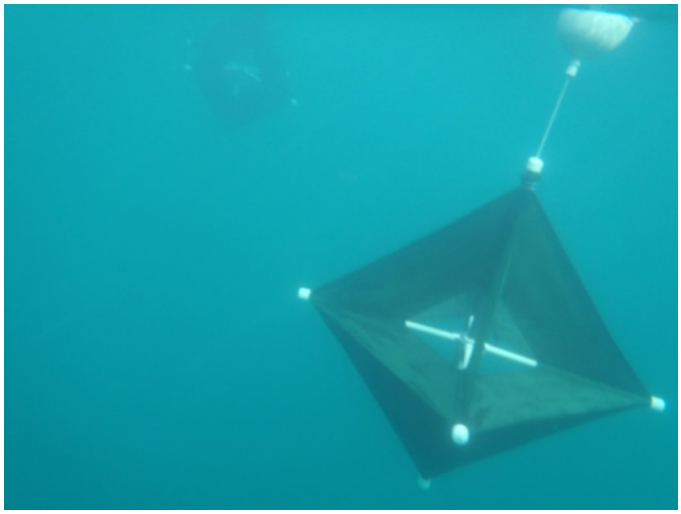

Figure 3. Underwater photo of a Microstar drifter in operation. Note the structure of the drogue and the white, semi-submerged surface float.

Figure 4. Aerial photo of two Microstar drifters offshore of Wainwright in 2013 (Photograph is courtesy of Vikki Beaver and Janet Clarke).

Figure 5. iSphere surface drifters (manufactured by Metocean).

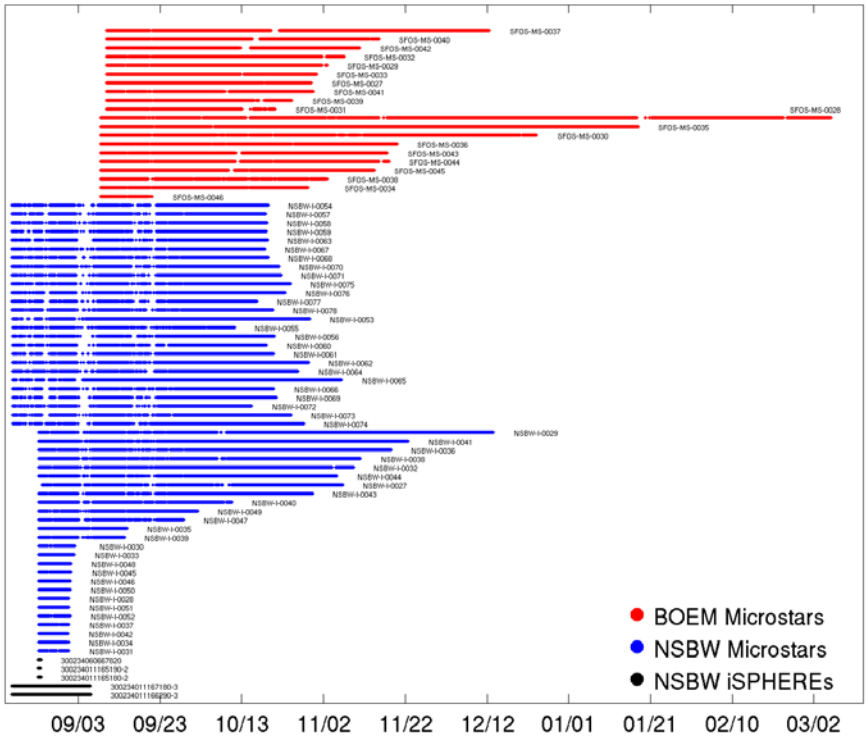

Figure 6. Time of occurrence (solid colors) of high quality position data for the drifters deployed in 2013. High quality position data is derived from three GPS satellites.

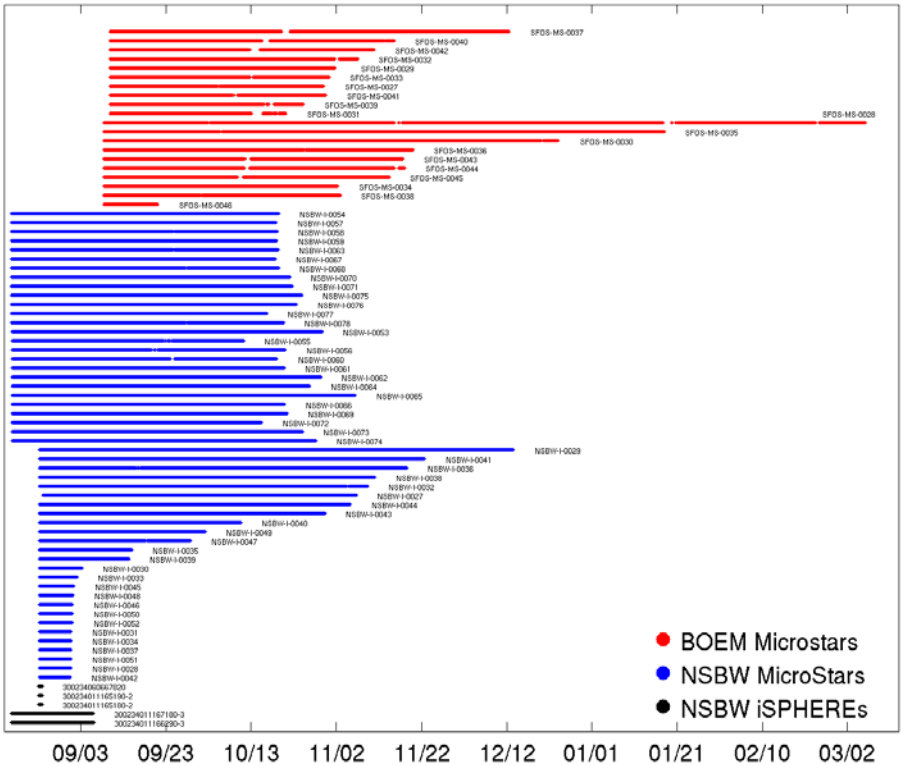

Figure 7. Time of occurrence (solid colors) of all quality position data for the drifters deployed in 2013. The remaining gaps were linearly interpolated through time.

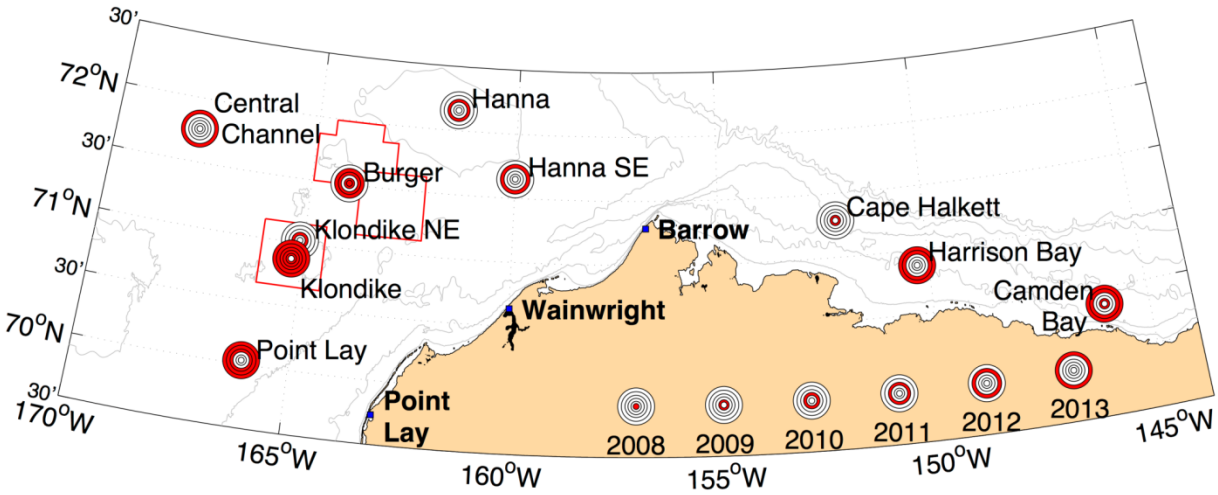

Figure 8. Locations of meteorological buoys in the Chukchi and Beaufort Seas since 2008. Colored ring on each buoy indicates the year for which data is available.

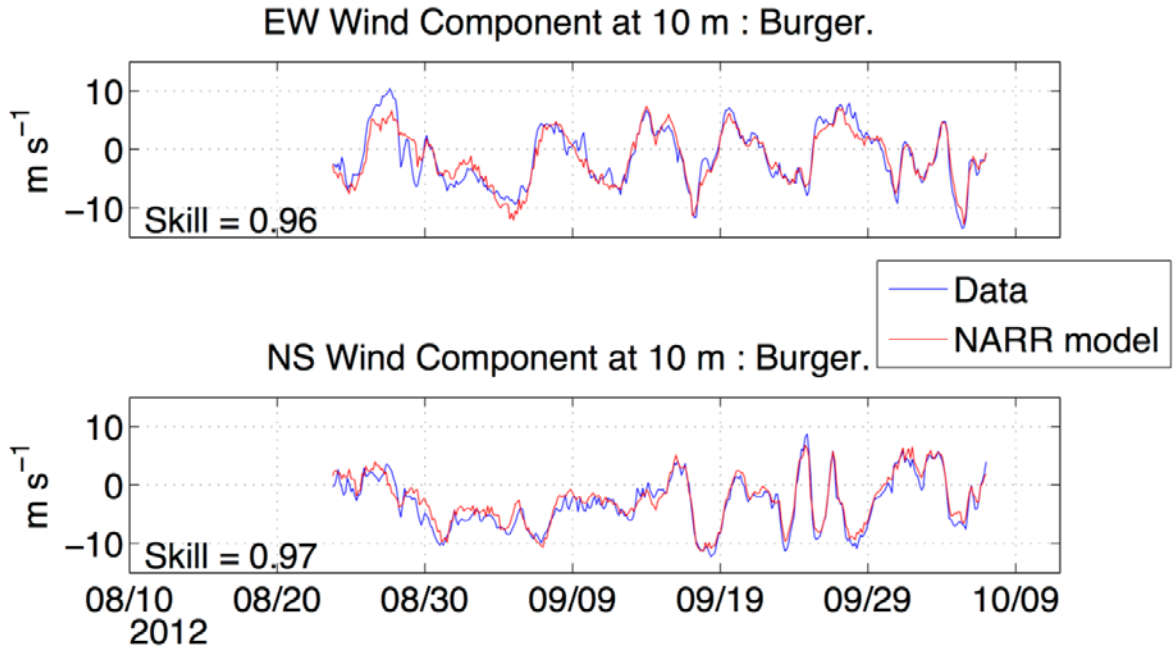

Figure 9. Time series of winds based on the NARR model and observed at the Burger meteorological buoy in 2012. Upper panel shows the east-west wind component and lower panel shows the north-south wind component. The skill in both cases is >0.95.

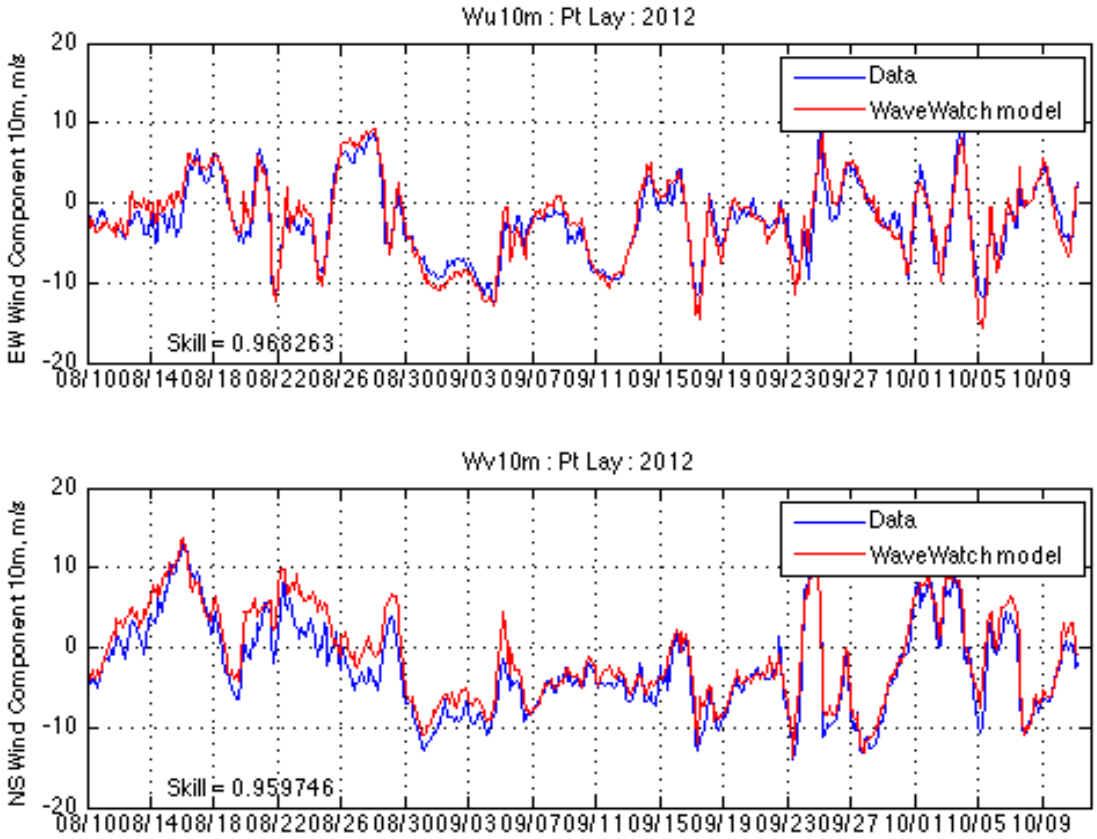

Figure 10. Time series of winds based on the WaveWatch model and observed at the Pt. Lay meteorological buoy in 2012. Upper panel shows the east-west wind component and lower panel shows the north-south wind component. The skill in both cases is >0.95.

A description of the interannual variability in the winds over the Chukchi Sea are based on the NARR winds at grid point 71° 3.75'N, 165°3.75'W, located within Klondike. The wind estimates are generated at three-hourly intervals and the NARR ice-edge positions are mapped based on the analyses of the National Ice Center.

The drifter deployments in 2011 and 2012 were made in the areas shown in **Figure 11**. These deployments were conducted in regions providing supplementary data that included shipboard and/or towed conductivity-temperature-depth (CTD), subsurface moorings, and surface velocities. The latter were obtained from shore-based high-frequency radars (HFR) located in the communities of Barrow, Wainwright, and Pt. Lay.

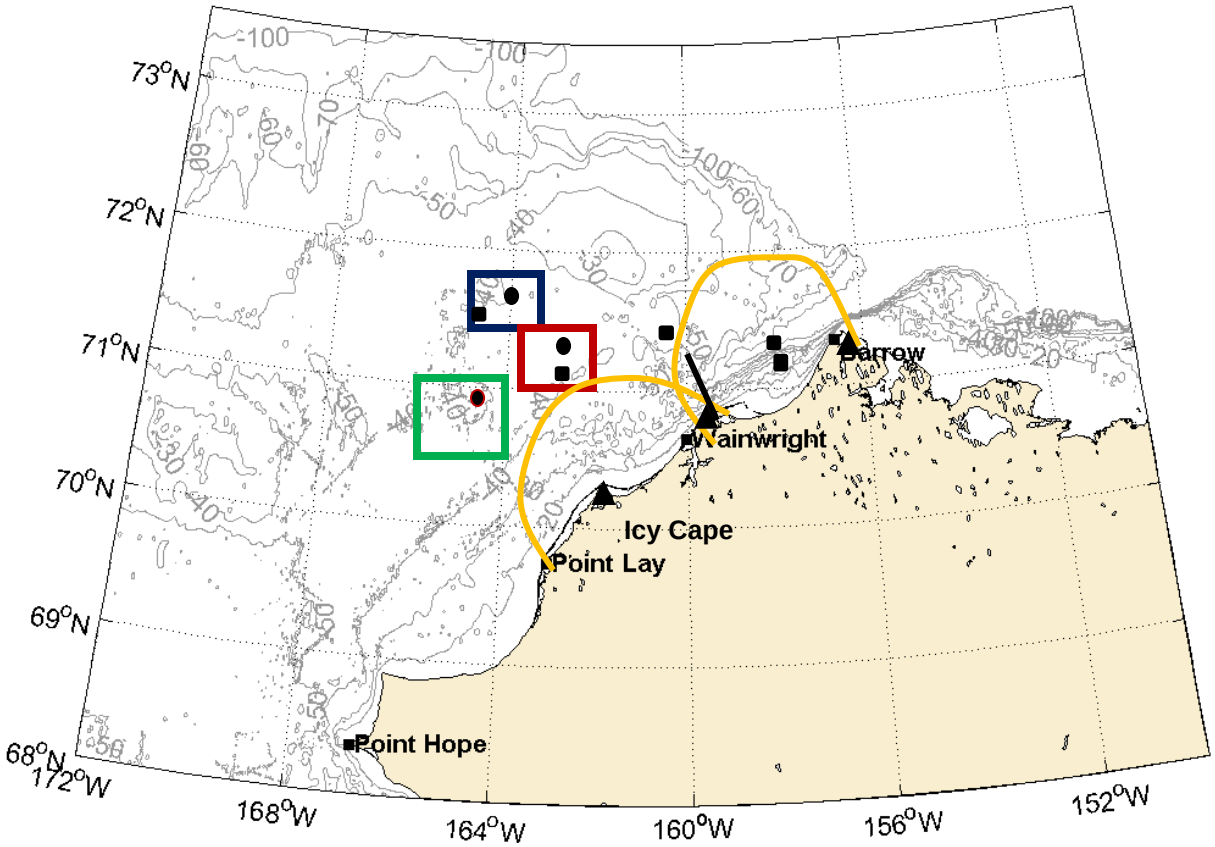

Figure 11. Bathymetric map of the Chukchi Sea showing the approximate location of the Statoil (dark blue box), Burger (red box), and Klondike (green box) prospects. The orange arcs show the approximate radar masks for HFRs at Pt. Lay, Wainwright, and Barrow. The solid black line extending northwest from Wainwright encompasses an array of six subsurface moorings present during the 2011 period. Approximate locations of UAF drifter releases in 2011 (circles) and 2012 (squares) are shown. The approximate locations of NSBW drifter deployments in 2012 are shown by triangles.

Drifter trajectories were updated daily and posted to a website available to the public at http://dm.sfos.uaf.edu/chukchi-beaufort/data/drifters/. The website also contains the data files for each drifter. Individual trajectories and their time series of derived velocities and temperatures, can be viewed at http://dm.sfos.uaf.edu/chukchi-beaufort/data/drifters/2012_png/ for 2012 deployments, http://dm.sfos.uaf.edu/chukchi-beaufort/data/drifters/2013_png/ for drifters deployed in 2013, and http://dm.sfos.uaf.edu/chukchi-beaufort/data/drifters/2014_png/ for drifter deployments carried out in 2014 by BSEE and the North Slope Borough-Shell Baseline studies programs. An animation of the 2012 drifter trajectories can be viewed at http://mather.sfos.uaf.edu/drifters/Chukchi2012/Plots/DrifterMovieC.html.

IIIb. Hydrographic Data

Hydrographic data was shared with this program from other programs, including the CSESP program and the BOEM-funded "Characterization of the Circulation on the Continental Shelf Areas of the Northeast Chukchi and Western Beaufort Seas". The CSESP CTD data were

collected using a Seabird, Inc. SBE-19+V2 CTD sampling at 4 Hz and lowered through the water column at ~10 m min^{-1}. The CTD data were processed following the manufacturer's procedures and were then averaged into 1 dbar bins (*Weingartner et al.*, 2013a). Comparison of pre- and post-season calibrations (performed by Seabird) of the temperature and conductivity sensors indicate that the data are accurate to better than 0.005°C for temperature and 0.02 for salinity. The BOEM CTD data were obtained from a towed, CTD vehicle (Acrobat). The Acrobat vehicle yo-yos between the surface and bottom and samples with a high horizontal resolution. Its data were averaged into 1-dbar bins to produce water column profiles with a nominal 250 m horizontal spacing.

IIIc. Drifter Clusters: Relative Dispersion and Kinematic Characteristics

Relative dispersion is the mean square distance between pairs of drifters and indicates how a group of particles spreads through time about the center of mass of a cluster of drifters (*LaCasce and Ohlmann*, 2003; *LaCasce*, 2008). The calculation depends upon the initial starting point and the initial drifter pair separation distance. The relevant quantities are computed as follows:

$$D_x^2(t) = \frac{1}{M}\sum_{i\neq j}\left(x_i(t) - x_j(t)\right)^2$$

$$D_y^2(t) = \frac{1}{M}\sum_{i\neq j}\left(y_i(t) - y_j(t)\right)^2$$

$$D^2(t) = D_x^2(t) + D_y^2(t)$$

$$D_{xy}(t) = \frac{1}{M}\sum_{i\neq j}\left(x_i(t) - x_j(t)\right)\left(y_i(t) - y_j(t)\right)$$

Here, $x(t)$ [$y(t)$] is the zonal [meridional] position of drifters i and j, relative to the center of mass of the cluster at time t. The terms $D_x^2(t)$ and $D_y^2(t)$ are the mean square dispersion in the zonal and meridional directions, respectively. The last two equations represent the relative mean square dispersion ($D^2(t)$) and the cross-correlation ($D_{xy}(t)$). The variable M is the number of drifter pairs used in the estimate. Schematically, the calculation is performed as indicated in **Figure 12**, beginning with the initial drifter separation distances at time = t_0 and proceeding through time = t_n.

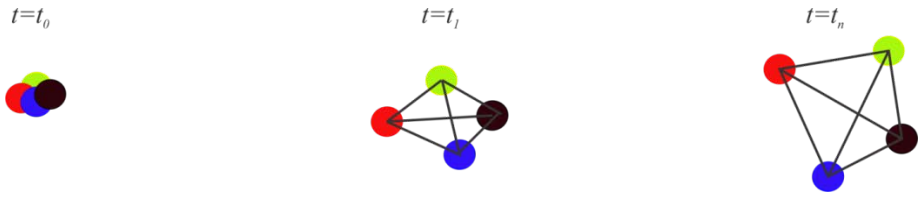

Figure 12. Example schematic of a cluster of drifters dispersing through time. The dispersion calculations are made amongst all possible drifter pairs.

We calculated the dispersion quantities in the Chukchi Shelf domain only based on several sets of MS drifters from 2012 and 2013. There are three reasons for this approach. First, these clustered deployments were all within several meters of one another at the time of deployment. Second, given the observed differences in the wind-drifter regressions we do not include the SVP-drifter results in these calculations. There were too few SVP trajectories available for a meaningful estimate of relative dispersion at 10 m depth. Third, we do not include drifters that entered Barrow Canyon in this calculation, since the dynamical regime (and presumably the dispersion characteristics) within the canyon is different from that of the shelf. Five clusters satisfied these criteria; one cluster from 2012 that was deployed in Burger on 2 September and four clusters deployed in 2013. The 2013 clusters used include two deployed offshore of Pt. Lay, another cluster deployed northeast of Hanna Shoal, and a fourth deployed northwest of Hanna Shoal. Each cluster involved from 9 – 13 drifters and the dispersion calculations are based on time series ranging from about 25 – 40 days depending upon the varying attrition rate of the drifters in the clusters. We excluded drifters that entered ice in the dispersion calculations.

Okubo and Ebbesmeyer (1976) presented a convenient way to summarize many of the kinematic properties of drifter trajectories based on clusters (groups of drifters deployed close to one another). Based on observed positions and observed velocities of each drifter (*i*) in the cluster, $\left[u_i(t), v_i(t)\right]$ is, at each time step, expanded in a Taylor series about the centroid position located at $\left[\bar{x}(t), \bar{y}(t)\right]$ accordingly:

$$\underbrace{u_i(t)}_{observed} = \underbrace{\bar{u}(t)}_{tbd} + \underbrace{\frac{\partial \bar{u}(t)}{\partial x}}_{tbd}\underbrace{\left[x_i(t) - \bar{x}(t)\right]}_{known} + \underbrace{\frac{\partial \bar{u}(t)}{\partial y}}_{tbd}\underbrace{\left[y_i(t) - \bar{y}(t)\right]}_{known} + u_\varepsilon(t)$$

$$\overbrace{v_i(t)}^{observed} = \overbrace{\bar{v}(t)}^{tbd} + \overbrace{\frac{\partial \bar{v}(t)}{\partial x}}^{tbd}\overbrace{\left[y_i(t) - \bar{y}(t)\right]}^{known} + \overbrace{\frac{\partial \bar{v}(t)}{\partial y}}^{tbd}\overbrace{\left[y_i(t) - \bar{y}(t)\right]}^{known} + v_\varepsilon(t)$$

The terms denoted indicated by "*tbd*" are determined from a least squares fit based on all the drifters in the cluster. The higher order terms $u_\varepsilon(t), v_\varepsilon(t)$ are considered turbulent motions not discussed herein. The results allow us to estimate the centroid velocity components $\left[\bar{u}(t), \bar{v}(t)\right]$ and the velocity gradients. The following kinematic quantities were then estimated:

Horizontal divergence: $\gamma(t) = \partial\bar{u}/\partial x + \partial\bar{v}/\partial y$

Relative vorticity: $\zeta(t) = \partial\bar{v}/\partial x - \partial\bar{u}/\partial y$

Stretching deformation rate: $\alpha(t) = \partial\bar{u}/\partial x - \partial\bar{v}/\partial y$

Shearing deformation rate: $h(t) = \partial\bar{v}/\partial x + \partial\bar{u}/\partial y$

By considering a "box" to denote a water parcel captured by a drifter, these terms can then be described schematically as follows:

1. Horizontal divergence describes increases (divergence) or decreases (convergence) in parcel's area:

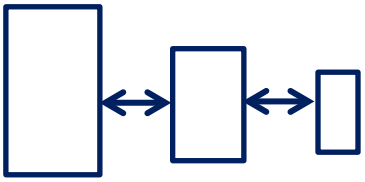

2. Relative vorticity describes the rotation of the parcel:

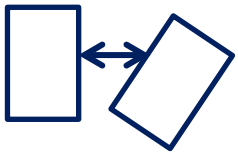

3. Stretching deformation describes dilatation of the parcel along a particular axis without changing the area of the parcel:

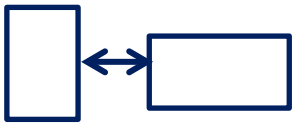

4. Shearing Deformation describes distortion of the parcel due to the velocity gradients:

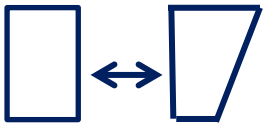

Note that a parcel may undergo one, some, or all of these changes simultaneously. The time rate of change of the fluid's absolute vorticity ($\zeta+f$) is given by:

$$\underbrace{\frac{d}{dt}(\zeta+f)}_{\substack{\text{rate of change}\\ \text{of absolute vorticity}}} + \underbrace{(\zeta+f)\left(\frac{\partial u}{\partial x}+\frac{\partial v}{\partial y}\right)}_{\text{stretching vorticity}} = \text{ sources and sinks for } (\zeta+f)$$

The first time on the right describes the rate of change of the absolute vorticity and the second term is vortex tube stretching due to convergence or divergence within the fluid. Vorticity sources or sinks arise from torques associated with the surface wind or bottom stresses, or baroclinic torques arising from the density field. Our data allow us to evaluate the terms on the left hand side only. If there are no vorticity sources or sinks then the left hand side should sum to zero.

IV. Results and Discussion

IVa. Winds

On long-term average, the winds over the northeast Chukchi Sea Shelf are from the east-northeast (*Brower et al,. 1988*) and roughly oppose the mean bathymetrically-steered flow established by the pressure gradient between the Pacific and Arctic oceans. Based on moored measurements, *Weingartner et al.* (1999) found that the Alaskan Coastal Current reversed and flowed southwestward in Barrow Canyon when northeasterly wind speeds were $\geq$5 m s^{-1}. Northeasterly winds also promote coastal upwelling along the Chukchi coast, which should include a southwestward alongshore flow and an offshore flow at the surface. *Weingartner et al.* (2013a) found that, in summer, the currents in Klondike reversed from being eastward to being westward when winds had a westward component that exceeded ~6 m s^{-1}. Both sets of observations are consistent with the high-frequency radar measurements of the regional surface currents south of 71.5°N reported by *Weingartner et al.* (2013b). The radar data sets also indicate that the winds explain ~50% of the surface current variance in ice-free regions. With these results in mind, we briefly review the October – November wind fields for 2011 – 2013 in the form of three-hourly vector plots based on the NARR grid point in Klondike (**Figure 13**).

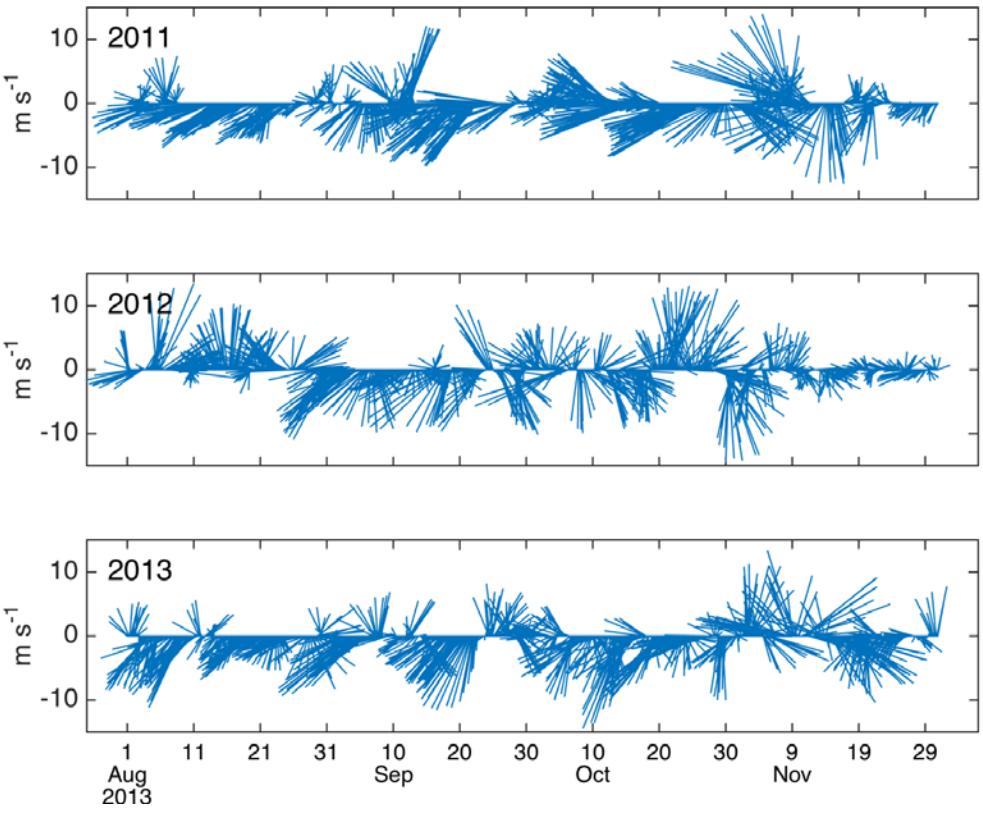

Figure 13. Vector plots of winds from the central Chukchi Sea Shelf from August through November for 2011 (top), 2012 (middle) and 2013 (bottom). North is oriented toward the top of the page and the vectors point in the direction *toward* which the wind is blowing.

As seen in the figure, winds were primarily from the northeast in each of these years, but there was considerable interannual variability both seasonally and synoptically. For example, northeasterly winds were dominant from August through October in 2011 and 2013 and, compared to 2012, there was relatively little synoptic variability. In November of 2011 and 2013, the wind directions were much more variable with nearly equal frequencies of southerly and northerly winds. In contrast, the winds in 2012 were from southerly quadrants in August and through much of October. There was considerable directional variability in the winds in November of all years, however, wind speeds in November 2012 were generally <5 m s^{-1}, much weaker than in either November of 2011 or 2013. While the NARR winds provide an overview of the regional winds, we have used winds prepared by NOAA's WaveWatch wave prediction model for most of the statistical analyses between winds and currents derived from the drifters. As shown previously, both products agree well with measured winds, and with one another.

IVb. Sea Ice Distribution

From the perspective of this drifter study, sea ice plays two roles. As will be seen, it is a major source of cold, dilute seawater that influences the hydrography, especially the stratification and frontal structures. Sea ice will respond differently to the winds than the ocean so that drifters caught in ice are likely to not reflect the ocean currents. Maps of the ice-edge position over the northeastern Chukchi Shelf for selected dates (1 and 15 August; 1 and 15 September) for 2008 – 2013 are shown in **Figure 14**. The seasonal pattern of ice retreat consists primarily of a northward regression of the ice-edge such that by mid-September the region south of Hanna Shoal is completely ice free (although this was not the case in 2012). Note that the ice retreat does not proceed uniformly across the region. Ice lingers longer over Herald Shoal, centered at 70.5°N and 170°W, than to the east of the shoal where by mid-August the ice-edge is typically at 71°N. Similarly, ice frequently persists over Hanna Shoal even though the shelf to the west (e.g., within the Central Channel) and to the east of the Shoal may be ice free.

The interannual variations in ice-edge position were substantial. The heaviest ice years occurred in 2008, 2012, and 2013. In each of these years the ice-edge was nearly zonally-oriented along ~71°N south of Hanna Shoal and varied little in position throughout August. In 2008 and 2013 the ice retreated to northwest of Hanna Shoal and over the outer shelf by mid-September. The same northwestward retreat occurred in 2012, but ice remained over Hanna Shoal through mid-September. It appears that in both 2012 and 2013 heavily-deformed ice grounded atop Hanna Shoal in late winter and that much of this ice remained grounded well into summer (Dr. A. Mahoney, UAF, personal communication, January 2015). The lightest ice years were in 2009 and 2011. In 2009, the ice retreated very rapidly between 1 and 15 August such that the northeastern shelf was completely ice free by mid-August. In 2011, the northeastern shelf was virtually ice-free in early August. The ice retreat in 2010 was modest in comparison to the heavy and light ice years. By early August 2010, ice had retreated northward in the Central Channel, but still encompassed Herald Shoal and extended eastward along 71.5°N between 165°W and the

coast. By mid-August the ice had retreated to the north of 72°N and by 1 September the shelf was largely free of ice.

The causes of this interannual variability are not at all clear and may depend upon a number of factors discussed later. We note, however, that these differences in ice extent are not simply related to the local winds. For example, the winds during August and September of 2008 and 2013 (heavy ice) and 2011 (light ice) were persistently from the northeast. In contrast, winds were from the south and southwest in 2009 (light ice) and in August of 2012 (heavy ice) while winds were variable in both direction and strength in 2010.

Figures 15 and 16 show the ice concentrations based on AMSRE and/or AMSR2 satellite imagery for the Pacific Arctic sector including the Chukchi and Beaufort Seas. Note that this imagery is based on passive microwave satellites and is acquired at a coarser horizontal resolution than the NIC ice edges of the previous figure. In all years, the main concentrations of ice in the Chukchi sector were north of 73°N through September. In 2011 and 2012, ice remained north of this latitude through the end of October. In 2013, the ice was further south, between 72°N and 73°N by mid-October, and advancing to between 70°N and 72°N by the end of October. Ice advanced rapidly southward through early November, with this advance being largest in 2012 and least in 2011. Much of the Chukchi Shelf was covered by ice by the end of October in all years. Over the Beaufort Shelf, the main concentrations of ice remained north of 72°N through the middle of October in all years and through the end of October in 2012. In 2011 and 2013, the ice expanded westward along the Beaufort Shelf to between 145° and 150°W and to the south of 72°N through the end of October. By mid-November, ice had encompassed the entire Beaufort Shelf, except for a small fraction of the shelfbreak region in 2013.

IVc. Hydrography

We begin the discussion of hydrographic variability using the CSESP data from 2011 – 2013. These data have been published in the associated annual reports for that program (*https://www.chukchiscience.com/Downloads*). Here, we present the data in terms of plan views of temperature and salinity averaged over the surface and bottom 10 m of the water column for each cruise in each of these years, with two vertical sections from 2011 and 2012 for comparison. Additional hydrography from 2013 is presented in the form of vertical sections taken from either gliders or the Acrobat vehicle. As a prelude to this section we include a temperature-salinity diagram (**Figure 17**) that illustrates the water masses present. The diagram is based on the 2011 and 2013 CSESP data (2012 T/S diagrams are similar to 2013 so not shown). Three basic water masses and mixtures are generally present. These include Winter Water (WW), which is very cold (near freezing) and saline, warm and moderately saline Bering Sea Water (BSW), and Meltwater (MW), which is fresh and cool. All of these water masses were present in 2012 and 2013, but MW was absent in 2011. There was an additional water mass present in 2013 on some of the Acrobat sections discussed later. This is Alaskan Coastal Water

(ACW), which is as warm or warmer than BSW, but fresher, with salinities generally <30. With this nomenclature established, we next consider the hydrographic properties of the shelf in these years.

In August 2011 (**Figure 18**) the surface waters over the central shelf were largely occupied by BSW with the warmest and most saline surface waters found in Klondike. Recall that the ice-edge in August 2011 was far to the north by 1 August and so the survey area had been flushed of MW by the time of the sampling. Bottom water properties in Burger and Statoil consisted primarily of WW, while those in Klondike were warmer and fresher, suggesting that some mixing had occurred between the BSW and WW. In September, BSW occupied the entire surface layer so that horizontal temperature and salinity gradients were weak. In contrast, there was considerable spatial variability in the bottom waters. Those in Klondike consisted of BSW, while bottom waters in Burger and those to the north and east of Hanna Shoal consisted entirely of WW. Bottom waters in Statoil had warmed and freshened compared to the prior month indicating infiltration of BSW into this area.

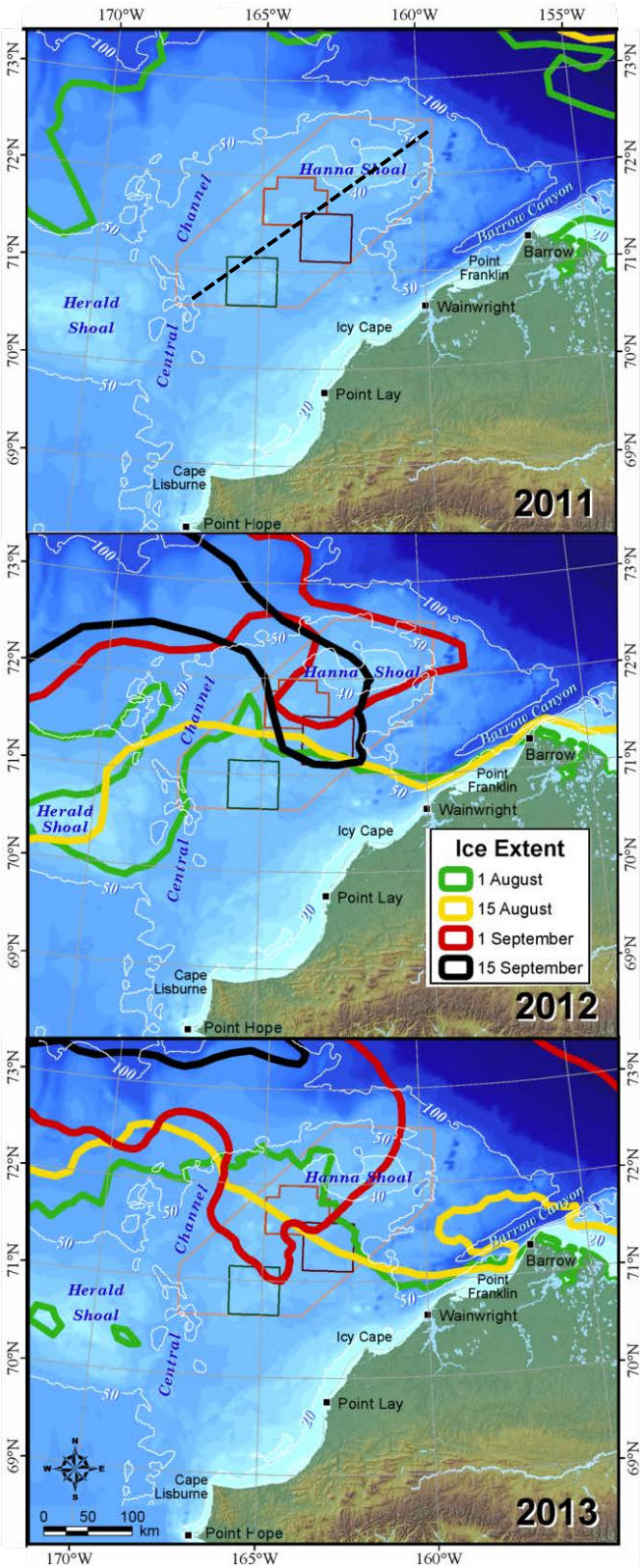

Figure 14. Ice-edge location as a function of year and date between August and September. The dashed line in the 2011 map shows the location of the vertical sections for 2011 and 2012 shown in **Figure 21**.

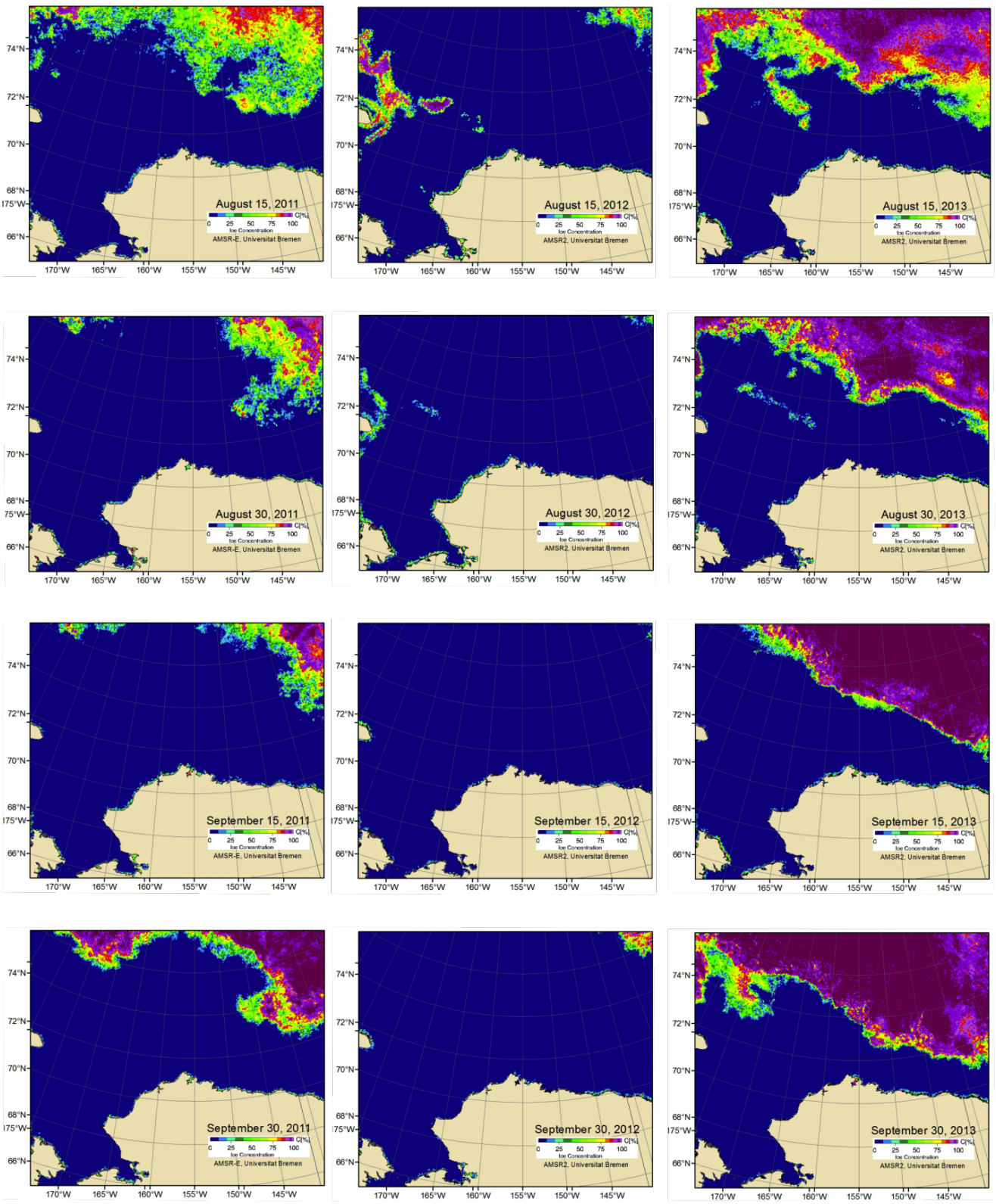

Figure 15. Regional ice concentration maps by year (columns) and date (rows) for August 15 and 30, and September 15 and 30.

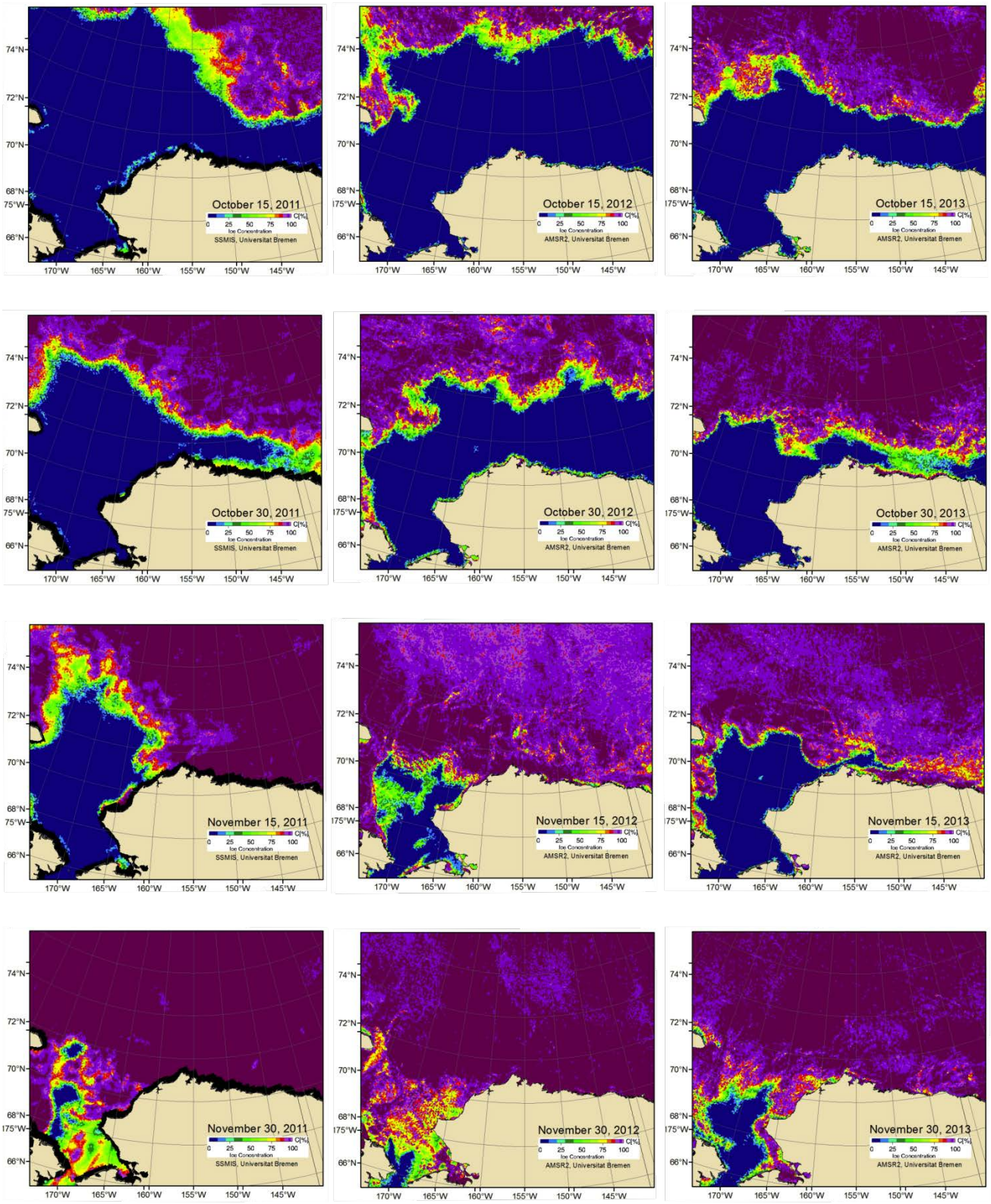

Figure 16. Regional ice concentration maps by year (columns) and date (rows) for October 15 and 30, and November 15 and 30.

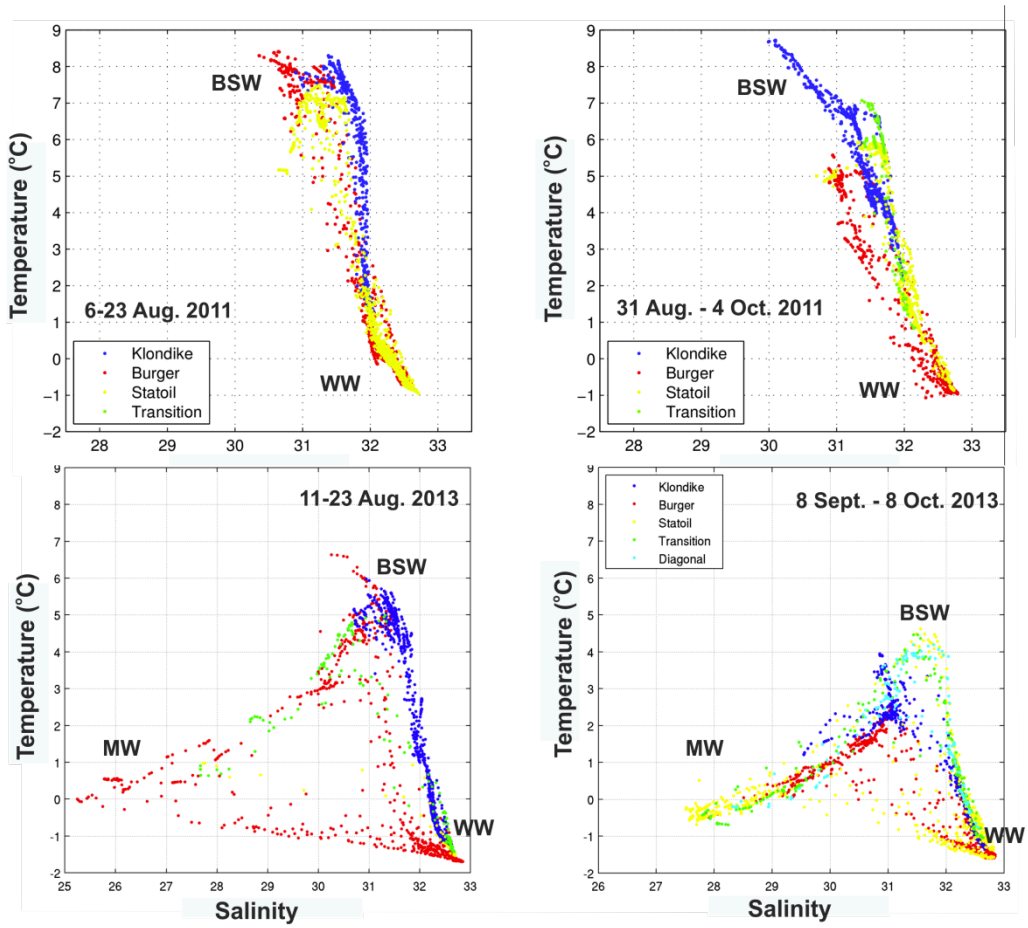

Figure 17. Temperature-salinity diagrams from the CSESP stations in the central Chukchi Sea for 2011 (upper panels) and 2013 (lower panels).

The conditions in 2012 (**Figure 19**) were quite different from those in 2011. Although BSW occupied Klondike in August, surface temperatures and salinities decreased toward the northeast indicating the presence of MW in both Statoil and Burger. Bottom water properties in Klondike were cooler and saltier than the surface layer, but nonetheless these suggest that BSW had displaced much of the WW. Within Statoil and Burger, the bottom water properties consisted of WW. By September, MW occupied the surface waters in the entire region north of 71.5°N, except over the westernmost portion of the survey area. Here a tongue of water with BSW properties extended northward within the Central Channel and to the west of Statoil. With the exception of the coastal stations near Wainwright, September bottom waters consisted of cold BSW in the southwestern portion of the study area with these being colder and saltier in September than in August. Hence, in 2012, the typical seasonal progression in Klondike bottom water properties was reversed. Elsewhere WW prevailed, with the coldest and saltiest waters found encircling the southern flank of Hanna Shoal.

In many ways 2013 conditions were similar to 2012. In August of 2013 (**Figure 20**), a prominent surface front extended along 71.25°N and separated BSW in the south from MW to the north. Although bottom waters were cold throughout the area, the salinities increased from the south to the north suggesting the intrusion of cold BSW into Klondike. By September, surface temperatures had cooled and the frontal structure evident in the salinity field had weakened, however, there was little change in the distribution of bottom water properties.

We next examine vertical sections of temperature and salinity from September 2011 and 2012 (**Figure 21**). The sections consist of the same stations along a transect that extends from the southeast corner of Klondike, skirts the eastern side of Hanna Shoal (indicated by "HS" in the figure) and continues to the northeast side of Hanna Shoal (the location of the section is shown on the 2011 ice-edge map in **Figure 14**). In 2011, the upper 25 m of the entire section contained BSW with salinities between 31 and 32. There was very little horizontal variability in the upper layer, except for the weak thermal gradient at ~km 100. The pycnocline was centered at ~25 m depth across the entire section and varied in strength along the section. Southwest of km 100 it coincided with a weak halocline (0.05 m^{-1}) and a modest (~0.2°Cm^{-1}) thermocline. Northeast of this location the pycnocline strengthened due to a much stronger halocline (0.2 m^{-1}) and thermocline (~0.8°Cm^{-1}). The strengthening of the pycnocline was a consequence of the change in bottom water properties; cold (<0^{o}C), salty (>32) winter waters occupied the bottom 15 m of the water column on either side of Hanna Shoal. In contrast to the upper layer, the bottom waters included a strong thermohaline front at ~km 100, which separated the BSW to the southwest from the WW to the northeast. The corresponding section in 2012 was substantially different in two important respects. First, the upper layer was substantially more heterogeneous in consisting of both BSW and MW. The latter was largely centered over Hanna Shoal and separated from the BSW to the southwest by a strong thermohaline front at ~km 125. Second, a prominent pycnocline extended across the entire section, although it was stronger to the northeast than to the southwest. Northeast of the front the pycnocline was shallow, centered at ~15m depth, and largely due to the vertical salinity gradient (~0.5 m^{-1}). In contrast, the pycnocline to the southwest was deeper (~22m) and associated with vertical gradients in both temperature and salinity. Third, there is the suggestion of an anticyclonic eddy embedded in the pycnocline in 2012. This feature is indicated by the patch of 2.5^{o}C water centered at ~km 210 on the transect, and it is accompanied by vertical spreading of the isohalines. As outlined later, this feature was likely an eddy shed baroclinic instability of the MW/BSW front.

In spite of the large hydrographic differences between 2011 and 2012, the vertical sections shared a common feature in terms of the large pool of WW that was distributed to the south and north of Hanna Shoal. Indeed, this pool of WW and its location appears to be a conspicuous and recurrent feature of the shelf hydrography as evidenced by the September bottom water property distributions in **Figures 18–20** and in previous years as described by *Weingartner et al.* (2013a). While there are variations between years in the temperature and salinity of the WW (in 2011 it was somewhat warmer and fresher than in 2012), these differences are much smaller than the

large interannual variations in temperature and salinity observed at the surface and along the bottom elsewhere throughout this region.

As will be seen, most of the 2011 and 2012 drifters deployed on the Chukchi Sea Shelf moved into Barrow Canyon and out onto the Beaufort and Chukchi shelfbreaks. However, the drifters deployed in 2013 mainly remained on the Chukchi Sea Shelf throughout their lifetime. A considerable amount of hydrography collected by Dr. Winsor (UAF) under separate BOEM funding in September 2013 from the northeast Chukchi Sea Shelf is relevant to the 2013 drifters. This hydrographic data set provides a glimpse of the hydrographic structure of the shelf that many of the drifters passed across within their first month. We first review a subset of these vertical sections. The Acrobat measured temperature, salinity, chlorophyll, particle concentrations, and color-dissolved organic matter (CDOM) as a function of pressure, depth and density were computed from temperature, salinity, and pressure.

From 10 – 14 August, and just prior to the release of the Pt. Lay drifters, glider 191 (deployed by Dr. Winsor) transited eastward from the Central Channel toward the Alaskan coast along 69.5^{o}N completing a nearly 120 km long section. **Figure 22** shows the glider transect its related vertical section. (Note that the glider did not extend inshore of ~30 isobath and only came within ~40 km of the coast.) Warm (8 – 9^{o}C), fresh (<29.5) ACW occupied the uppermost 20 m of the section between km 100 – 120. Beneath this layer, waters were cooler (~1^{o}C) and saltier (31). This region was separated from offshore waters by a front located at ~km 100. Seaward of the front, waters were cooler (7 – 8^{o}C) and saltier (>~30) and more weakly stratified. Below 20 m depth, temperatures were 5 – 6^{o}C and salinities were ~31. The winds at the time of this transect were upwelling-favorable and very likely the offshore extent of the ACW reflects surface near-surface displacement by Ekman transport. We do not, however, see evidence of coastal upwelling in the form of upward sloping isopycnals toward the coast on this section. The most likely reason is that the glider did not come sufficiently close to the coast to capture upwelling of subsurface waters into the surface layer.

In the following paragraphs we describe the hydrography collected by the Acrobat-CTD system. Leg H (**Figure 23**), occupied on September 11 – 12, extended ~260 km westward from offshore of Wainwright and across the Central Channel. Nearshore surface temperatures were cool (2 – 3^{o}C) and moderately fresh (<31) while offshore temperatures were warmer (>3^{o}C) and slightly saltier (~31.5). Maximum temperatures were ~6 ^{o}C along the eastern side of the Central Channel and are associated with the northward flow of BSW within the Channel. Cold (< 0^{o}C), salty (32.5) waters occupied the lower half of the water column everywhere but along the eastern flank of the Central Channel. Density stratification was moderate over the entire section, except in the eastern portion of the Central Channel, where the water column was weakly stratified. Thus surface temperatures along the western end of this section were cooler than those observed by the glider in mid-August.

Leg D, occupied on 10 September, extended from the west side of Hanna Shoal to the head of Barrow Canyon offshore of Wainwright (**Figure 24**). The lower half of the water column consisted of cold ($\leq 0^{o}$C), salty (~32.5) WW. Surface waters between km 0 and 80 were cool (~1^{o}C) and fresh (~27) indicating MW. Between km 100 – 190, there was a plume of warmer (~3 – 4^{o}C) and saltier (29 – 31.5) surface waters, most likely ACW that was displaced offshore by the upwelling-favorable winds. Colder and saltier waters were found within 20 km of the coast. Here the isopycnals bowed upward toward the surface nearing the coast, indicative of wind-induced coastal upwelling. Across the whole transect, with the exception of this coastal upwelling band, the water column was heavily stratified. Leg G (**Figure 25**), from 8 September, is a shorter transect extending 60 km offshore of Wainwright to the coast where it ended ~50 km southwest of Leg D. This section also reflects coastal upwelling, with the upwelling signature present inshore to at least the 10 m isobath. Seaward of the 25 m isobath (km 15), the surface waters were the warmest (~3^{o}C) observed on this section and had a salinity of ~32. Given the prevalence of upwelling-favorable winds in August and September, these hydrographic conditions were likely similar to those prevailing at the time of the Wainwright drifter deployments on 24 August.

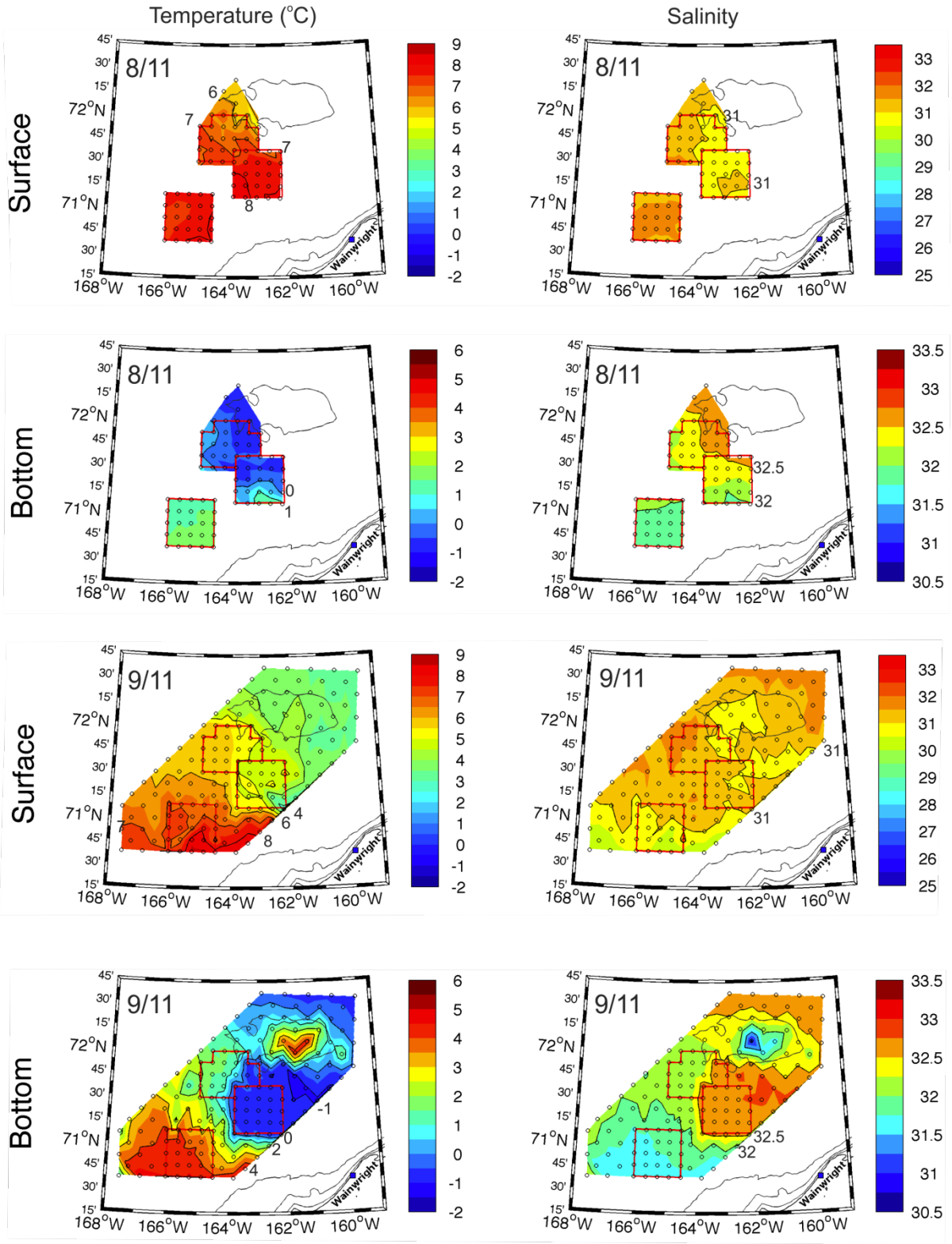

Figure 18. Plan views of surface and bottom temperatures and salinities averaged over the upper and lower 10 m of the water column in August and September 2011. Note that the temperature and salinity scales differ between the surface and bottom maps.

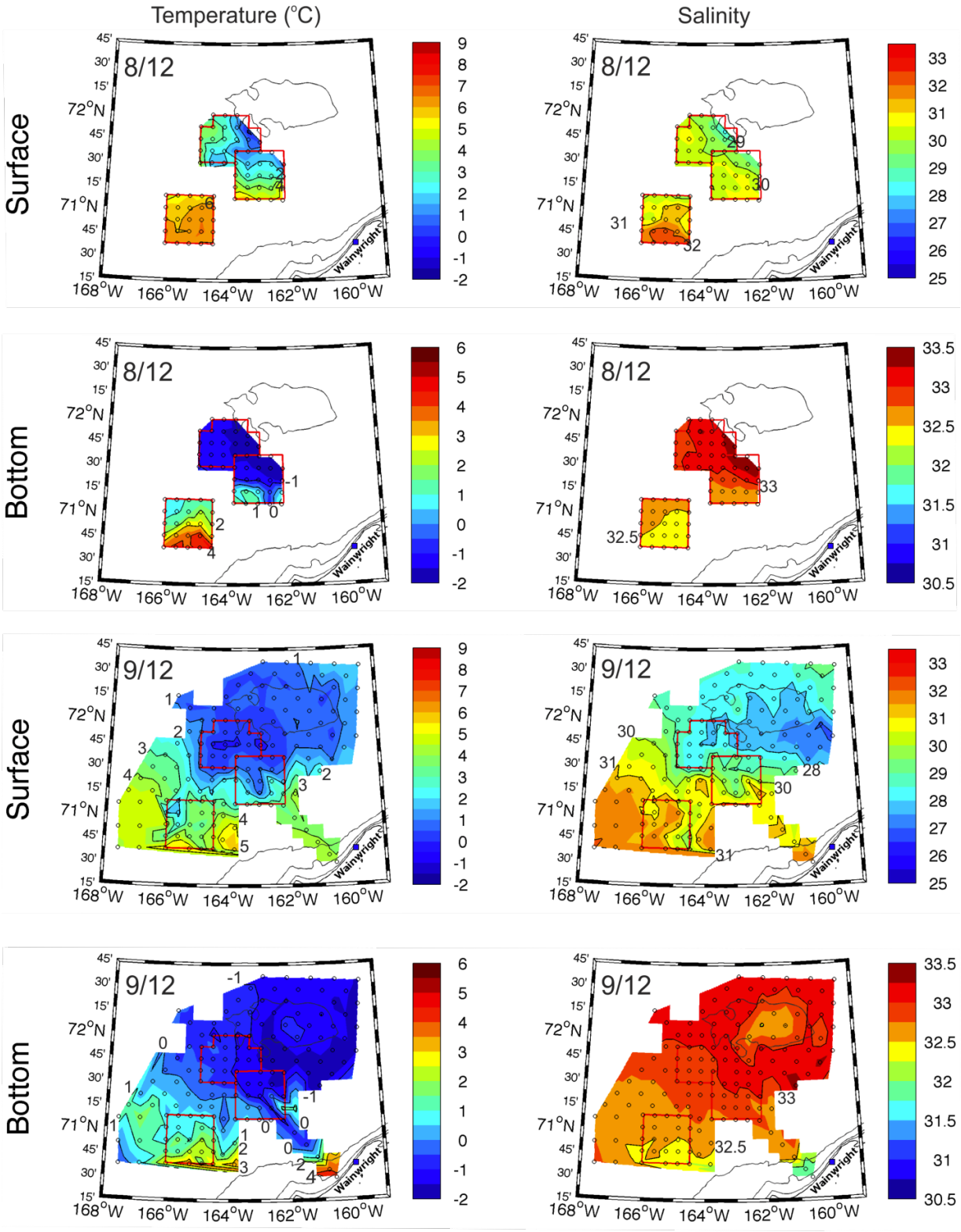

Figure 19. Plan views of surface and bottom temperatures and salinities averaged over the upper and lower 10 m of the water column in August and September 2012. Note that the temperature and salinity scales differ between the surface and bottom maps.

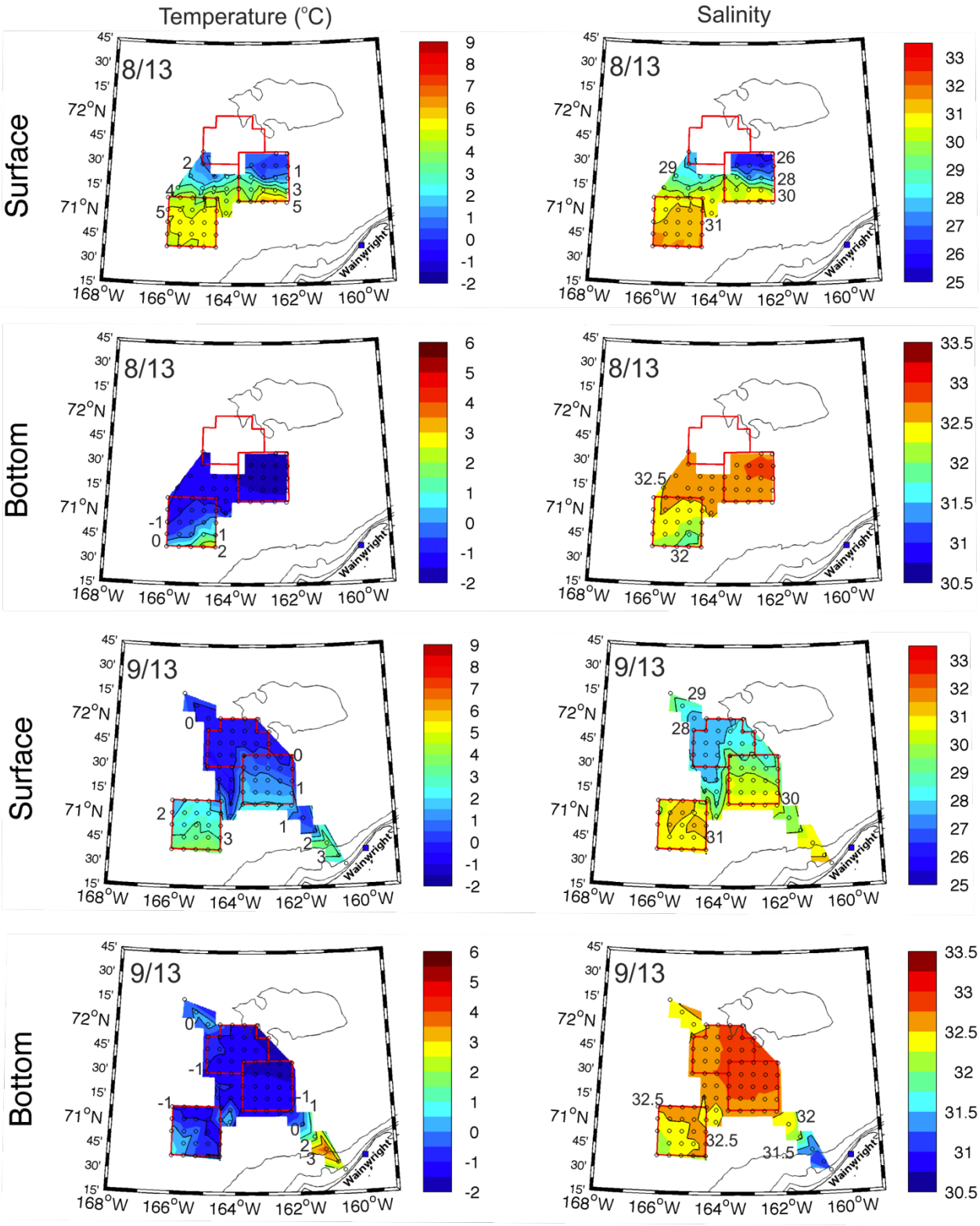

Figure 20. Plan views of surface and bottom temperatures and salinities averaged over the upper and lower 10 m of the water column in August and September 2013. Note that the salinity scales differ between the surface and bottom.

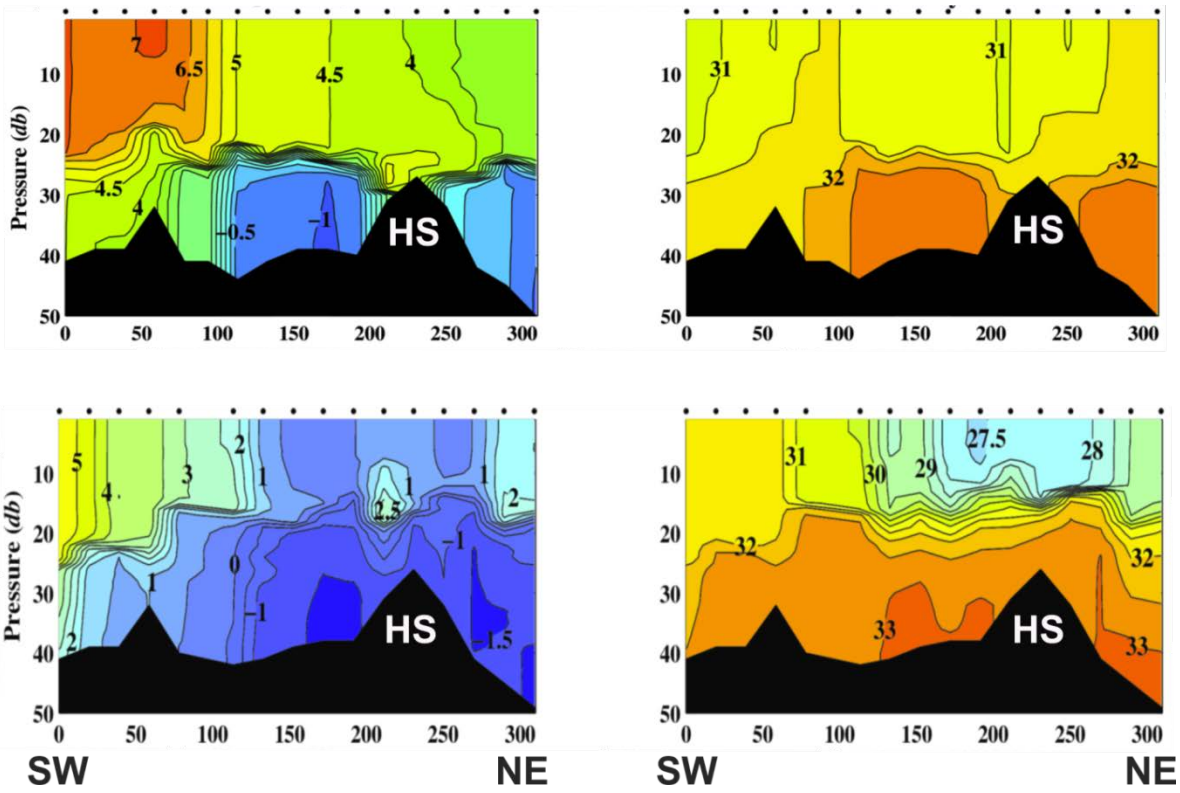

Figure 21. Vertical sections of temperature (left) and salinity (right) from 2011 (top row) and 2012 (bottom row) along the southwest (SW) to northeast (NE) transect shown in **Figure 14**. The location of Hanna Shoal is indicated by "HS".

Leg Q (16 – 17 September; **Figure 26**) extends ~220 km northward from offshore of Wainwright to the north side of Hanna Shoal. Proceeding northward along the transect, the hydrographic properties over the first 80 km consists of warm (3 – 6^{o}C) and moderately salty (~31) BSW in the upper 20 m and much colder (<0^{o}C) and saltier ($\geq$ 32.3) waters within the lower half of the water column. The stratification over this part of the transect is modest, changing by 2 kg m^{-3} over 2 m depth, and centered at ~25 m depth. On approaching the southern flank of Hanna Shoal, between km 80 – 220, the water column stratification nearly doubles, with the surface layer consisting of meltwaters and the bottom layer being winter water. A 20-km wide prominent front, confined to the upper 20 m, occurs at km 80 and separates warmer saltier waters to the south from cooler, fresher waters to the north. Leg H, which extends westward offshore of Wainwright and across the Central Channel (**Figure 27**) reflects properties in the upper 20 m of the water column similar to those south of the front found on Leg Q. Note, however, that within the Channel, the surface waters are warmer and saltier on the east side of the channel than those on the west side.

Legs B, O, and R (**Figures 28 – 29**) characterize the water properties on the shelf between the east side of Hanna Shoal and Barrow Canyon and atop Hanna Shoal. In aggregate, these sections indicate a strongly stratified water column, a consequence of the fresh, cold meltwaters in the

upper 20 m and the saline, colder winter waters below 25 m depth. This strong stratification persists even over the shallow (~25 m deep) Hanna Shoal (Leg R; **Figure 29**). None of these sections show evidence of the warmer and moderately salty water that was observed on the legs farther south. This suggests that either these waters have yet to arrive in this region, or that dynamical processes are inhibiting their infiltration into this part of the shelf.

Leg C, occupied on 9 September, extended ~70 km northwestward from the western side of Hanna Shoal (**Figure 30**). This section's properties were similar to those found on the eastern side of Hanna Shoal in being primarily a composition of surface meltwaters and subsurface winter waters. However, there are lenses of warm, moderately salty water embedded in the pycnocline along this section, most noticeably between km 5 – 30 and 40 – 60. These lenses are signatures of warm (~3 – 4^{o}C) moderately saline (~31.5) waters derived from the south (most likely from the northward flow of BSW in the Central Channel; cf., Leg H in **Figure 23**).

In summary, the hydrographic structure of the northeast Chukchi Sea Shelf was similar in many regards in 2012 and 2013. Features in common include surface fronts that separated weakly and/or modestly stratified BSW and ACW in the south from strongly stratified water columns consisting of MW at the surface and WW at depth. These fronts tended to be oriented from west to east along about 71.5°N (and south of Hanna Shoal) in both years. Not surprisingly, these fronts were also approximately aligned with the August ice-edge in both years.

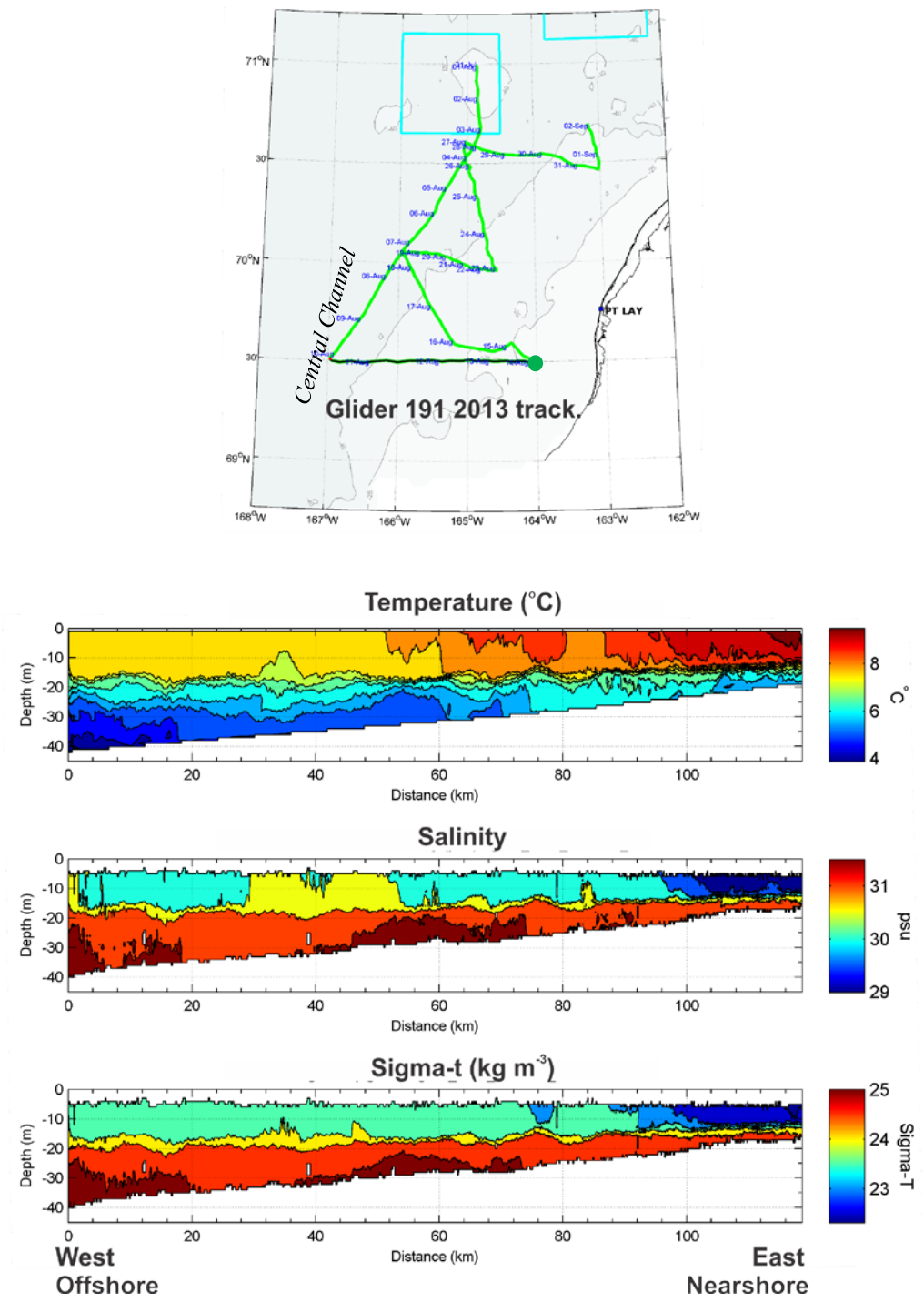

Figure 22. Top: location (black line) of the west-to-east transect of glider 191 from 10 – 14 August, 2013. The green dot indicates the start of the transect. Bottom: Vertical sections of temperature (top), salinity (middle), and density (expressed as sigma-t; bottom) along the transect. The westernmost end of the transect is on the left of the figure.

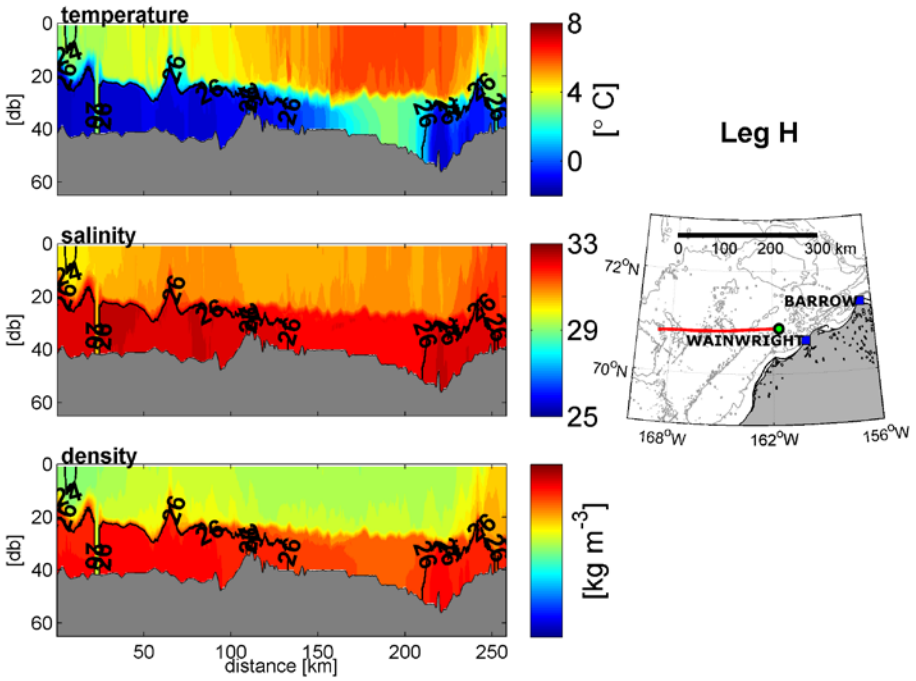

Figure 23. The Leg H vertical section derived from the towed-CTD (Acrobat) on 11 – 12 September 2013. The section extends from the coast to the Central Channel as indicated by red line on the inset map. The black and green circle indicates the beginning of the transect. From top to bottom: temperature, salinity, and density. The westernmost end of the transect is on the right.

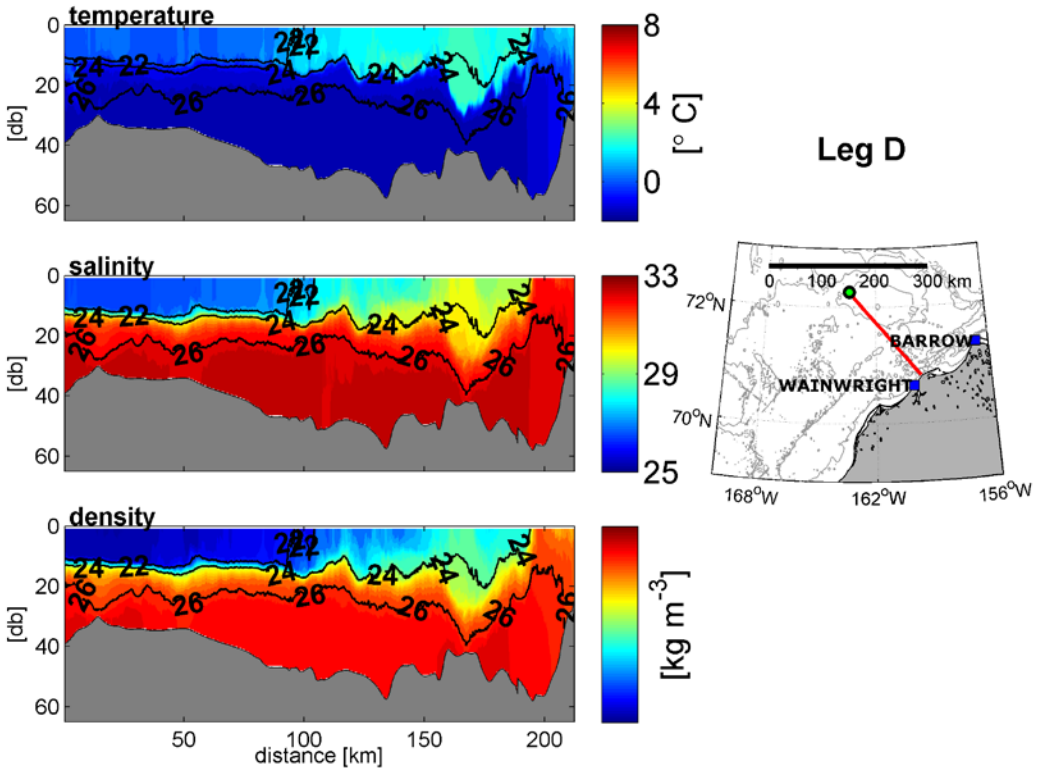

Figure 24. As in Figure 23, but for Leg D, from northwest of Hanna Shoal to the coast.

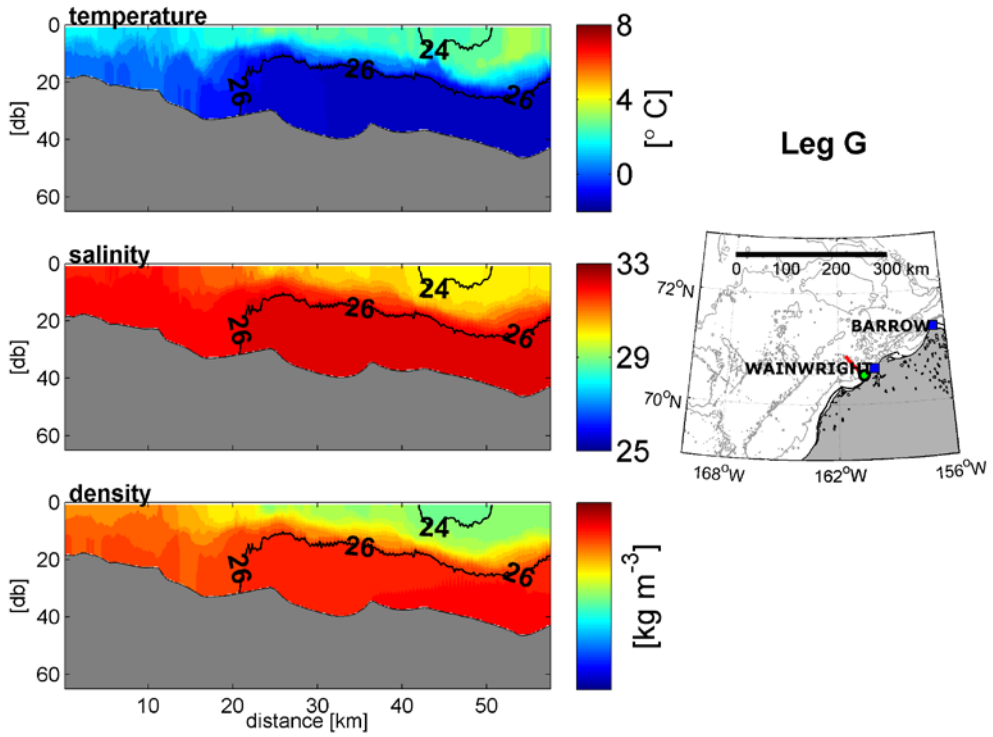

Figure 25. As in Figure 23, but for Leg G, a short transect offshore of Wainwright.

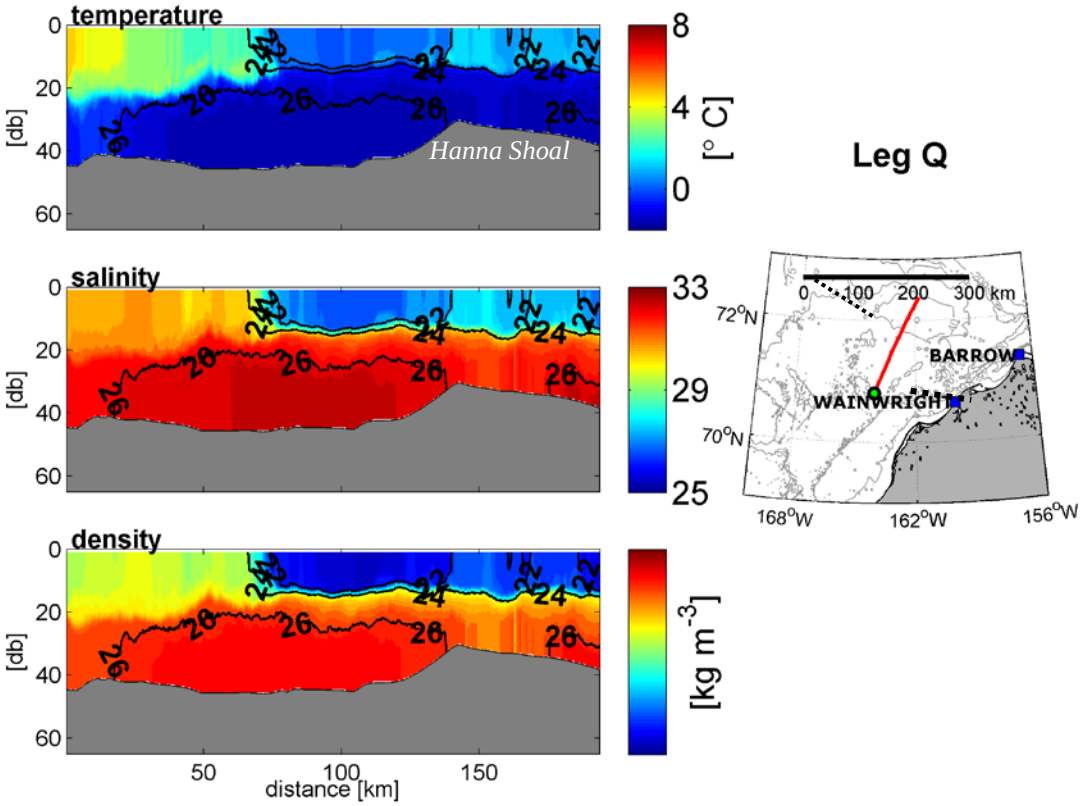

Figure 26. As in Figure 23, but for Leg Q, a south to north transect across Hanna Shoal. The black dotted line on the map insert shows the approximate location of the front at km = 80.

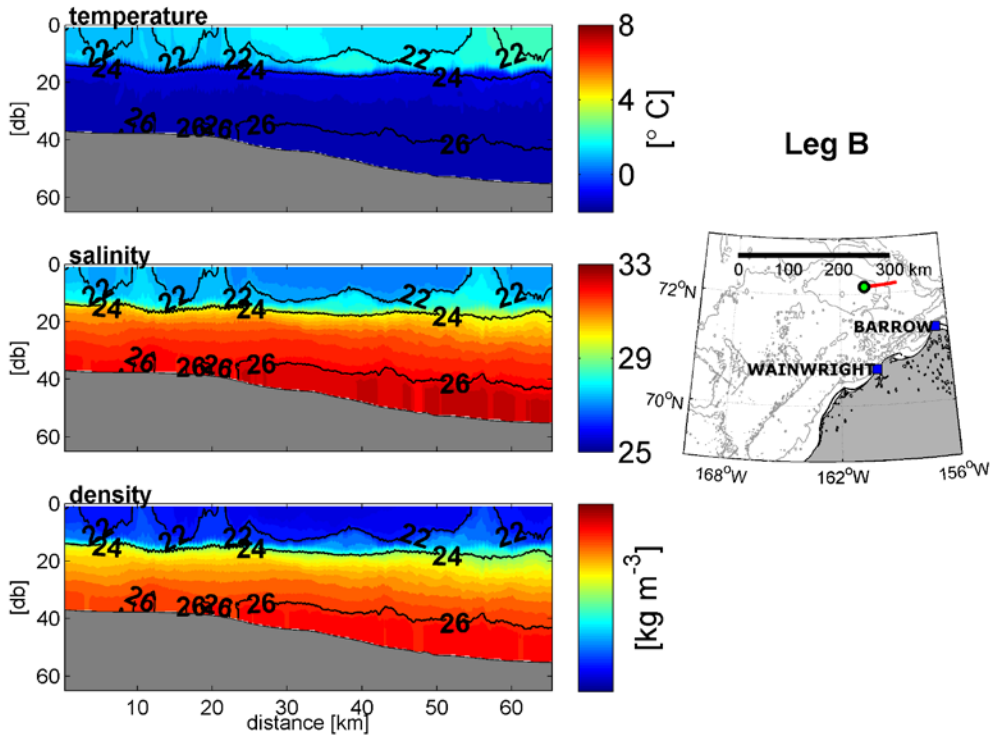

Figure 27. As in Figure 23, but for Leg B, a short west to east transect along the northeastern flank of Hanna Shoal.

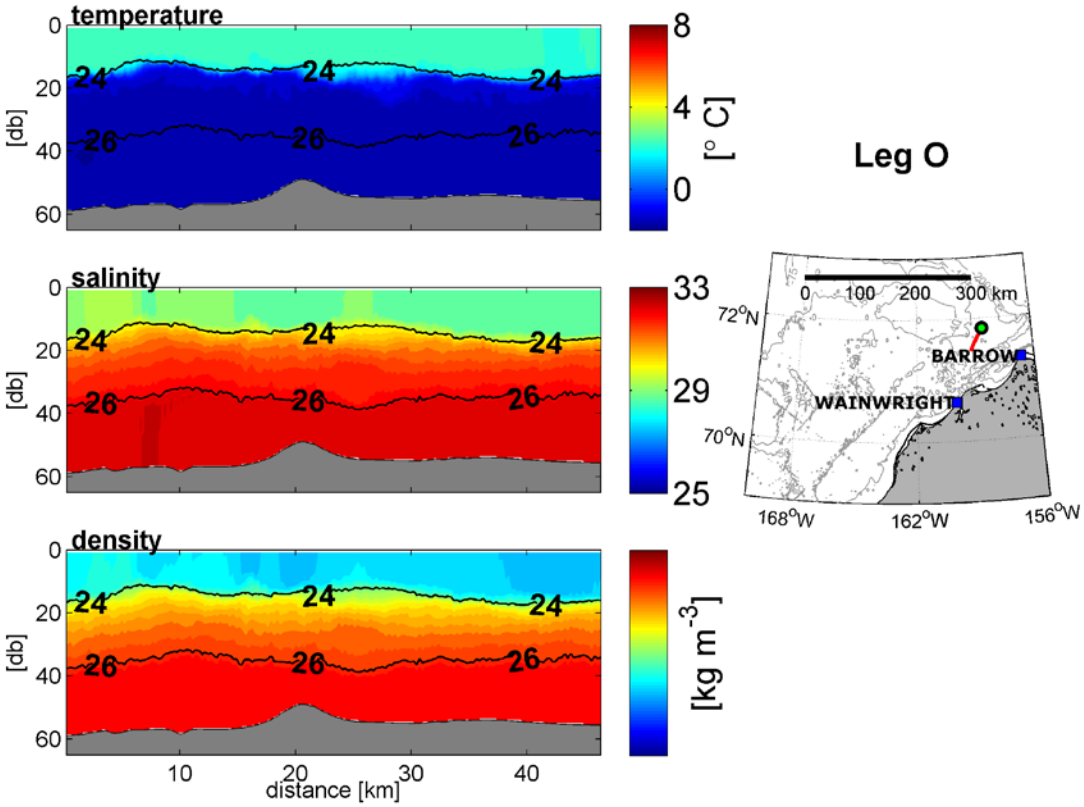

Figure 28. As in Figure 23, but for Leg O, a short north to south transect along the northeastern flank of Hanna Shoal.

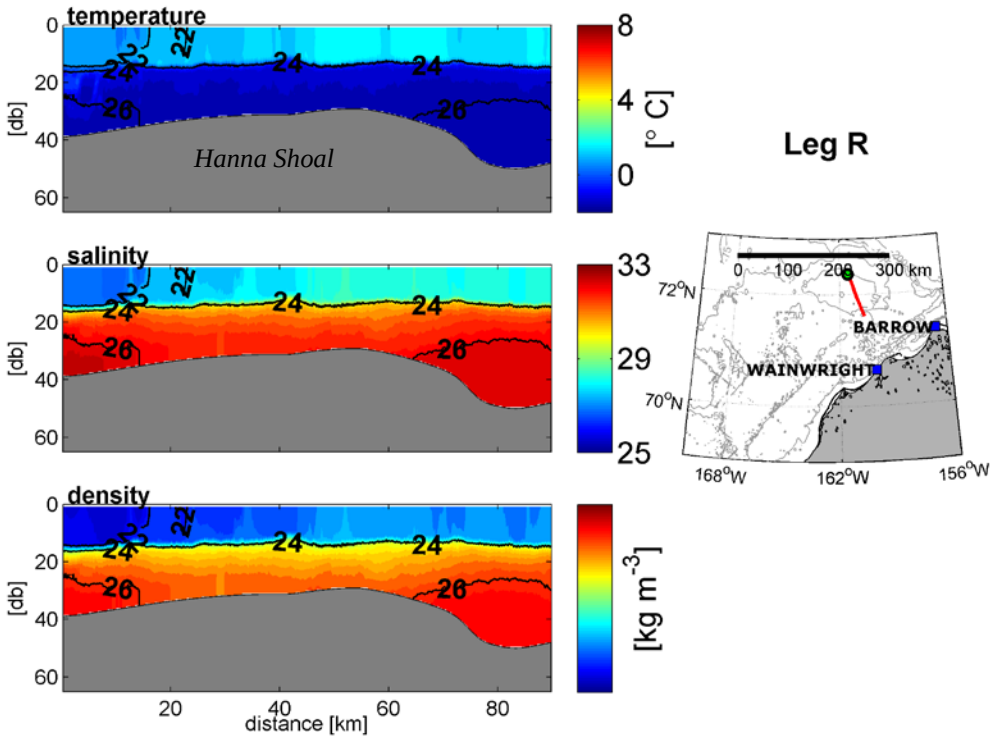

Figure 29. As in Figure 23, but for Leg R, a short north-south transect across Hanna Shoal.

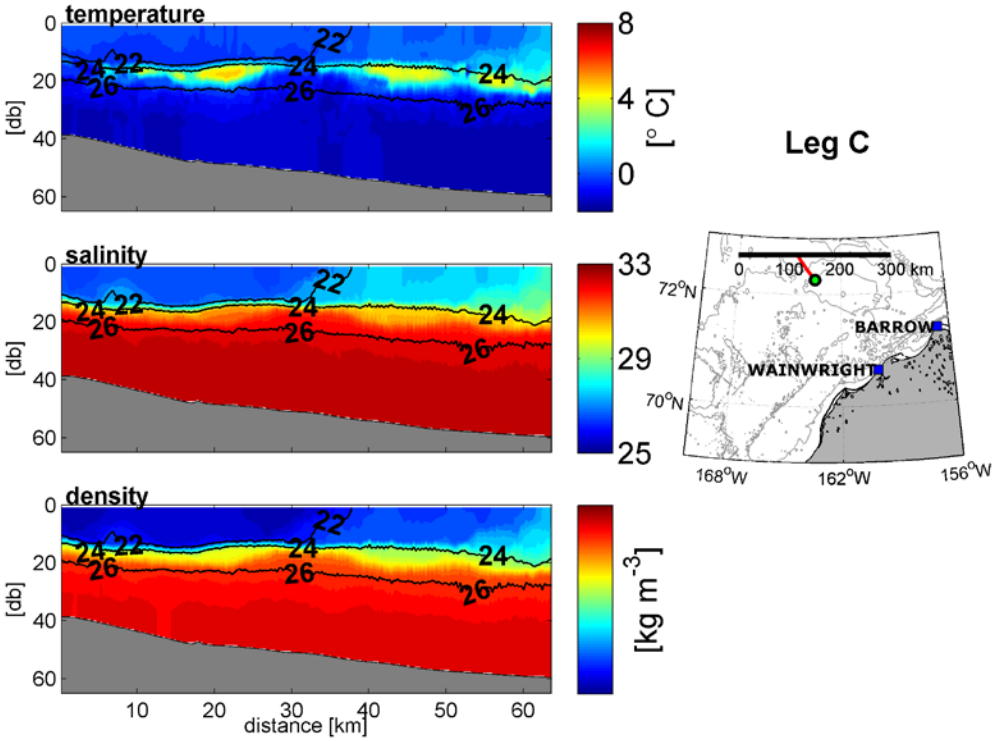

Figure 30. As in Figure 23, but for Leg C, a short transect along the northwestern side of Hanna Shoal.

IVd. Overview of Selected Trajectories

In this section we provide a descriptive overview of the diversity and complexity of a subset of the drifter trajectories. Those drifter labels prefixed with MS denote the Microstar, or 1-m drogued drifters and those with the SVP prefix denote the 10-m drogued drifters.

Given the problems with the 2011 drifters, the data distribution was insufficient to address many of our goals and hence our discussion of this data set is limited. **Figure 31** shows the trajectories of drifters deployed in mid-August 2011 (and whose lifetimes exceeded four days). All of the functioning 10-m drogued drifters moved eastward from south of Hanna Shoal toward Wainwright (**Figure 32**) in August under easterly winds that averaged 4 ms^{-1} (the background geostrophic flow more than compensated for the westward surface wind stress). All but one of these drifters then moved northeastward down Barrow Canyon to the shelfbreak, and then turned westward along the Chukchi shelfbreak (under the influence of strong westward winds in fall). In contrast, immediately after deployment three of the 1-m drogued drifters moved southwestward (also under strong northeasterly winds) from Hanna Shoal and into the Central Channel in August. From there, they moved northward toward the Chukchi shelfbreak in accordance with both historical (*Weingartner et al.*, 2005b) and recent (*Weingartner et al.*, 2013a) current meter data from the Central Channel.

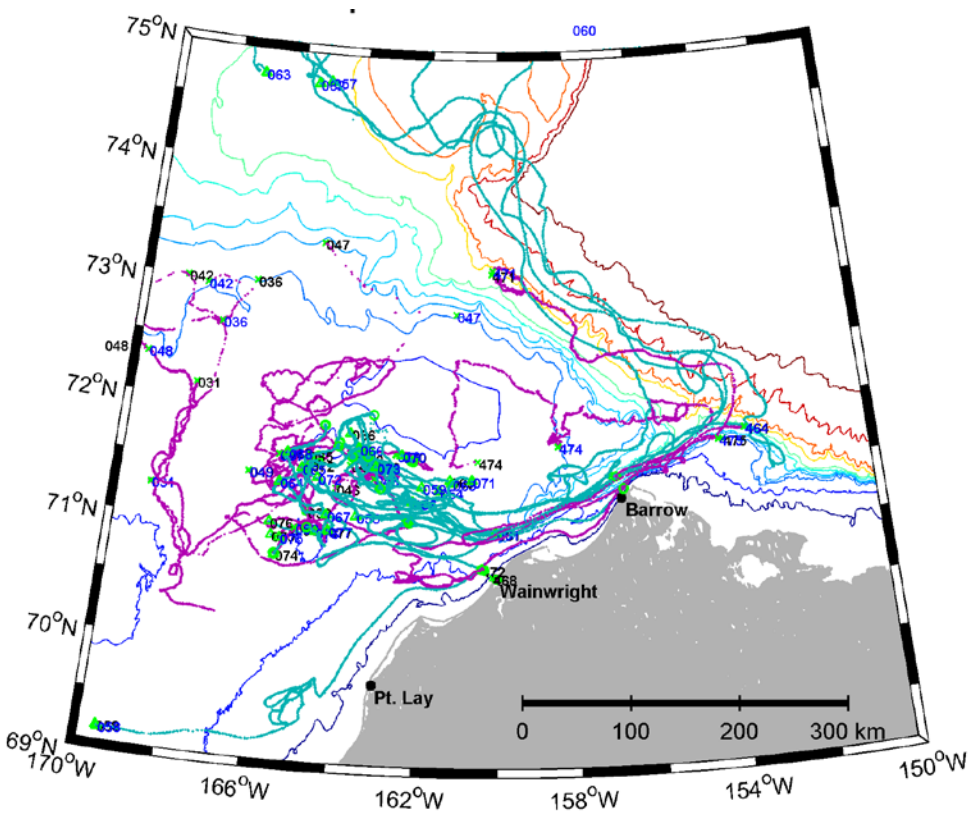

Figure 31. Trajectories of all drifters between mid-August and 22 November 2011, released in the central Chukchi Sea. Green lines are SVP drifters and purple lines are the 1-m drogued drifters.

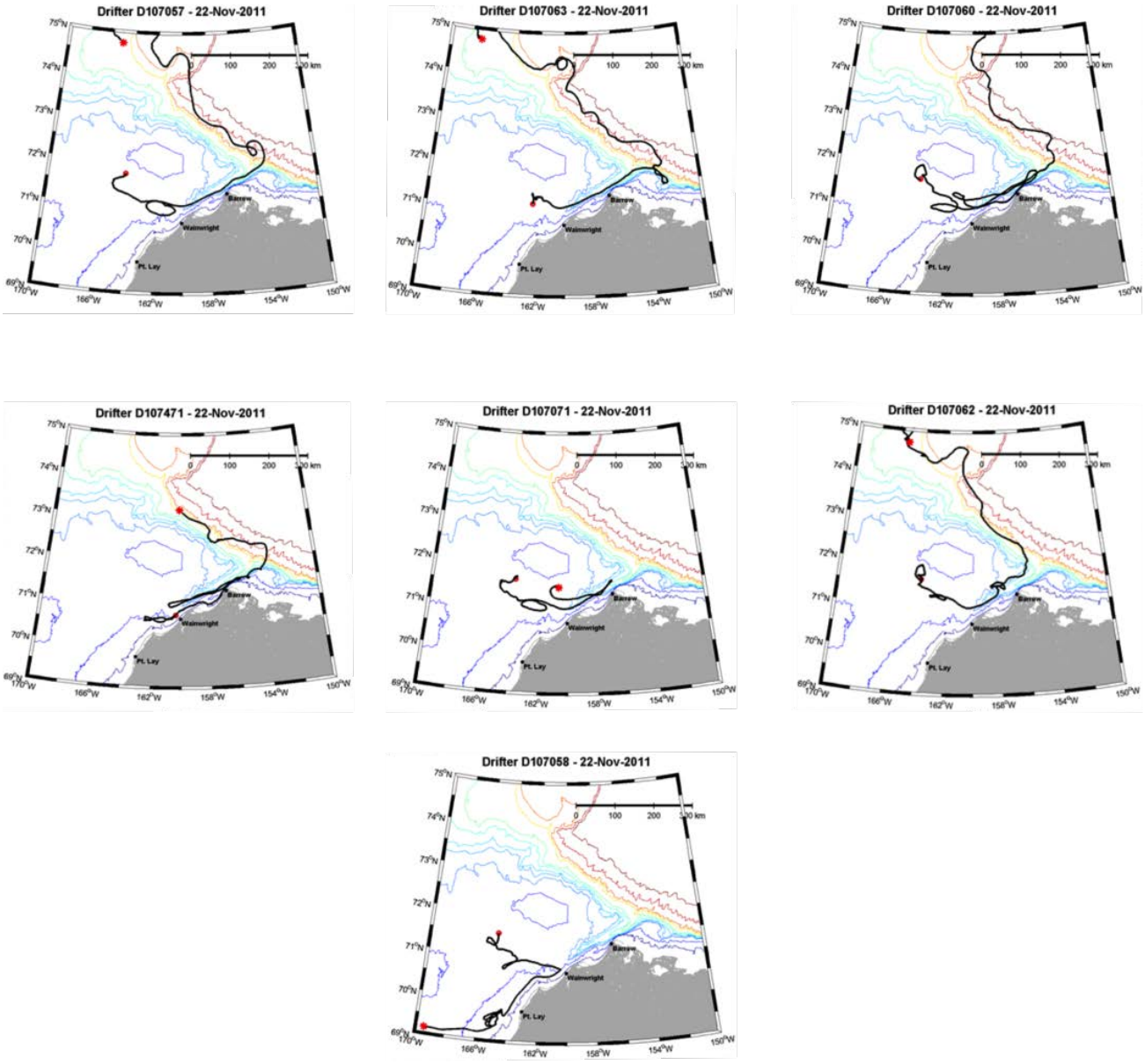

Figure 32. Trajectories of 10-m drogued drifters between mid-August and 22 November, 2011, released in the central Chukchi Sea.

2012 Drifter Deployments and Data Distribution

Deployments in 2012 were staggered in time and space. Deployments planned for northwest and northeast of Hanna Shoal in early August from the USCG Healy were prevented due to heavy ice in these regions. Instead, deployments were made along the western side of the Statoil and on the southeast side of Hanna Shoal. Unfortunately, several of these drifters were destroyed in ice (≤30% concentration) shortly after deployment. **Figure 33** shows the deployment distribution times and locations for the UAF and NSBW drifters. **Figure 34** shows the eventual data distribution over the Chukchi Sea in terms of number of observations in each 15' x 15' grid cell.

The various panels show the data distribution for all drifters as well as for each drifter type. It is evident (**Figure 34)** that the iSphere drifters had a distribution distinctly different than the Microstars and SVPs. For example, almost all the drifter observations south of 70°N were iSpheres. Many of these initially drifted northeastward into Barrow Canyon, then turned westward over the Chukchi shelfbreak before being carried back onto the shelf and southward.

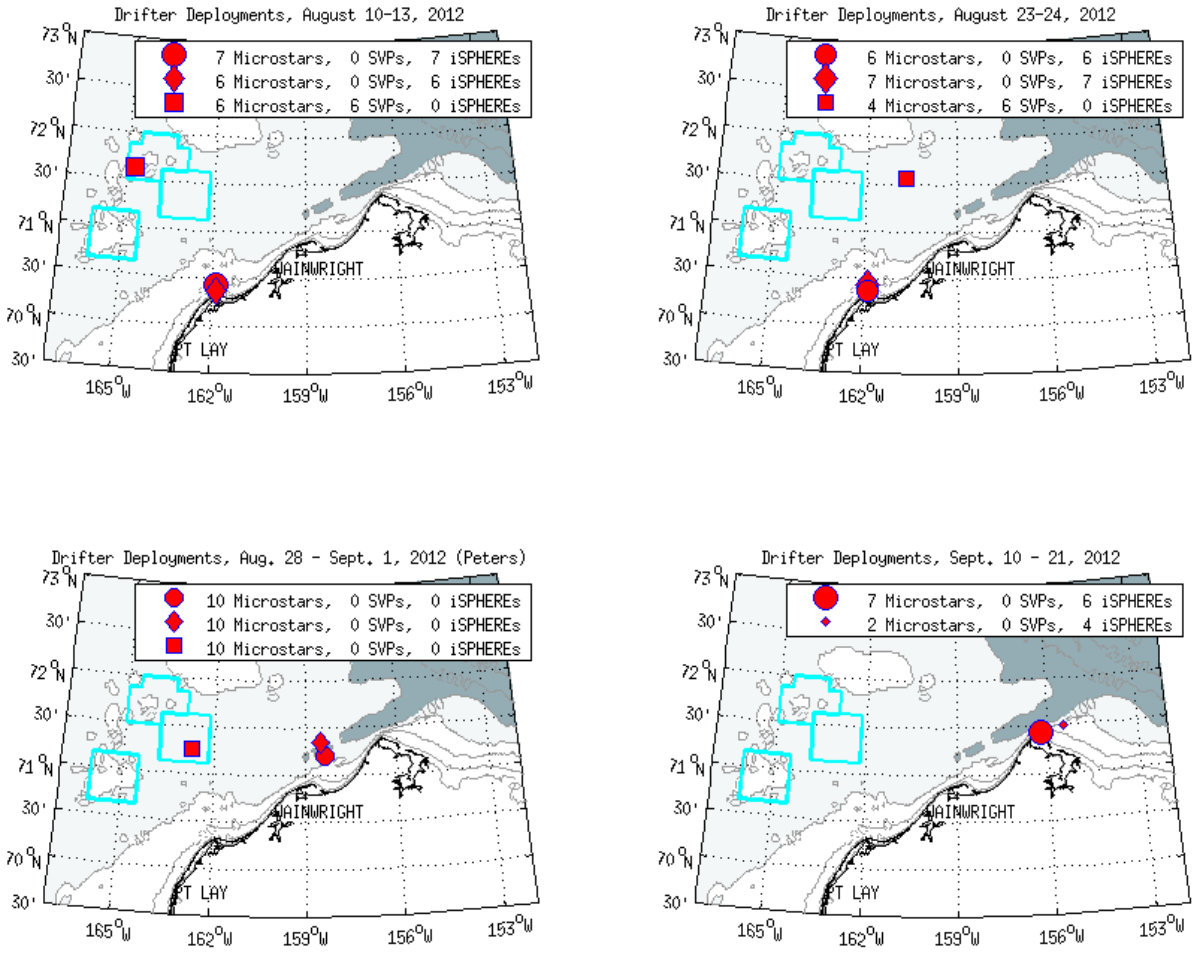

Figure 33. Deployment times, locations, and drifter types for the UAF and NSBW drifters used in 2012.

All of the drifters released in 2012 were eventually crushed in ice by late fall. However, five continued to transmit as late as February 2013. One of these traveled ~200 km north of Wrangel Island and a second was eventually trapped in the landfast ice zone of the Mackenzie Shelf. A third was trapped in the landfast ice in Peard Bay, and two drifted slowly eastward in the pack ice over the Alaskan Beaufort Shelf. Each of these drifters were of the SVP-type. It is emphasized that once entrapped by ice these drifters move with the ice and no longer characterize the water motion.

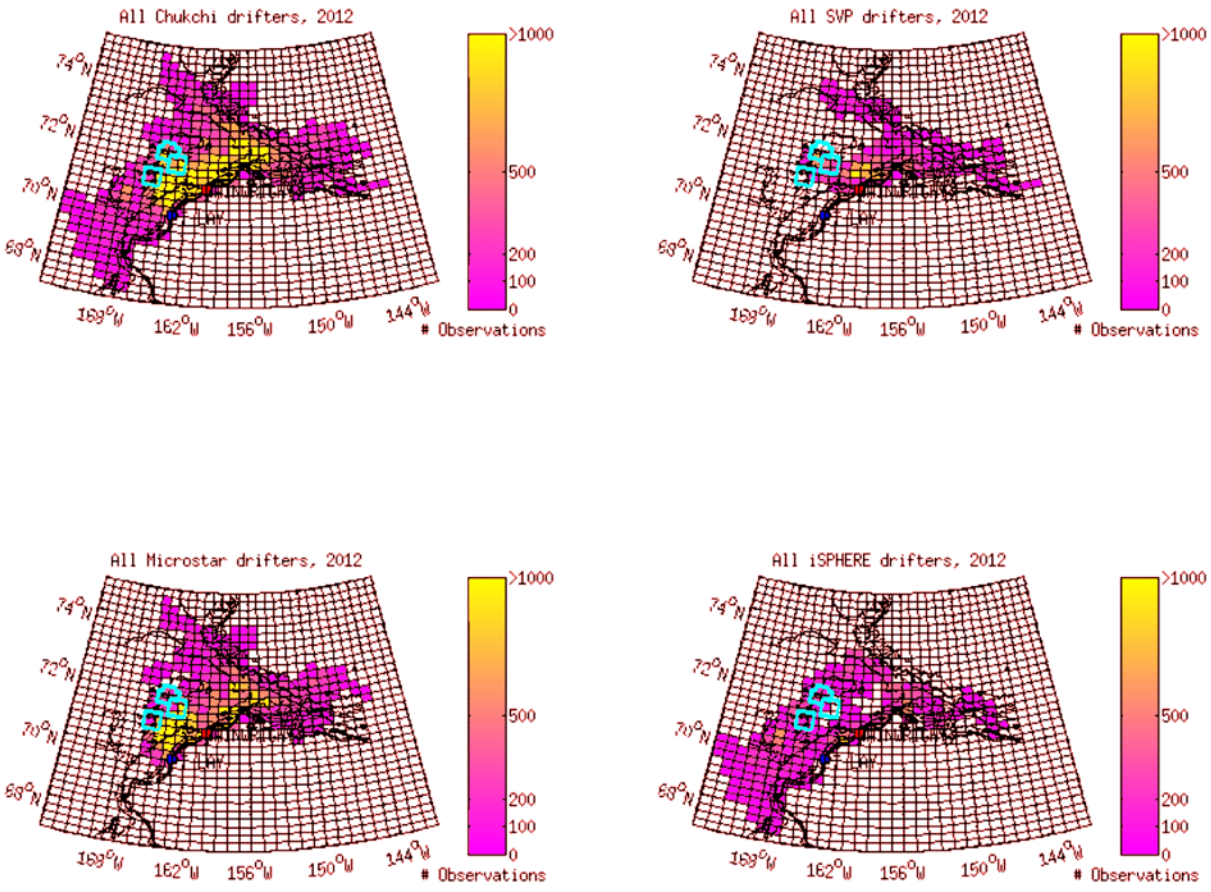

Figure 34. Data distribution in 15'x15' grid cells for all drifters (upper left), SVP drifters (10 m drogue; upper right), Microstar (1-m drogue; lower left) drifters, and iSphere drifters (lower right) for the UAF and NSBW deployments in 2012.

13 August 2012 Deployments: Central Chukchi Shelf

The Statoil deployment consisted of five MS drifters and six SVP drifters. All were deployed in the northeast corner of Statoil on August 13. The drifters were deployed sequentially and as rapidly as possible from the stern of the USCG Healy as it moved westward at ~2 kts. Separation distances between individual drifters were about 50 – 100 m. A few of the trajectory maps include time series of the zonal (U), meridional (V) and sea surface temperature (SST). These time series include both the hourly data (light lines) and the 35-hour low-pass filtered data (thick red line). For this deployment, the MS drifters are shown in **Figures 35 – 38** and the SVP drifters are in **Figures 39 – 45**.

From 13 – 30 August, MS-4, 7, and 9 first moved northward and then southeastward across the northern side of Statoil and Burger. MS-1 and 5 initially moved northward also, then proceeded southward until 21 August when these drifters moved southeastward across the southern portions of Statoil and Burger. At this time, winds were generally from the south so that these drifter

motions were not simply related to the wind field. On 29 August, winds began blowing from the northeast and all of these drifters moved to the southwest. Winds were generally from the northeast (or north) through first half of September, with the drifters making variously sized loops between 70^{o} and 71^{o}N and between 162^{o} and 165^{o} W. Note that as the drifters moved southward, the SST increased rapidly from $<3^{o}$C to $\sim5^{o}$C, indicating that they crossed a frontal system with cool meltwaters present north of the front and warmer Bering Sea summer waters south of the front. By mid-September most of the drifters resumed a northeastward trajectory and entered Barrow Canyon in the last few days of September.

After entering the canyon, the drifters moved northeastward (down-canyon) for ~8 days and then either beached (MS-1 and 6) near Barrow or turned eastward onto the Beaufort Shelf by October 8. Drifter MS-7 moved onto the shelfbreak at the mouth of Barrow Canyon, and then meandered back and forth across the canyon before eventually beaching at Barrow. In summary the MS drifters deployed within Statoil drifted over the northeast shelf for 1 – 1.5 months before entering Barrow Canyon. While on the Chukchi Shelf, MS-1 and 7 conducted a number of mesoscale meanders and loops, with these meanders accompanied by rapid changes in SST. The remaining drifters generally moved eastward (more or less) across the shelf and toward Barrow Canyon. All of the MS drifters then spent approximately 8 – 10 days moving rapidly to the northeast through Barrow Canyon. Drifter velocities on the shelf were variable with speeds typically ~10 cm s^{-1}. Within the canyon, velocities were northeast at an average speed of ~25 cm s^{-1}, however, maximum speeds in the canyon were between 50 and 100 cm s^{-1}.

The SVP drifters generally had a longer life-time as they were less prone to beaching or losing their drogue to wave action. Hence their trajectories encompassed a much broader area than the MS drifters. All of the SVP drifters moved eastward across Burger. Recall from the discussion of the hydrography that there was a thermohaline BSW/WW front oriented zonally across the center of Burger in 2012. This front is reflected in the drifter data as those to the north of the front measured SSTs of 2 – 3^{o}C, while drifters to the south of the center of Burger recorded SSTs of 4 – 5^{o}C. All of the SVP drifters took from 1 and 2 months to move into Barrow Canyon and many of them underwent a number of complex meanders and eddying motions that are not evidently related to the winds as they moved toward the canyon. Most likely these mesoscale motions are with frontal instabilities as described later. The fact that not all the drifters were caught in such motions reflects the fact that these instabilities are spatially and temporally variable in their occurrence along the front.

After passing through the canyon, most of the SVP drifters moved to the mouth of the canyon and then proceeded eastward along the shelfbreak. (Recall that the MS drifters proceeded eastward along the inner Beaufort Shelf). SVP-2 and 3 were trapped in ice on about 8 November and stopped transmitting shortly thereafter. Upon exiting Barrow Canyon on 8 October, SVP-5 moved rapidly eastward over the next 30 days before getting trapped in the landfast ice of the Mackenzie Shelf at ~135^{o}W where it was immobile through the winter and spring of 2013. Upon

landfast ice breakup in late June 2013, SVP-5 slowly looped around the Mackenzie Shelf and then drifted westward through mid-July until it reached the head of the Mackenzie Canyon, north of Herschel Island. From here, it moved northwestward along the western flank of the canyon, then westward along the Alaskan Beaufort Sea shelfbreak before it stopped transmitting in late July. During July, while on the Mackenzie Shelf, SVP-5 recorded large (amplitude ~10^{o}C) ~diurnal oscillations in SST. These oscillations may be associated with diurnal variations in solar heating. Drifter SVP-6 also moved eastward along the shelfbreak after exiting Barrow Canyon. Its drift was interrupted by 2 – 3 cyclonic excursions that carried SVP-6 ~80 km seaward of the break and slowly westward. It then resumed its eastward movement along the shelfbreak until it reached ~140^{o}W where it was caught in ice and drifted westward, episodically, with the ice. The episodic nature of the drift suggests that ice motion occasionally stalled, possibly because it was temporarily attached to, or incorporated into, the landfast ice zone along the 30 m isobath. SVP-6 continued to transmit through the winter but registered little movement until late April. At that point it meandered to the east and to the west several times before beginning a long westward excursion through June and into early July whereupon it moved eastward to offshore of Mikkelsen Bay. In late July it drifted westward again and stopped transmitting near Oliktok Pt. in the first week of August. SVP-8 entered Barrow Canyon twice. Initially this occurred in late August passing by Pt. Barrow in early September. Afterwards, it drifted to the southwest, meandered over the shelf east of Hanna Shoal for the next month and then re-entered the canyon and sped rapidly to the shelfbreak by 25 October. From there it moved eastward to about 152^{o}W, then regressed westward, before resuming eastward motion on 7 November. Over the next 10 days it moved eastward rapidly (~50 cm s^{-1}) along the shelfbreak until it was caught in ice in late November and ceased transmitting. SVP-10 entered Barrow Canyon around 18 September and then made several up and down-canyon transits before exiting onto the Beaufort Shelf. It then drifted eastward before being entrapped in ice on 11 November. It continued eastward with the ice and stopped moving on 17 November, suggesting that this ice was incorporated into the landfast ice zone. It continued to transmit for the next few days but ceased working on 25 November.

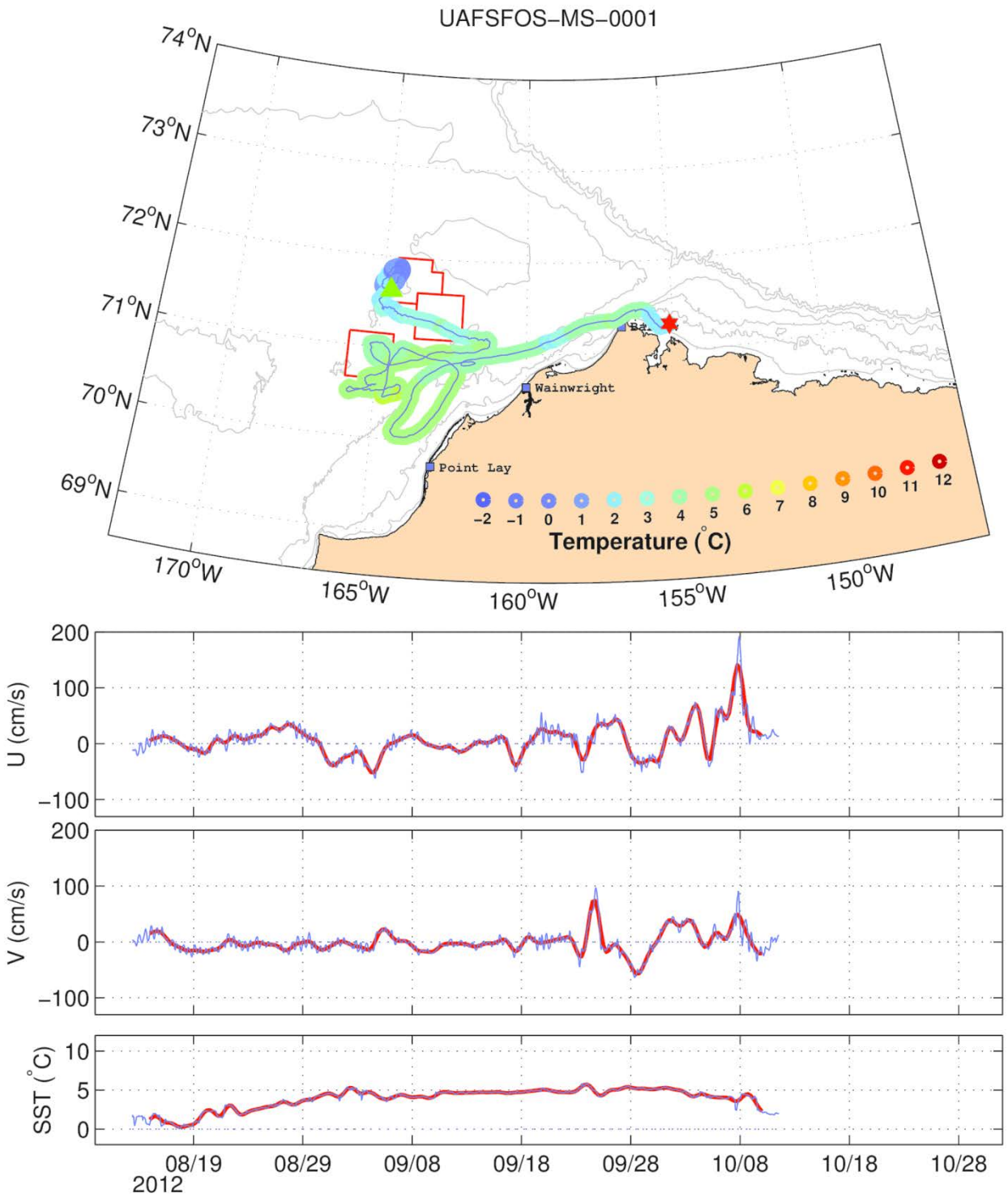

Figure 35. The trajectory of MS-1 and the time series of its zonal (U), meridional (V), and sea surface temperature (SST) record. The colors along the drifter trajectory are color-coded according to SST. The green triangle and red star show start and end of the trajectory, respectively. The light lines in the time series are raw data and the heavy red lines are the 35-hour low-pass filtered data.

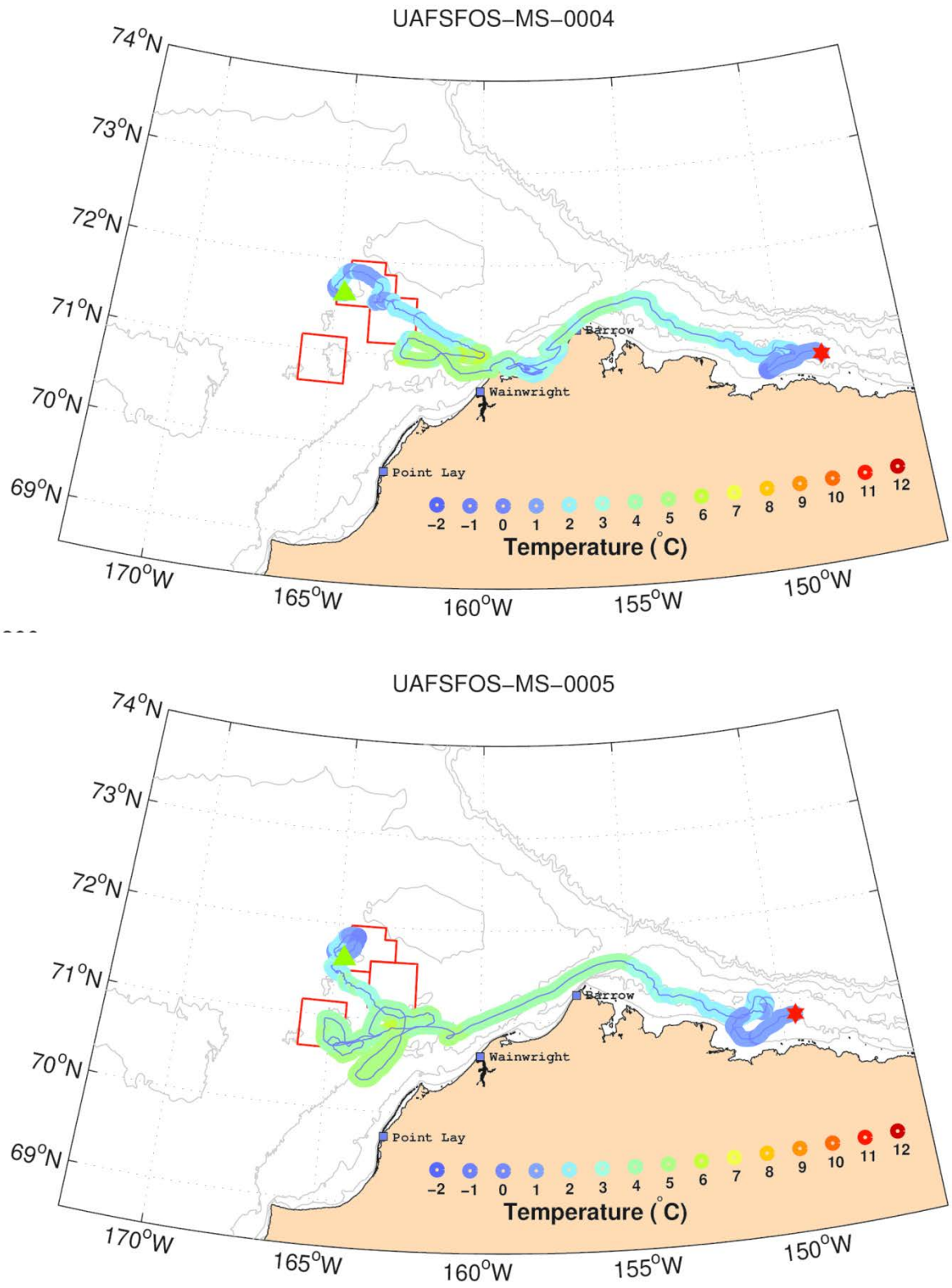

Figure 36. The trajectories of MS-4 (top) and 5 (bottom). The colors along the drifter trajectories are color-coded according to SST. The green triangle and red star show start and end of the trajectories, respectively.

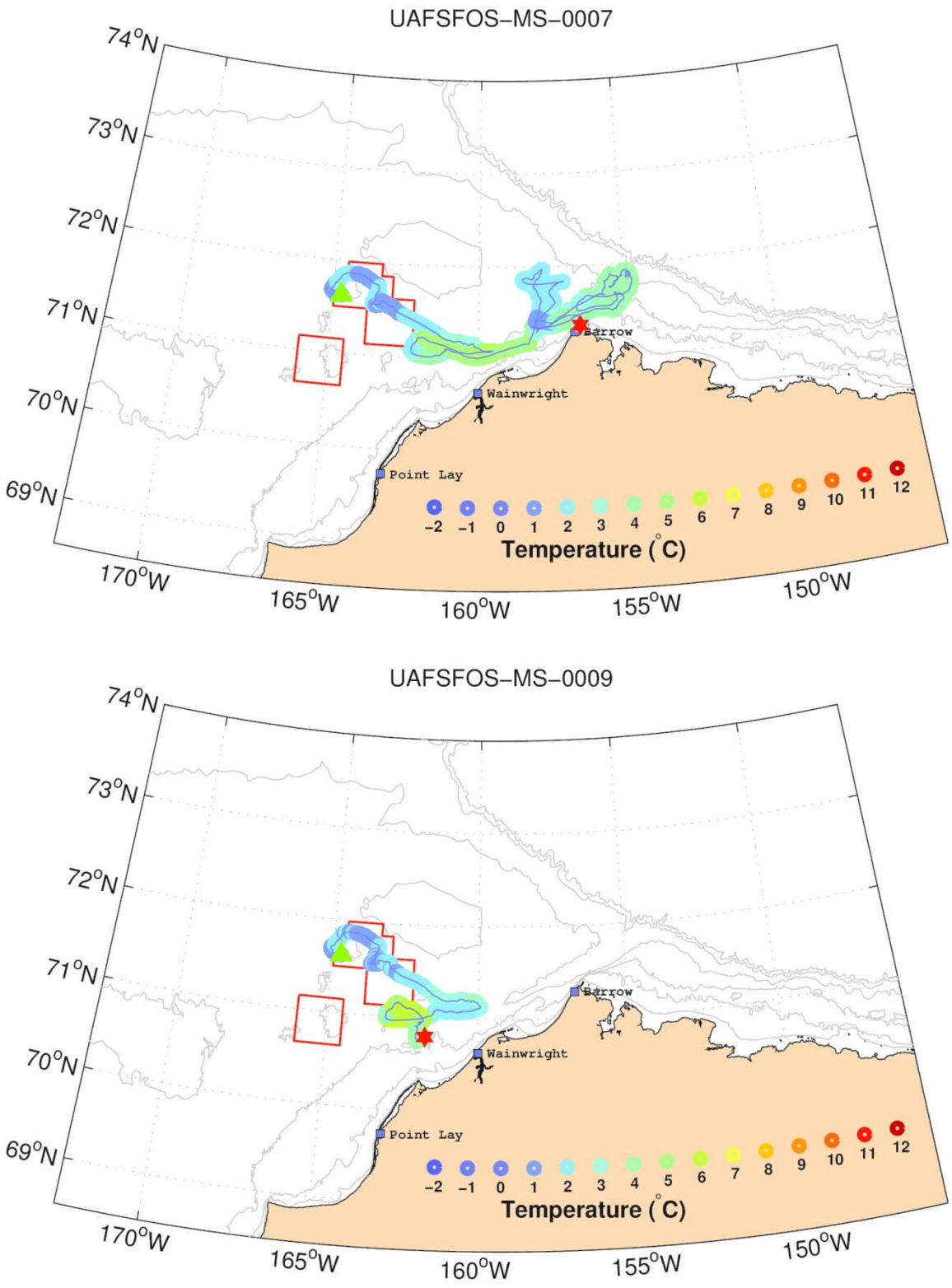

Figure 37. The trajectories of MS-7 (top) and 9 (bottom). The colors along the drifter trajectories are color-coded according to SST. The green triangle and red star show start and end of the trajectories, respectively.

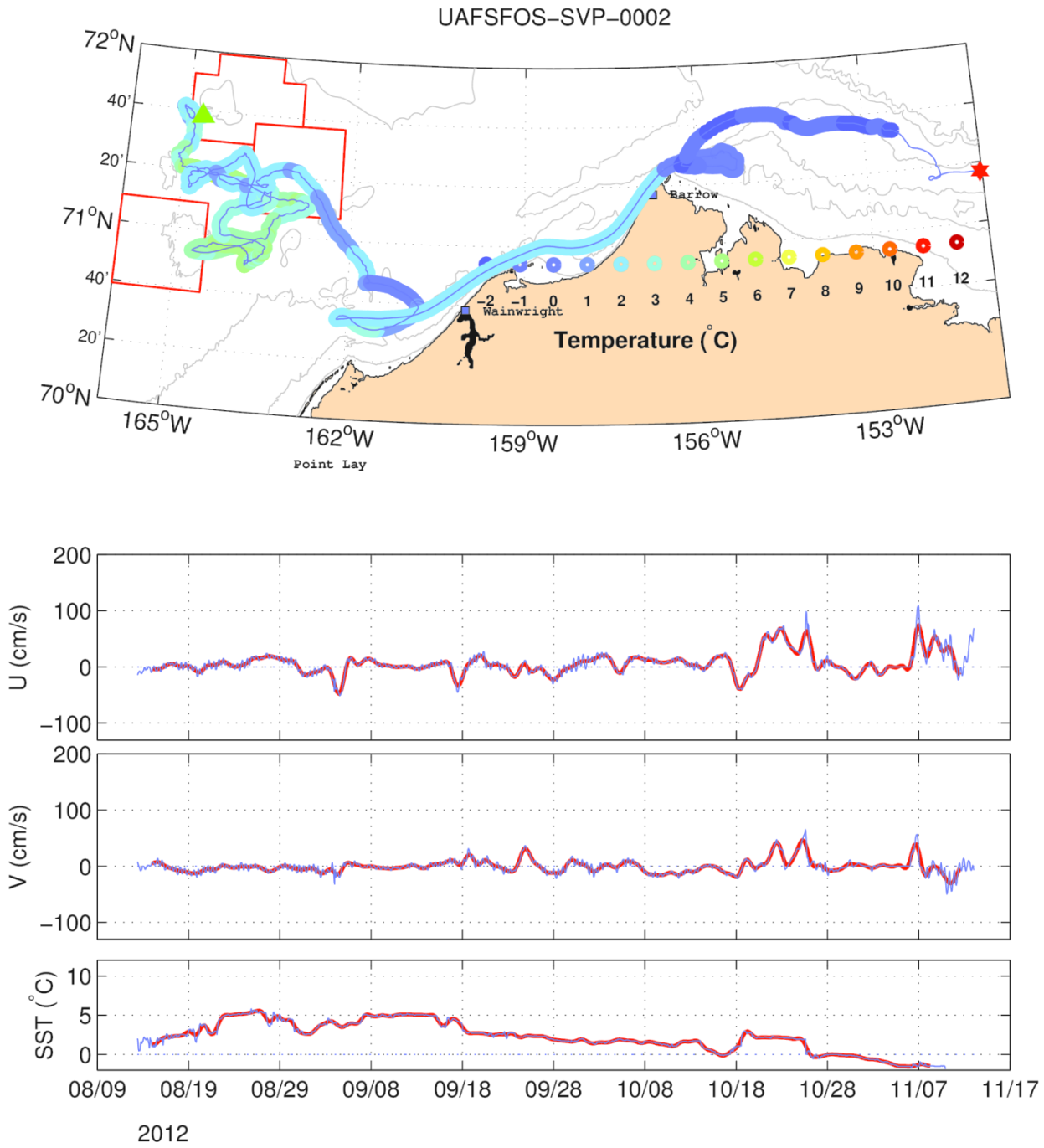

Figure 38. The trajectory of SVP-2 and the time series of its zonal (U), meridional (V), and sea surface temperature (SST) record. The colors along the drifter trajectory are color-coded according to SST. The green triangle and red star show start and end of the trajectory, respectively. The light lines in the time series are raw data and the heavy red lines are the 35-hour low-pass filtered data.

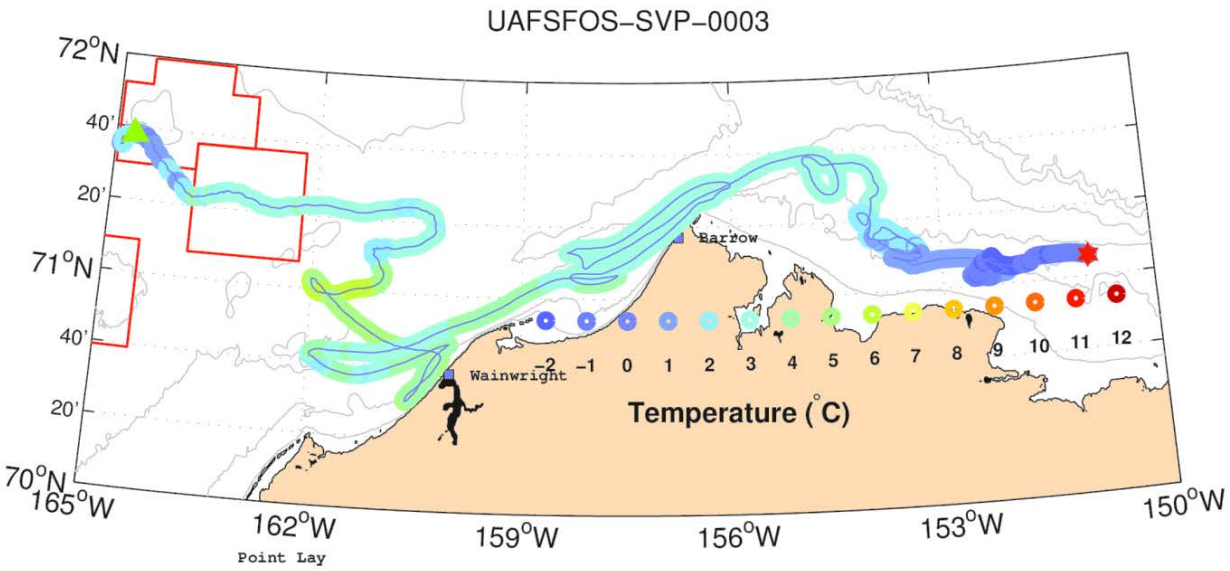

Figure 39. The trajectory of SVP-3. The colors along the drifter trajectory are color-coded according to SST. The green triangle and red star show start and end of the trajectory, respectively.

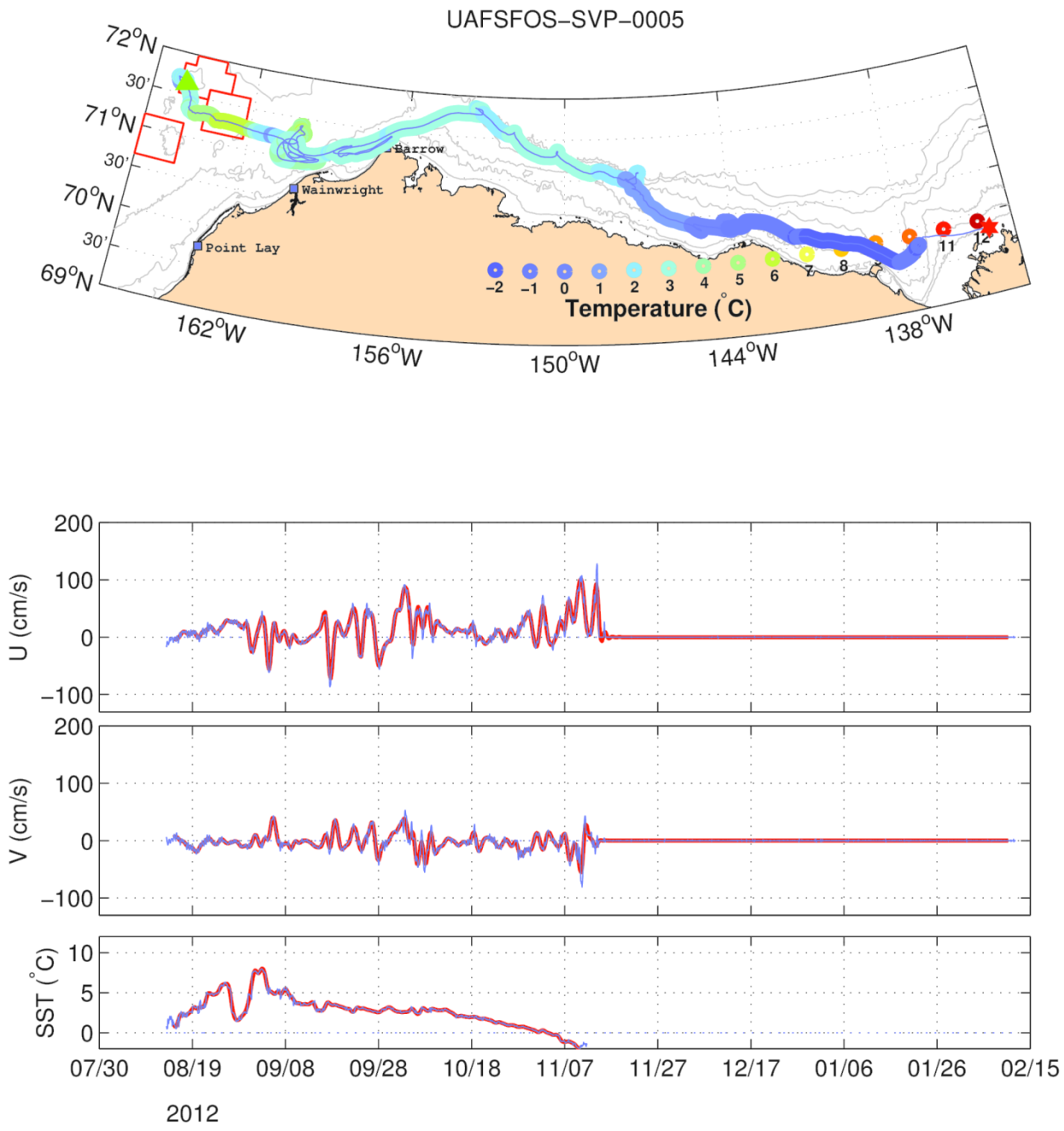

Figure 40. The 2012 trajectory of SVP-5 and the time series of its zonal (U), meridional (V), and sea surface temperature (SST) record. The colors along the drifter trajectory are color-coded according to SST. The green triangle and red star show start and end of the trajectory, respectively. The light lines in the time series are raw data and the heavy red lines are the 35-hour low-pass filtered data.

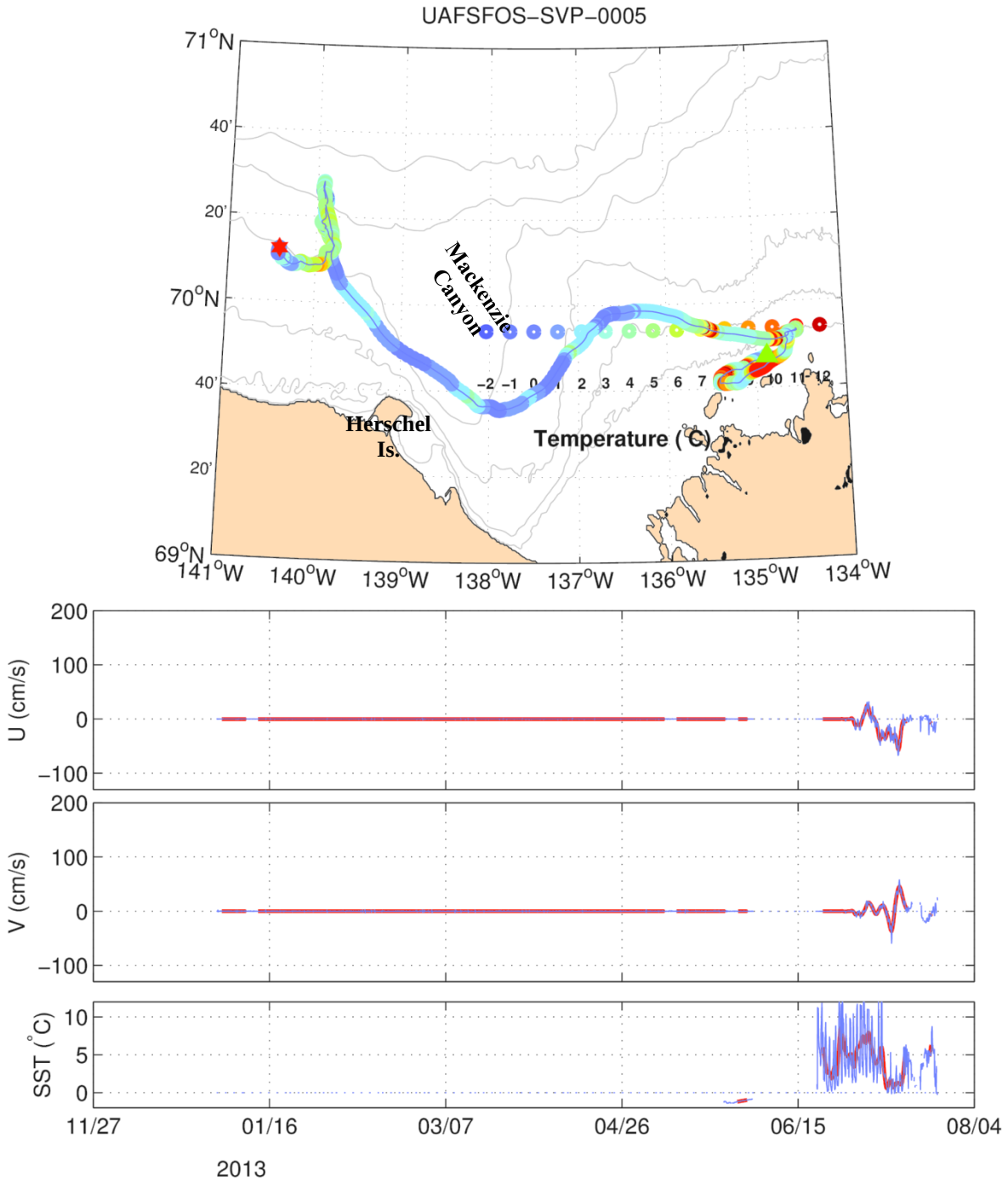

Figure 41. The 2013 trajectory of SVP-5 (top) the time series of its zonal (U), meridional (V), and sea surface temperature (SST) record. The colors along the drifter trajectory are color-coded according to SST. The green triangle and red star show start and end of the trajectory, respectively. The light lines in the time series are raw data and the heavy red lines are the 35-hour low-pass filtered data. This drifter overwintered in the landfast ice (cf. **Figure 30**) and continued operating through early August 2013.

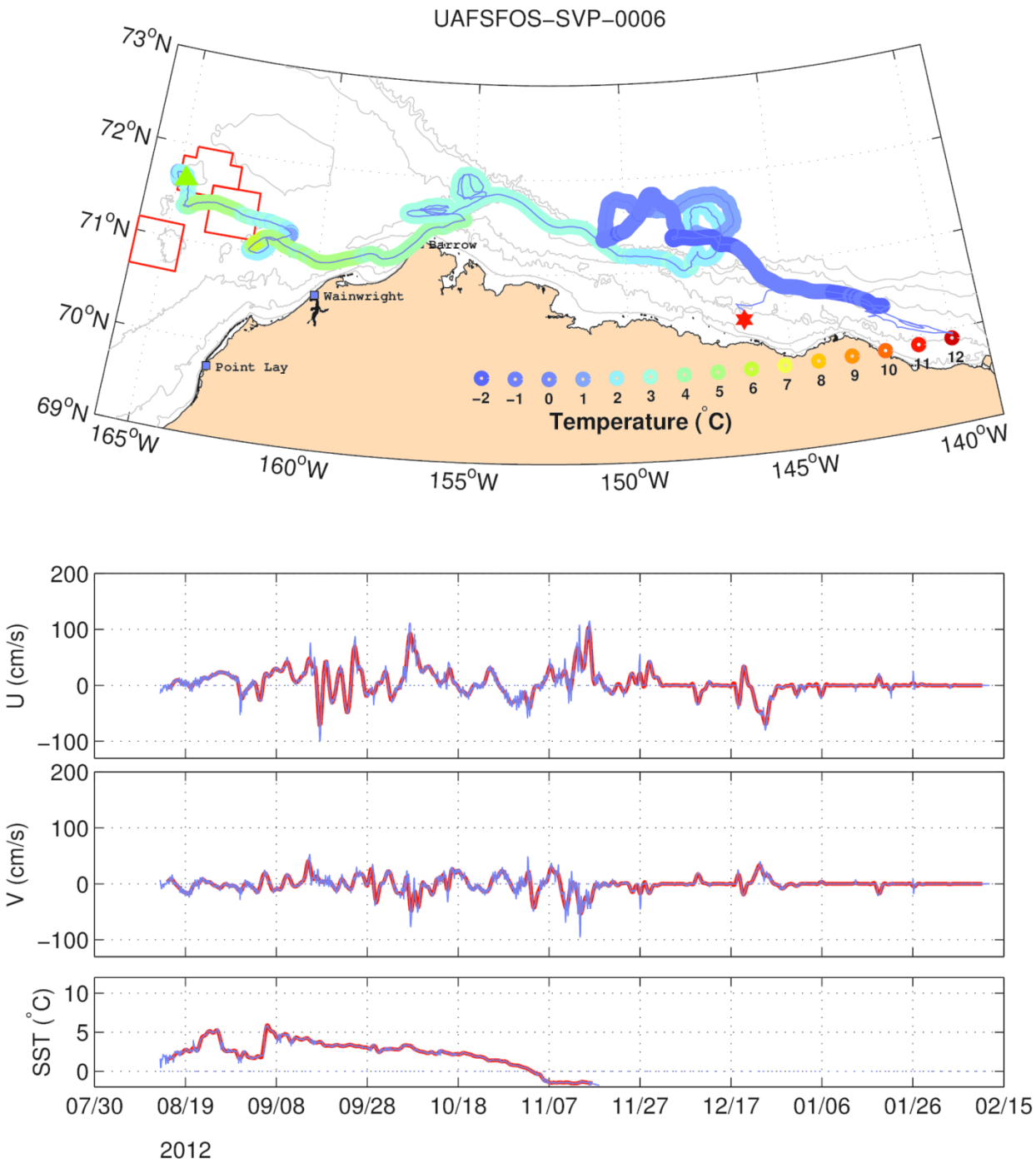

Figure 42. The 2012 trajectory of SVP-6 and the time series of its zonal (U), meridional (V), and sea surface temperature (SST) record. The colors along the drifter trajectory are color-coded according to SST. The green triangle and red star show start and end of the trajectory, respectively. The light lines in the time series are raw data and the heavy red lines are the 35-hour low-pass filtered data.

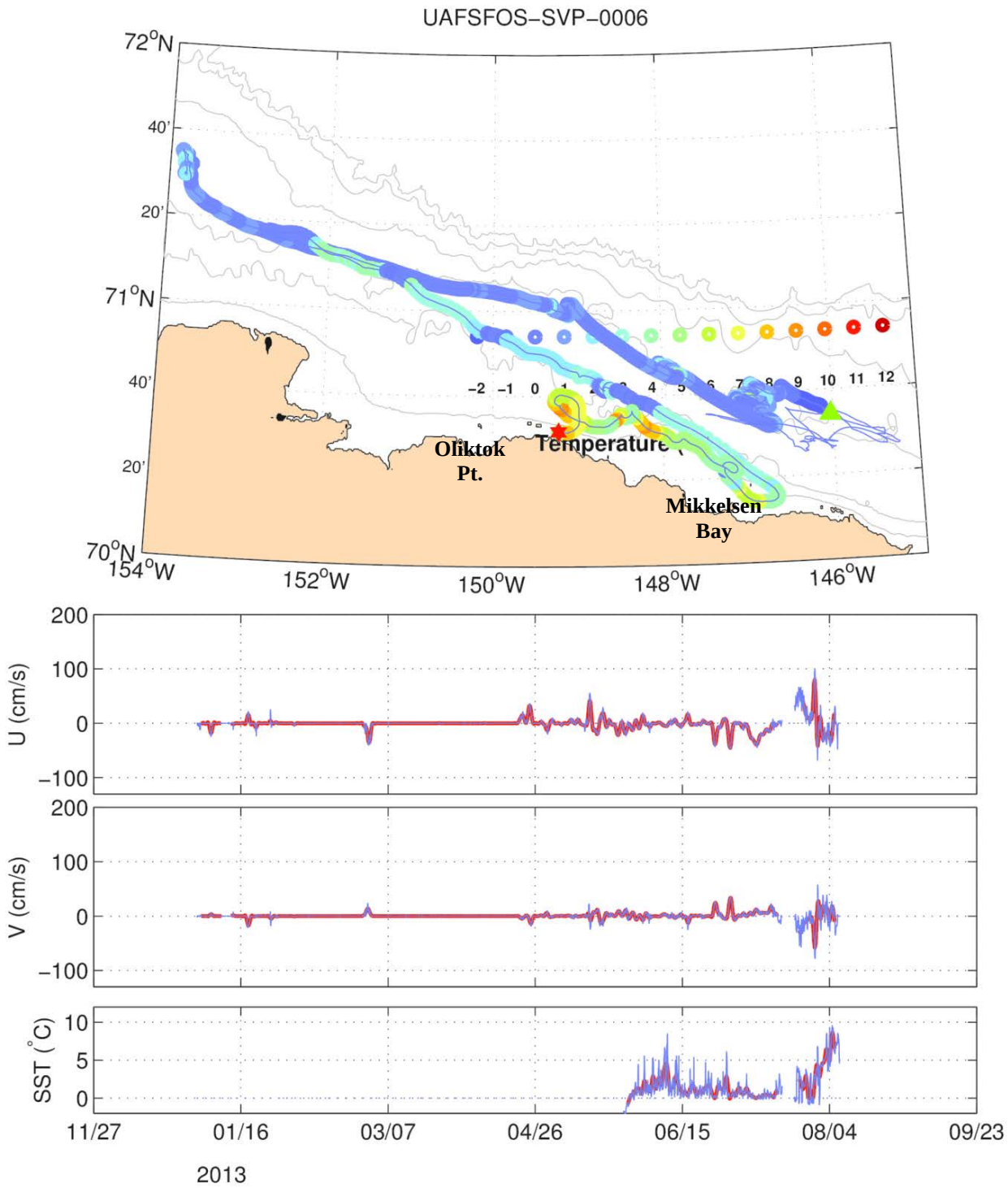

Figure 43. The 2013 trajectory of SVP-5 and the time series of its zonal (U), meridional (V), and sea surface temperature (SST) record. The colors along the drifter trajectory are color-coded according to SST. The green triangle and red star show start and end of the trajectory, respectively. The light lines in the time series are raw data and the heavy red lines are the 35-hour low-pass filtered data. This drifter overwintered in the landfast ice (cf. **Figure 42**) and continued operating through early August 2013.

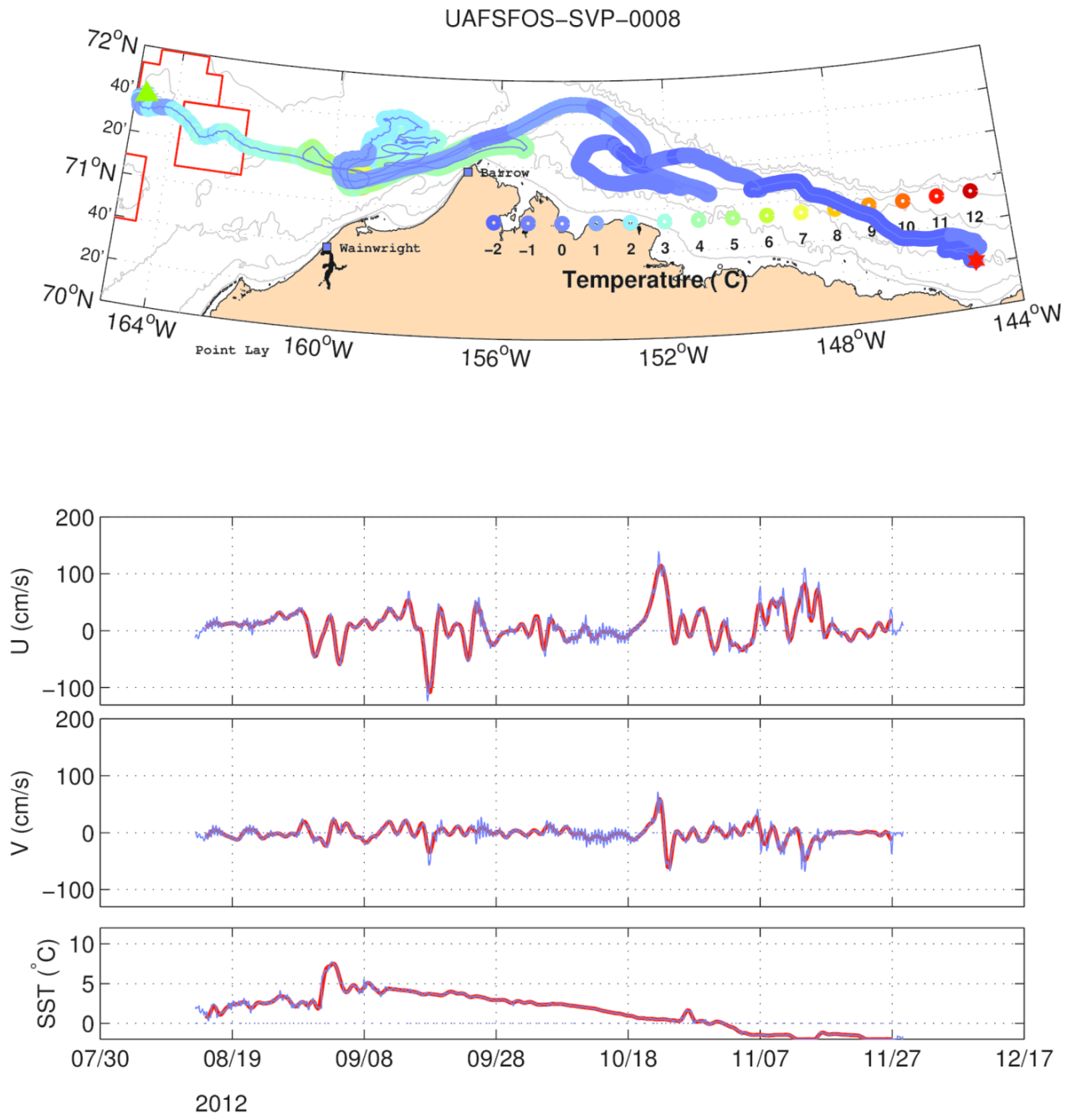

Figure 44. The trajectory of SVP-8 and the time series of its zonal (U), meridional (V), and sea surface temperature (SST) record. The colors along the drifter trajectory are color-coded according to SST. The green triangle and red star show start and end of the trajectory, respectively. The light lines in the time series are raw data and the heavy red lines are the 35-hour low-pass filtered data.

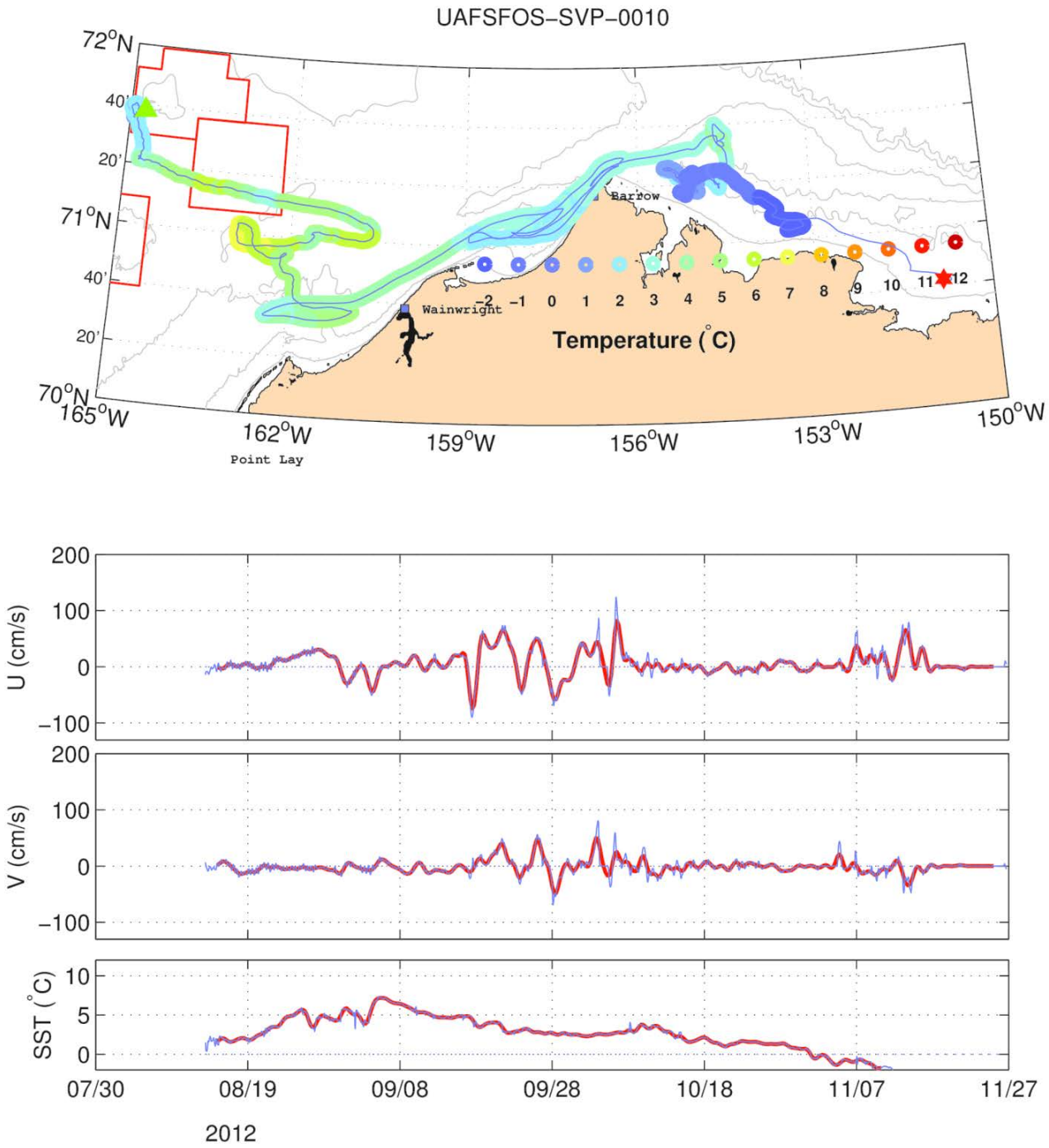

Figure 45. The trajectory of SVP-10 and the time series of its zonal (U), meridional (V), and sea surface temperature (SST) record. The colors along the drifter trajectory are color-coded according to SST. The green triangle and red star show start and end of the trajectory, respectively. The light lines in the time series are raw data and the heavy red lines are the 35-hour low-pass filtered data.

10 August 2012 Microstar Deployments: Inner Shelf of the Chukchi Sea

On 10 August, the NSBW deployed MS drifters offshore of Icy Cape in water depths of ~10 m. This section discusses the trajectories of the 13 MS drifters deployed at this time. **Figures 46 – 54** show the trajectories of some of the NSBW drifters. There was remarkable coherence in each of these trajectories at least over the first few days. For example, each took ~3 days to move from Icy Cape to Pt. Barrow and another day to reach the mouth of Barrow Canyon. They thus drifted over 175 km in ~4 days (with an average speed of ~50 cm s^{-1}). All turned eastward at the shelfbreak and most turned northward into the basin before reaching 150^{o}W. Note that each of these drifters were associated with warm (>4^{o}C) water into the basin by mid-August when heavy ice and cold meltwaters still covered the northern Chukchi Shelf. Drifters NSBW-2, 4, 9, 10, 11, 12, and 13 then continued to the west-northwest toward the Chukchi Sea shelfbreak. Drifters NSBW-1, 5, 6, 7, and 8 made one or more anti-cyclonic and/or cyclonic loops before moving to the west-northwest. In contrast, NSBW-3 made several anticyclonic loops in this same region and then drifted southeastward toward the Beaufort shelfbreak before ceasing transmissions in mid-October.

After reaching the Chukchi shelfbreak, NSBW-1 and 4 turned southward onto the Chukchi Shelf. NSBW-1 drifted eastward over the outer shelf and then re-entered Barrow Canyon where it moved toward the shelfbreak. From there it undertook two large looping excursions across the shelfbreak and slope followed by a southwestward excursion onto the Beaufort Shelf in late October. It then moved eastward until it ceased transmitting on 16 November. After reaching the Chukchi shelfbreak, NSBW-4 was carried southward over Hanna Shoal in early October and continued southward to the southeast side of Burger on 18 October. Over the next seven days it moved rapidly eastward to Pt. Barrow and then out the canyon to the shelfbreak. From there it moved southeastward and crossed the Beaufort Shelf nearly to the 10 m isobath. It continued drifting eastward until early November when it was caught in ice near 150^{o}W. It drifted with the ice as far as ~145^{o}W where it failed on 9 November. Among the other drifters that reached the Chukchi shelfbreak, drifters NSBW-5, 6, 7, 8, 11 and 12 all died in late September/early October. NSBW-2, 9, and 13 moved southward across Hanna Shoal and either died atop the Shoal or south of it in mid-October. After crossing the Chukchi shelfbreak, NSBW-10 drifted southwest towards the Central Channel and ceased transmissions on 4 October.

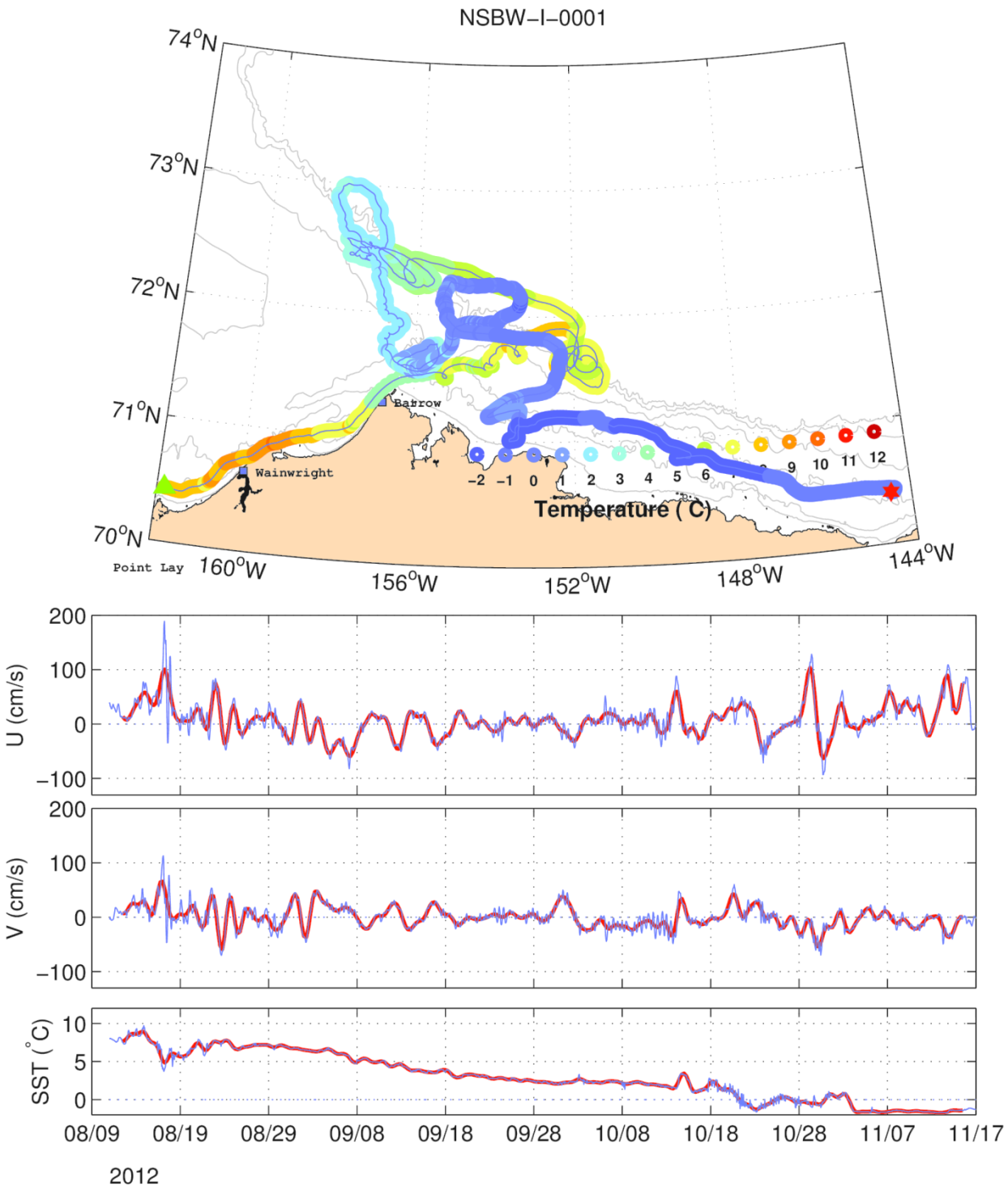

Figure 46. The trajectory of NSBW-1 and the time series of its zonal (U), meridional (V), and sea surface temperature (SST) record. The colors along the drifter trajectory are color-coded according to SST. The green triangle and red star show start and end of the trajectory, respectively. The light lines in the time series are raw data and the heavy red lines are the 35-hour low-pass filtered data.

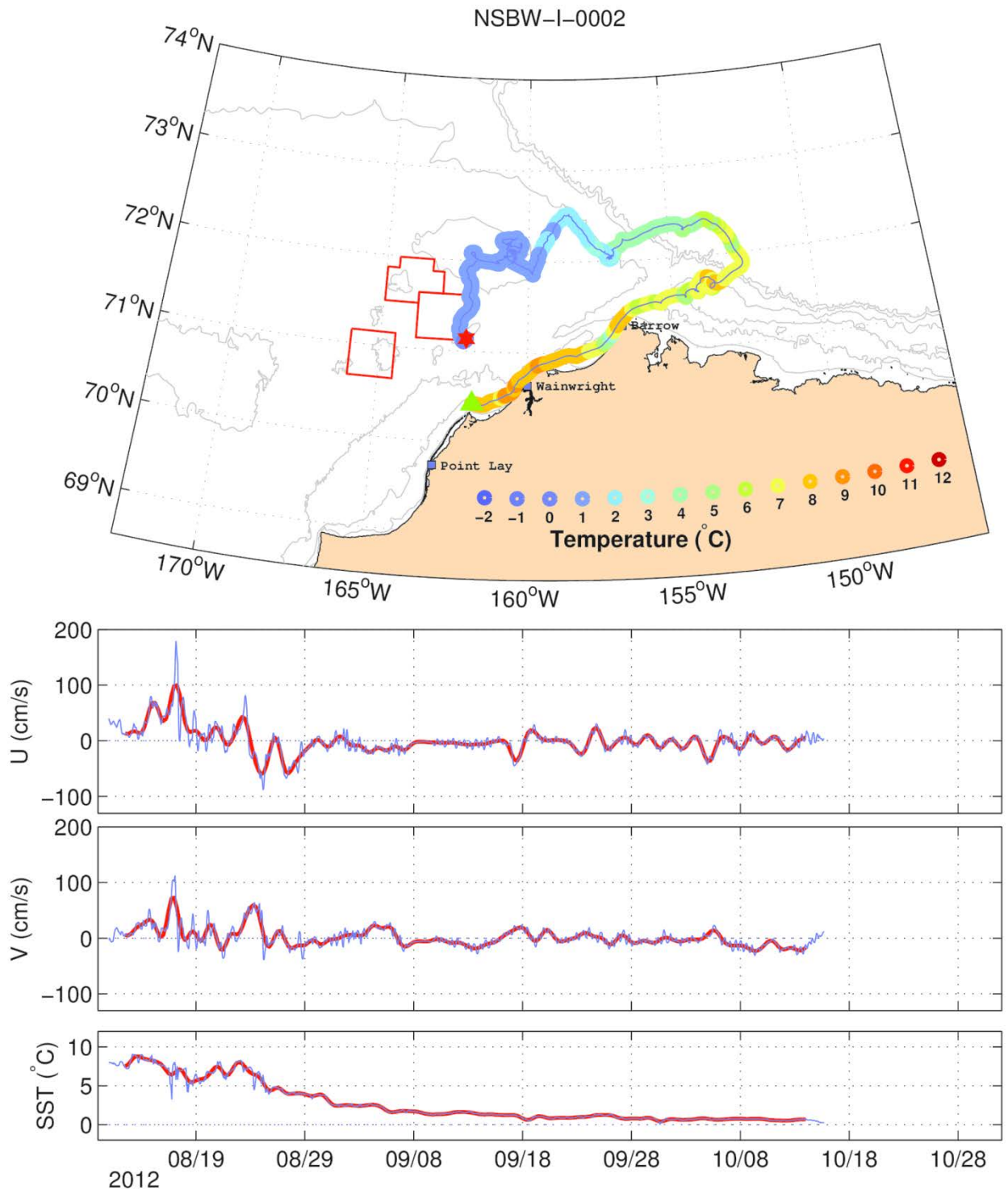

Figure 47. The trajectory of NSBW-2 and the time series of its zonal (U), meridional (V), and sea surface temperature (SST) record. The colors along the drifter trajectory are color-coded according to SST. The green triangle and red star show start and end of the trajectory, respectively. The light lines in the time series are raw data and the heavy red lines are the 35-hour low-pass filtered data.

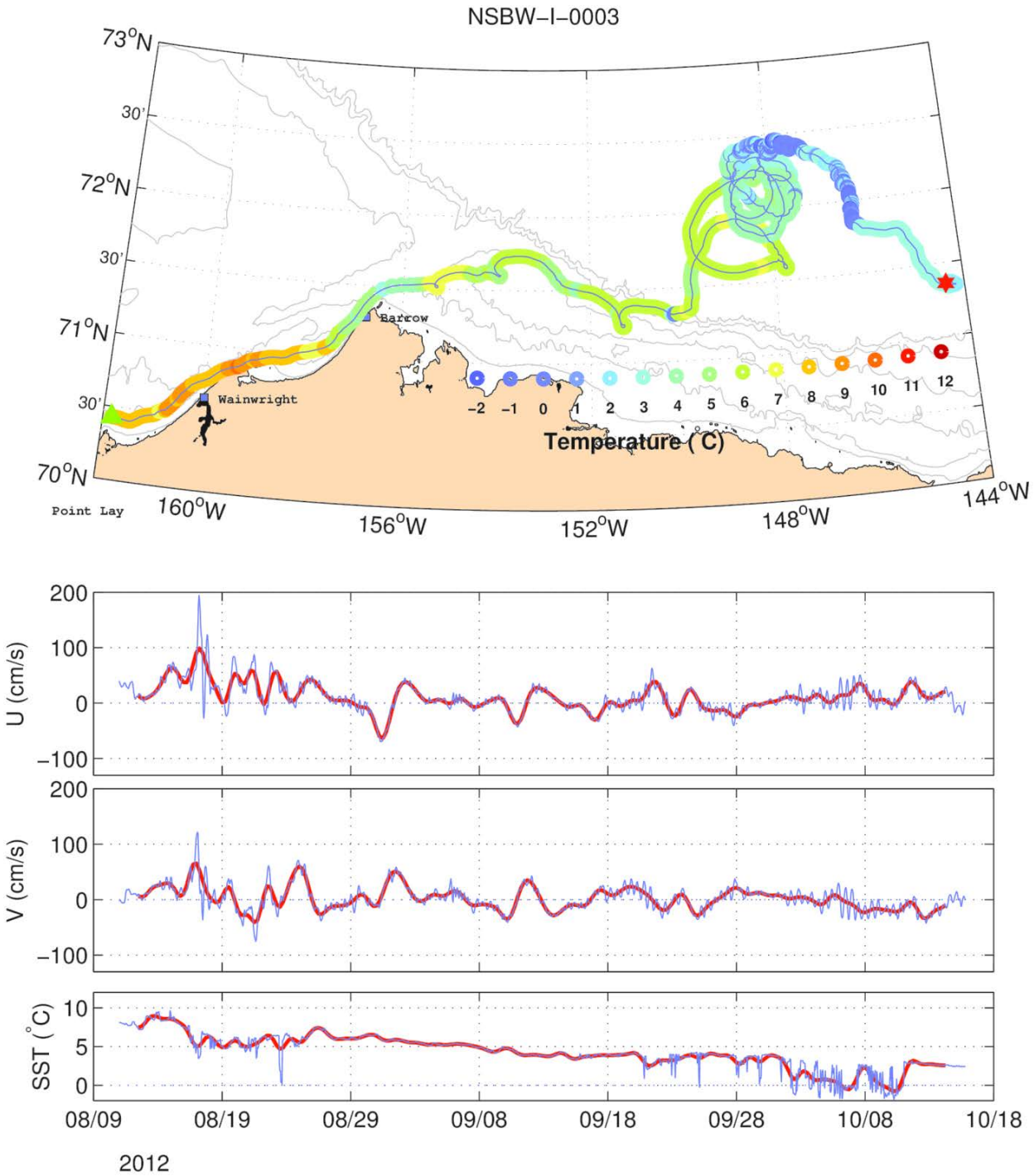

Figure 48. The trajectory of NSBW-3 and the time series of its zonal (U), meridional (V), and sea surface temperature (SST) record. The colors along the drifter trajectory are color-coded according to SST. The green triangle and red star show start and end of the trajectory, respectively. The light lines in the time series are raw data and the heavy red lines are the 35-hour low-pass filtered data.

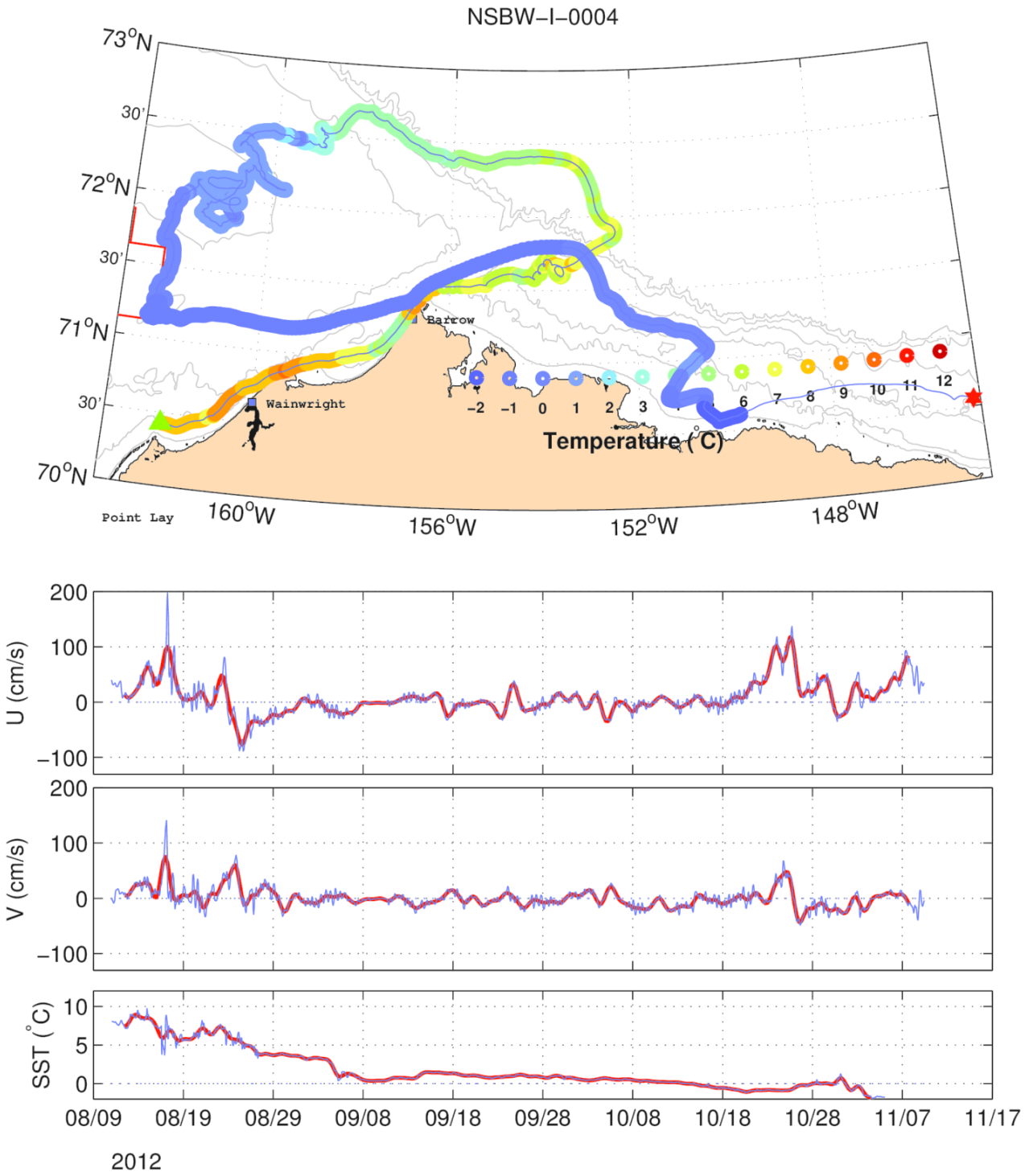

Figure 49. The trajectory of NSBW-4 and the time series of its zonal (U), meridional (V), and sea surface temperature (SST) record. The colors along the drifter trajectory are color-coded according to SST. The green triangle and red star show start and end of the trajectory, respectively. The light lines in the time series are raw data and the heavy red lines are the 35-hour low-pass filtered data.

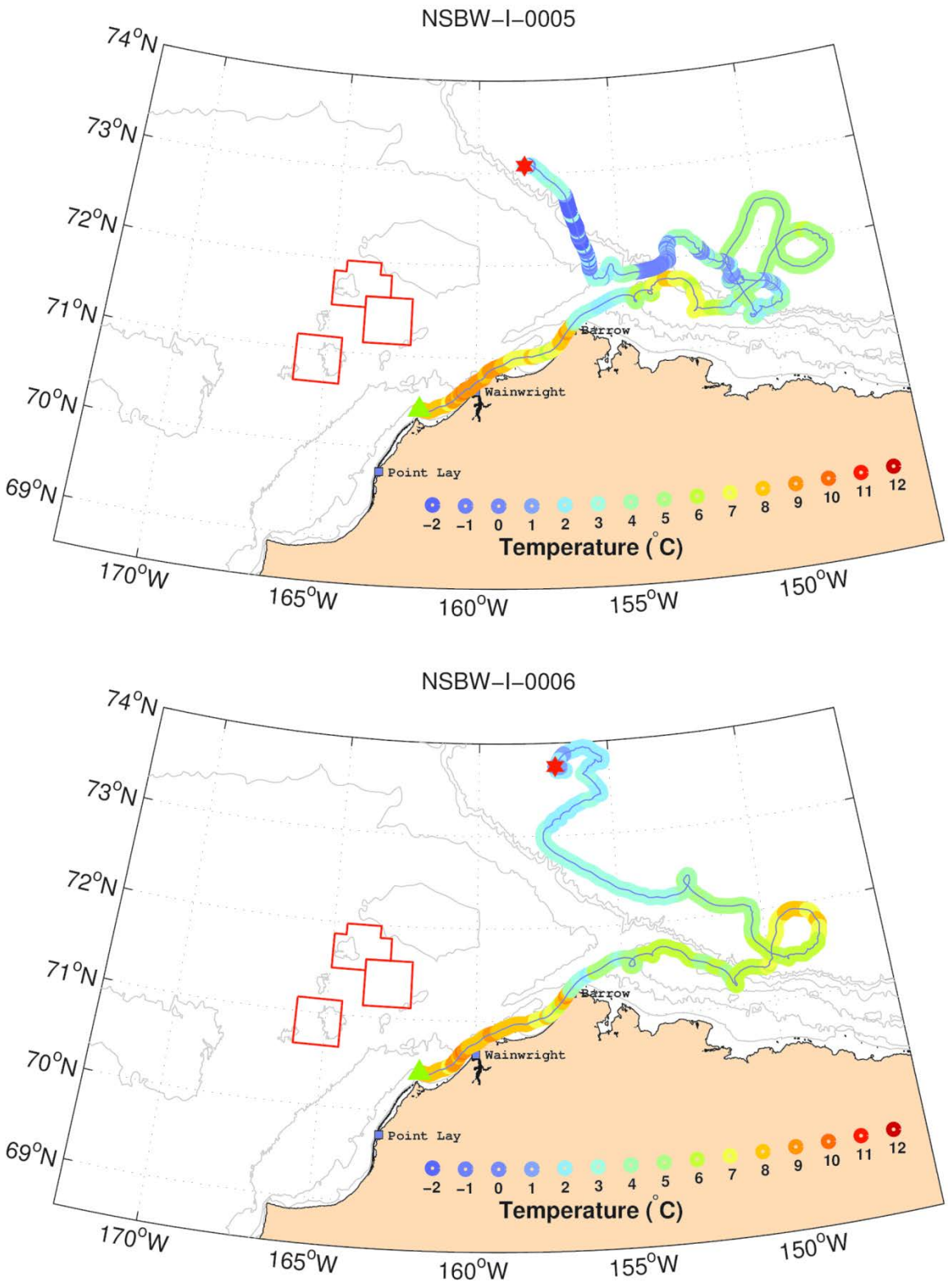

Figure 50. The trajectories of NSBW-5 (top) and 6 (bottom). The colors along the drifter trajectories are color-coded according to SST. The green triangle and red star show start and end of the trajectories, respectively.

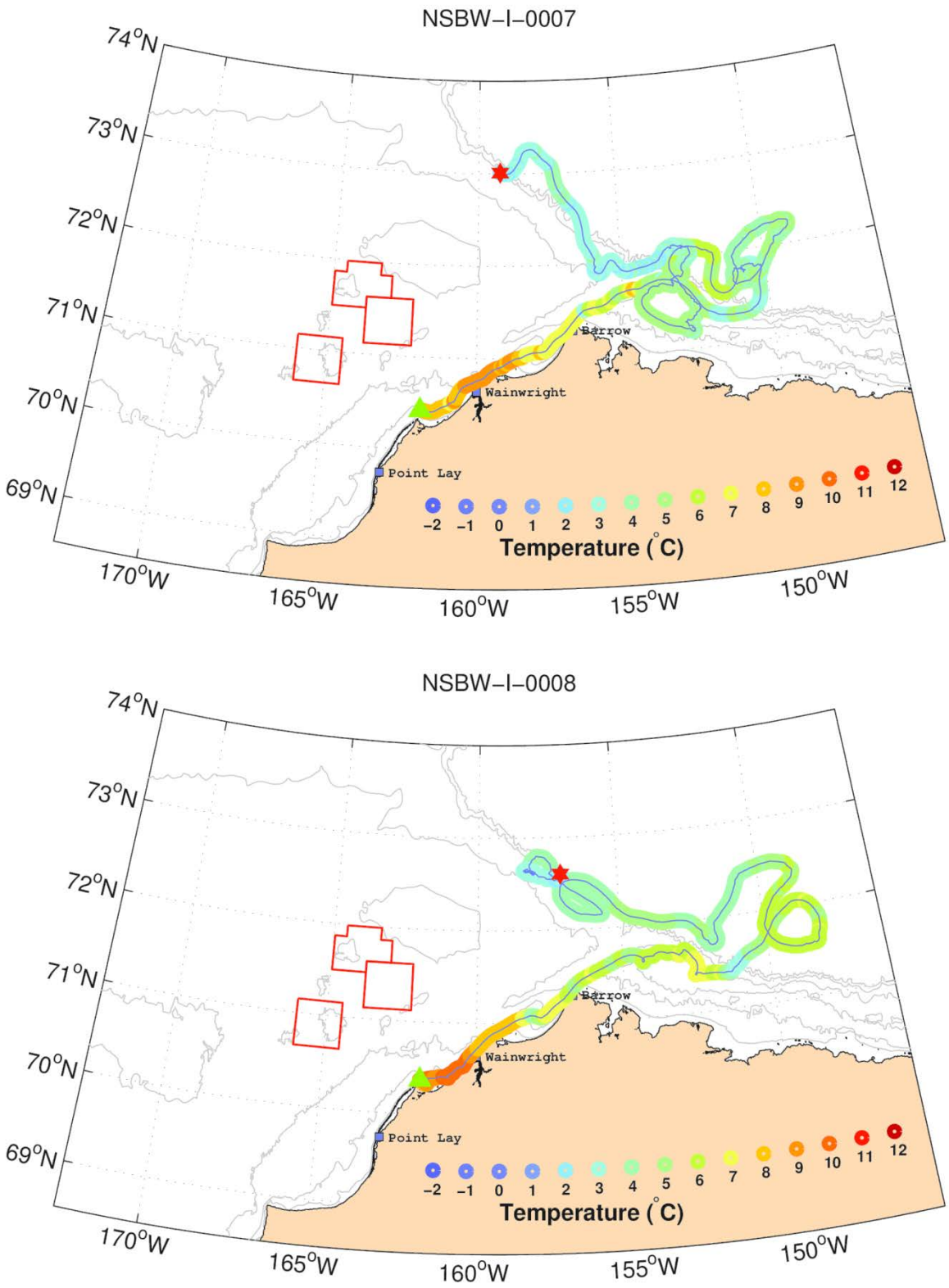

Figure 51. The trajectories of NSBW-7 (top) and 8 (bottom). The colors along the drifter trajectories are color-coded according to SST. The green triangle and red star show start and end of the trajectories, respectively.

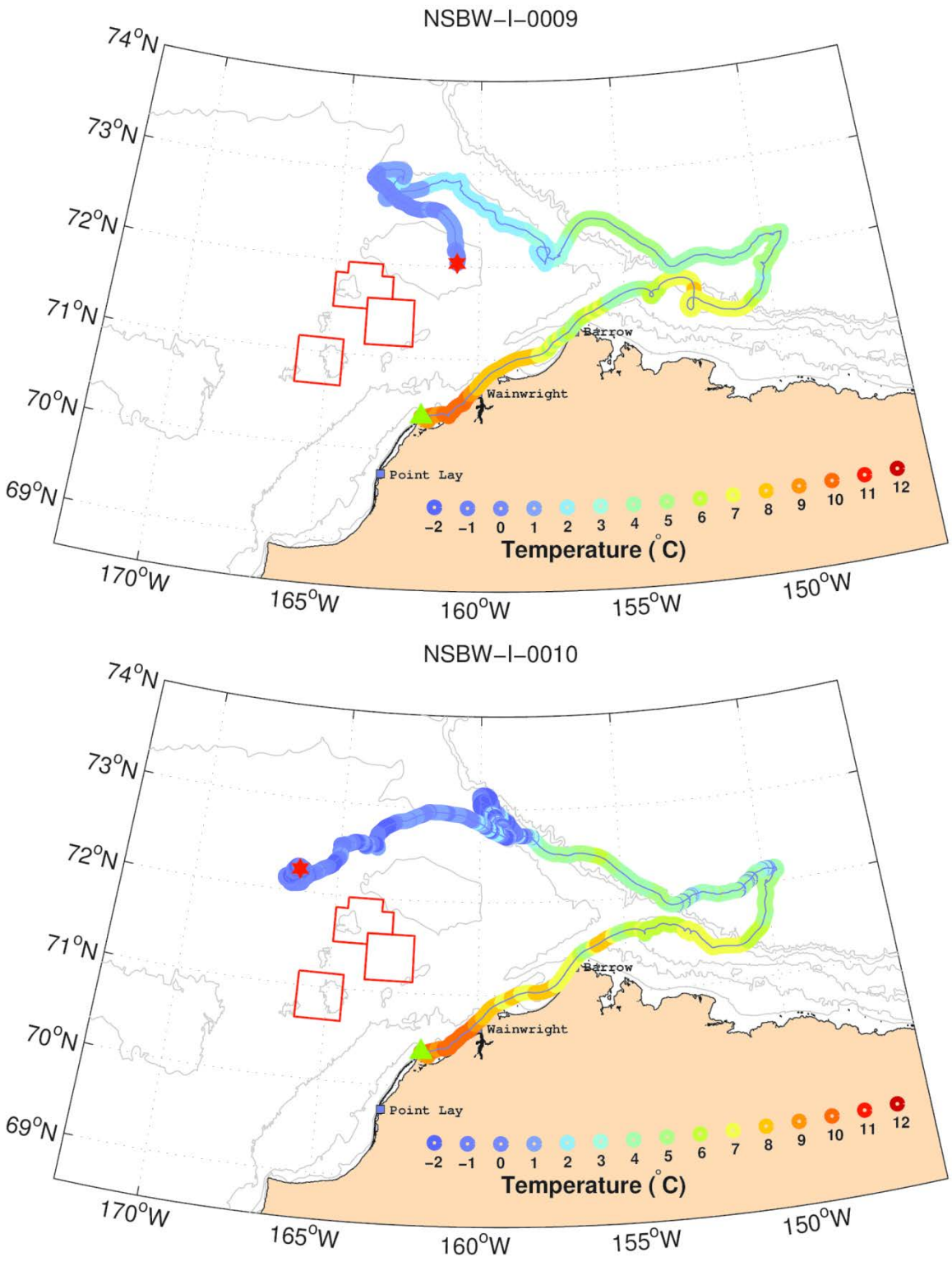

Figure 52. The trajectories of NSBW-9 (top) and 10 (bottom). The colors along the drifter trajectories are color-coded according to SST. The green triangle and red star show start and end of the trajectories, respectively.

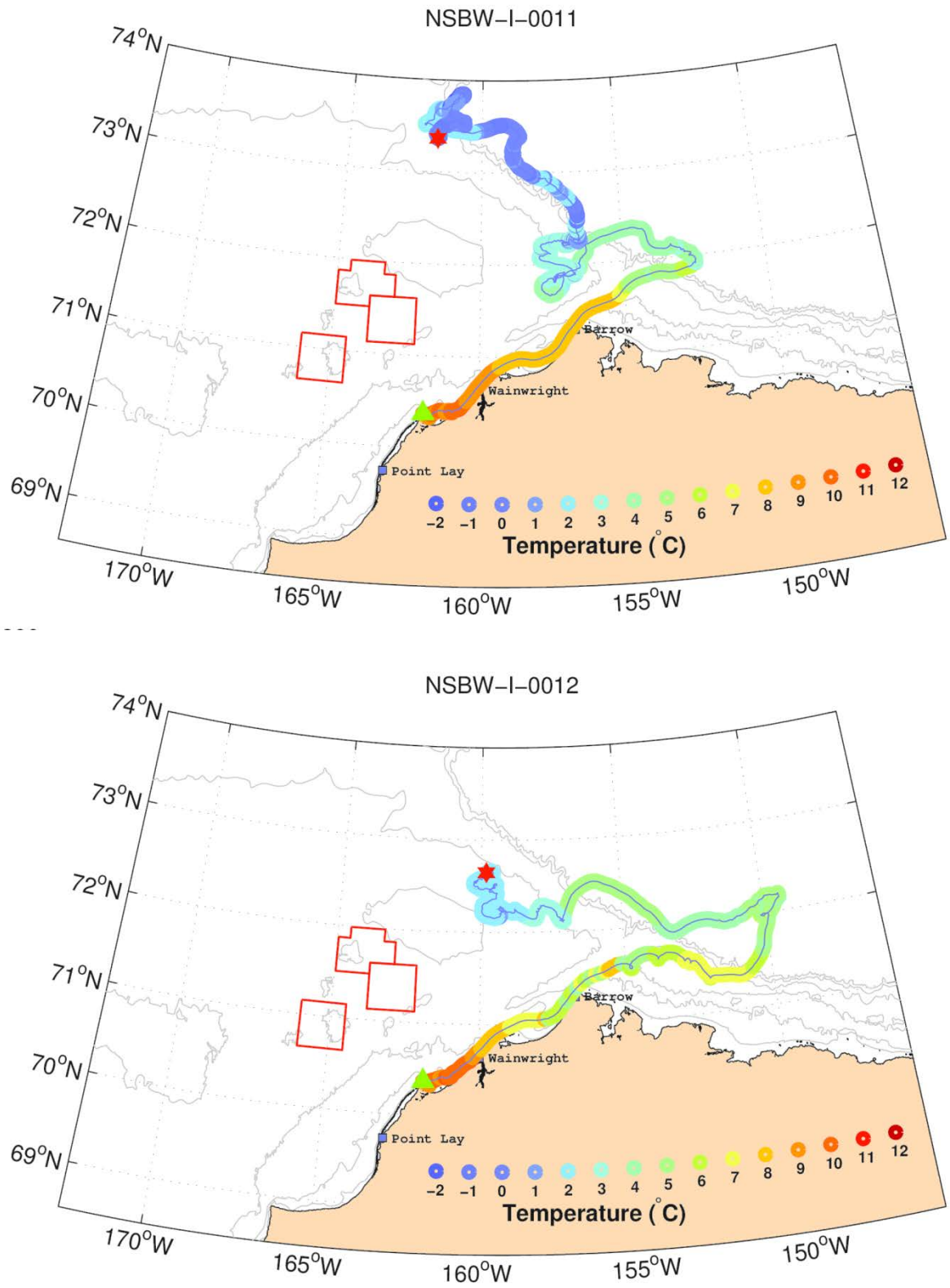

Figure 53. The trajectories of NSBW-11 (top) and 12 (bottom). The colors along the drifter trajectories are color-coded according to SST. The green triangle and red star show start and end of the trajectories, respectively.

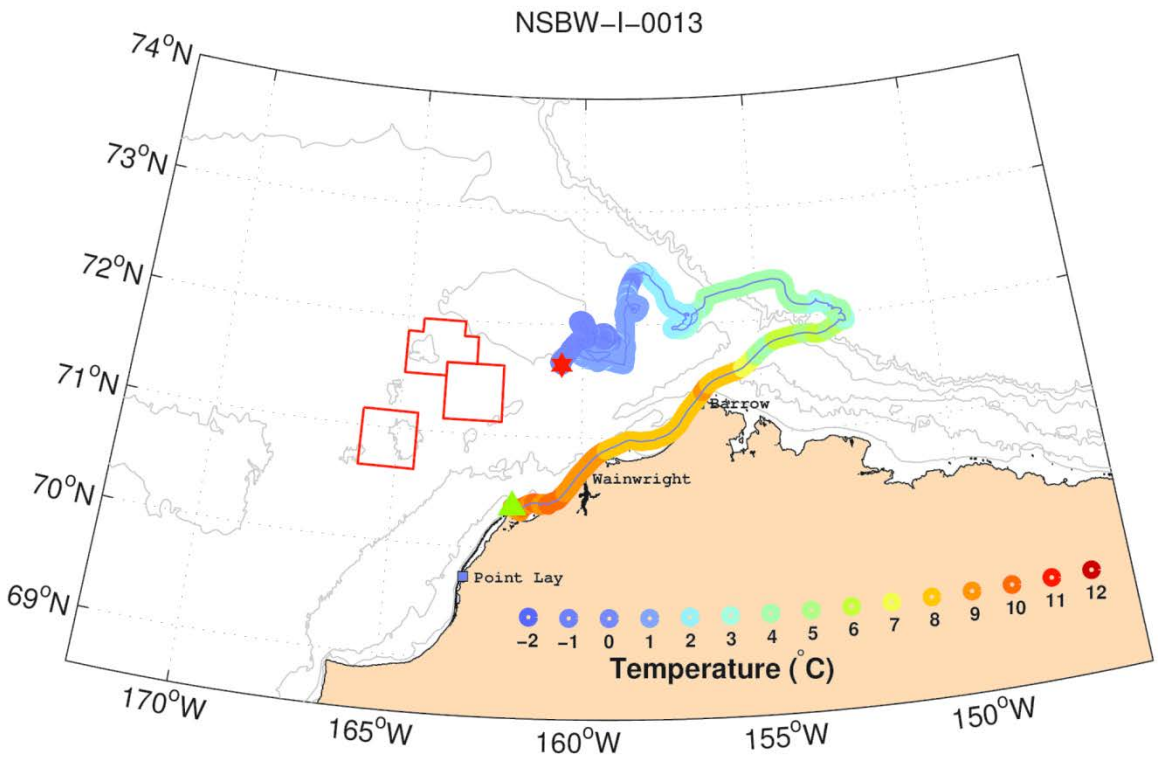

Figure 54. The trajectory of NSBW-13. The colors along the drifter trajectory are color-coded according to SST. The green triangle and red star show start and end of the trajectory, respectively.

10-11 August 2012 iSphere Deployments: Inner Shelf of the Chukchi Sea

NSBW made two separate deployments of iSphere drifters with the first of these coincident with the MS deployments on 10 August on the inner shelf of the Chukchi Sea near Icy Cape. A subset of iSphere trajectories is shown in **Figures 55 – 59**. Note that we include only one velocity record (from 63180) as the velocity records of the other iSphere drifters were quite similar**.** Initially, the iSphere trajectories were similar to those of the MS drifters deployed at the same time, e.g., they moved northeastward along the coast and through Barrow Canyon to the shelfbreak within 4 – 5 days. Upon reaching the shelfbreak all iSpheres veered northwestward along the Chukchi shelfbreak presumably in response to the intensification of the easterly and southeasterly winds on 19 August. None of the iSpheres turned eastward at the mouth of the canyon, which contrasts sharply with the MS drifters in this deployment. Recall that the MS drifters first moved eastward along the Beaufort shelfbreak, with many moving to the east of 152°W, before turning offshore and then to the northwest. All of the iSpheres moved northwestward to ~161°W along the Chukchi shelfbreak and then they drifted southward on 29 August (in response to northeasterly winds) and crossed Hanna Shoal. Of particular interest is that the SSTs along the shelfbreak were warm (~5°C) compared to the SSTs (~0°C) over Hanna Shoal. Because the iSpheres were initially deployed in waters with an SST of ~9°C, the trajectories suggest that at least some of the warm water moving through Barrow Canyon

contributed to ice melt along the Chukchi shelfbreak north of Hanna Shoal. Drifters 65180 and 65190 moved to the east of Burger on crossing the Shoal and subsequently beached near Wainwright in late September. The remaining drifters moved across Statoil and Klondike and into the Central Channel between 165^{o} and 170^{o}W. On proceeding southward, SSTs for all these drifters increased from ~0^{o}C at ~72^{o}N to 4 – 6^{o}C at 71^{o}N, suggesting that the drifters crossed the meltwater front south of Hanna Shoal and into warmer Bering Sea waters. Many of these drifters reached the vicinity of Pt. Hope by ~20 October. Drifter 60180 passed Pt. Hope and proceeded to 67.5^{o}N on 20 October. It then turned northward, passed Pt. Hope, and eventually ran aground near Pt. Lay on 30 October. Drifters 61180, 63180, 64180, and 66180 performed similarly and all died in Ledyard Bay between Pt. Lay and the Lisburne Peninsula. Drifter 60190 made two large north-south loops in late October and early November, first south of Herald Shoal and then offshore of Pt. Lay, before passing Pt. Hope. In late November it was caught in ice and drifted south toward the Siberian coast before ending transmissions in mid-December. Drifter 62300 beached near Pt. Hope on about 18 October.

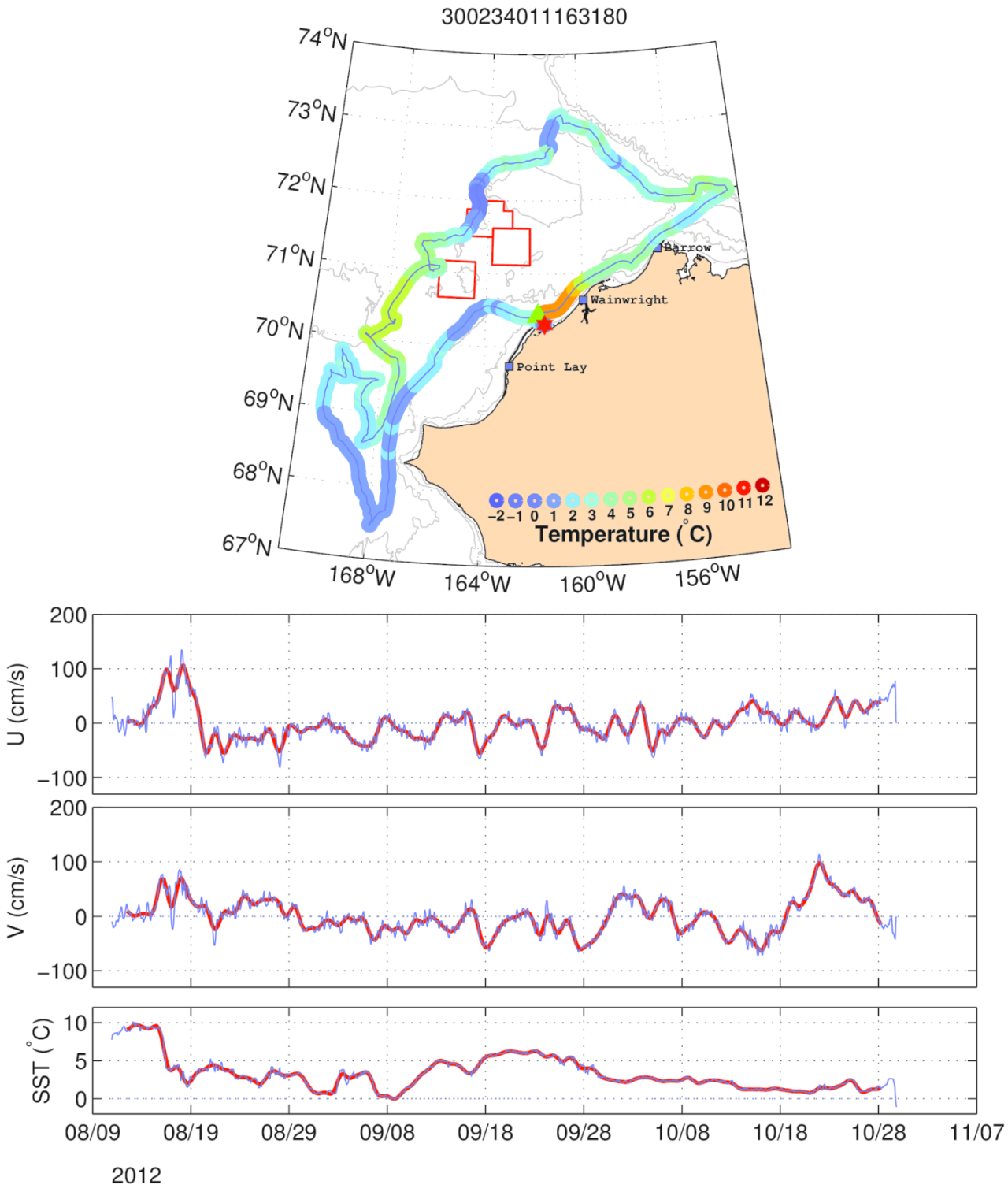

Figure 55. The trajectory of iSphere-63180 and the time series of its zonal (U), meridional (V), and sea surface temperature (SST) record. The colors along the drifter trajectory are color-coded according to SST. The green triangle and red star show start and end of the trajectory, respectively. The light lines in the time series are raw data and the heavy red lines are the 35-hour low-pass filtered data.

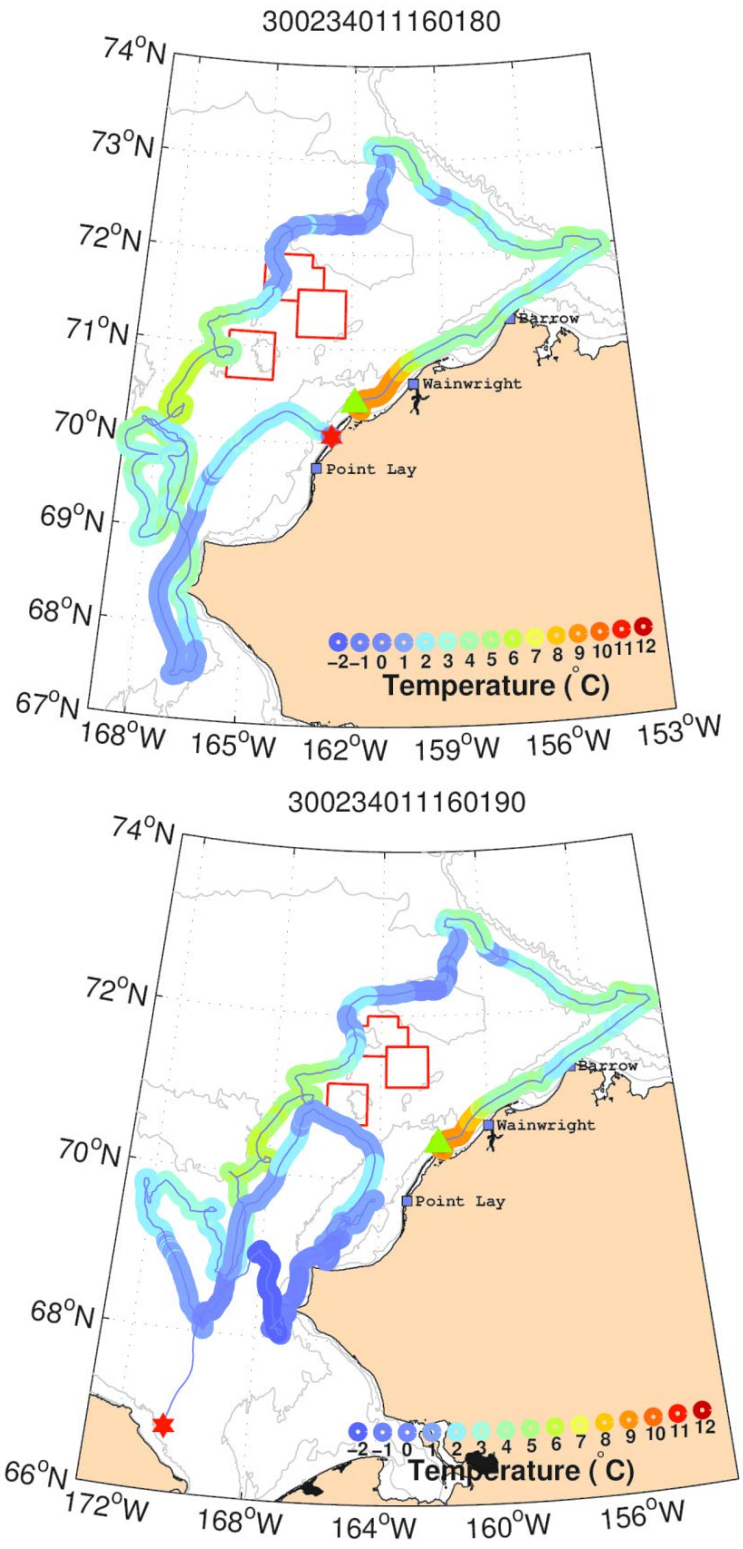

Figure 56. The trajectories of iSphere-60180 (top) and 60190 (bottom).). The colors along the drifter trajectories are color-coded according to SST. The green triangle and red star show start and end of the trajectories, respectively.

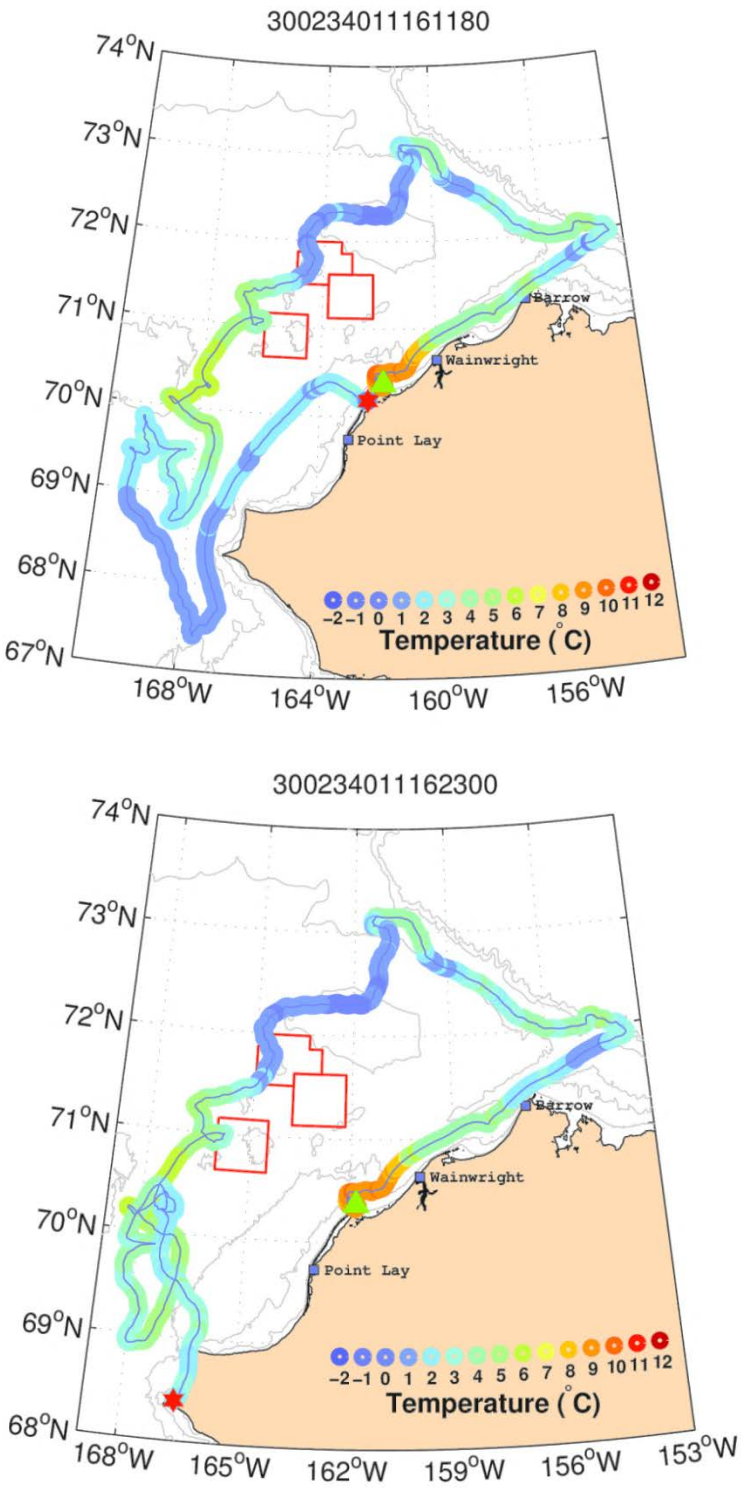

Figure 57. The trajectories of iSphere-61180 (top) and 62300 (bottom). The colors along the drifter trajectories are color-coded according to SST. The green triangle and red star show start and end of the trajectories, respectively.

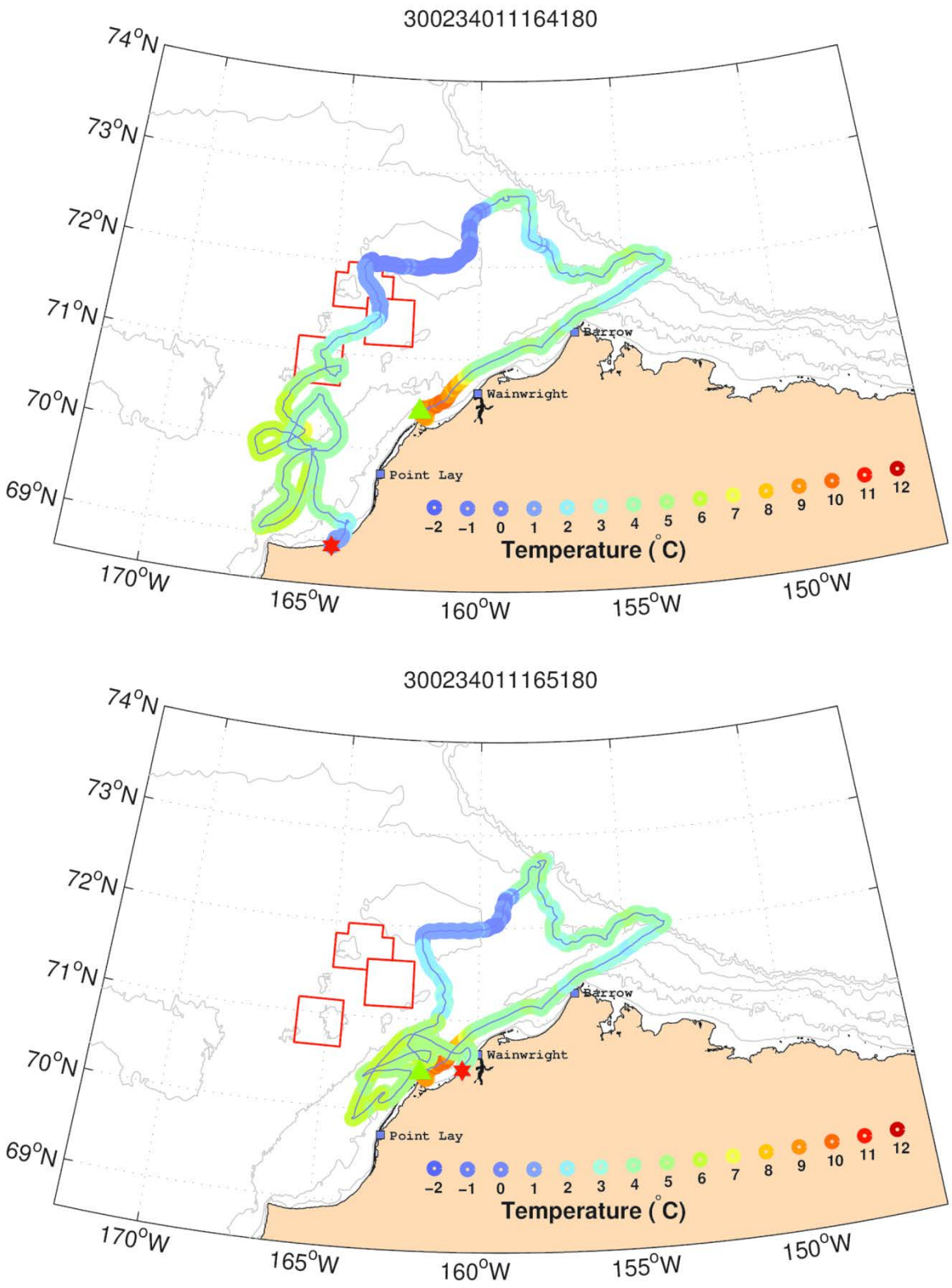

Figure 58. The trajectories of iSphere-64180 (top) and 65180 (bottom). The colors along the drifter trajectories are color-coded according to SST. The green triangle and red star show start and end of the trajectories, respectively.

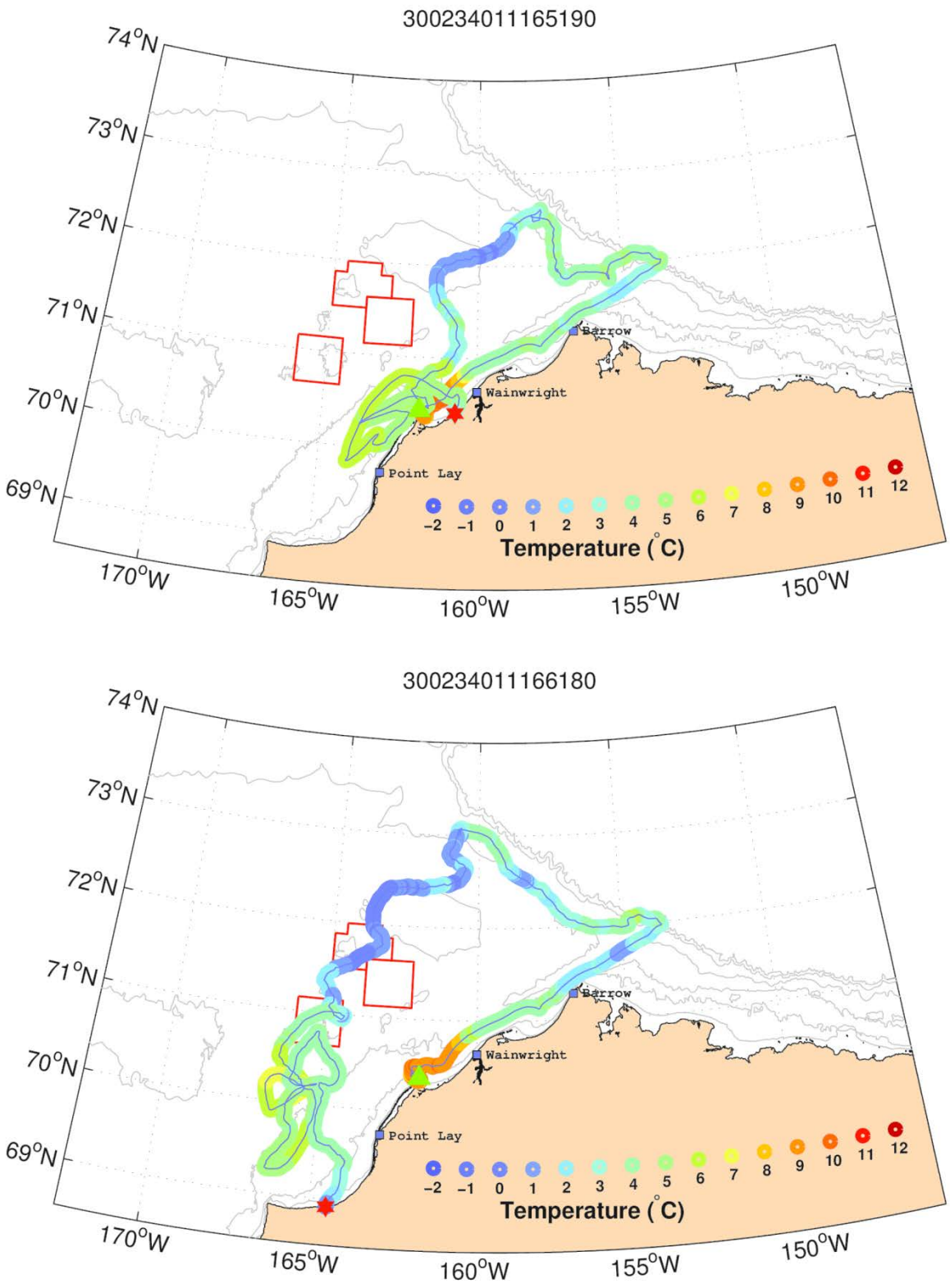

Figure 59. The trajectories of iSphere-65190 (top) and 66180 (bottom). The colors along the drifter trajectories are color-coded according to SST. The green triangle and red star show start and end of the trajectories, respectively.

2 September 2012 MS Drifter Deployments in Burger

The final set of deployments that we include from 2012 consists of ten MS drifters that were deployed in the southeast quadrant of Burger on 2 September. The trajectories, shown in **Figures 60 – 65**, were remarkably similar to one another over much of the time. Given the similarities in the velocity records, we show only one time series of velocity. Through ~24 September, each drifter moved southward and made three to four east-to-west excursions until they reached ~70^{o}N, offshore of Pt. Lay and approximately 150 km south of the deployment position. As they moved southward they crossed a meltwater front along the southern boundary of Burger where the temperature rose from ~2^{o}C to 5^{o}C. After reaching 70^{o}N, each drifter then moved ~100 km to the northeast and then eastward toward the coast over the next several days. This was followed by a southwestward excursion along the coast until about 1 October. Thereafter, the drifters reversed course and, again, proceeded to the northeast. All of the drifters, except MS 11-2 and 12-2, went ashore between Pt. Lay and Pt. Franklin from 9 – 10 October, presumably due to the onset of winds from the northwest. Drifter MS 11-2 was caught in the main current in Barrow Canyon and proceeded to Barrow where it grounded on 9 October. Drifter MS 13-2 rounded Pt. Barrow on 9 October. Winds continued to be from the northwest or north at this time so the drifter moved eastward over the inner portion of the Beaufort Sea Shelf until it grounded in Harrison Bay on 18 October.

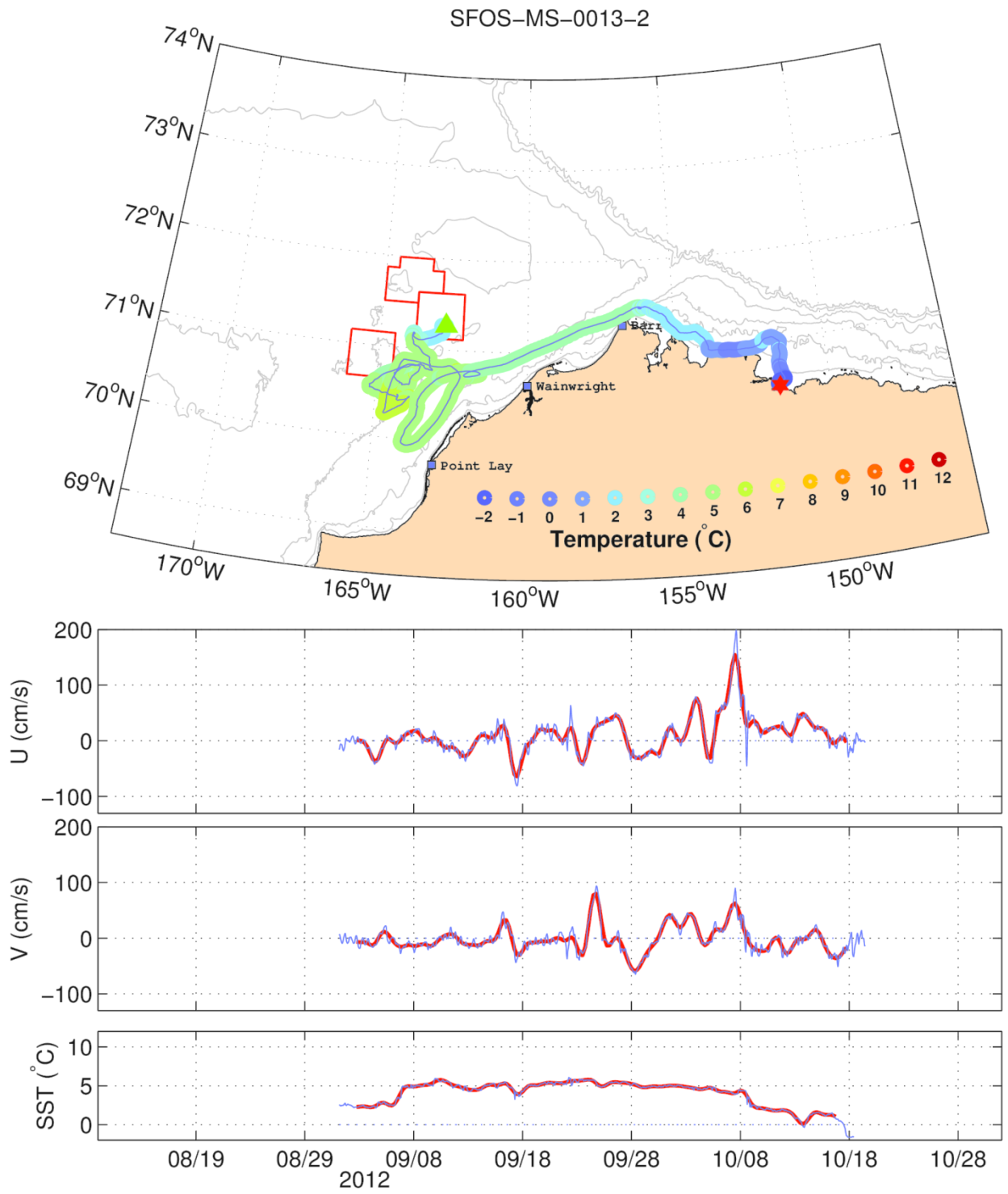

Figure 60. The trajectory of MS-13-2 and the time series of its zonal (U), meridional (V), and sea surface temperature (SST) record. The colors along the drifter trajectory are color-coded according to SST. The green triangle and red star show start and end of the trajectory, respectively. The light lines in the time series are raw data and the heavy red lines are the 35-hour low-pass filtered data.

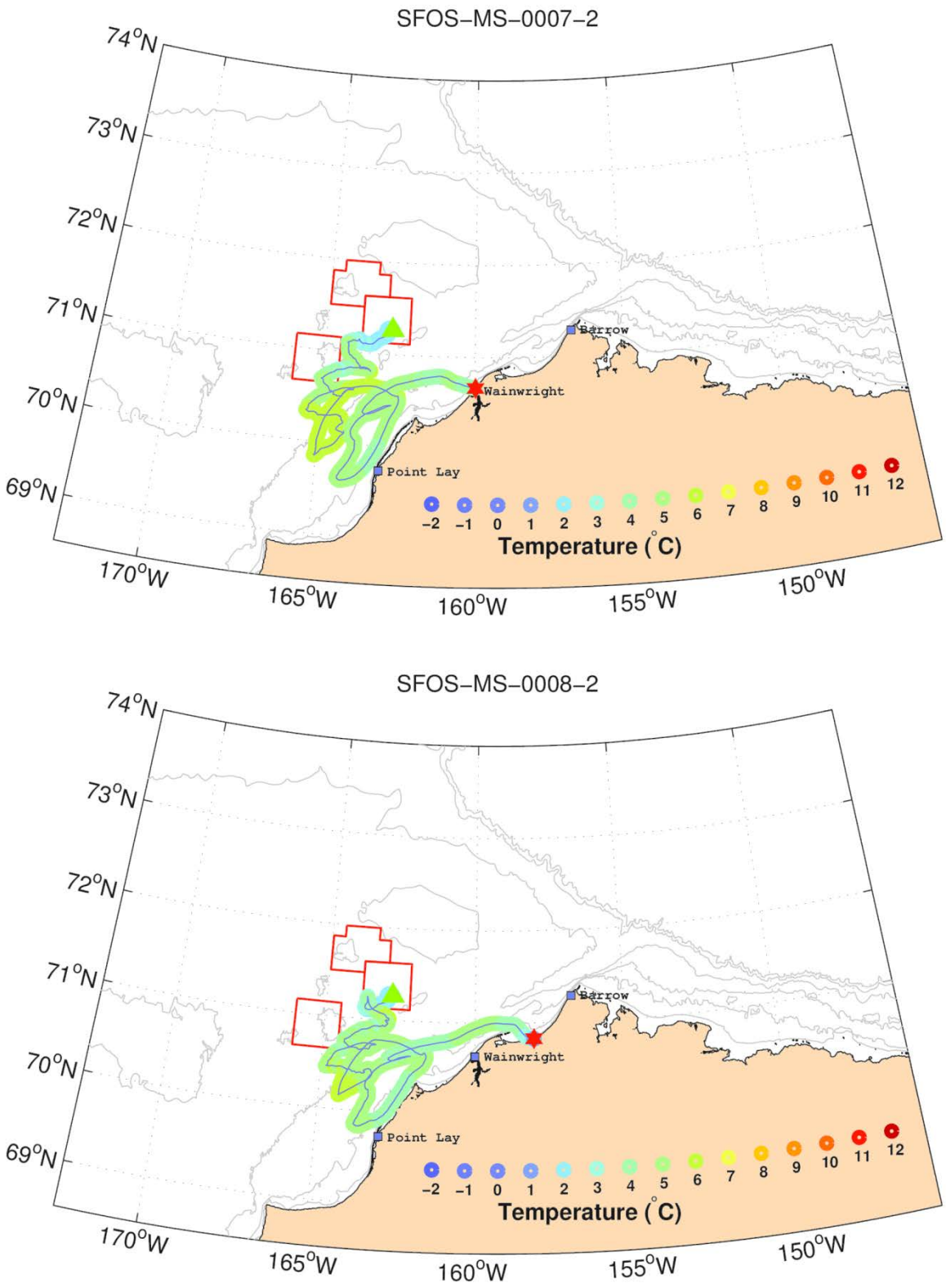

Figure 61. The trajectories of MS-7-2 (top) and 8-2 (bottom). The colors along the drifter trajectories are color-coded according to SST. The green triangle and red star show start and end of the trajectories, respectively.

-035

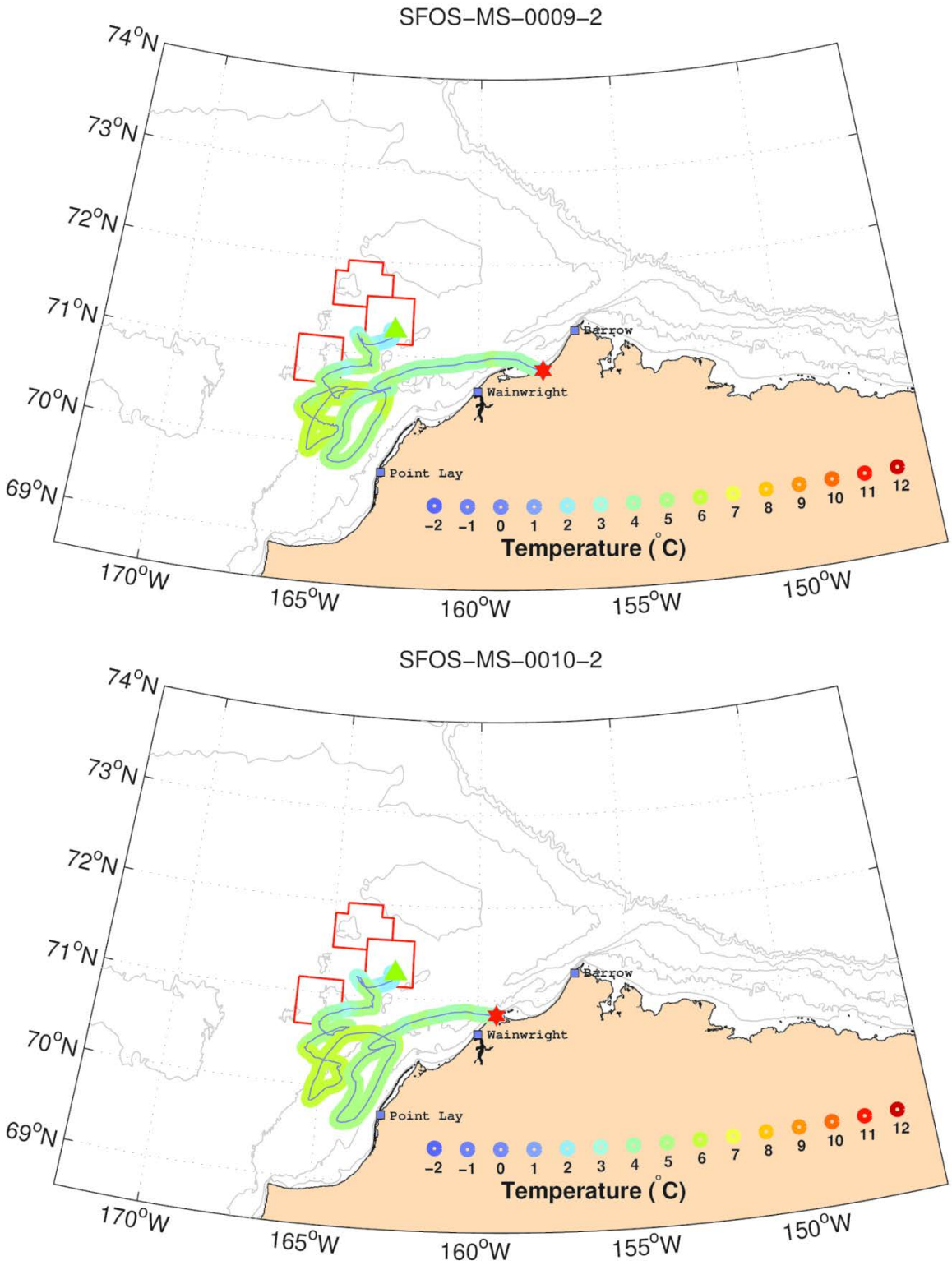

Figure 62. The trajectories of MS-9-2 (top) and 10-2 (bottom). The colors along the drifter trajectories are color-coded according to SST. The green triangle and red star show start and end of the trajectories, respectively.

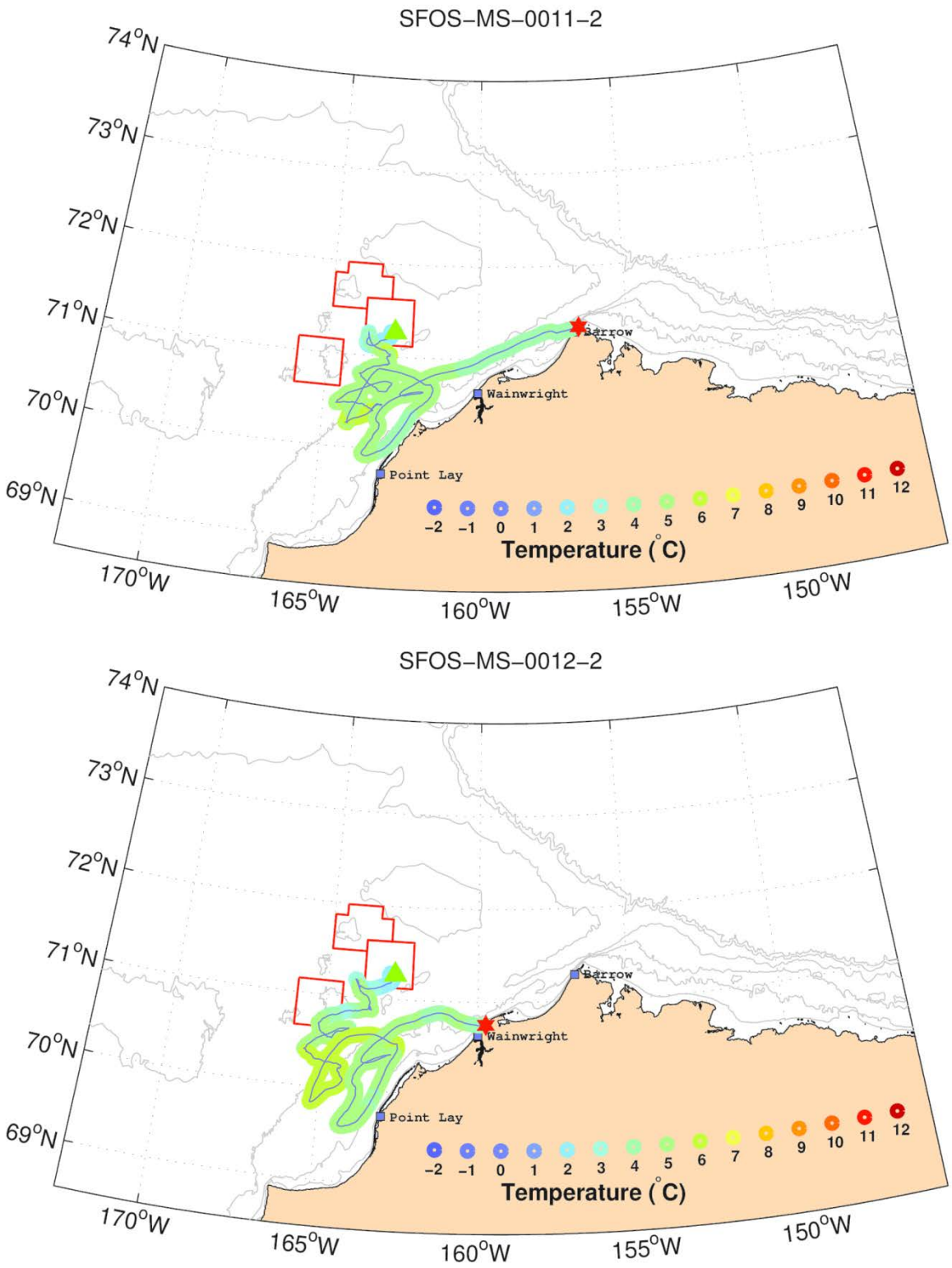

Figure 63. The trajectories of MS-11-2 (top) and 12-2 (bottom). The colors along the drifter trajectories are color-coded according to SST. The green triangle and red star show start and end of the trajectories, respectively.

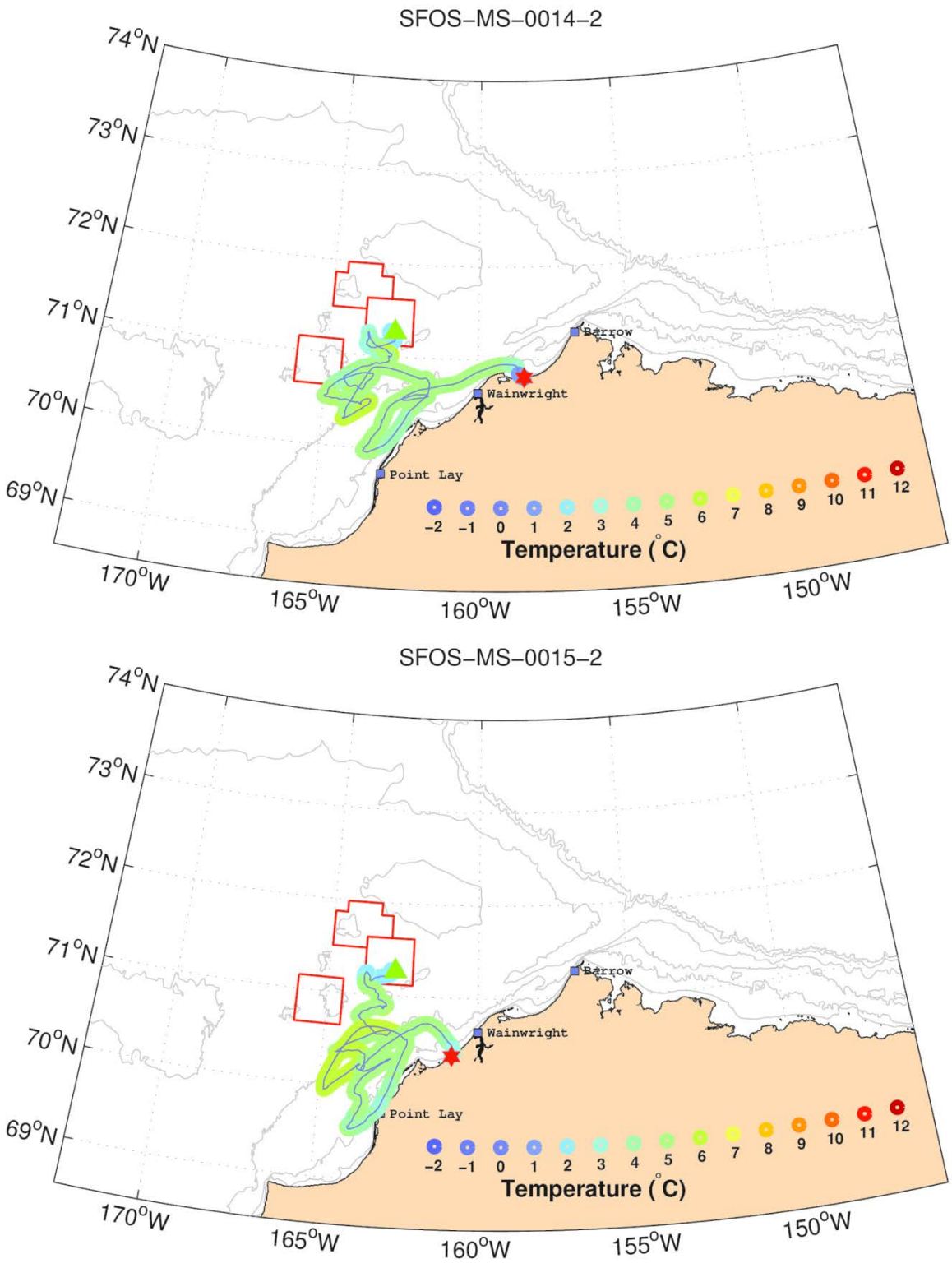

Figure 64. The trajectories of MS-14-2 (top) and 15-2 (bottom). The colors along the drifter trajectories are color-coded according to SST. The green triangle and red star show start and end of the trajectories, respectively.

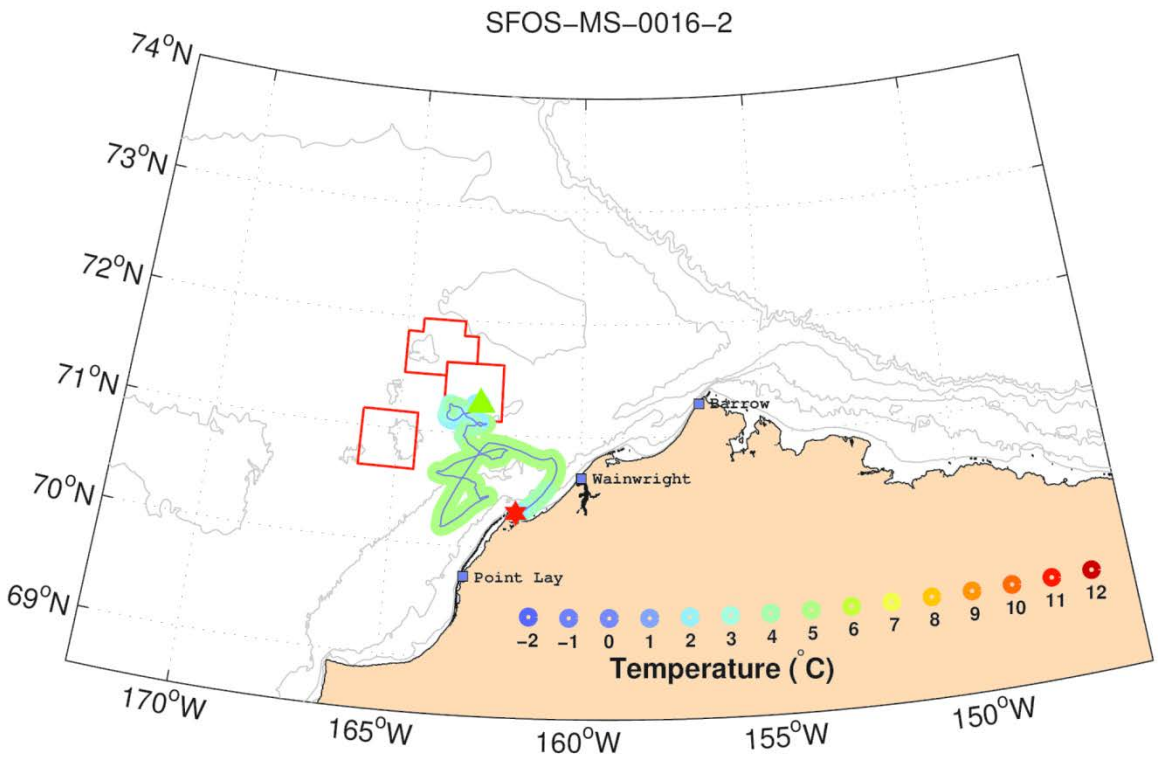

Figure 65. The trajectory of MS-16-2. The colors along the drifter trajectory are color-coded according to SST. The green triangle and red star show start and end of the trajectory, respectively.

17 August 2013 Deployments: Pt. Lay Inshore and Offshore (NSBW-Shell)

The NSBW deployed drifters MS-53 to MS-78 in two separate clusters (13 drifters each) within a few kilometers of one another seaward of Pt. Lay. We refer to these as the Pt. Lay Inshore cluster and the Pt. Lay Offshore cluster. The clustered deployments were designed to assess cross-shore gradients in the along-shore flow near the coast. In particular, we hypothesized that the Alaskan Coastal Current included nearshore horizontal shears that would be identified by this deployment scheme. As it turns out the winds during this deployment were initially upwelling-favorable and both clusters behaved similarly. The trajectories of the Pt. Lay Inshore cluster are shown in **Figures 66 – 73** and the Offshore cluster trajectories are in **Figures 74 – 78**.

From 17 August to 7 September, all of these drifters moved ~200 km westward toward Herald Shoal and the Central Channel at a speed of ~15 cm s^{-1}. Initially, the inshore cluster moved southwestward, while the offshore cluster had a more westerly set. The drifters were moving ~40^{o} to the right of the wind, consistent with Ekman dynamics, with the drift speeds being ~2% of the wind speed.

Near the coast, SSTs were ~6^{o}C, but temperatures increased to 8 – 9^{o}C offshore before decreasing again west of 165^{o} W. These cross-shore temperature differences are consistent with the hydrography obtained from the glider and Leg H (**Figures 22** and **23**) in suggesting that

coastal upwelling was occurring (e.g., cooler water was inshore and warmer waters were offshore.

On about 7 September, many of the drifters approached Herald Shoal and then moved northward along the eastern side of the Central Channel. This northward movement occurred even though the winds often blew strongly from the northeast and is consistent with prior observations, which indicate the flow here is often northward even when northerly winds prevail (*Weingartner et al*., 2005a; *Weingartner et al.,* 2013a). By early October, the drifters had migrated to the western side of the Channel and then started moving southward again as northerly wind speeds increased. Many of the drifters moved across Herald Shoal and then southward toward the Chukotkan coast. Those that did approach the coast often moved along-shore and toward the southeast, suggesting that these might have been entrained into the Siberian Coastal Current (*Weingartner et al*., 1999).

24 August 2013 Deployments: Wainwright Inshore and Offshore (NSBW-Shell)

Drifters MS-27 to MS-52 were deployed in two separate clusters (13 drifters each) within a few kilometers of one another seaward of Wainwright. As with the Pt. Lay drifters, the two clusters were designed to assess cross-shore gradients in the along-shore flow. However, both clusters behaved similarly and are, therefore, not discussed separately. Their trajectories are shown in **Figures 79 – 83**. Thirteen of these drifters ran aground shortly after deployment so their trajectories are not shown.

During the first seven days after deployment these drifters moved offshore in response to upwelling-favorable winds and then, with the brief wind relaxation in late August, they drifted to the northeast. During this brief northeastward excursion, many of the drifters beached just north of Wainwright. From early September to mid-October, these drifters made several (to many) offshore-to-onshore excursions apparently in response to the waxing and waning of upwelling-favorable winds. Consistent with the hydrography that indicated coastal upwelling, the drifters moved into warmer water as they were carried offshore and into colder water as they moved onshore. By mid-October the clusters had begun dispersing with some heading northeast and out through Barrow Canyon (MS-27, 32, 44) and others drifting southwest or west over the Chukchi Sea Shelf (MS-36, 38, 41, 43). All of these drifters died by early to mid-November. Note that the trajectories of the 2013 Pt. Lay and Wainwright drifters contrast sharply with the trajectories of the nearshore drifters deployed in 2012. In that year, virtually all of the nearshore drifters moved rapidly through Barrow Canyon and onto the outer shelf and slope of the Chukchi and Beaufort Seas. These differences are largely associated with the wind conditions at the time of deployment. In 2012, the winds were from the southwest in early August. In 2013, wind speeds exceeded 6 m s^{-1} from the northeast at the time of deployment.

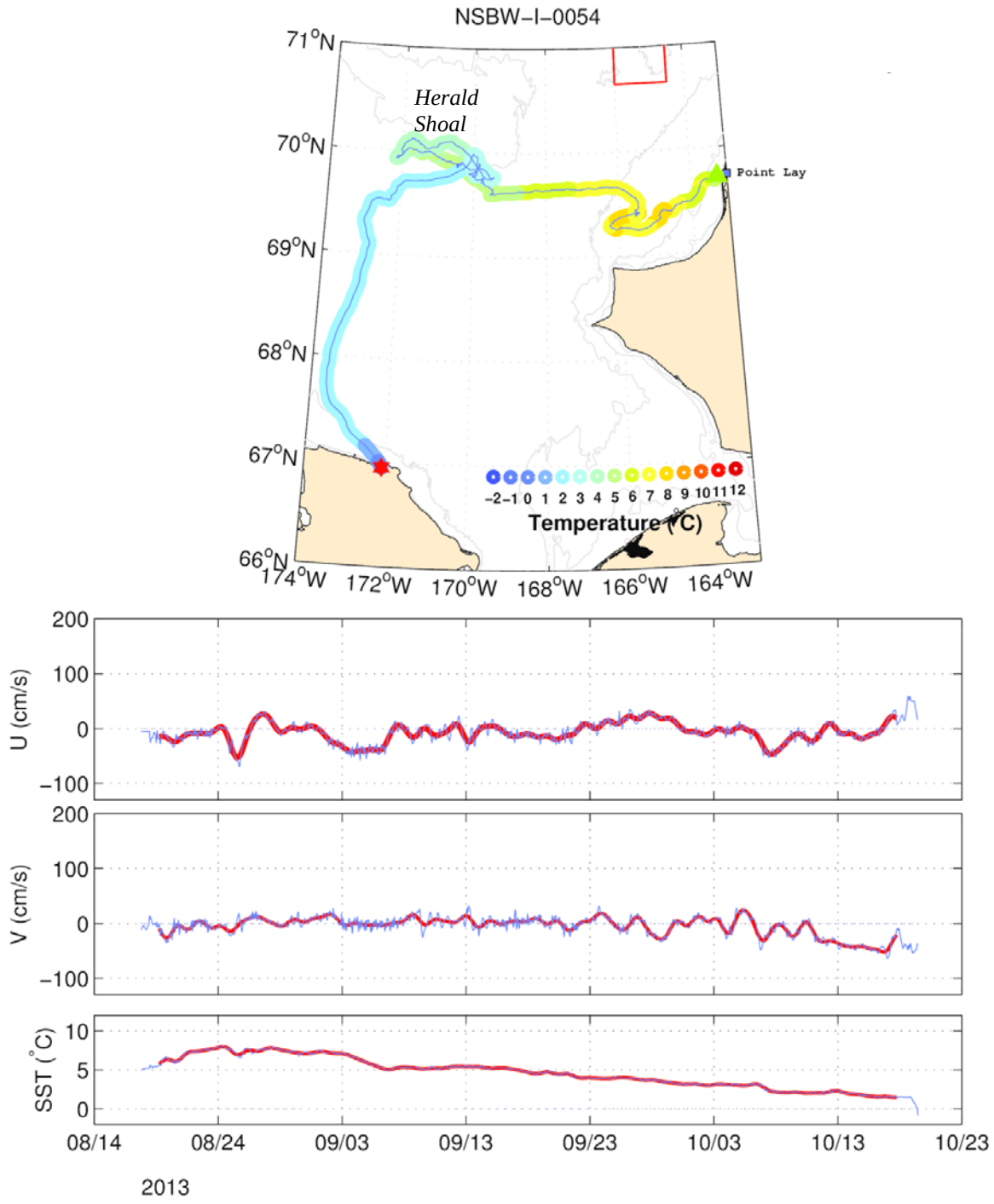

Figure 66. The Pt. Lay Inshore trajectory of MS-54 and the time series of its zonal (U), meridional (V), and sea surface temperature (SST) record. The colors along the drifter trajectory are color-coded according to SST. The green triangle and red star show start and end of the trajectory, respectively. The light lines in the time series are raw data and the heavy red lines are the 35-hour low-pass filtered data.

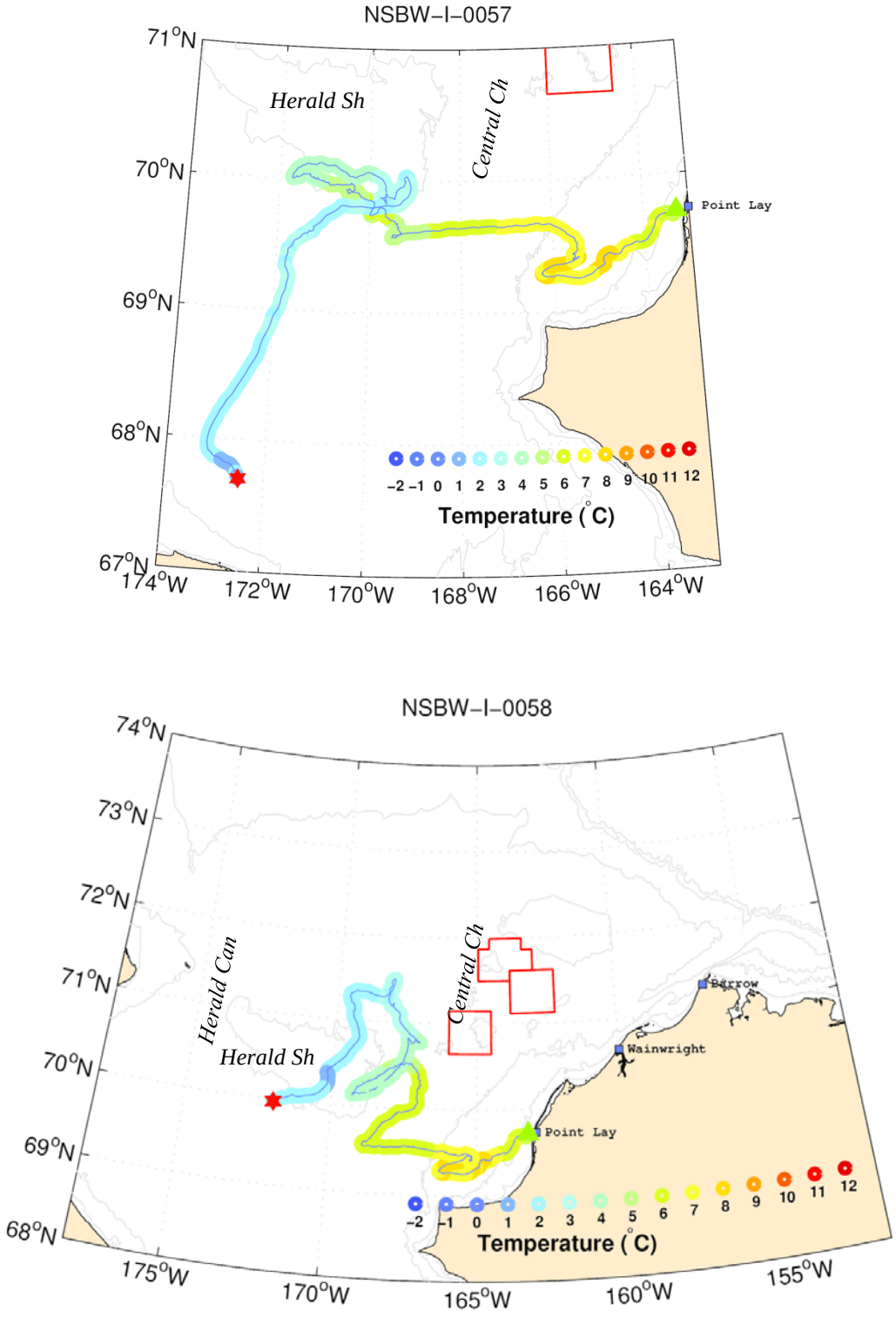

Figure 67. The Pt. Lay Inshore trajectories of MS-57 (top) and 58 (bottom). The colors along the drifter trajectories are color-coded according to SST. The green triangle and red star show start and end of the trajectories, respectively.

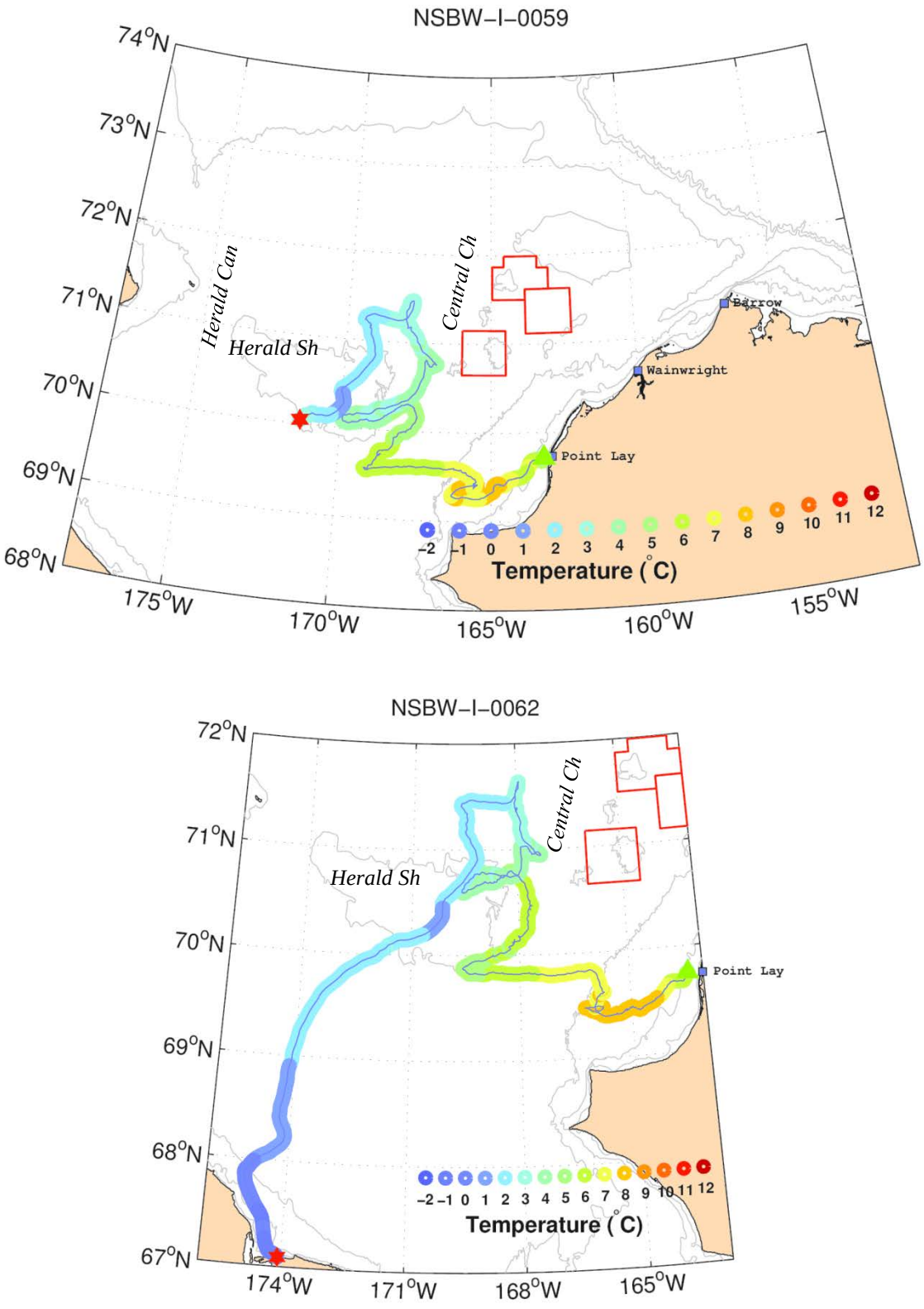

Figure 68. The Pt. Lay Inshore trajectories of MS-59 (top) and 62 (bottom). The colors along the drifter trajectories are color-coded according to SST. The green triangle and red star show start and end of the trajectories, respectively.

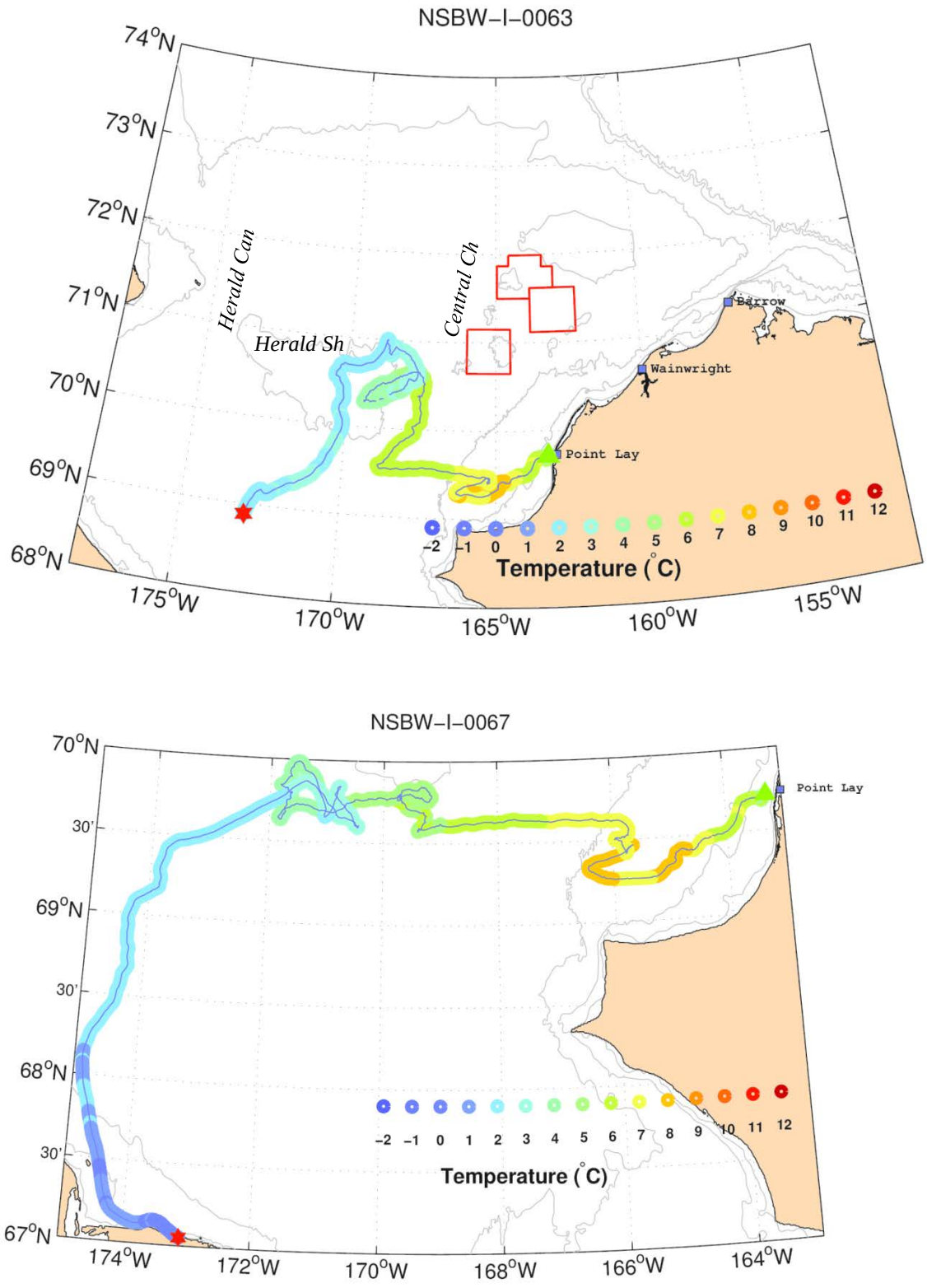

Figure 69. The Pt. Lay Inshore trajectories of MS-63 (top) and 67 (bottom). The colors along the drifter trajectories are color-coded according to SST. The green triangle and red star show start and end of the trajectories, respectively.

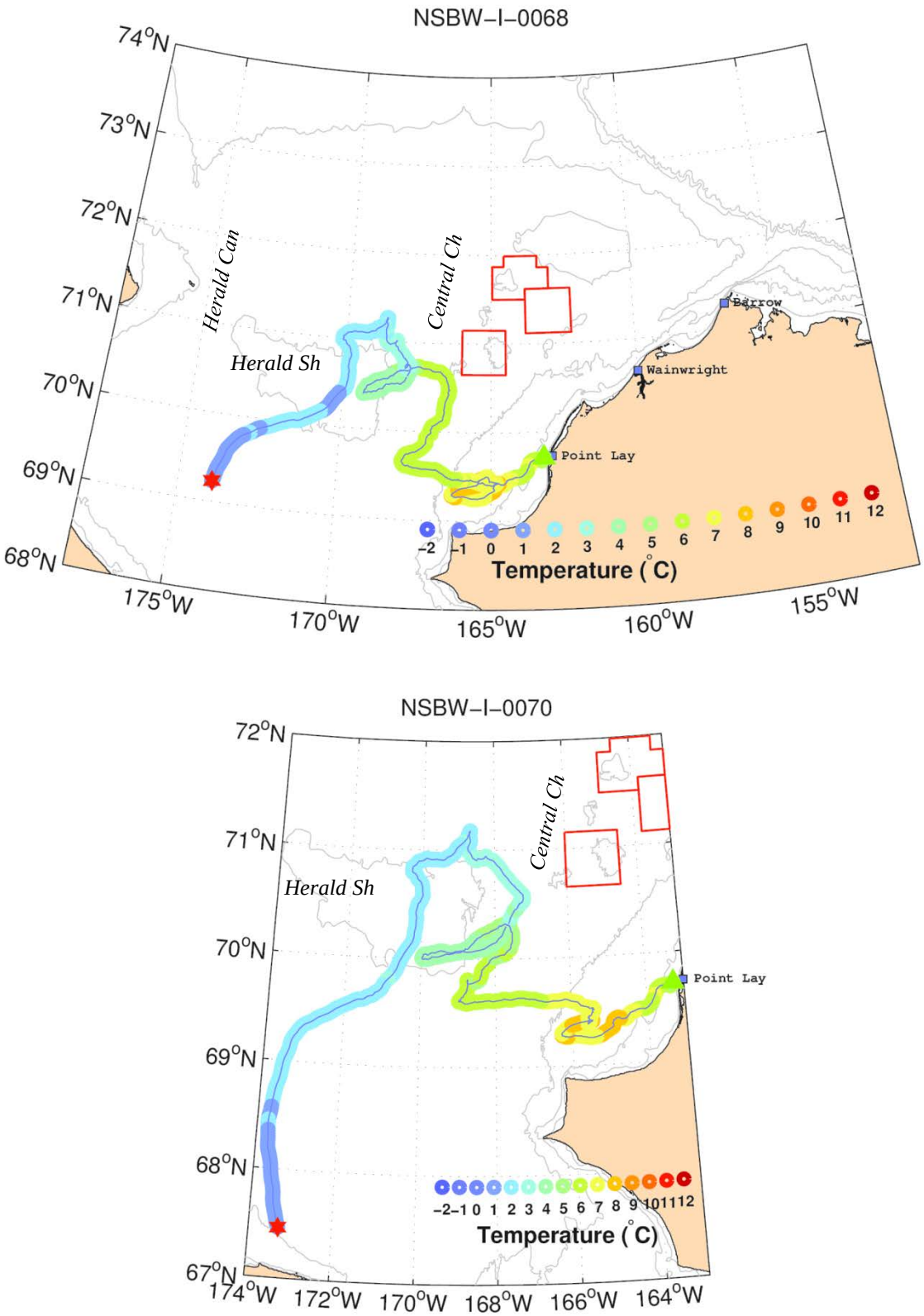

Figure 70. The Pt. Lay Inshore trajectories of MS-68 (top) and 70 (bottom). The colors along the drifter trajectories are color-coded according to SST. The green triangle and red star show start and end of the trajectories, respectively.

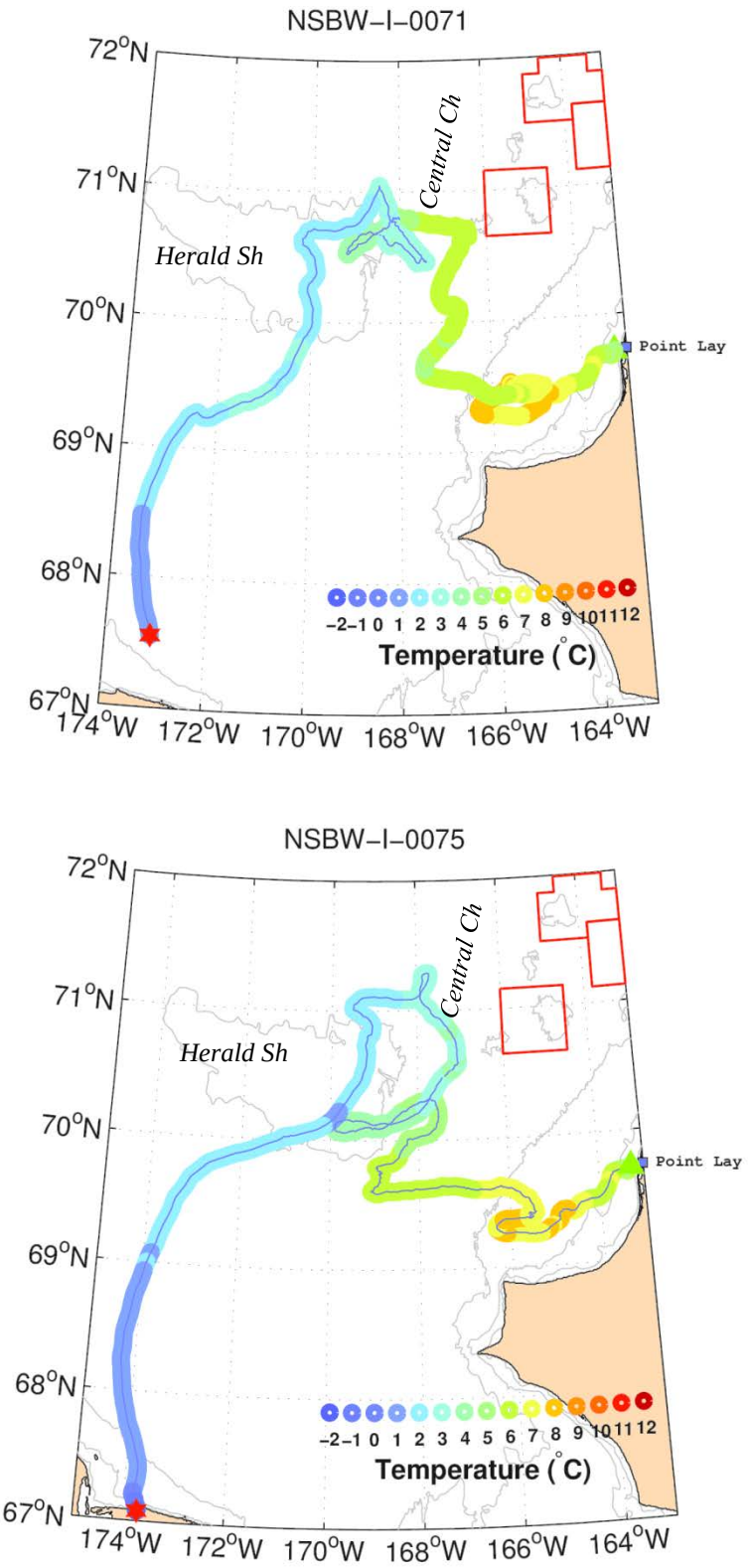

Figure 71. The Pt. Lay Inshore trajectories of MS-71 (top) and 75 (bottom). The colors along the drifter trajectories are color-coded according to SST. The green triangle and red star show start and end of the trajectories, respectively.

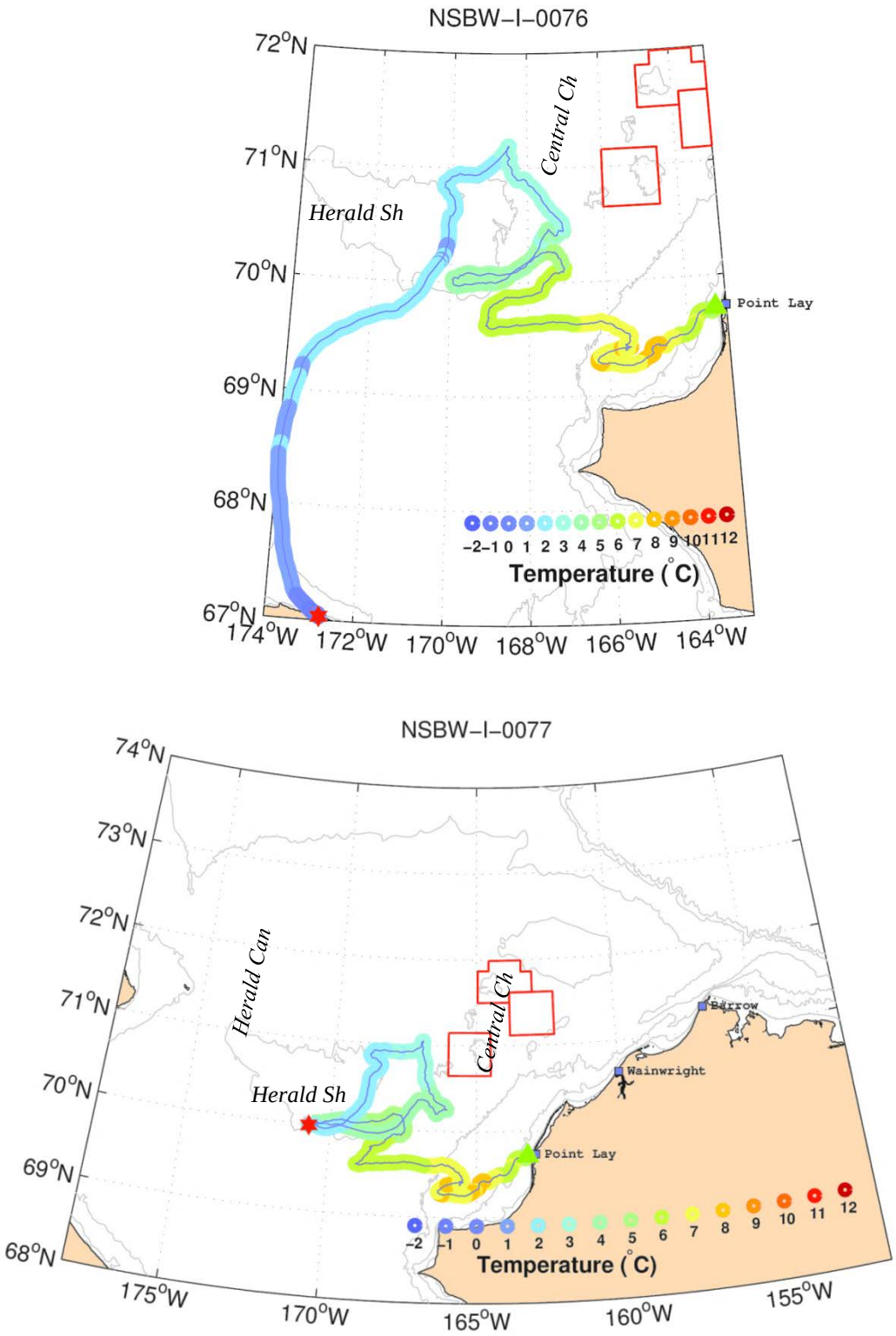

Figure 72. The Pt. Lay Inshore trajectories of MS-76 (top) and 77 (bottom). The colors along the drifter trajectories are color-coded according to SST. The green triangle and red star show start and end of the trajectories, respectively.

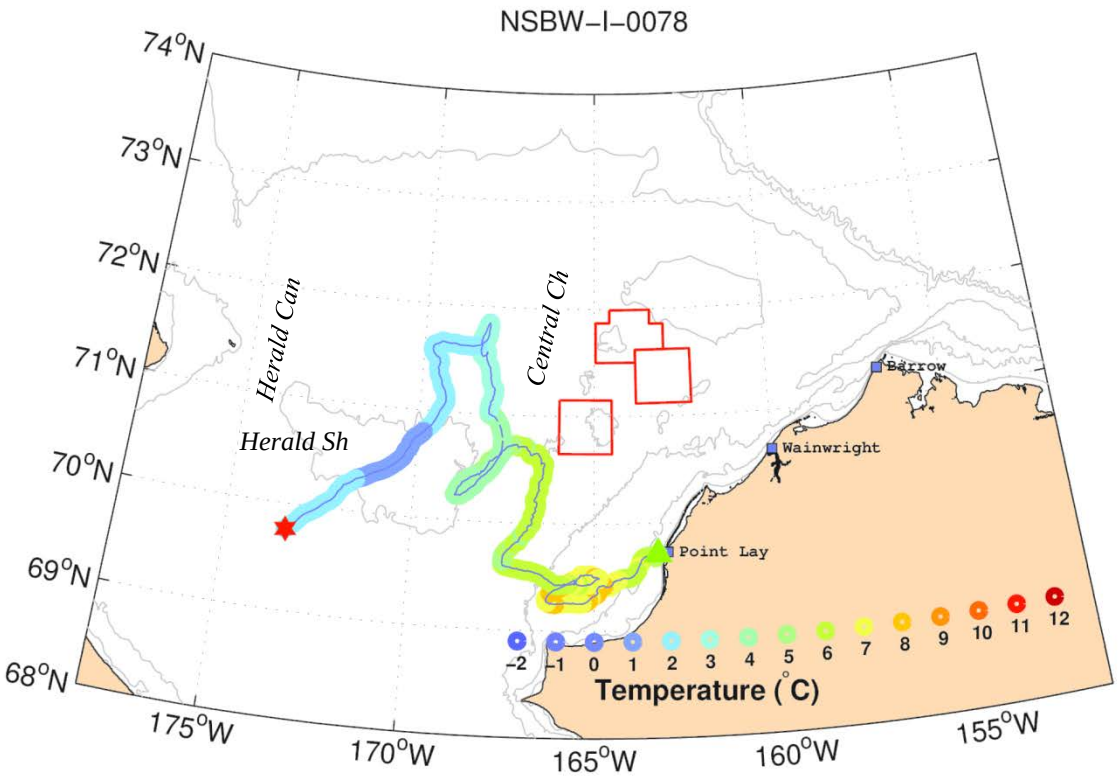

Figure 73. The Pt. Lay Inshore trajectory of MS-78. The colors along the drifter trajectory are color-coded according to SST. The green triangle and red star show start and end of the trajectory, respectively.

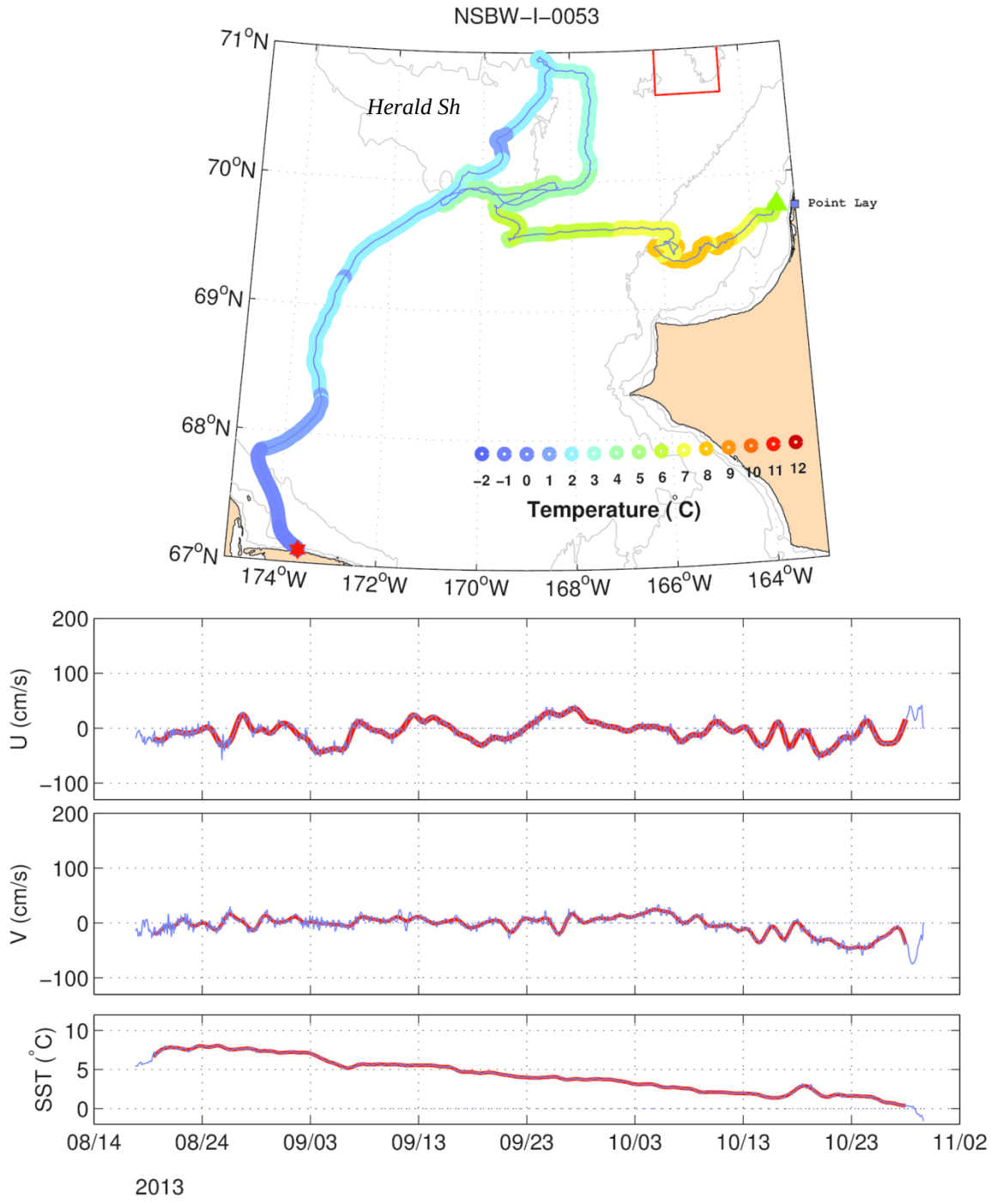

Figure 74. The Pt. Lay Offshore trajectory of MS-53 and the time series of its zonal (U), meridional (V), and sea surface temperature (SST) record. The colors along the drifter trajectory are color-coded according to SST. The green triangle and red star show start and end of the trajectory, respectively. The light lines in the time series are raw data and the heavy red lines are the 35-hour low-pass filtered data.

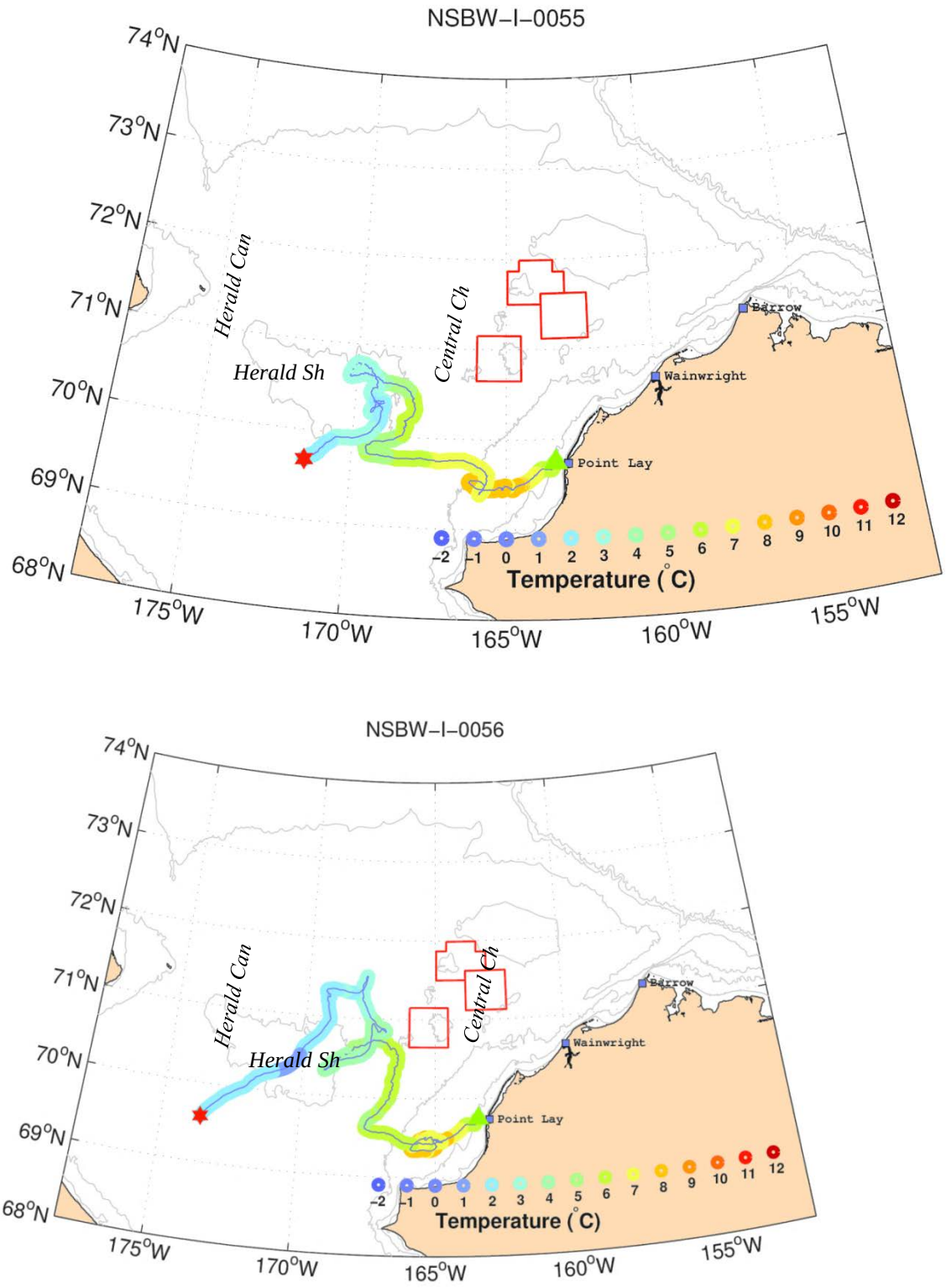

Figure 75. The Pt. Lay Offshore trajectories of MS-55 (top) and 56 (bottom). The colors along the drifter trajectories are color-coded according to SST. The green triangle and red star show start and end of the trajectories, respectively.

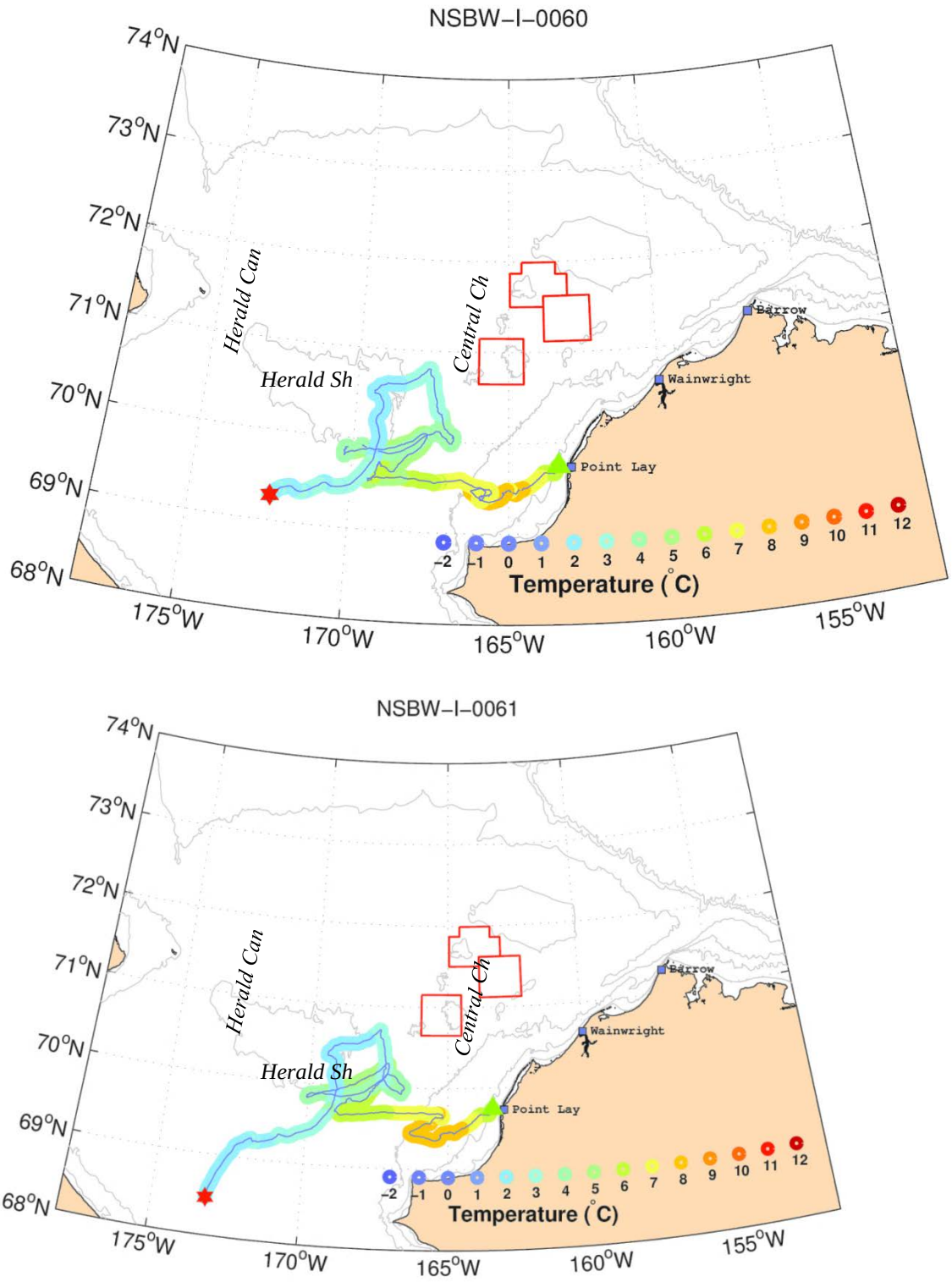

Figure 76. The Pt. Lay Offshore trajectories of MS-60 (top) and 61 (bottom). The colors along the drifter trajectories are color-coded according to SST. The green triangle and red star show start and end of the trajectories, respectively.

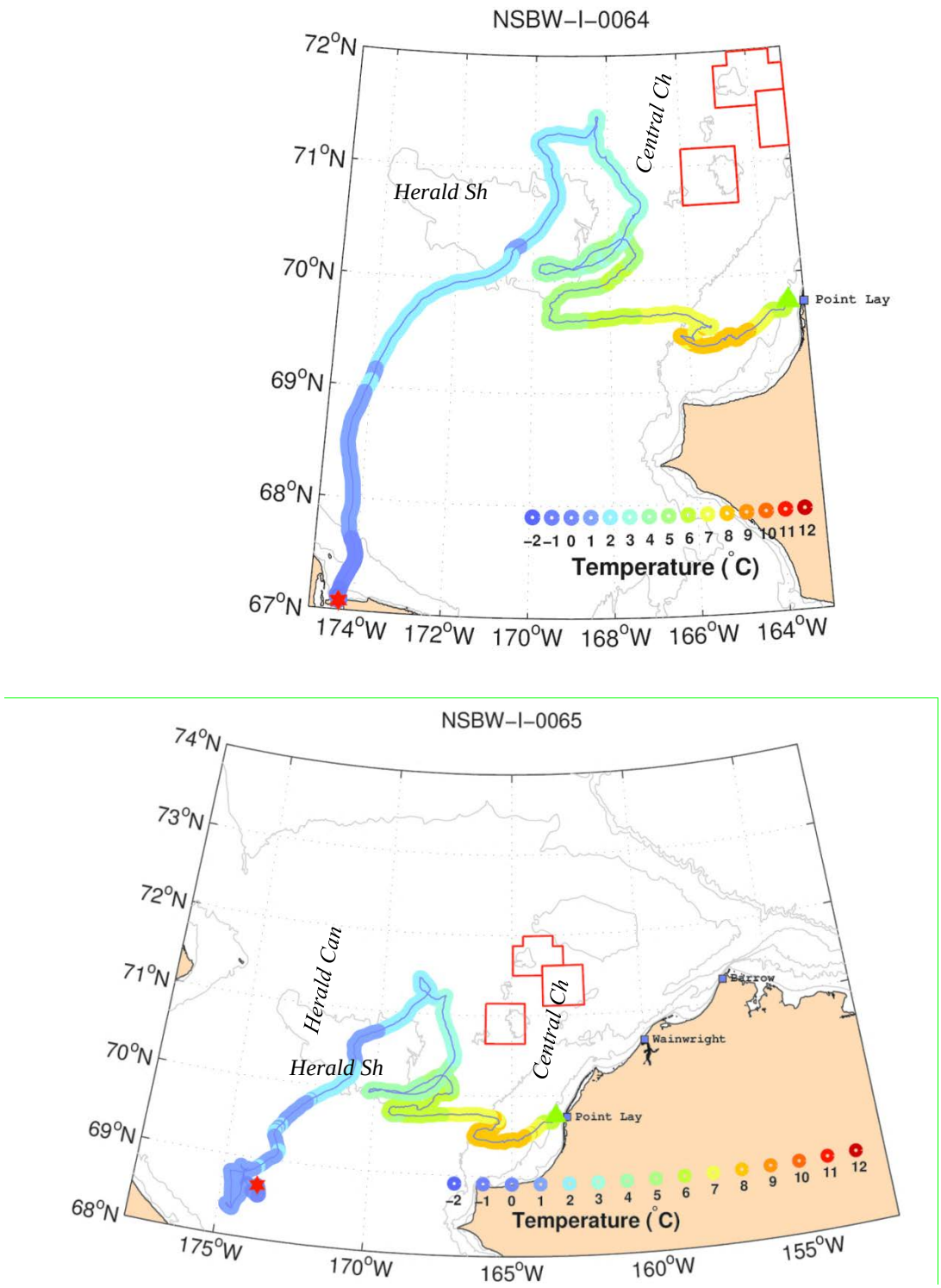

Figure 77. The Pt. Lay Offshore trajectories of MS-64 (top) and 65 (bottom). The colors along the drifter trajectories are color-coded according to SST. The green triangle and red star show start and end of the trajectories, respectively.

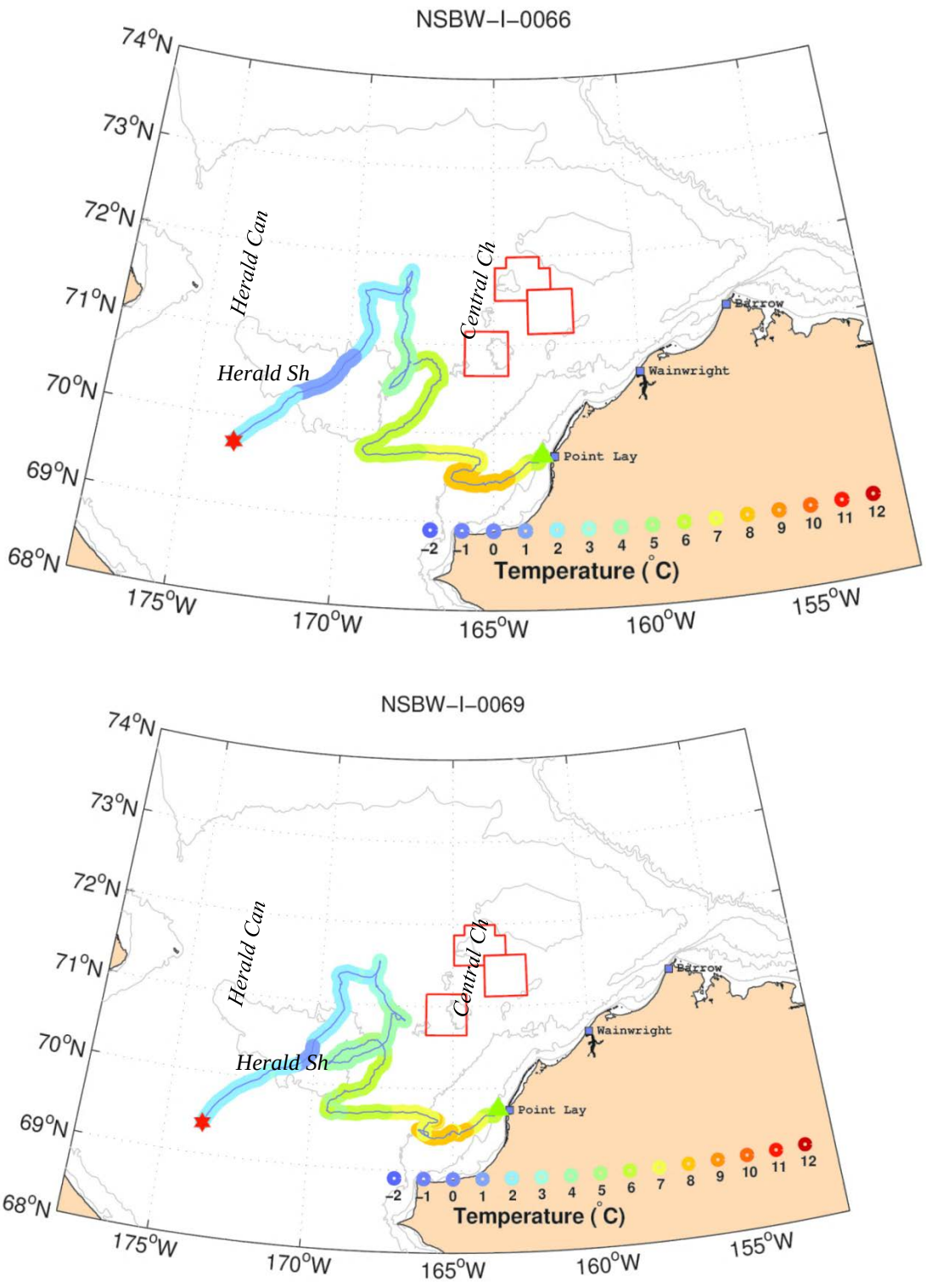

Figure 78. The Pt. Lay Offshore trajectories of MS-66 (top) and 69 (bottom). The colors along the drifter trajectories are color-coded according to SST. The green triangle and red star show start and end of the trajectories, respectively.

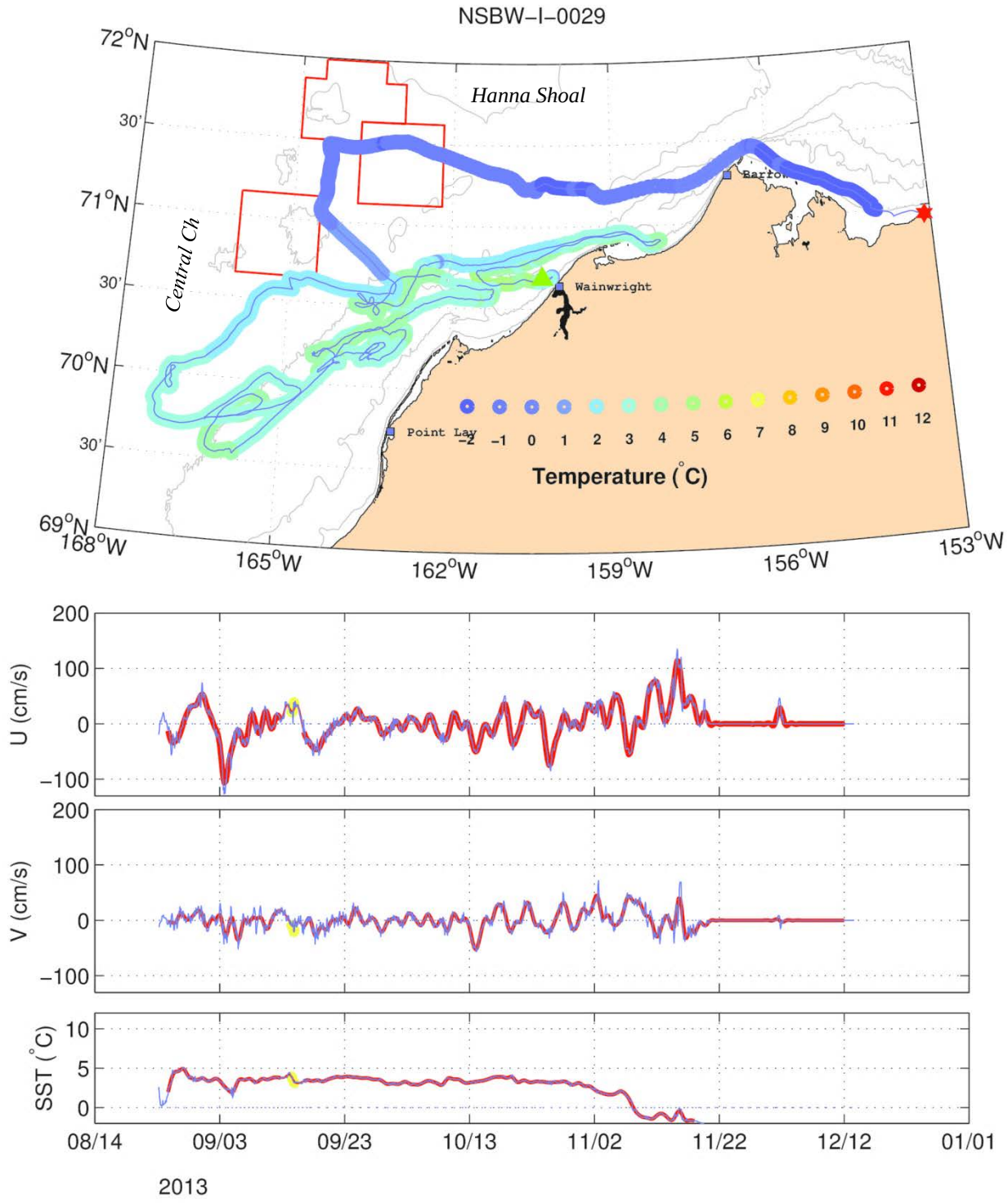

Figure 79. The trajectory of MS-29 and the time series of its zonal (U), meridional (V), and sea surface temperature (SST) record. The colors along the drifter trajectory are color-coded according to SST. The green triangle and red star show start and end of the trajectory, respectively. The light lines in the time series are raw data and the heavy red lines are the 35-hour low-pass filtered data.

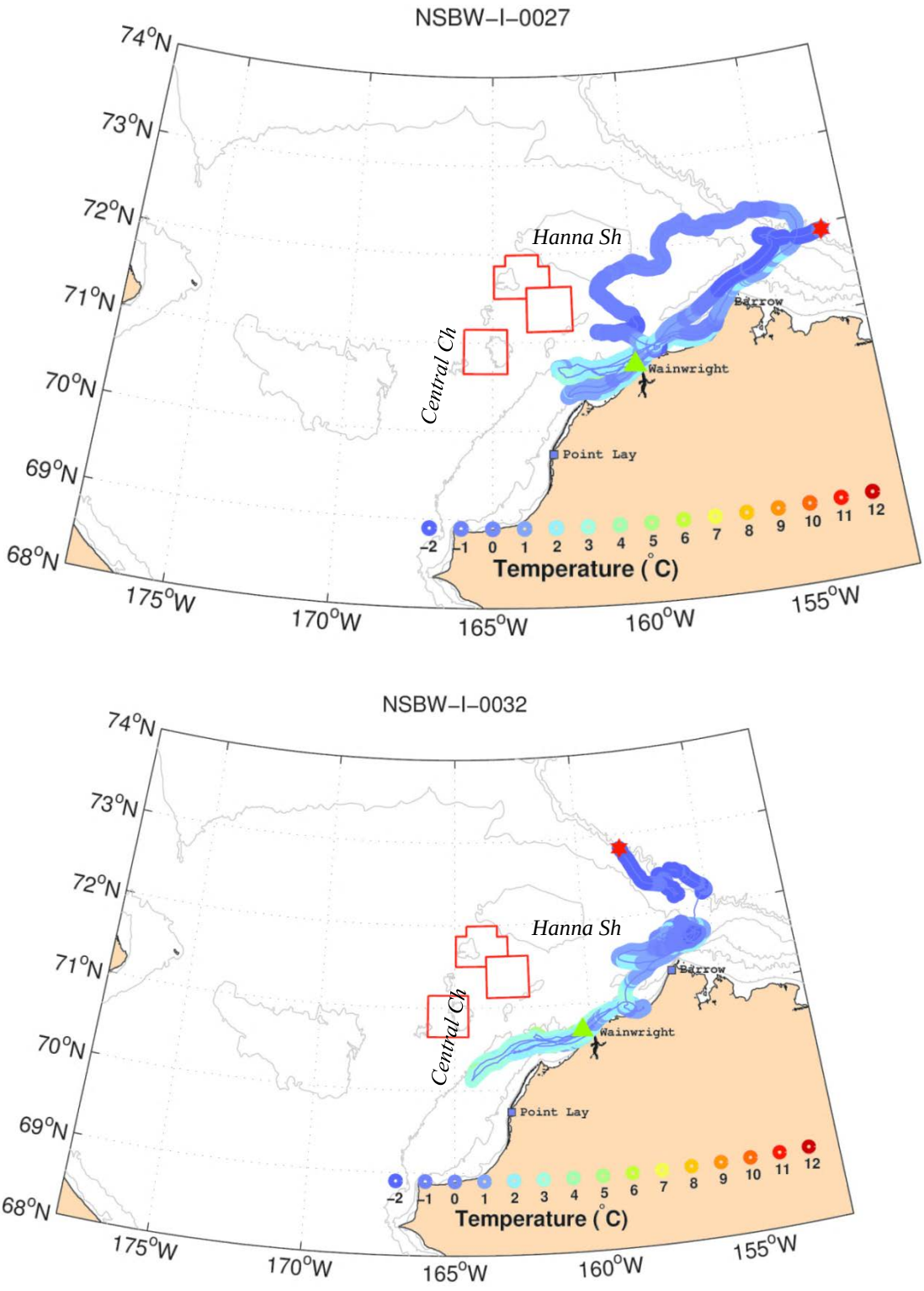

Figure 80. The trajectories of MS-27 (top) and 32 (bottom). The colors along the drifter trajectories are color-coded according to SST. The green triangle and red star show start and end of the trajectories, respectively.

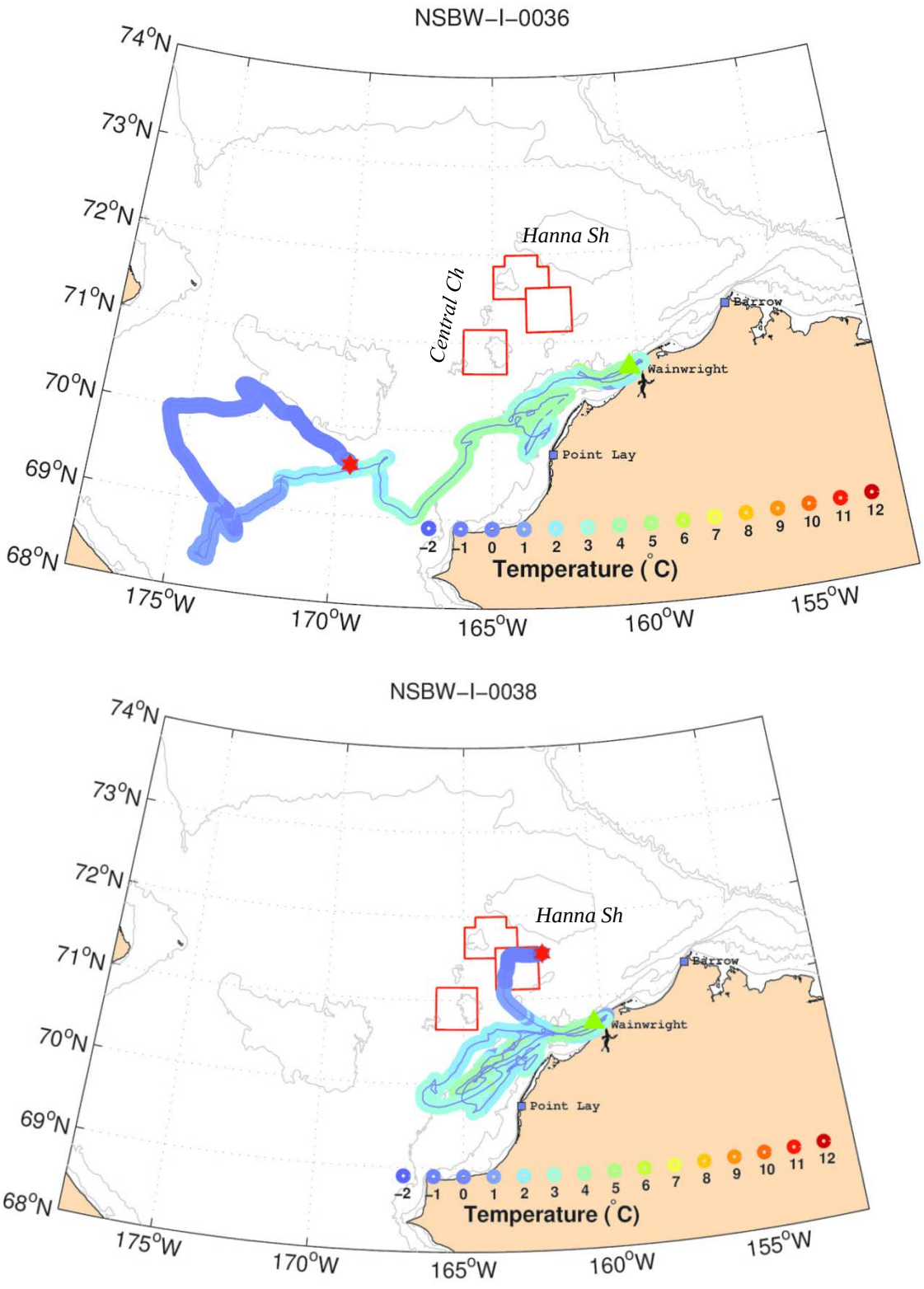

Figure 81. The trajectories of MS-36 (top) and 38 (bottom). The colors along the drifter trajectories are color-coded according to SST. The green triangle and red star show start and end of the trajectories, respectively.

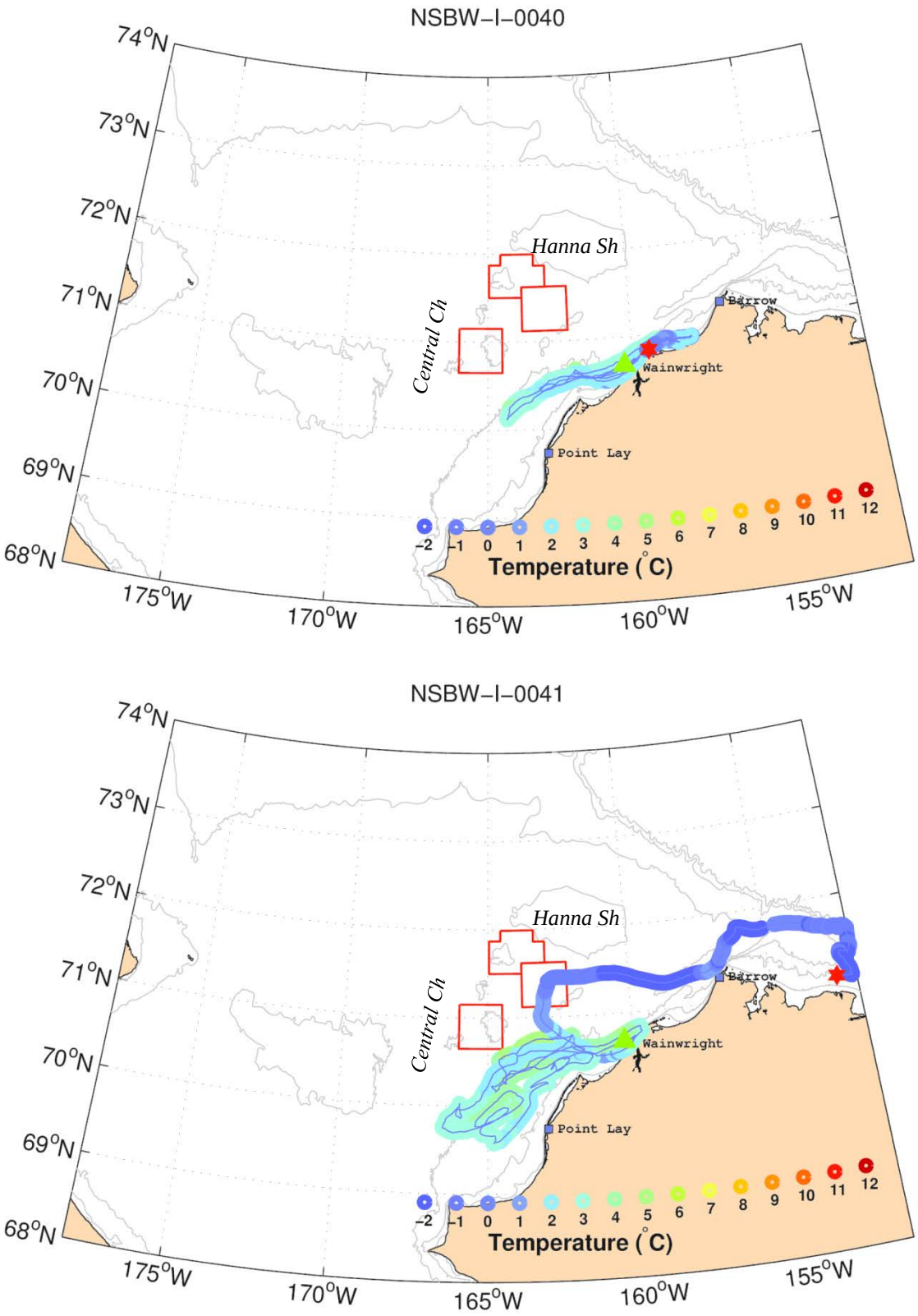

Figure 82. The trajectories of MS-40 (top) and 41 (bottom). The colors along the drifter trajectories are color-coded according to SST. The green triangle and red star show start and end of the trajectories, respectively.

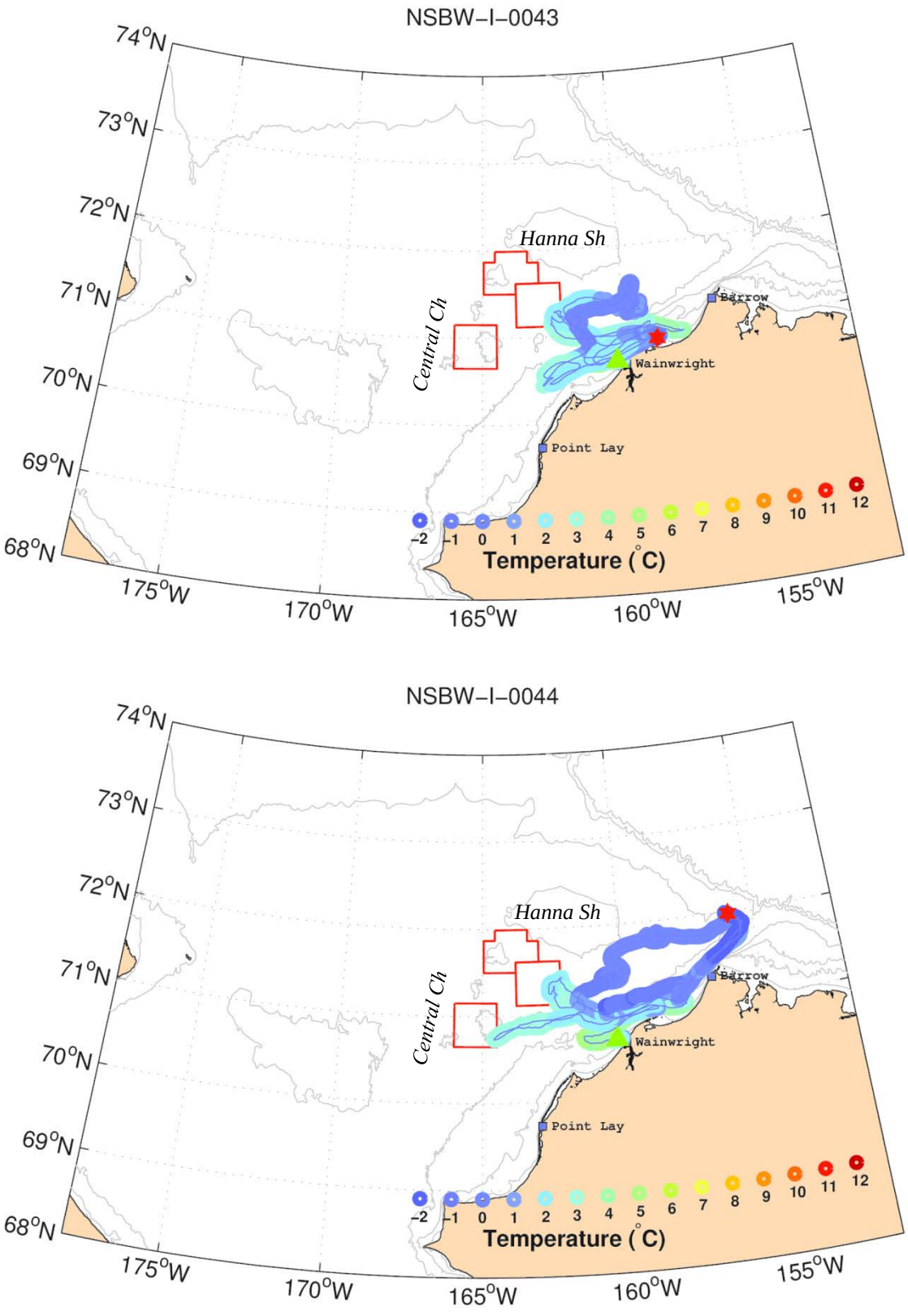

Figure 83. The trajectories of MS-43 (top) and 44 (bottom). The colors along the drifter trajectories are color-coded according to SST. The green triangle and red star show start and end of the trajectories, respectively.

8 September 2013 Deployments: Northeast Hanna Shoal (BOEM)

Ten MS drifters were deployed in a single cluster within a few meters of one another northeast of Hanna Shoal. Their trajectories are shown in **Figures 84 – 89**. Initially all of these drifters moved slowly westward and over Hanna Shoal while remaining close to one another. They crossed the Shoal in early October and then began dispersing. Drifters MS-35, 38, 43 moved southwest toward the Central Channel, and then northward in the Channel to about 72.75^{o}N. Note that this northward excursion within the Channel occurred when winds were from the northeast during the latter half of October. They then turned to the southeast where they either died or were caught in ice. Of interest is that these drifters moved into the middle of the Central Channel before beginning their northward loops. Several others (MS-30, 36, 44, 45) also continued to the southwest after crossing the Shoal, but appear to have adhered to the eastern flank of the Central Channel before drifting to the east. The results suggest that along-channel flow in the Central Channel was sheared; drifters that skirted the eastern side of the Channel separated quickly from those that entered closer to the center of the Channel.

Drifters MS-28, 30, and 35 survived long enough to get trapped in and drift with sea ice. Both MS-28 and 30 drifted with the ice northward through Barrow Canyon and exited to the west of the Canyon along the Chukchi slope. MS-28 continued westward along the slope and outer Chukchi Sea Shelf, then southward in the Central Channel reaching ~72^{o}N by the third week of January. It then drifted westward over the shelf north of Herald Shoal and died in early March 2014. MS-30 underwent a similar excursion except that it returned to its deployment position where it died in the latter half of December.

Drifter MS-35 was among those carried northward in the Central Channel before drifting southeastward across the west side of Hanna Shoal. It entered the ice around 1 December and drifted southwestward at speeds that often exceeded 30 cm s^{-1}. It crossed Herald Shoal around 1 January and then turned southward and died at around 69.25^{o}N in late January.

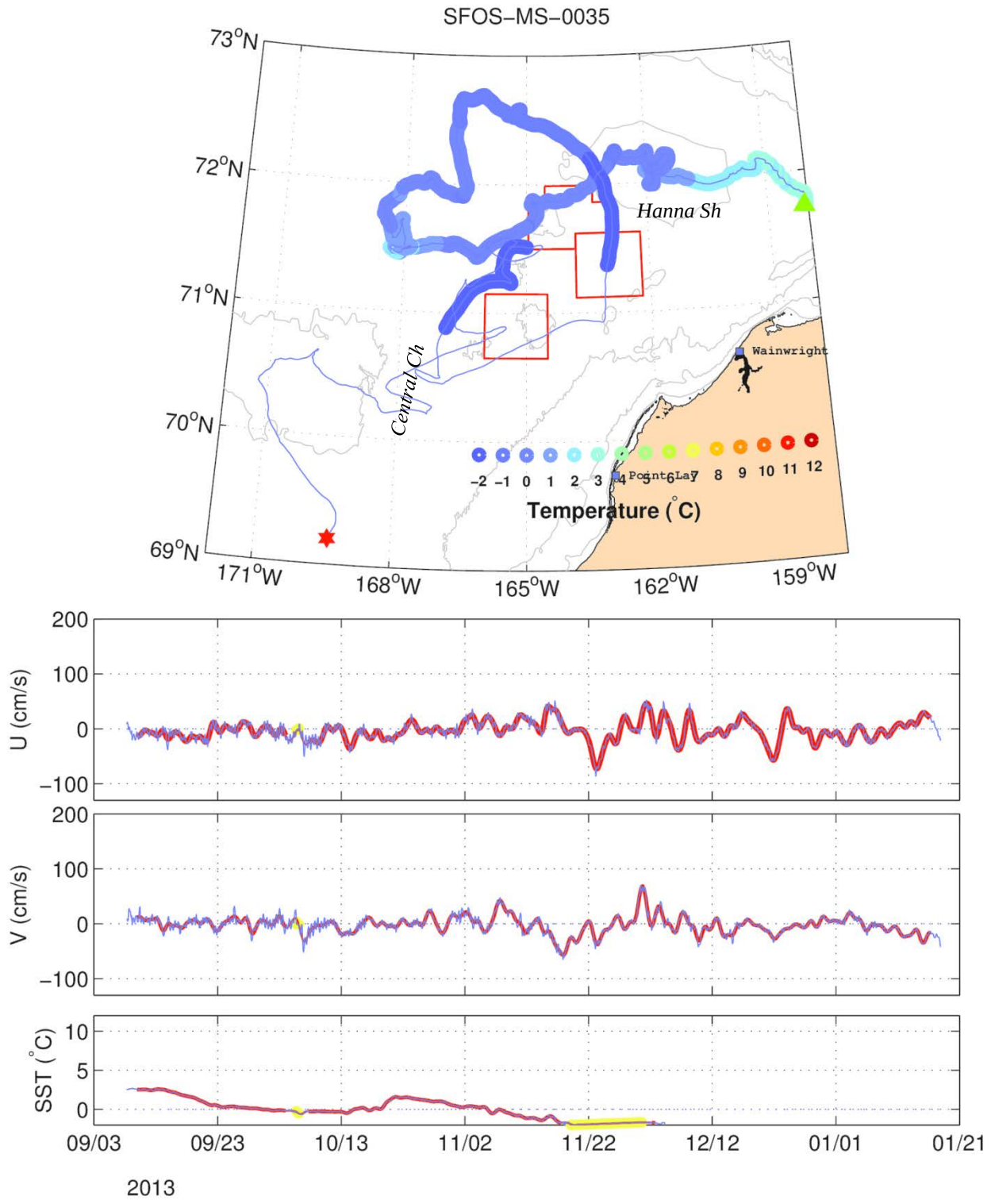

Figure 84. The trajectory of MS-35 and the time series of its zonal (U), meridional (V), and sea surface temperature (SST) record. The colors along the drifter trajectory are color-coded according to SST. The green triangle and red star show start and end of the trajectory, respectively. The light lines in the time series are raw data and the heavy red lines are the 35-hour low-pass filtered data.

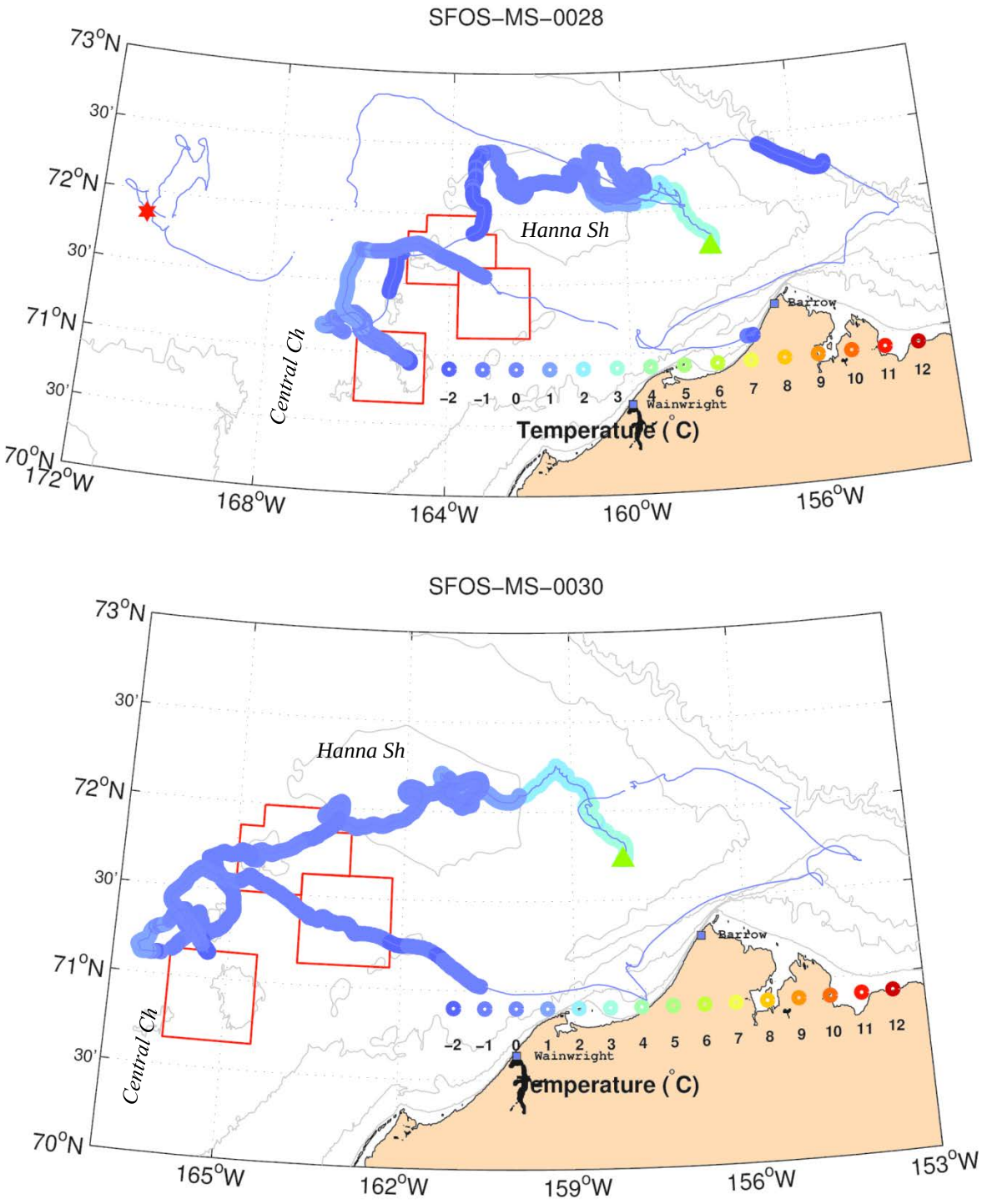

Figure 85. The trajectories of MS-28 and 30. The colors along the drifter trajectories are color-coded according to SST. The green triangle and red star show start and end of the trajectories, respectively.

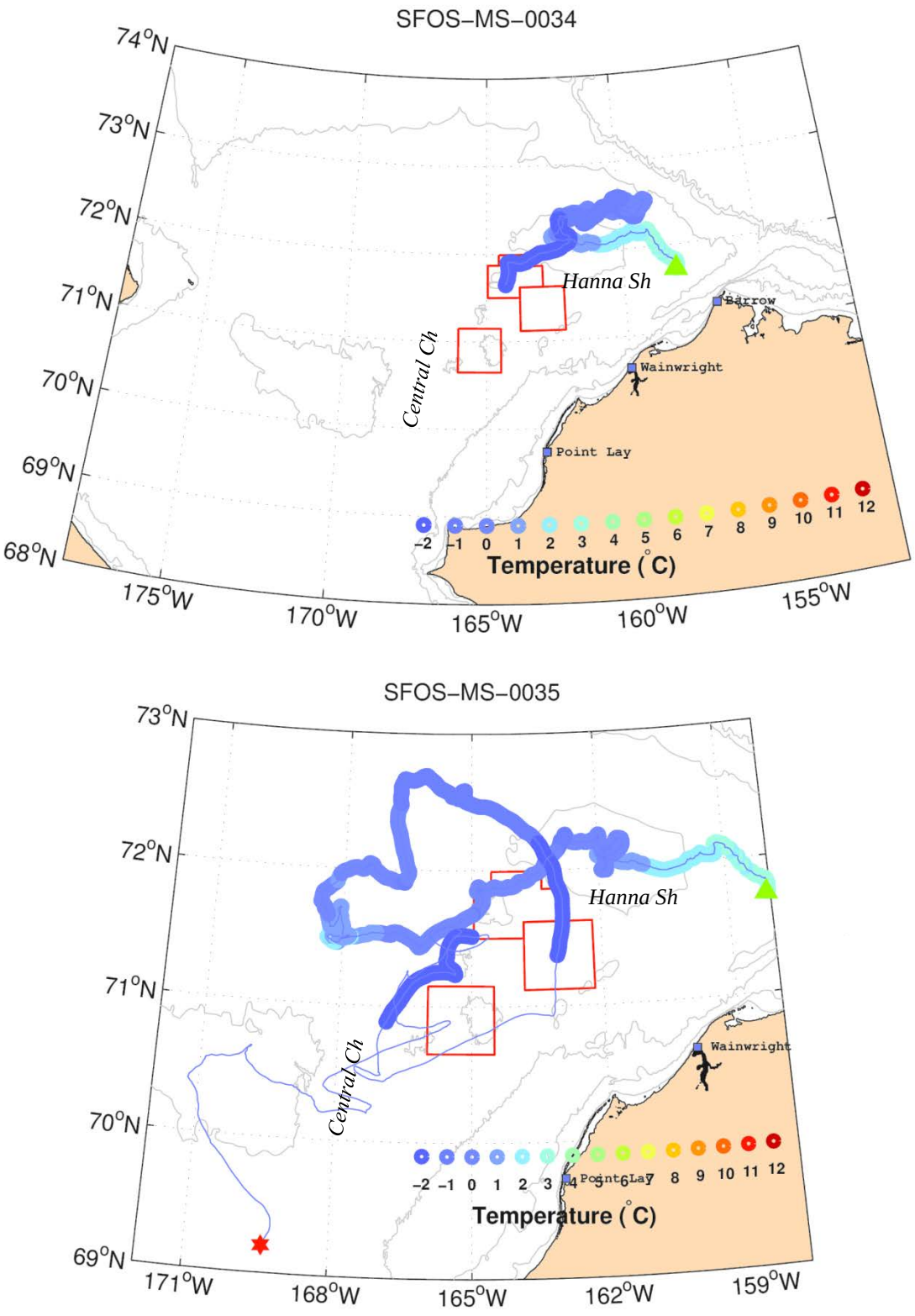

Figure 86. The trajectories of MS-34 and 35. The colors along the drifter trajectories are color-coded according to SST. The green triangle and red star show start and end of the trajectories, respectively.

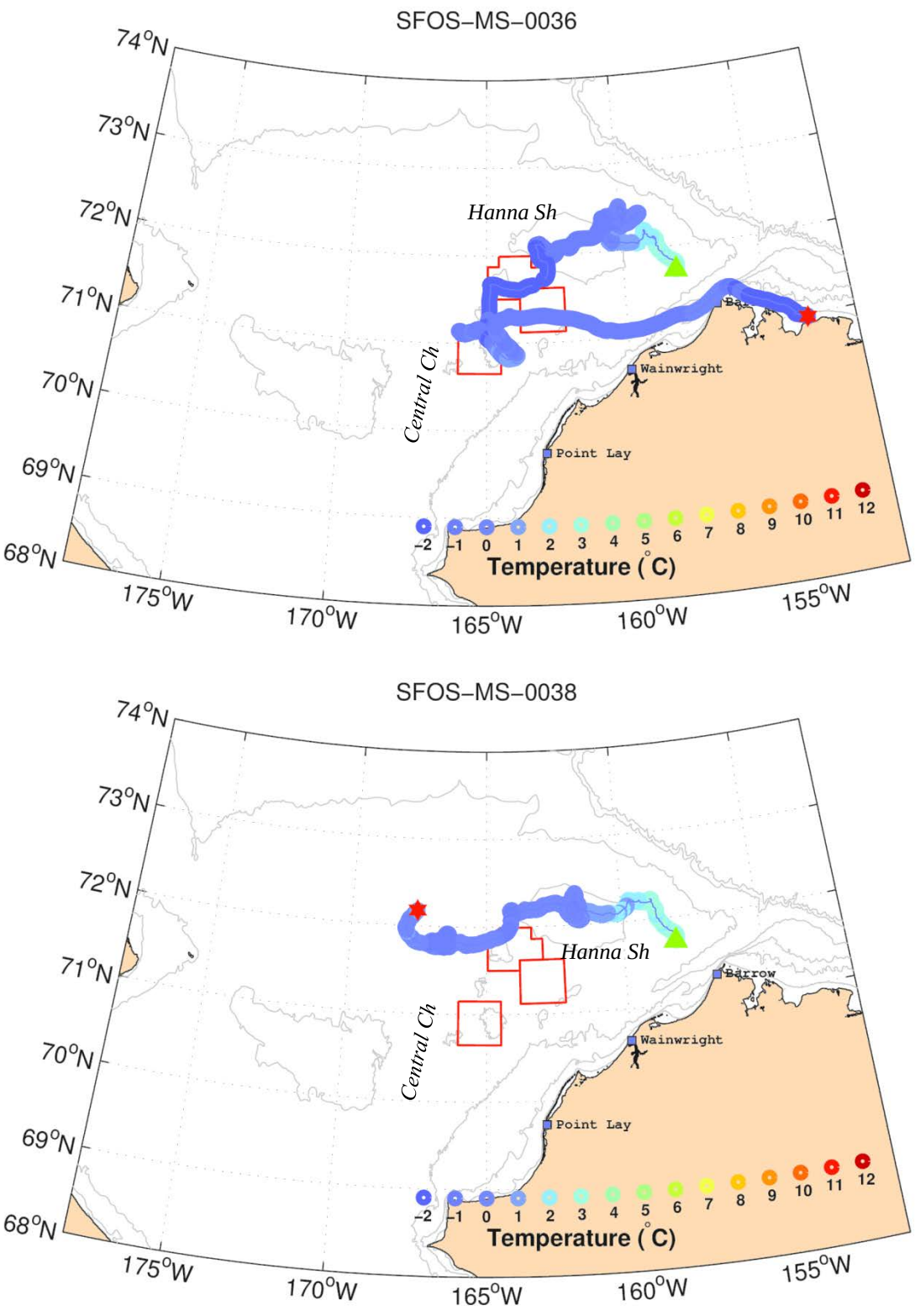

Figure 87. The trajectories of MS-36 and 38. The colors along the drifter trajectories are color-coded according to SST. The green triangle and red star show start and end of the trajectories, respectively.

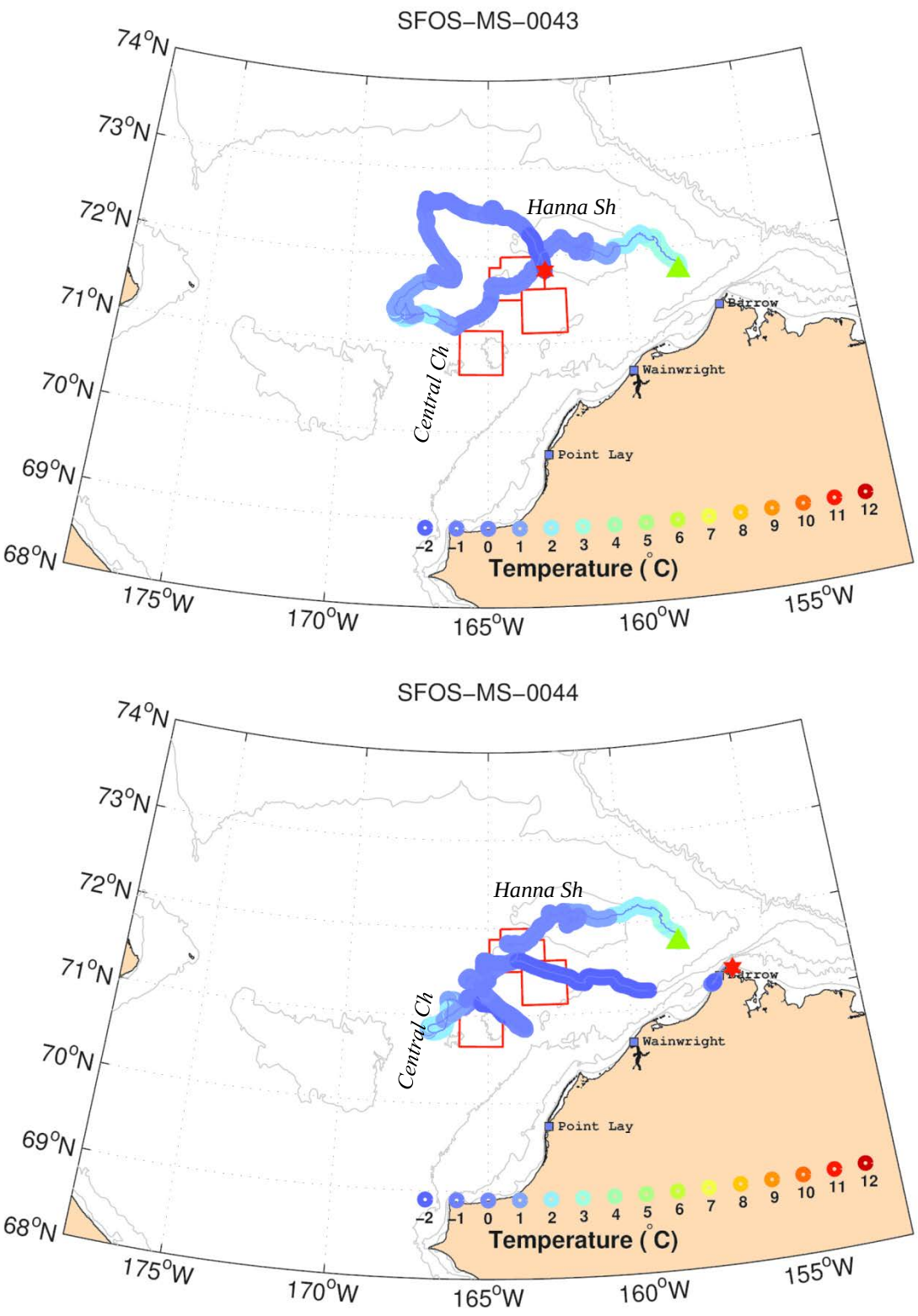

Figure 88. The trajectories of MS-43 and 44. The colors along the drifter trajectories are color-coded according to SST. The green triangle and red star show start and end of the trajectories, respectively.

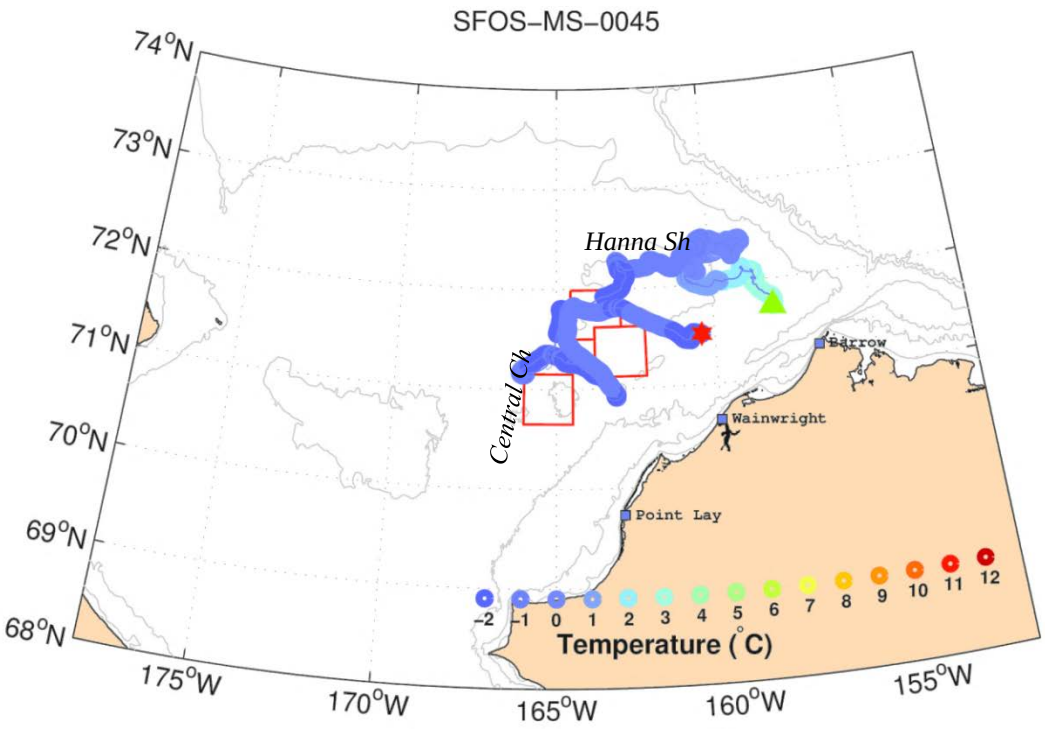

Figure 89. The trajectory of MS-45. The colors along the drifter trajectory are color-coded according to SST. The green triangle and red star show start and end of the trajectory, respectively.

9 September 2013 Deployments: Northwest Hanna Shoal (BOEM)

Eleven drifters were deployed in a single cluster within a few meters of one another northwest of Hanna Shoal. A subset of their trajectories is shown in **Figures 90 – 94**. Initially, all proceeded west-northwestward at speeds of 10 – 30 cm s^{-1}. Most crossed into the Russian EEZ on 4 October and continued westward until about 10 October when they started drifting southwestward into Herald Canyon. All but one (MS-37) entered or crossed to the west side of the canyon and then milled about the middle of the canyon before dying in late October/early November, one drifter (MS-39) moved southward along the west side of the canyon and died to the east of Wrangel Island on 25 October.

Throughout September, SSTs were 0 – 2°C, but decreased to <0°C in early October with minimum SSTs at latitude 73°N; the northernmost portion of the drifts. Based on the sea ice concentrations (**Figure 16**), the drifters were closest to the sea ice during this portion of their trajectories. Afterward, temperatures increased slightly as the drifters moved to the southwest along the western side of Herald Channel.

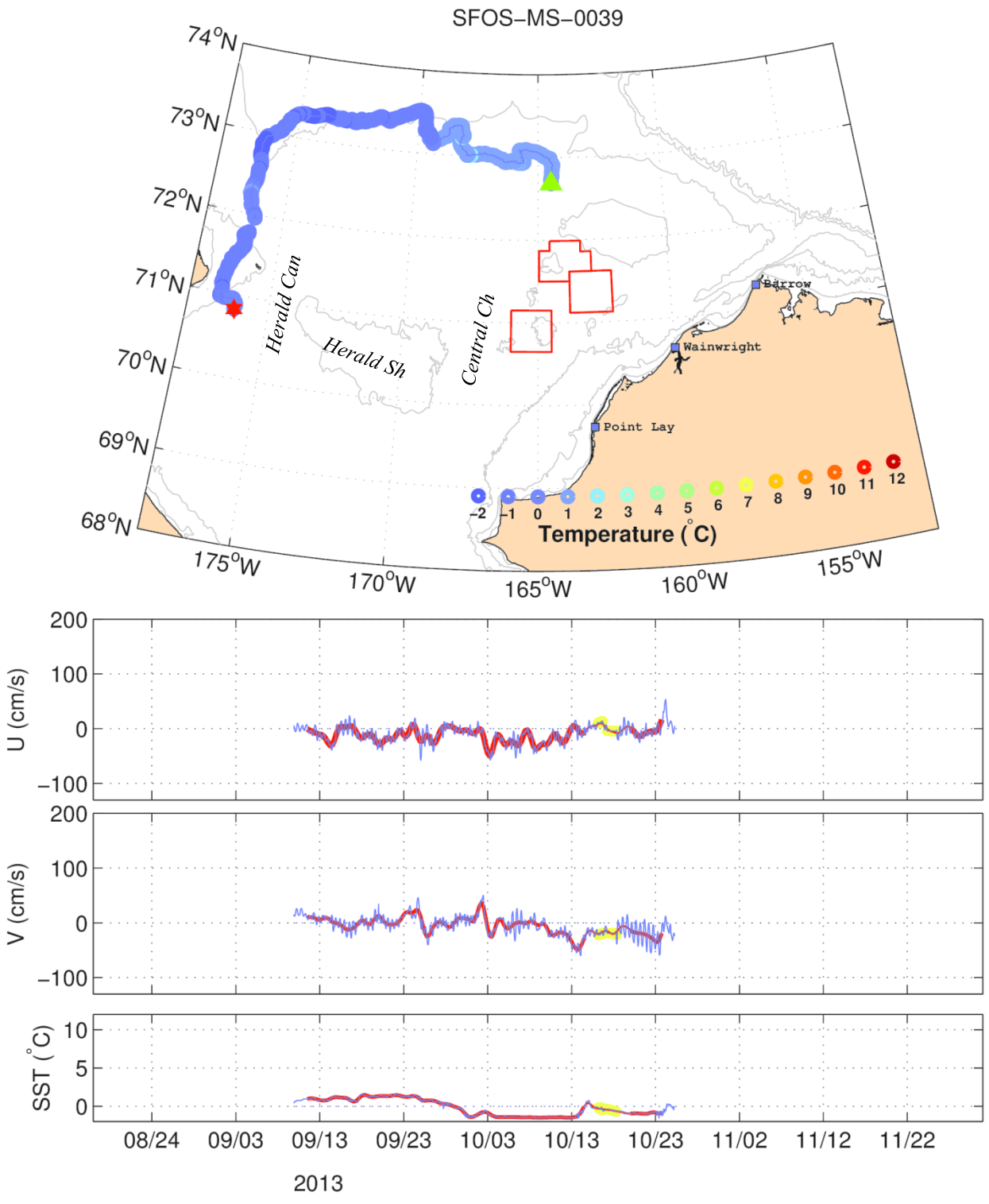

Figure 90. The trajectory of MS-39 and the time series of its zonal (U), meridional (V), and sea surface temperature (SST) record. The colors along the drifter trajectory are color-coded according to SST. The green triangle and red star show start and end of the trajectory, respectively. The light lines in the time series are raw data and the heavy red lines are the 35-hour low-pass filtered data.

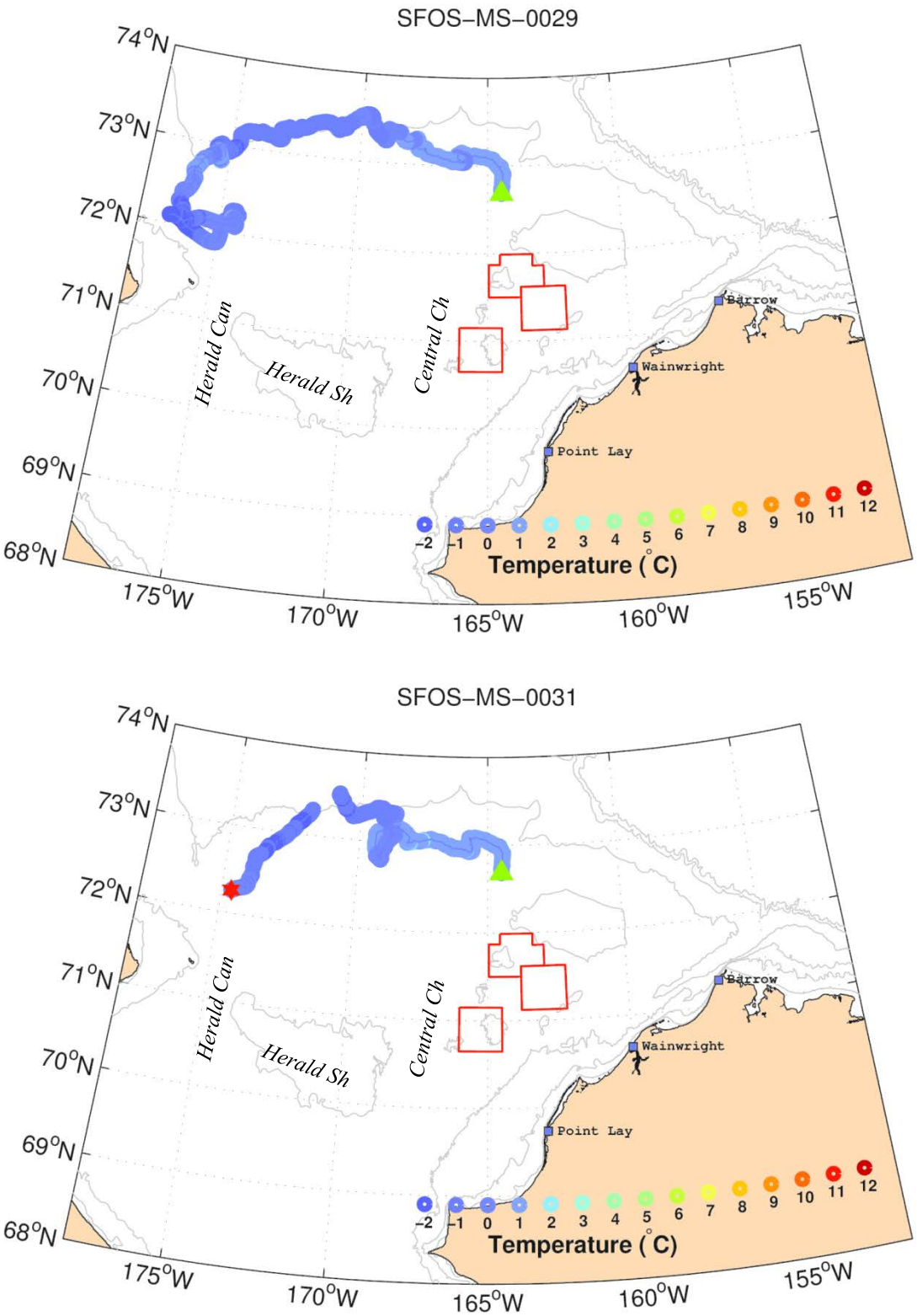

Figure 91. The trajectories of MS-29 (top) and 31 (bottom). The colors along the drifter trajectories are color-coded according to SST. The green triangle and red star show start and end of the trajectories, respectively.

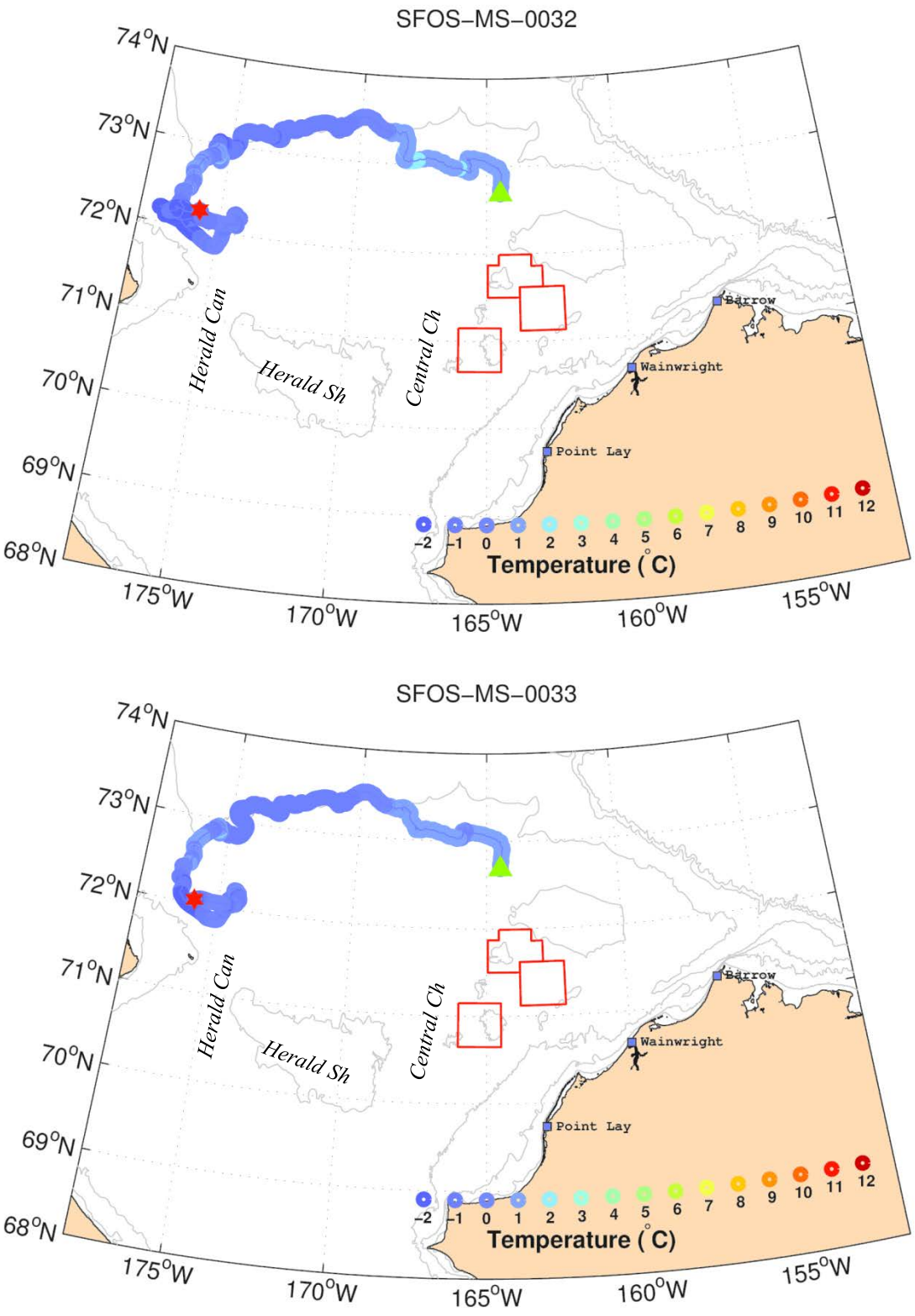

Figure 92. The trajectories of MS-32 (top) and 33 (bottom). The colors along the drifter trajectories are color-coded according to SST. The green triangle and red star show start and end of the trajectories, respectively.

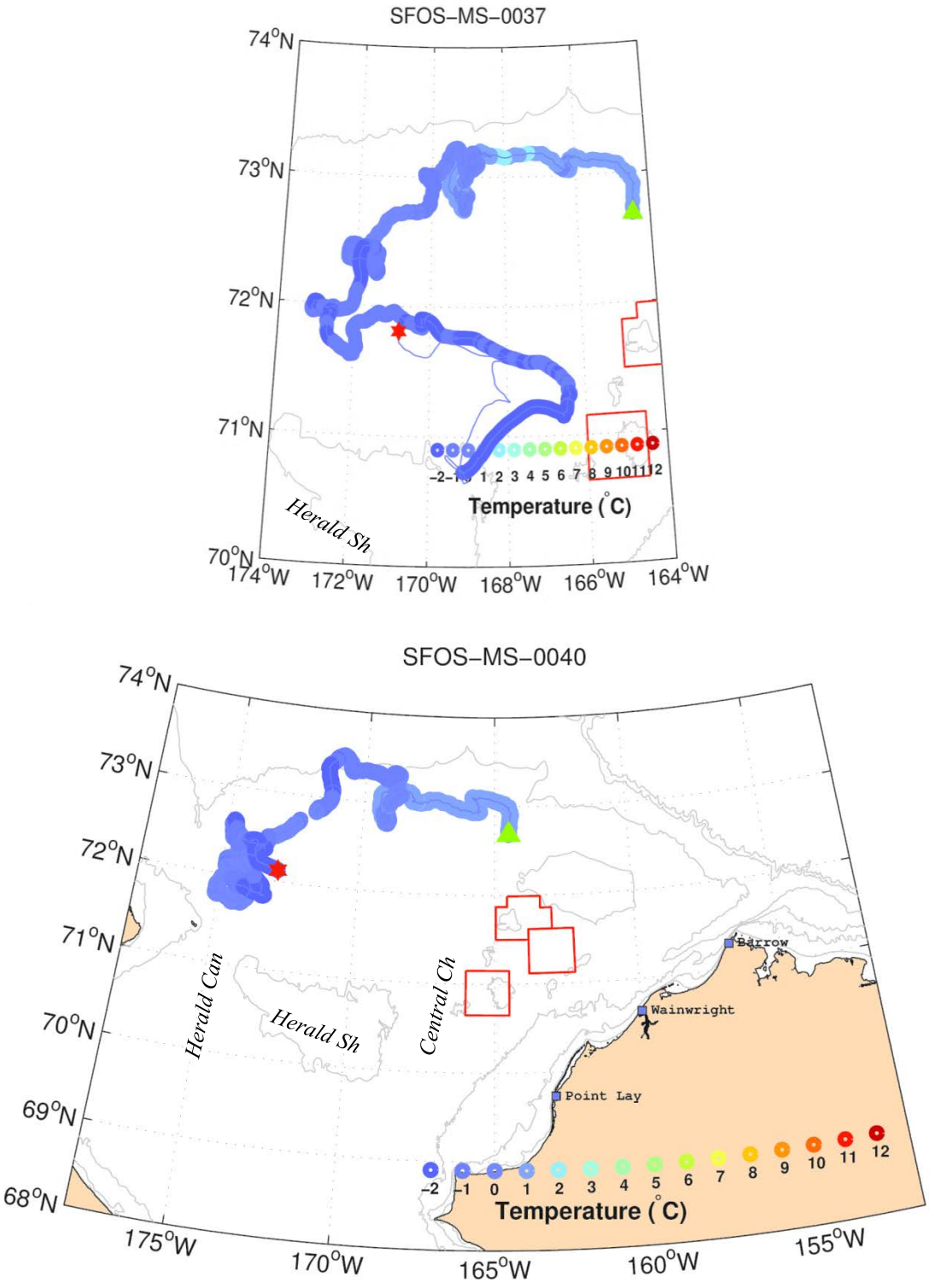

Figure 93. The trajectories of MS-37 (top) and 40 (bottom). The colors along the drifter trajectories are color-coded according to SST. The green triangle and red star show start and end of the trajectories, respectively.

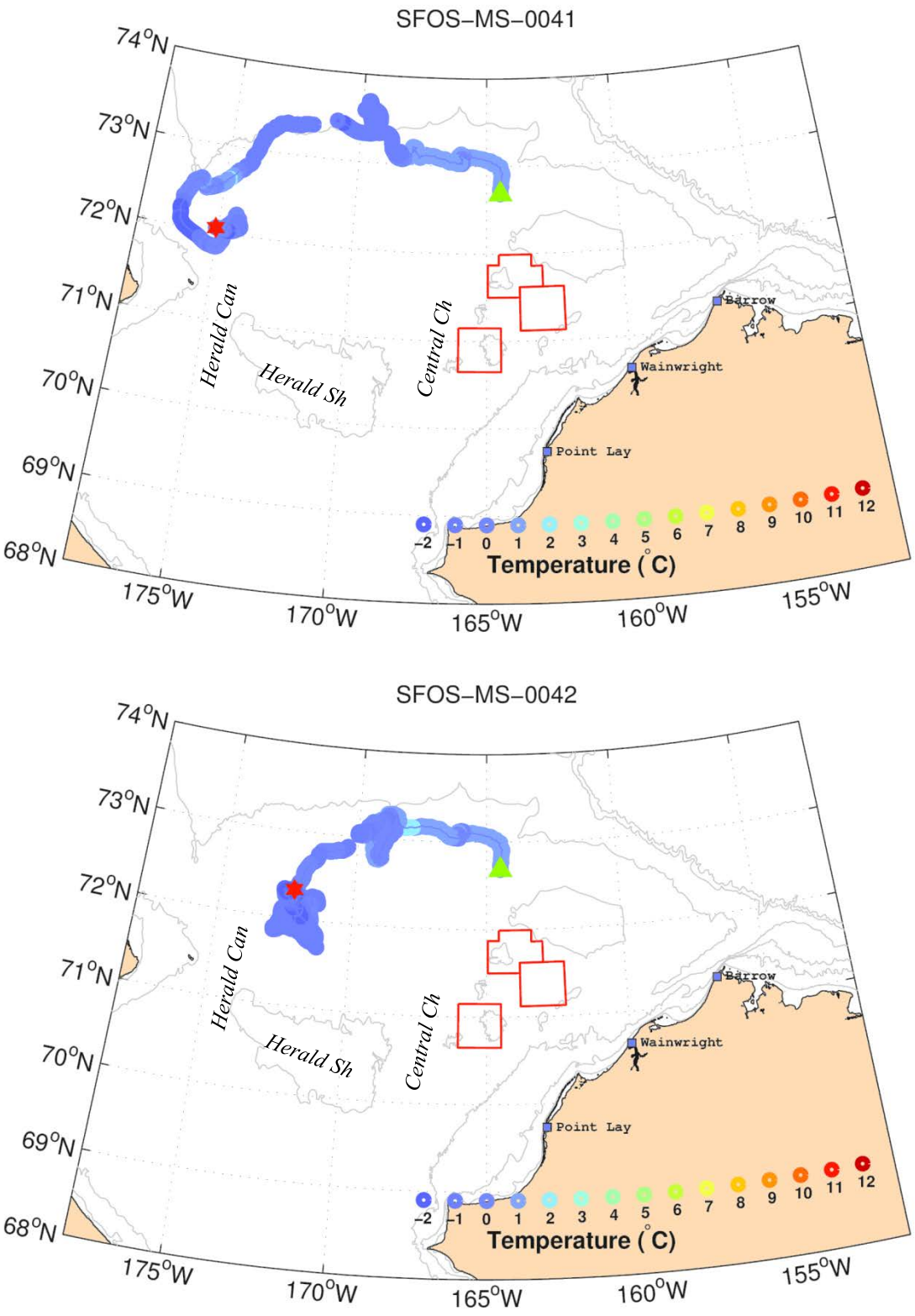

Figure 94. The trajectories of MS-41 (top) and 42 (bottom). The colors along the drifter trajectories are color-coded according to SST. The green triangle and red star show start and end of the trajectories, respectively.

IVe. Relative Dispersion and Kinematics

In this section we examine five drifter clusters in terms of their relative dispersion and kinematical characteristics. These clusters include one from September 2012 that was deployed in Burger (the Burger cluster) and four clusters from 2013. The 2013 clusters are the Pt. Lay Inshore and offshore clusters, and the two clusters from the northeast and northwest sides of Hanna Shoal.

Figure 95 shows the trajectories of all drifters deployed in the Burger cluster on 2 September 2012. The dispersion statistics were computed on this cluster for all drifters that remained west of 161°W, which we adopted as the cutoff longitude for drifters that entered Barrow Canyon. **Figure 96** shows a comparison of the time series between centroid velocities estimated by least-squares ("matrix method") with those computed directly by central-differencing the centroid positions at each time step. This figure also includes time series of the winds throughout the period considered. The least squares approach is in good agreement with the directly computed velocities and supports the validity of the least square estimates. Note the large temporal variability in the velocities, which are largely coherent with the wind variations. Through mid-September, drifter velocities were generally ~0.2 m s^{-1}, but later in the month they increased to between 0.4 m s^{-1} and 0.8 m s^{-1}. The drifters tended to move coherently throughout the region as they gradually spread apart over time.

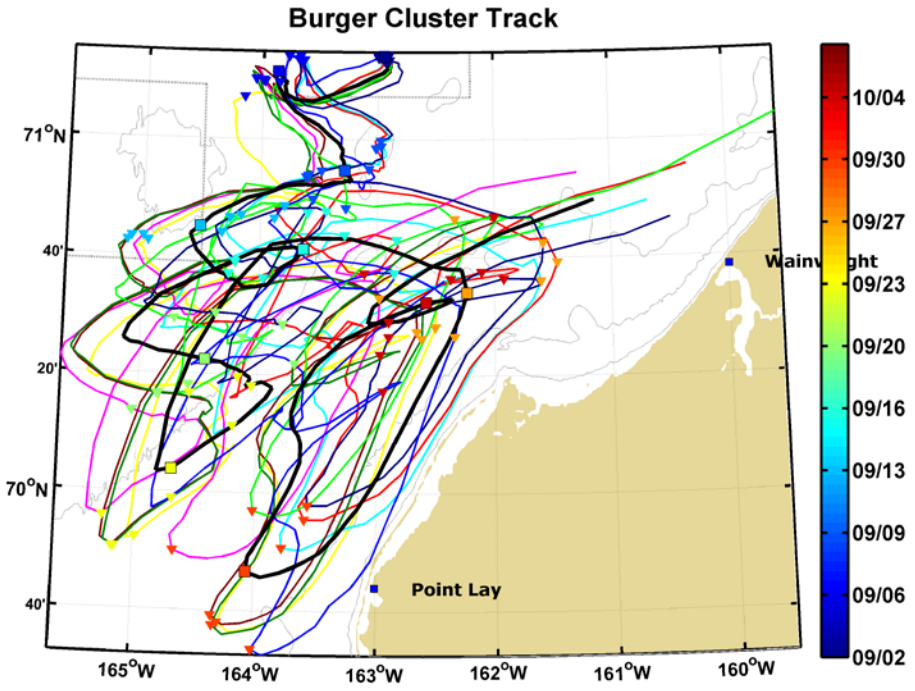

Figure 95. Drifter tracks (color-coded) and cluster centroid (black) for the cluster of drifters deployed in Burger in early September 2012. The color-coded date legend corresponds to the color of the various symbols (triangles for individual drifters and squares for the centroid) along the tracks.

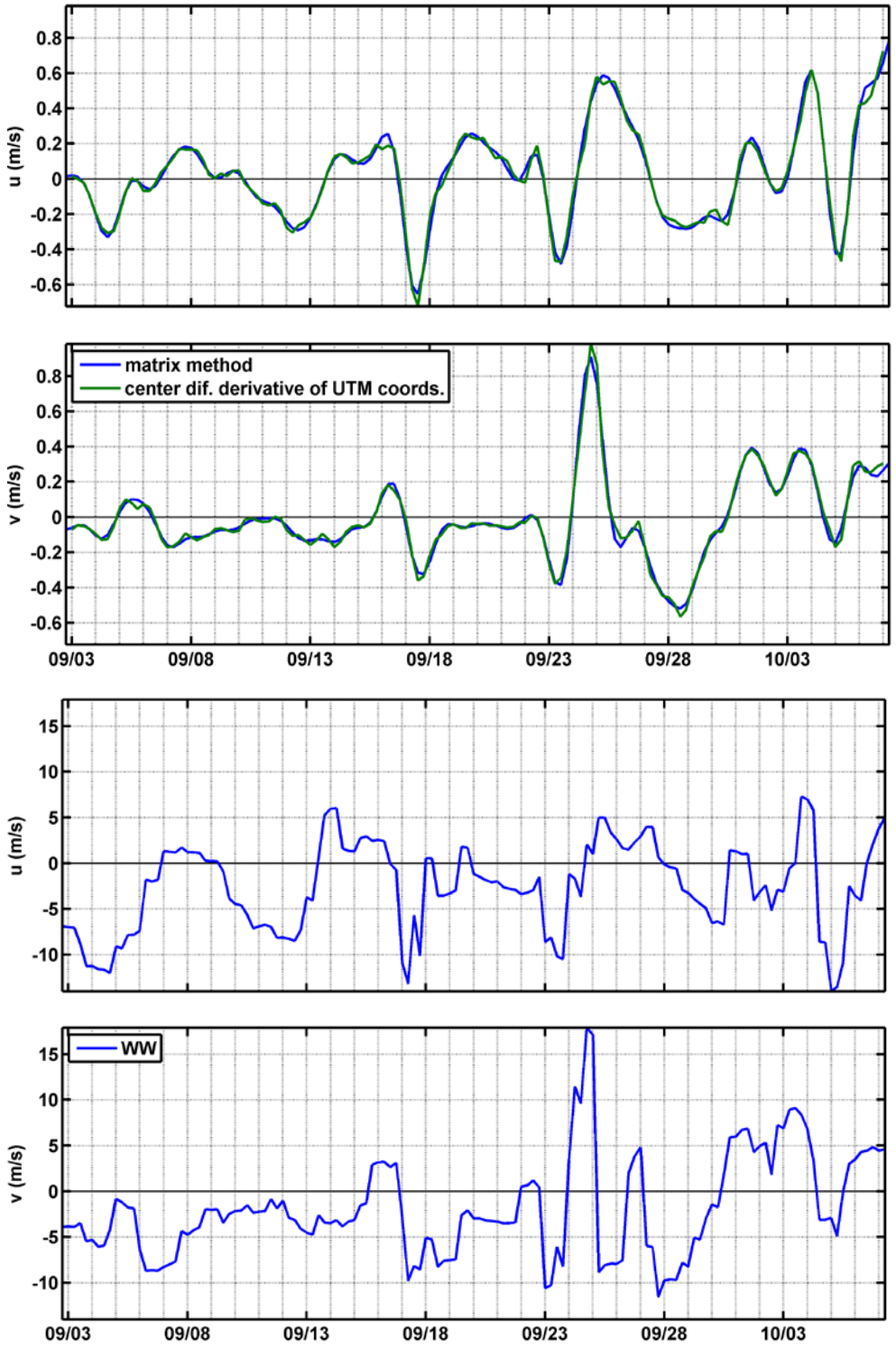

Figure 96. Mean zonal (top) and meridional (2nd from top) Burger drifter cluster centroid velocities and zonal (3rd from top) and meridional (bottom) WaveWatch wind velocities evaluated at the location of the centroid through time. For the drifter velocities, the blue line is based on the least squares solution and the green line is computed by centered differences of the centroid positions divided by the 6-hour time step.

Figure 97 summarizes the results of the relative dispersion components. The time series of D_x^2 (upper left panel) indicates that zonal dispersion increased more rapidly than the meridional dispersion (D_y^2; upper right panel), but then remained fairly constant at ~700 km^2 from 12 September to 3 October. D_y^2 remained fairly small until 24 September when it rapidly increased to ~1000 km^2 during a strong, but short-lived, burst of northward winds. Thereafter D_{xy} settled down to about 700 km^2 and remained at that level through the end of the record. The cross-correlation term (lower left panel), although variable through time, does have several large values. This is consistent the large cyclonic motions on 22 – 24 and 28 – 30 September, and in early October (**Figure 95)**. The relative dispersion (D^2*;* lower right panel) indicates that it remains nearly constant at ~1200 km^2 over most of the record.

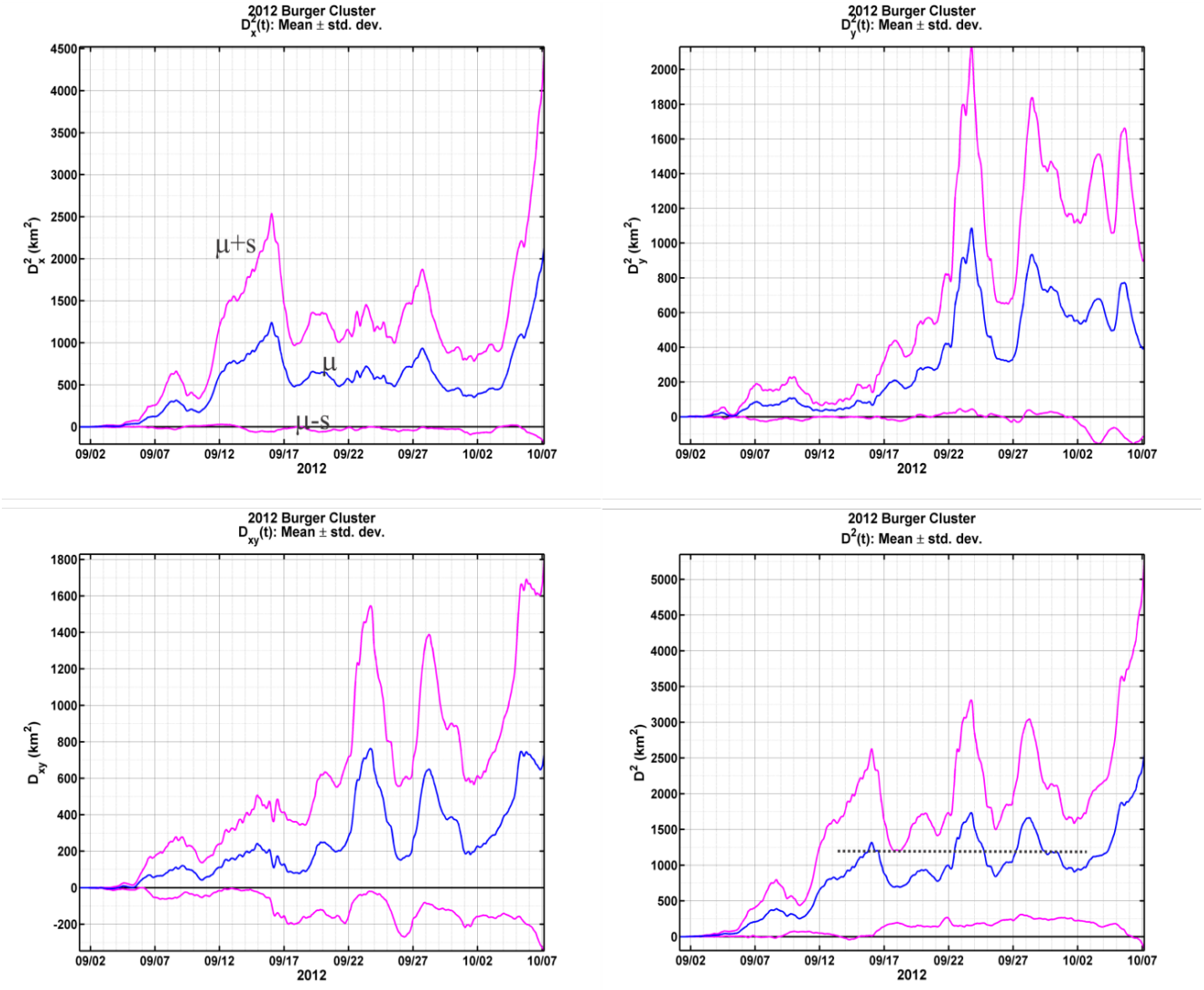

Figure 97. Time series of relative zonal (top left) and meridional (top right) dispersion, the cross-correlation in relative dispersion (bottom left), and the relative dispersion (bottom right) for the Burger drifter cluster.

Time series of the terms in the deformation tensor are shown in **Figure 101**. On average these are small (< 10^{-5} s^{-1}), but on occasion can be quite large. For example, both positive (counter-clockwise or cyclonic) and negative (clockwise or anticyclonic) relative vorticities ~ 2 x 10^{-5} s^{-1} (~20% the value of the Coriolis or planetary vorticity) occur early in the time series. These relative vorticity values imply a Rossby number of ~0.2, suggesting that non-linear motions may be important at these spatial scales. Of particular note is that all of these terms are much smaller after about 8 September. Recall (**Figures 60 – 65**) that shortly after deployment, these drifters detected a strong SST gradient associated with a MW/BSW zonally-oriented front present in Burger (**Figure 17**). The horizontal divergence term increases abruptly on 13 September coincident with an increase in zonal divergence, and the pulse-like changes in the meridional dispersion between 22 and 29 September are accompanied by relatively large changes in the associated vorticity, shearing, and stretching terms.

The absolute vorticity balance (**Figure 99**) indicates that the rate of change of absolute vorticity tends to compensate the stretching vorticity term, but not completely, which implies the presence of vorticity sources/sinks. The mechanism of these sinks or sources is not clear, but it is unlikely that they are due to small horizontal scale variations in surface wind stress, since wind-stress variations occur on much larger scales, typically hundreds of kilometers. Baroclinic instabilities (discussed in relation to **Figure 27)** are possible sinks/sources of vorticity.

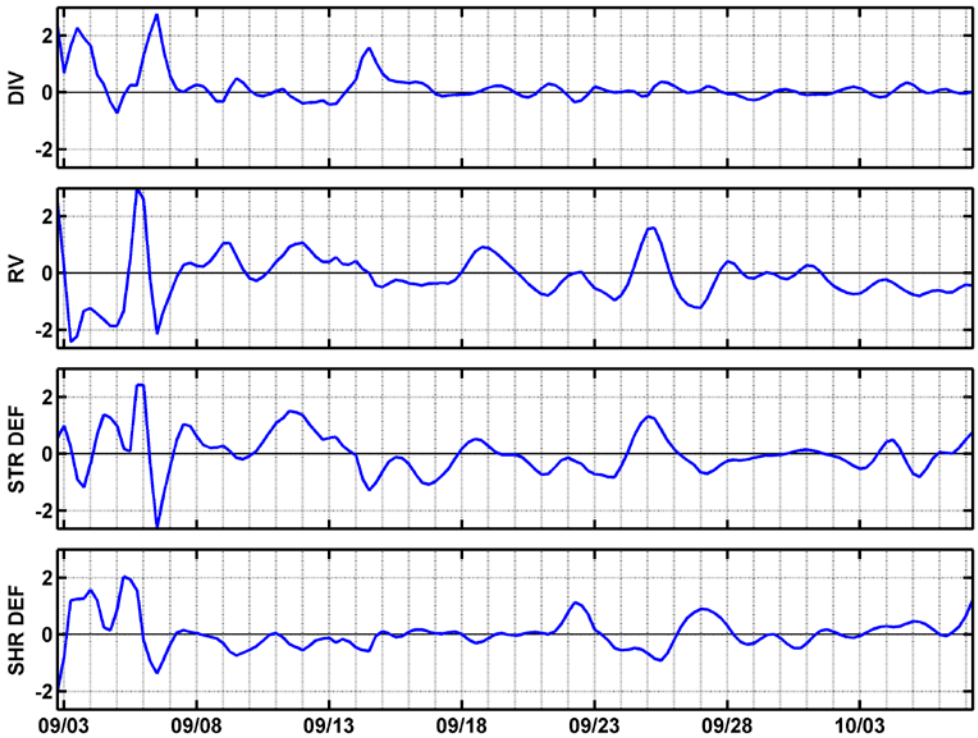

Figure 98. Time series of the horizontal divergence (top), relative vorticity (2nd from top), stretching deformation (3rd from top), and shearing deformation (bottom) for the 2012 Burger drifter cluster. Units are $10^{-5}s^{-1}$.

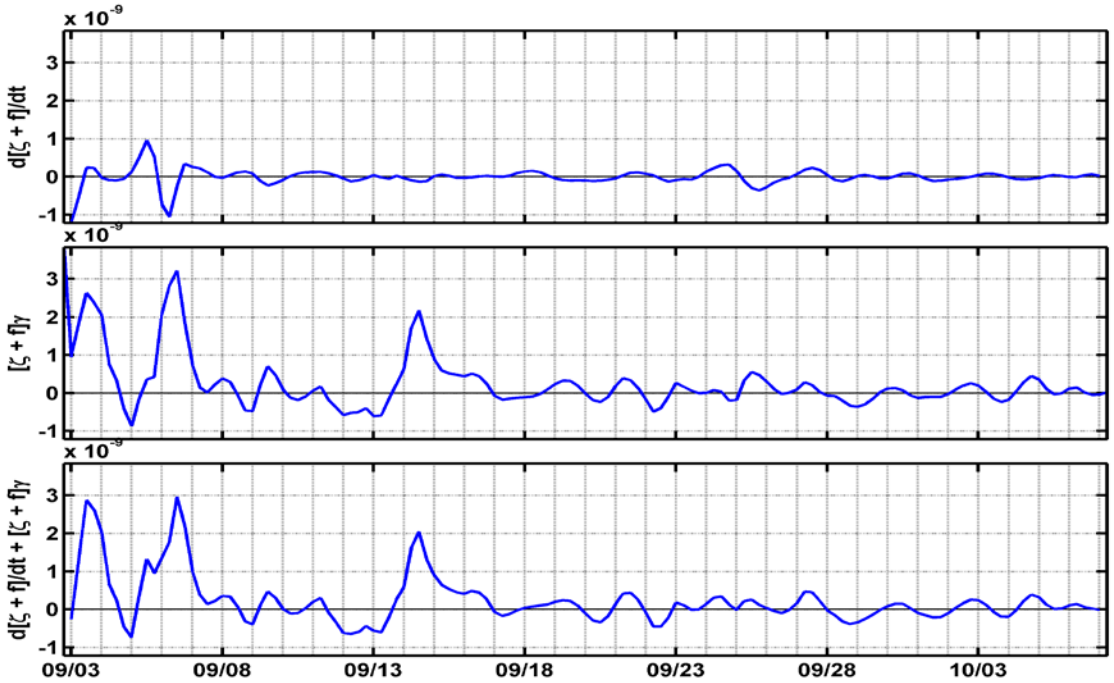

Figure 99. Time series of the terms comprising the absolute vorticity balance for the Burger drifter cluster. Units are s^{-2}.

We next consider the Pt. Lay Inshore and Offshore clusters **(Figures 100 and 101,** respectively**)** that were deployed in August 2013. We discuss both clusters together because they have similar features. The drifters remained tightly clustered as they drifted eastward from 19 August until approximately 11 September even though strong northeasterly winds dominated the first 20 days of the deployment. The winds then varied from southwesterly to northeasterly and the drifters began to disperse rapidly. Nevertheless, throughout the cluster lifetime, the drifter trajectories were coherent with one another. **Figures 102 and 103** show the centroid velocities for both clusters and the time series of the winds throughout the cluster's records. The temporal variation in centroid velocities were large and, to some degree, coherent with variations in the wind velocities. Note, however, that some of the large meridional wind speeds early in the record are not reflected in the meridional currents. In particular, the drifters moved northward between about 27 August and 13 September when they entered the Central Channel, even though winds at this time were mainly northeasterly at 5 – 10 m s^{-1}. The brief southward drift on ~20 September was associated with strong northerly winds. These winds caused the flow in the Central Channel to reverse southward, but the currents swiftly became northward again when the winds relaxed.

The dispersion results for the Pt. Lay clusters (**Figures 104 and 105**) indicate that little dispersion occurred as they drifted westward over the first 10 days or so of the deployment. Zonal dispersion was small until 3 September and then grew to ~3 – 4000 km^2 by 11 September. It increased slowly to ~4 – 5000 km^2 by early October and to ~8000 km^2 by mid-October. Meridional dispersion began around 11 September and remained small through late September as the drifters began their initial northward movement into the Central Channel. By late September the meridional (and total) dispersion increased rapidly to ~10000 km^2.

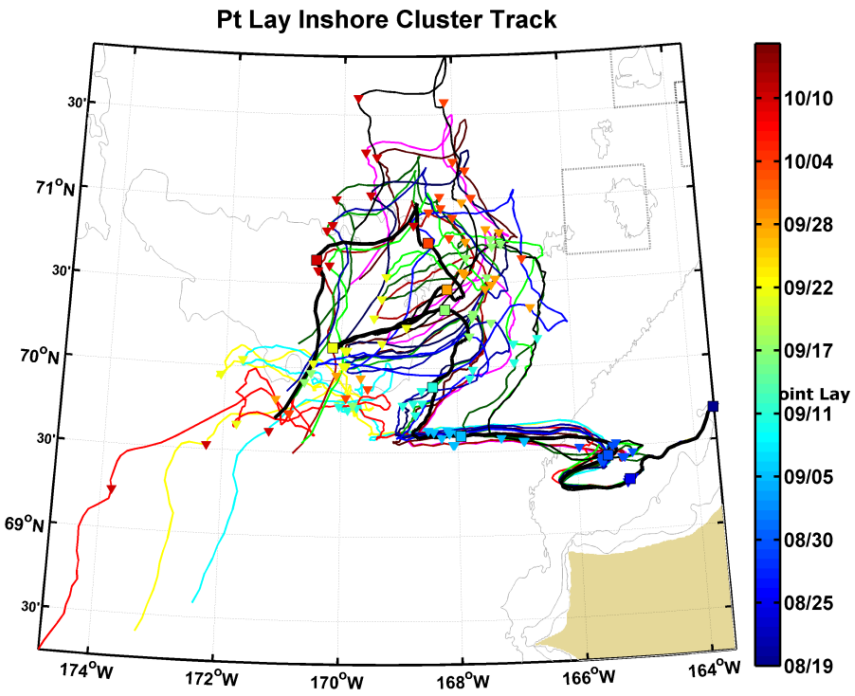

Figure 100. Mean cluster trajectory and individual drifter tracks for the Pt. Lay Inshore drifter cluster. The inverted triangles are color-coded by date and apply to individual drifter trajectories (in color) and the black line is the mean trajectory with dates indicated by color-coded squares.

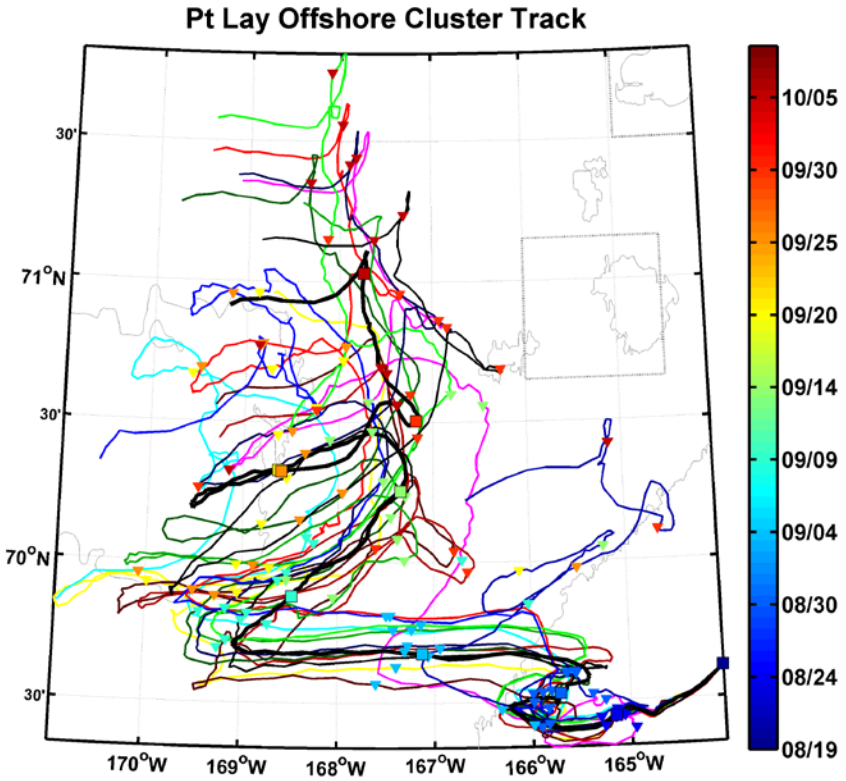

Figure 101. Mean cluster trajectory and individual drifter tracks for the Pt. Lay Offshore drifter cluster. The inverted triangles are color-coded by date and apply to individual drifter trajectories (in color) and the black line is the mean trajectory with dates indicated by color-coded squares.

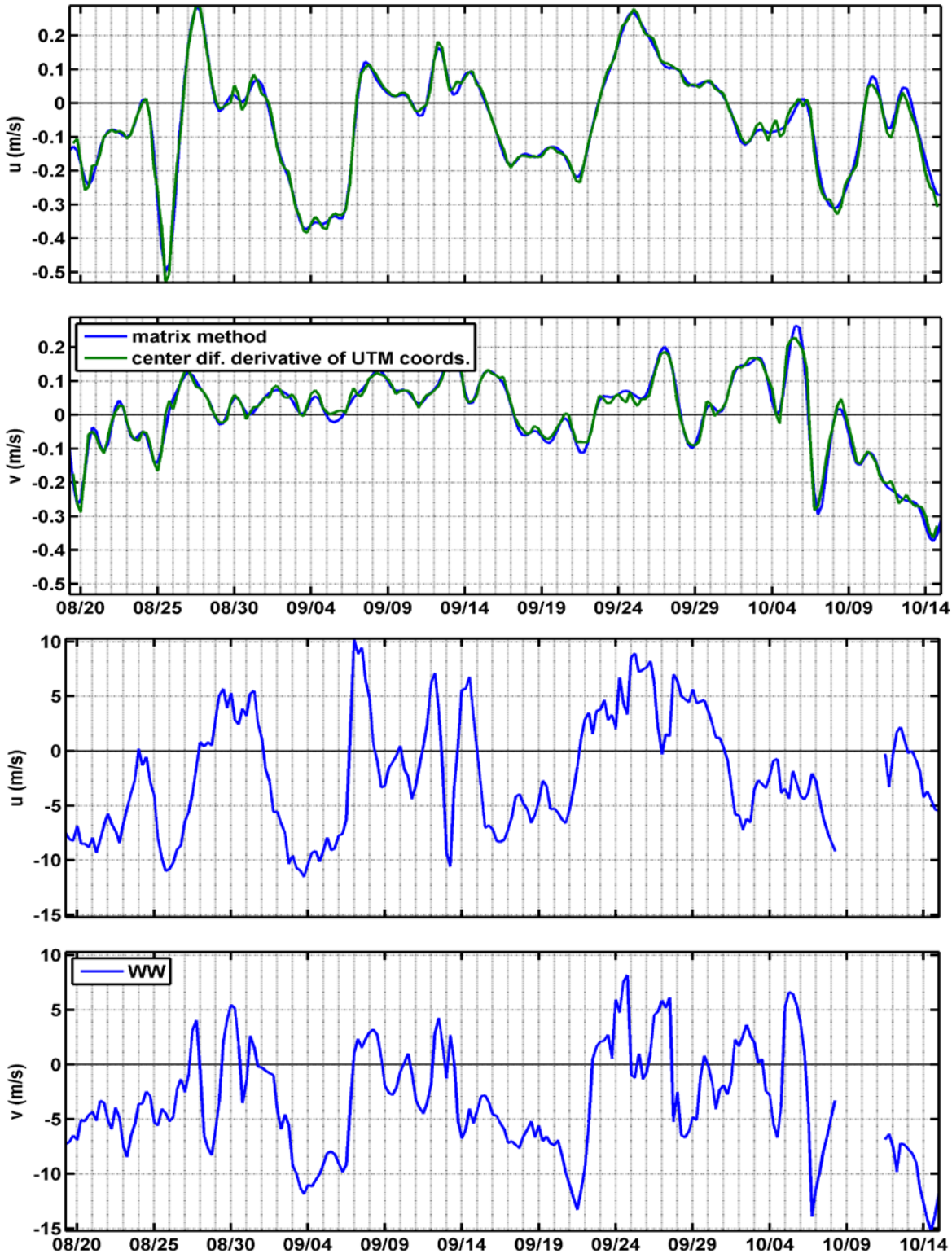

Figure 102. Mean zonal (top) and meridional (2nd from top) Pt. Lay Inshore drifter cluster centroid velocities, and zonal (3rd from top) and meridional (bottom) WaveWatch wind velocities evaluated at the location of the centroid through time. For the drifter velocities the blue line is based on the least squares solution and the green line is computed by centered differences of the centroid positions divided by the 6-hour time step.

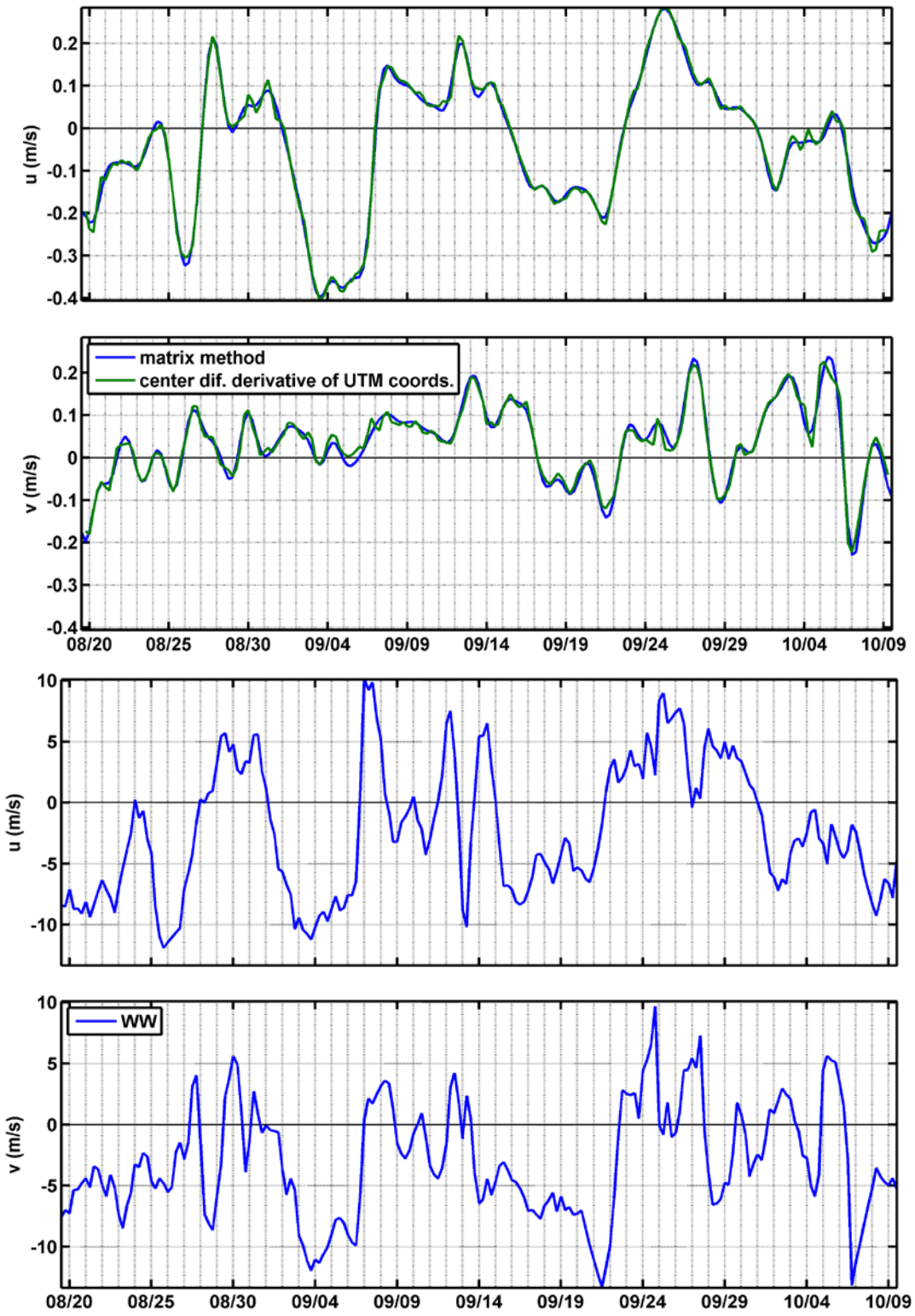

Figure 103. Mean zonal (top) and meridional (2nd from top) Pt. Lay Offshore drifter cluster centroid velocities, and zonal (3rd from top) and meridional (bottom) WaveWatch wind velocities evaluated at the location of the centroid through time. For the drifter velocities the blue line is based on the least squares solution and the green line is computed by centered differences of the centroid positions divided by the 6-hour time step.

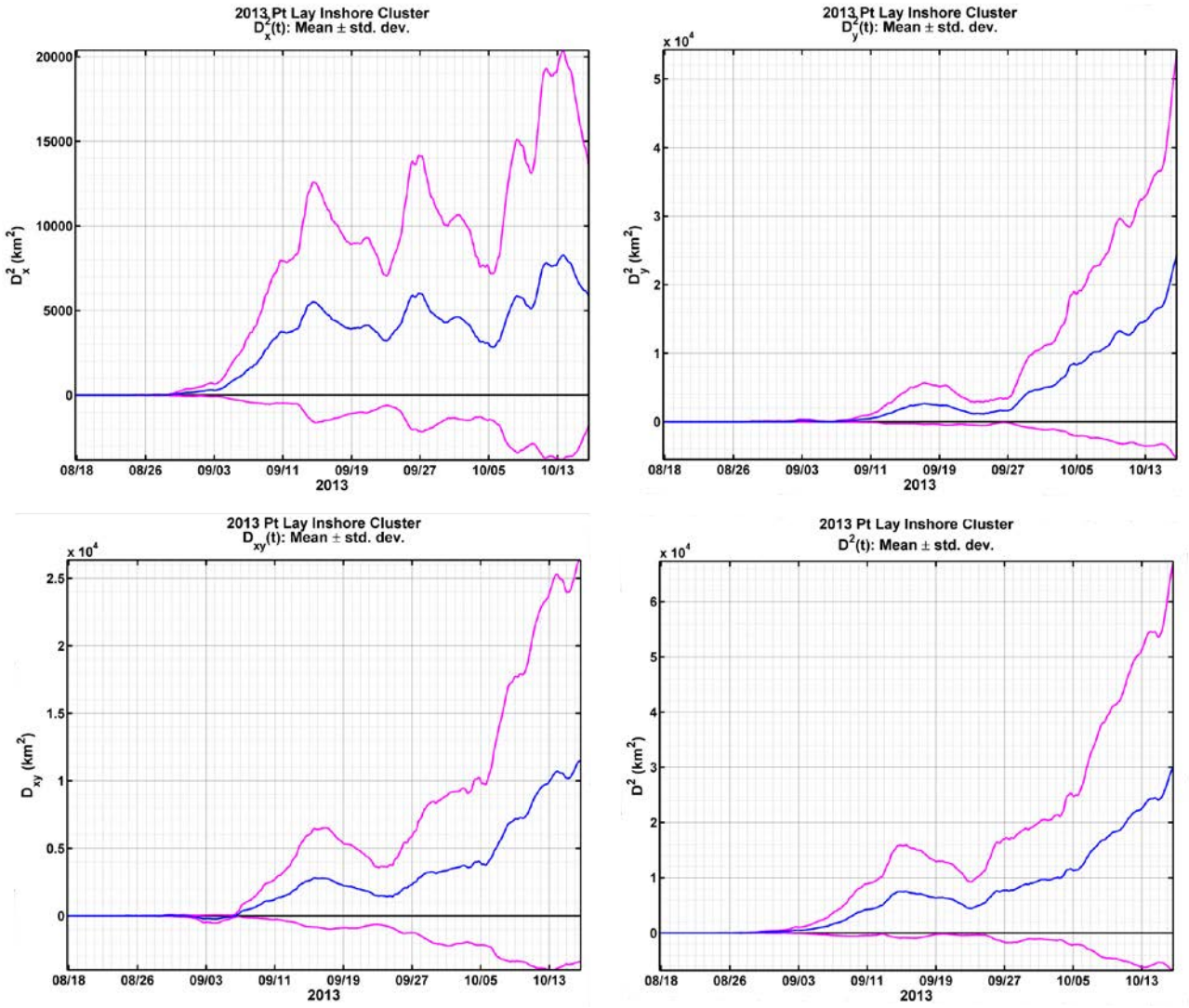

Figure 104. Time series of relative zonal (top left) and meridional (top right) dispersion, the cross-correlation in relative dispersion (bottom left), and the relative dispersion (bottom right) for the Pt. Lay Inshore drifter cluster.

Time series of the terms comprising the deformation tensor for both clusters are shown in **Figures 106** and **107**, respectively. These terms are always small ($<10^{-5}$ s^{-1}) for the offshore cluster and for the inshore cluster over most of the time series. The deformation terms did reach a large magnitude ($\sim10^{-4}$ s^{-1}) on around 24 – 25 August in conjunction with the large clockwise looping at 69.3°N, 166°W (cf. **Figure 100**) and the rapid westward acceleration of from 0 to -50 cm s^{-1} (**Figure 102**, upper panel) at this time.

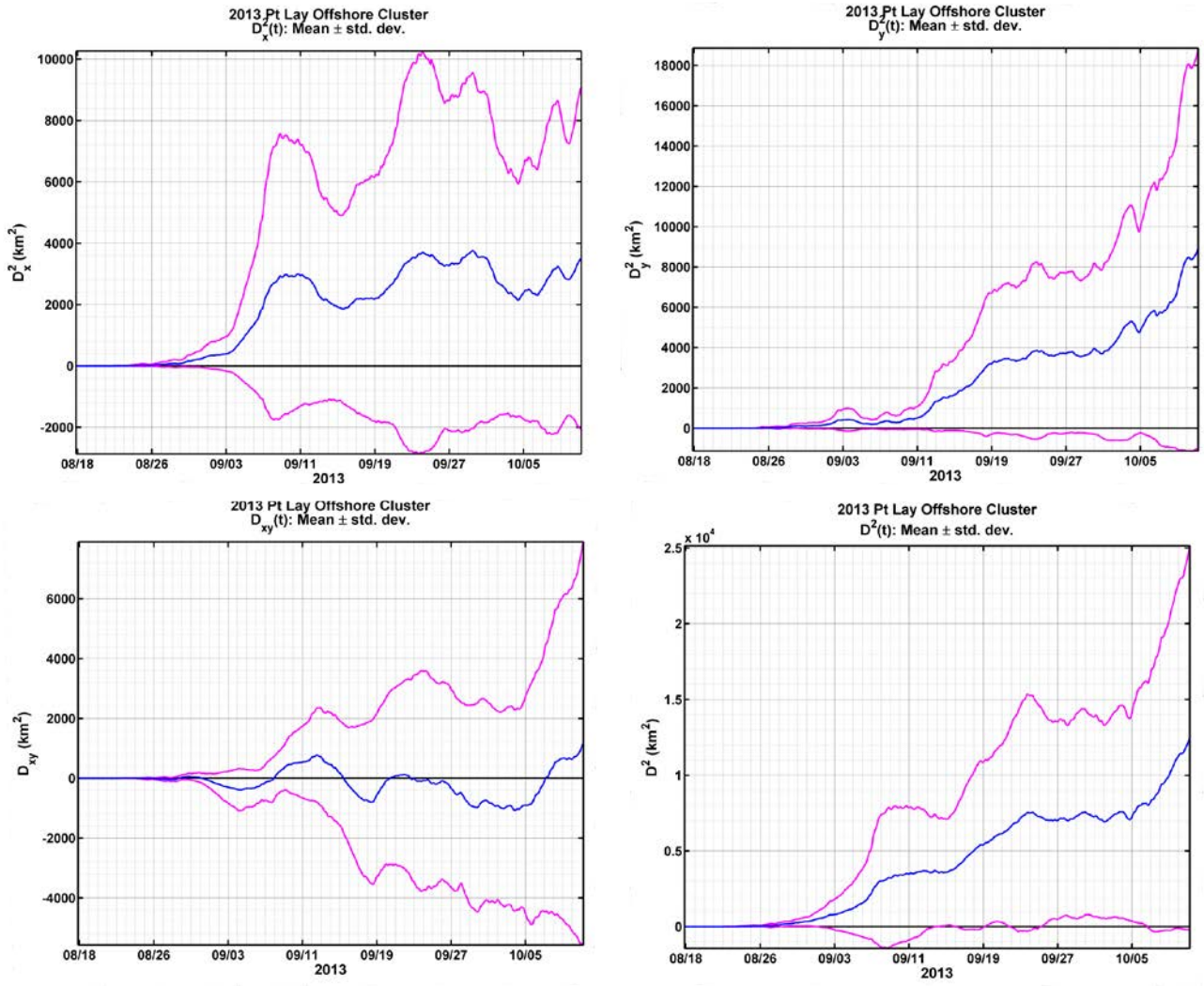

Figure 105. Time series of relative zonal (top left) and meridional (top right) dispersion, the cross-correlation in relative dispersion (bottom left), and the relative dispersion (bottom right) for the Pt. Lay Offshore drifter cluster.

The vorticity balance (**Figure 108**) for the inshore cluster indicates that the terms in the absolute vorticity equation vary little through time. The exception is from 24 – 25 August when the stretching term is not compensated for by the time rate of change in absolute vorticity. This imbalance occurred in conjunction with the looping motion followed by the rapid westward acceleration mentioned above. The implied vorticity source is unclear, though it may be due to baroclinic production of vorticity (at small scales) associated with the front seen in **Figure 18**. However, the time rate of change and stretching vorticity did not vary at all for the offshore cluster (**Figure 109**). The reasons for these different vorticity balances between the two clusters are not clear. If, however, baroclinic conversion in vorticity is indeed involved, then this process may be spatially and temporally episodic and thus not captured by the offshore cluster.

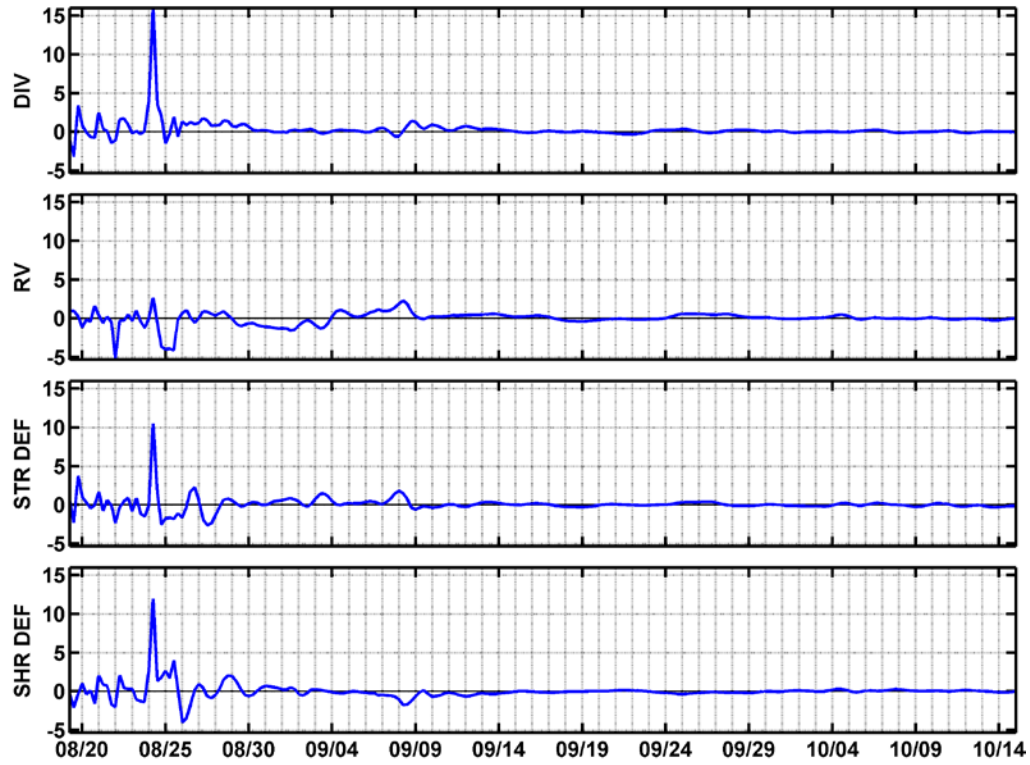

Figure 106. Time series of the horizontal divergence (top), relative vorticity (2nd from top), stretching deformation (3rd from top), and shearing deformation (bottom) for the Pt. Lay Inshore drifter cluster. Units are $10^{-5}s^{-1}$.

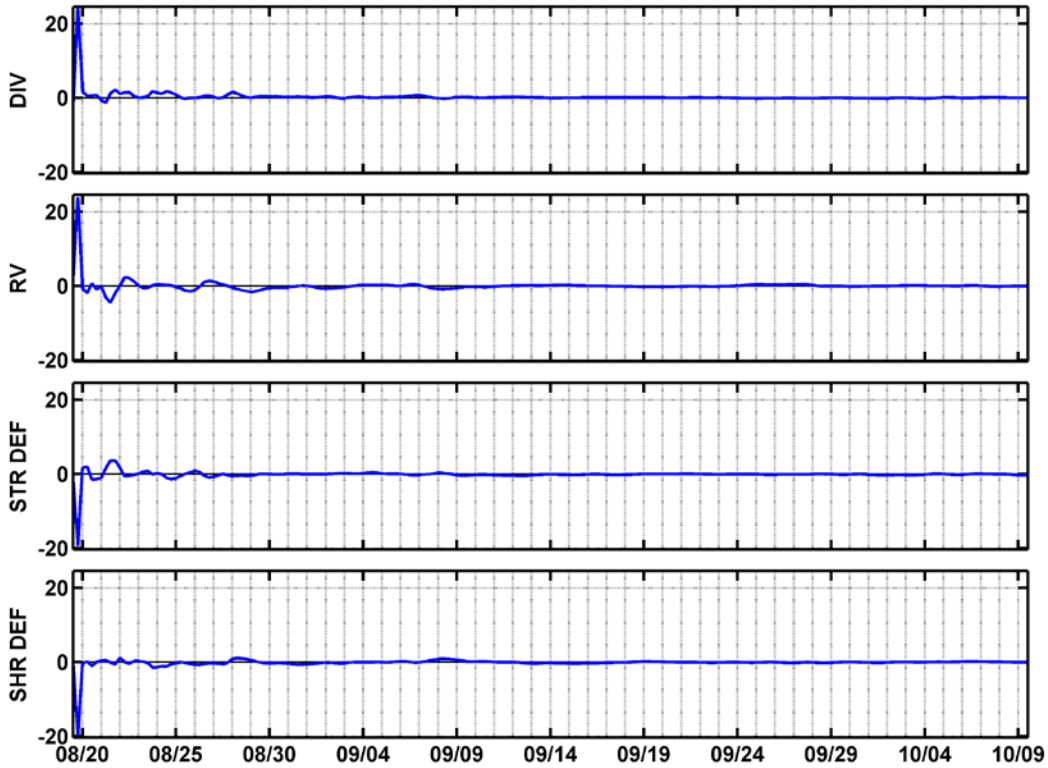

Figure 107. Time series of the horizontal divergence (top), relative vorticity (2nd from top), stretching deformation (3rd from top), and shearing deformation (bottom) for the Pt. Lay Offshore drifter cluster. Units are $10^{-5}s^{-1}$.

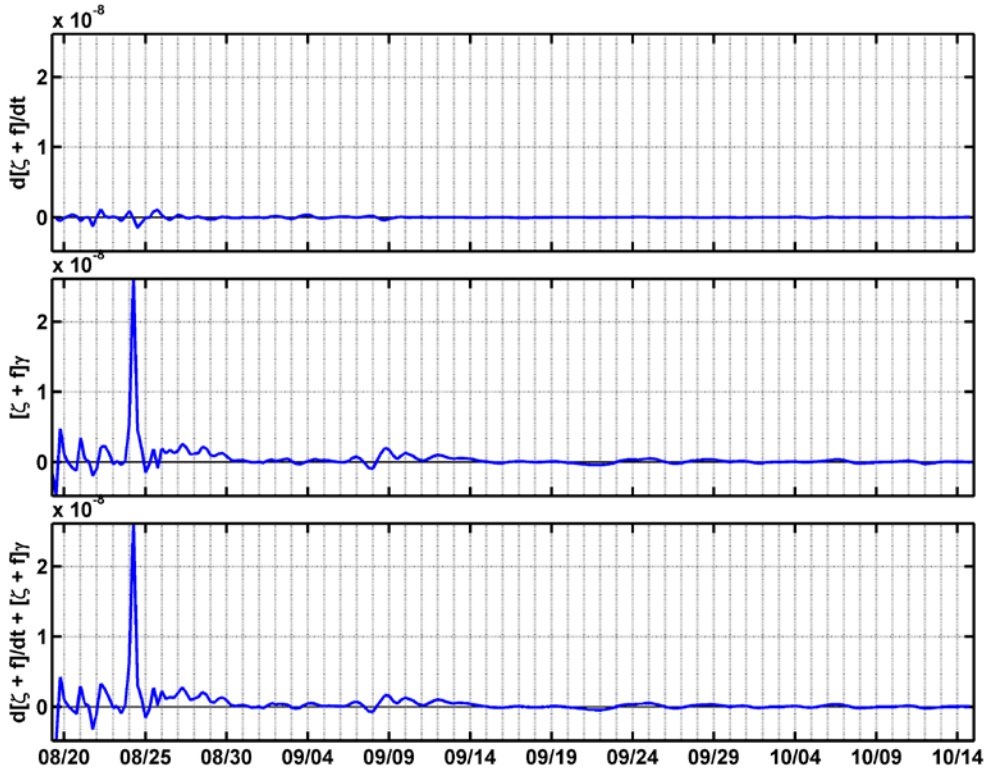

Figure 108. Time series of the terms comprising the absolute vorticity balance for the Pt. Lay Inshore drifter cluster. Units are s^{-2}.

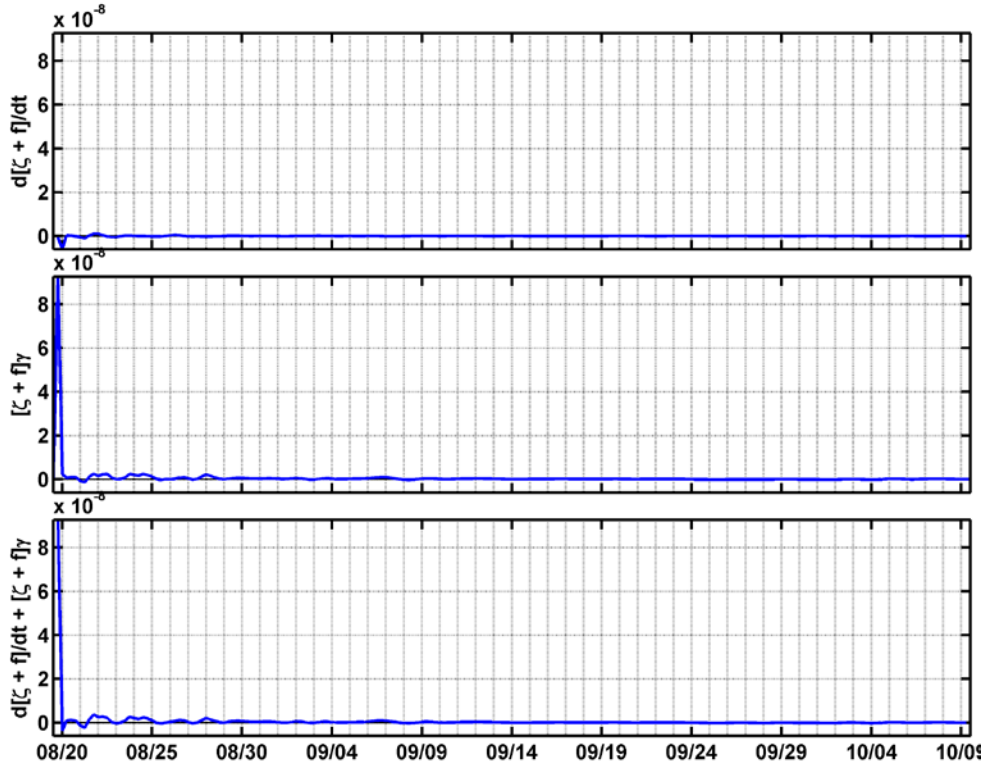

Figure 109. Time series of the terms comprising the absolute vorticity balance for the Pt. Lay Offshore drifter cluster. Units are s^{-2}.

The NE Hanna cluster centroid and individual tracks are shown in **Figure 110** for the period of 10 September through 27 October, and the accompanying current and time series are shown in **Figure 111**. This cluster's drift was primarily westward throughout the period of record. Initially the cluster drifted westward across Hanna Shoal under predominantly northeasterly winds. This drift stopped and reversed to the northeast over Hanna Shoal under southerly winds until about 5 October. Winds then became northeasterly (for the most part) again and the cluster drifted to the southwest across Statoil and north of Klondike into the Central Channel. By late October the cluster tracking was ended due to too many drifters being caught by ice. The NE Hanna cluster had much more modest speeds (e.g., $\pm$0.25 m s^{-1}) compared to the Burger and Pt. Lay clusters (speeds >0.5 ms^{-1}).

The dispersion characteristics for the NE Hanna cluster (**Figure 112**) show that zonal dispersion grew rapidly to 10000 km^2 through 10 October and remained nearly constant thereafter. Meridional dispersion developed much more slowly; it reached a maximum of 4000 km^2 by mid-October, and then diminished toward the latter end of the record. Overall, the total relative dispersion was primarily associated with zonal spreading of the drifters.

Time series of the terms comprising the deformation tensor for the NE Hanna Shoal cluster are shown in **Figure 113**. These terms are always small (< 10^{-5} s^{-1}) immediately after deployment, suggesting unsheared, non-divergent flows with little relative vorticity. Similarly, the vorticity balance (**Figure 114**) indicates that the absolute vorticity is conserved throughout the record.

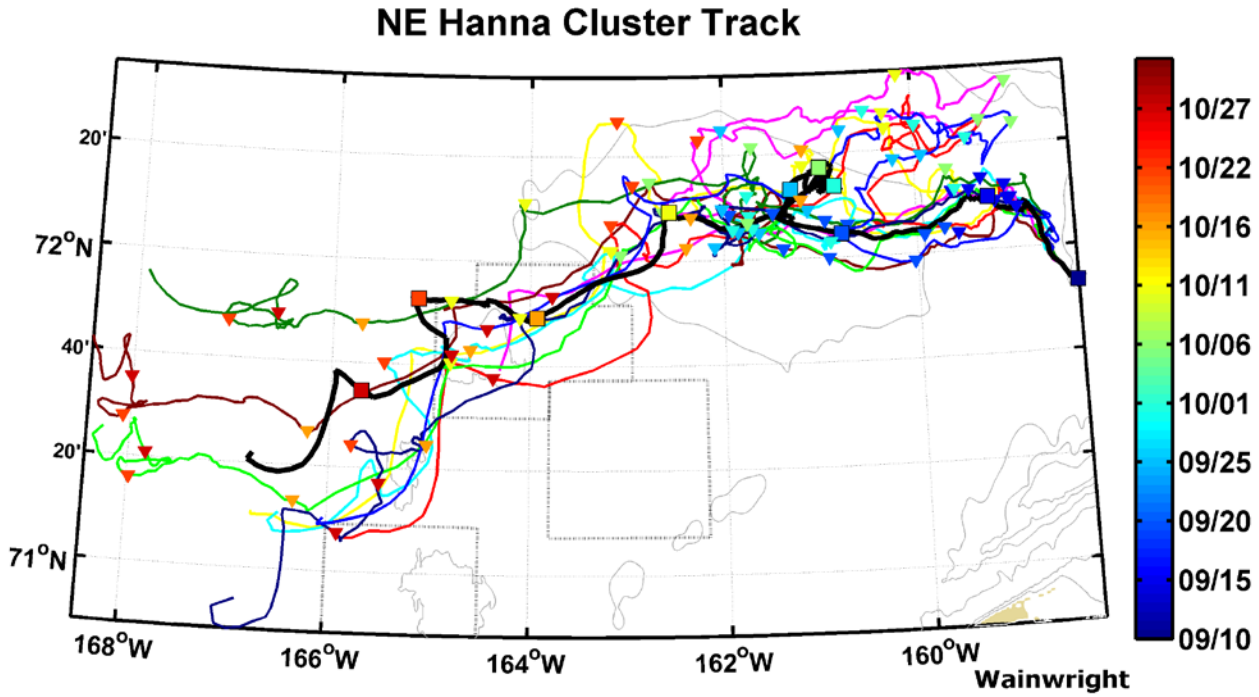

Figure 110. Mean cluster trajectory and individual drifter tracks for the Northeast Hanna Shoal drifter cluster. The inverted triangles are color-coded by date and apply to individual drifter trajectories (in color) and the black line is the mean trajectory with dates indicated by color-coded squares.

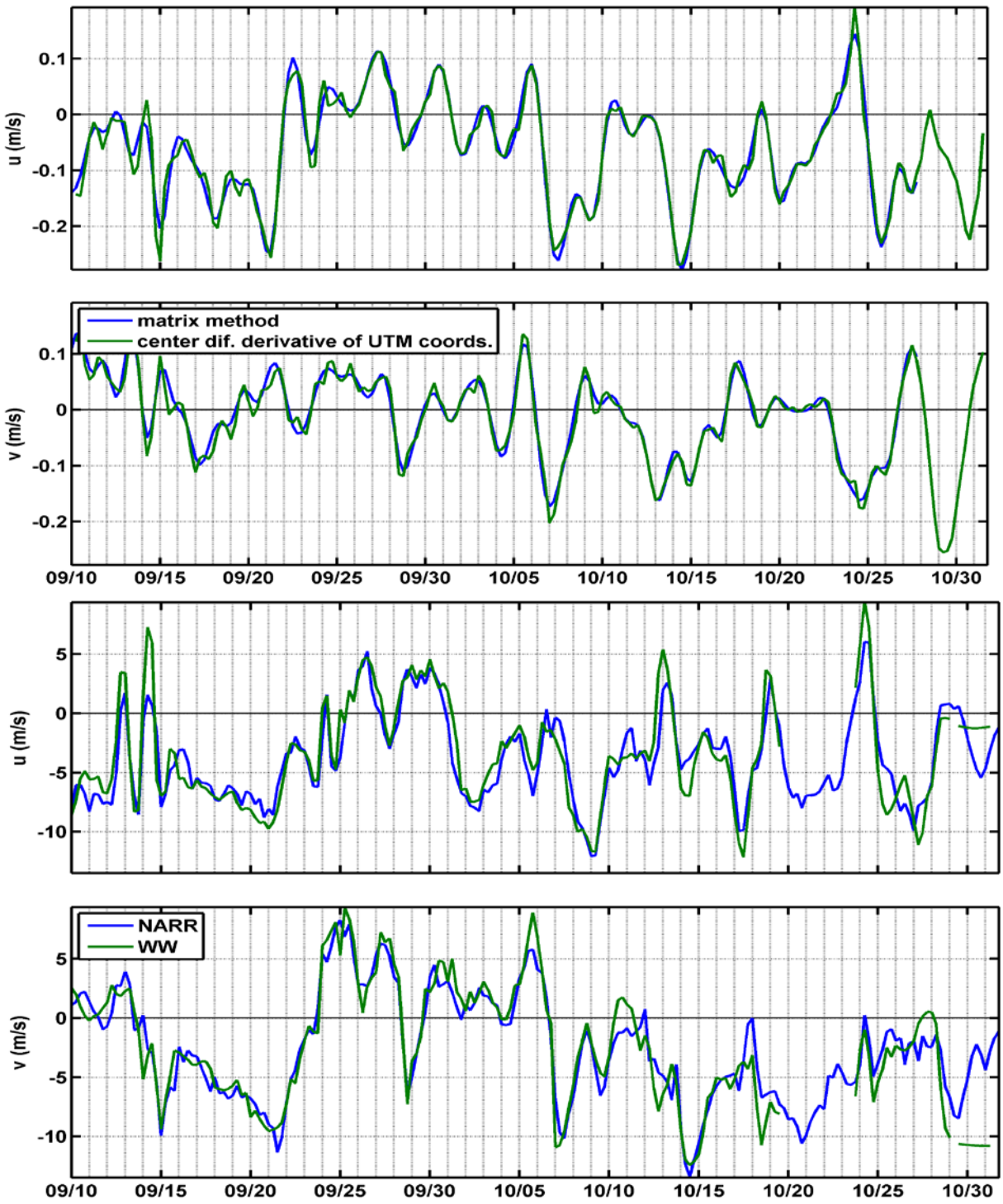

Figure 111. Mean zonal (top) and meridional (2nd from top) NE Hanna Shoal cluster centroid velocities and zonal (3rd from top) and meridional (bottom) wind velocities evaluated at the location of the centroid through time. For the drifter velocities the blue line is based on the least squares solution and the green line is computed by centered differences of the centroid positions divided by the 6-hour time step. For the wind components the green line is winds from the WaveWatch model and the blue line is the NARR winds.

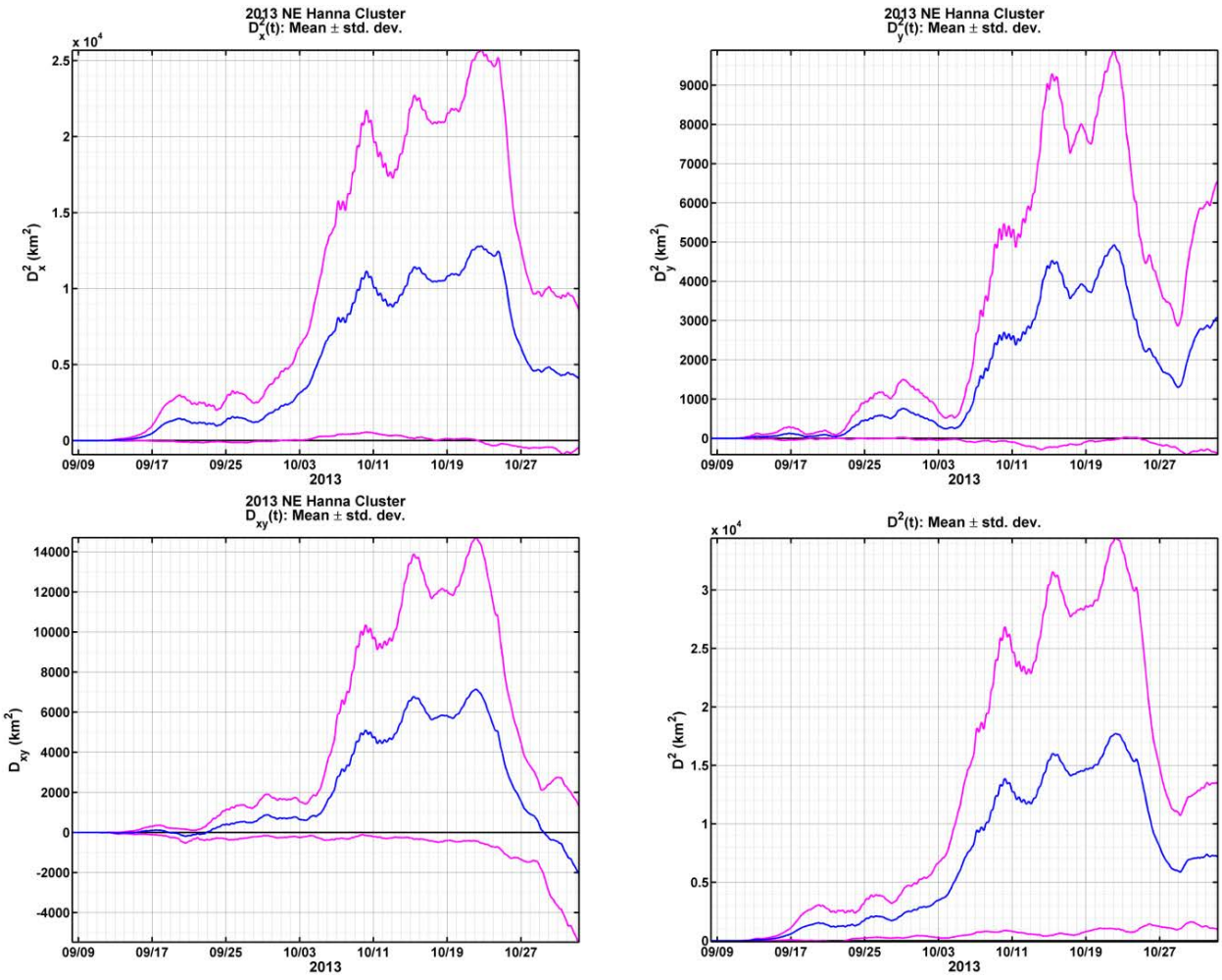

Figure 112. Time series of relative zonal (top left) and meridional (top right) dispersion, the cross-correlation in relative dispersion (bottom left), and the relative dispersion (bottom right) for the NE Hanna drifter cluster.

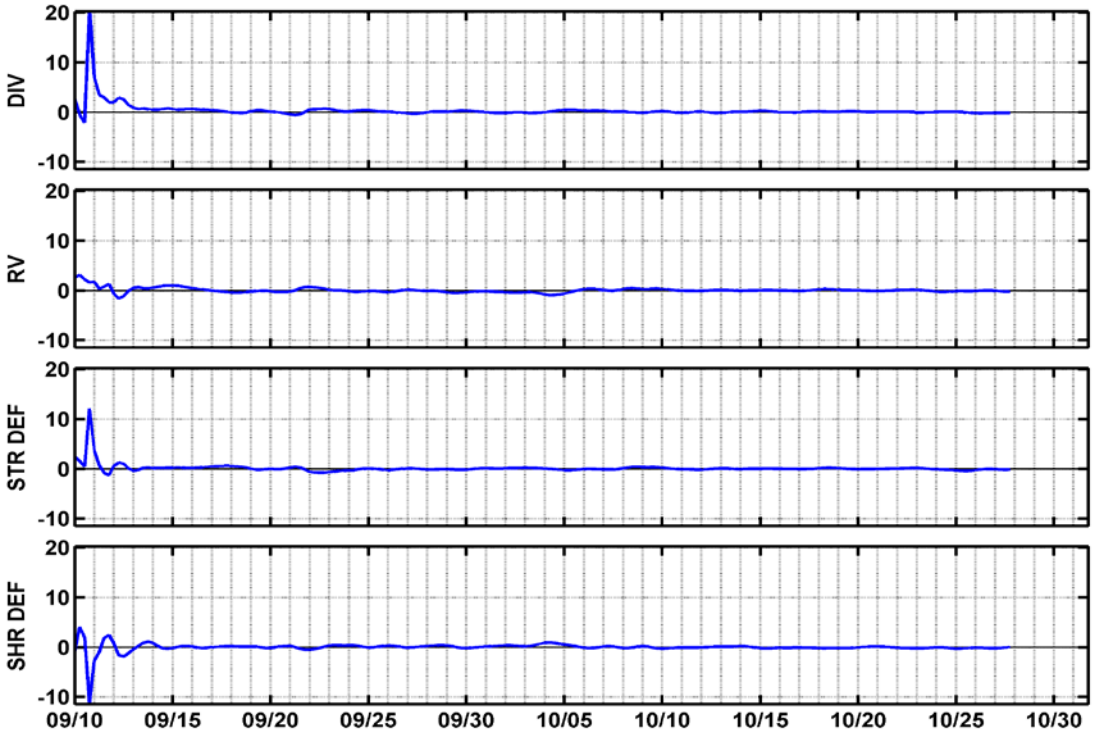

Figure 113. Time series of the horizontal divergence (top), relative vorticity (2nd from top), stretching deformation (3rd from top), and shearing deformation (bottom) for the NE Hanna drifter cluster. Units are 10^{-5} s^{-1}.

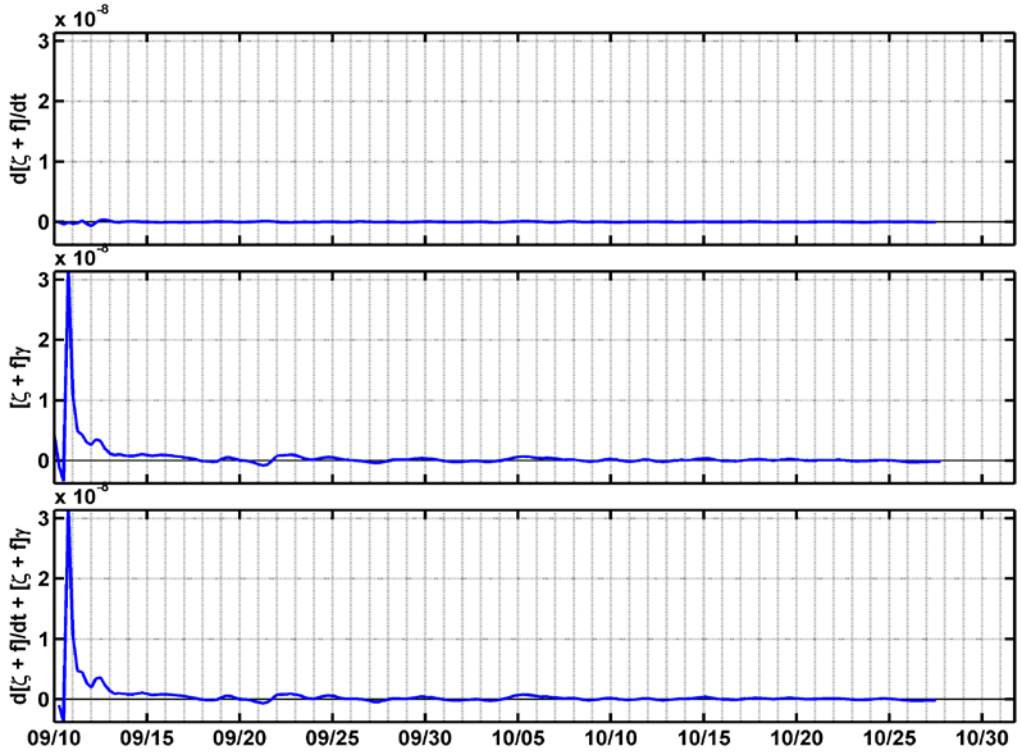

Figure 114. Time series of the terms comprising the absolute vorticity balance for the NE Hanna Shoal drifter cluster. Units are s^{-2}.

The NW Hanna cluster centroid and individual tracks for 11 September through 17 October are shown in **Figure 115** and their accompanying current and time series are shown in **Figure 116**. This cluster drifted west northwestward between 73°N and 72° 20'N from 11 September to 10 October. Until 22 September, this drift was westward at between 0.1 and 0.3 ms^{-1} and when winds were from the northeast at speeds of ~7ms^{-1}. The westward drift continued, but slowed, between 22 September and 6 October when the winds were from the southwest at 6 ms^{-1}. Winds were primarily from the north from 9 – 17 October and the cluster moved to the southwest through this period.

The dispersion characteristics for the NW Hanna cluster (**Figure 117**) indicate little dispersion in either direction before 28 September. Thereafter, zonal dispersion grew rapidly and reached 15000 km^2 by mid-October before decreasing to ~10000 km^2 by the end of the record. The meridional dispersion was markedly smaller; it increased to ~2000 km^2 in early October and then decreased to ~300 km^2 in mid-October before increasing again to ~2000 km^2 by the end of the record. The total dispersion was, therefore, largely related to zonal spreading of the drifters.

Time series of the terms comprising the deformation tensor for the NW Hanna Shoal cluster are shown in **Figure 118**. These terms are all small (<10^{-5} s^{-1}) after 17 September suggesting unsheared, non-divergent flows with little relative vorticity. Early on, all terms are large, especially the relative vorticity, which has a maximum value of 6 x 10^{-5} s^{-1} on 13 September. These large values are all associated with the counter-clockwise turning of all the drifters on this date near 166°W (**Figure 115**). The vorticity balance for this cluster (**Figure 119**) indicates that the rate of change in absolute vorticity tends to, but does not completely, compensate the

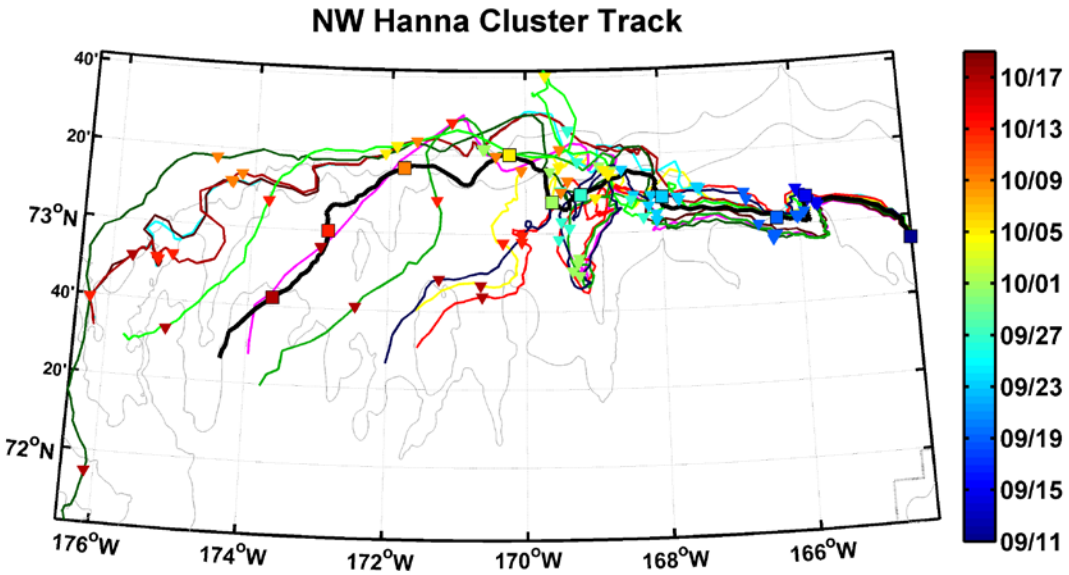

Figure 115. Mean cluster trajectory and individual drifter tracks for the Northwest Hanna Shoal drifter cluster. The inverted triangles are color-coded by date and apply to individual drifter trajectories (in color) and the black line is the mean trajectory with dates indicated by color-coded squares.

stretching vorticity term, indicating once again that there are vorticity sources and sinks present. The imbalance in the vorticity equations largely occurs before 17 September and we speculate that there may be meanders and/or eddies associated with meltwater fronts along the northwest side of Hanna Shoal.

A climatological picture of dispersion on the Chukchi Sea Shelf is established by averaging the dispersion properties of all drifters in the five clusters in a log-log plot of the total relative dispersion versus time (**Figure 120**). Dispersion increases by an order of magnitude from ~4 x 10^{-3} to 2 x 10^{-2} km^2 during the first 12 hours after deployment and then by another order of magnitude to ~4 x 10^{-1} km^2 over the next 12 hours. At time scales greater than two days, the approximate Lagrangian time scale (T_L) based on the autocorrelation functions for these drifters, the dispersion increases as a function of time to the 2.5 power.

Figure 121 shows log-log plots of the relative zonal and meridional dispersion calculations based on the average of the 2012 and four 2013 clusters. The data suggest anisotropic dispersion insofar as the zonal dispersion attains an average value ~6000 km^2 in 40 days, whereas the meridional dispersion is ~3000 km^2 over this duration. Relative diffusivities can be estimated from the dispersion curves to yield:

$K_{xx} = \frac{1}{2}\frac{dD_x^2}{dt} \sim 900 m^2 s^{-1}$ zonal diffusivity

$K_{yy} = \frac{1}{2}\frac{dD_y^2}{dt} \sim 450 m^2 s^{-1}$ meridional diffusivity,

where the calculation is based on values between day 2 and day 40.

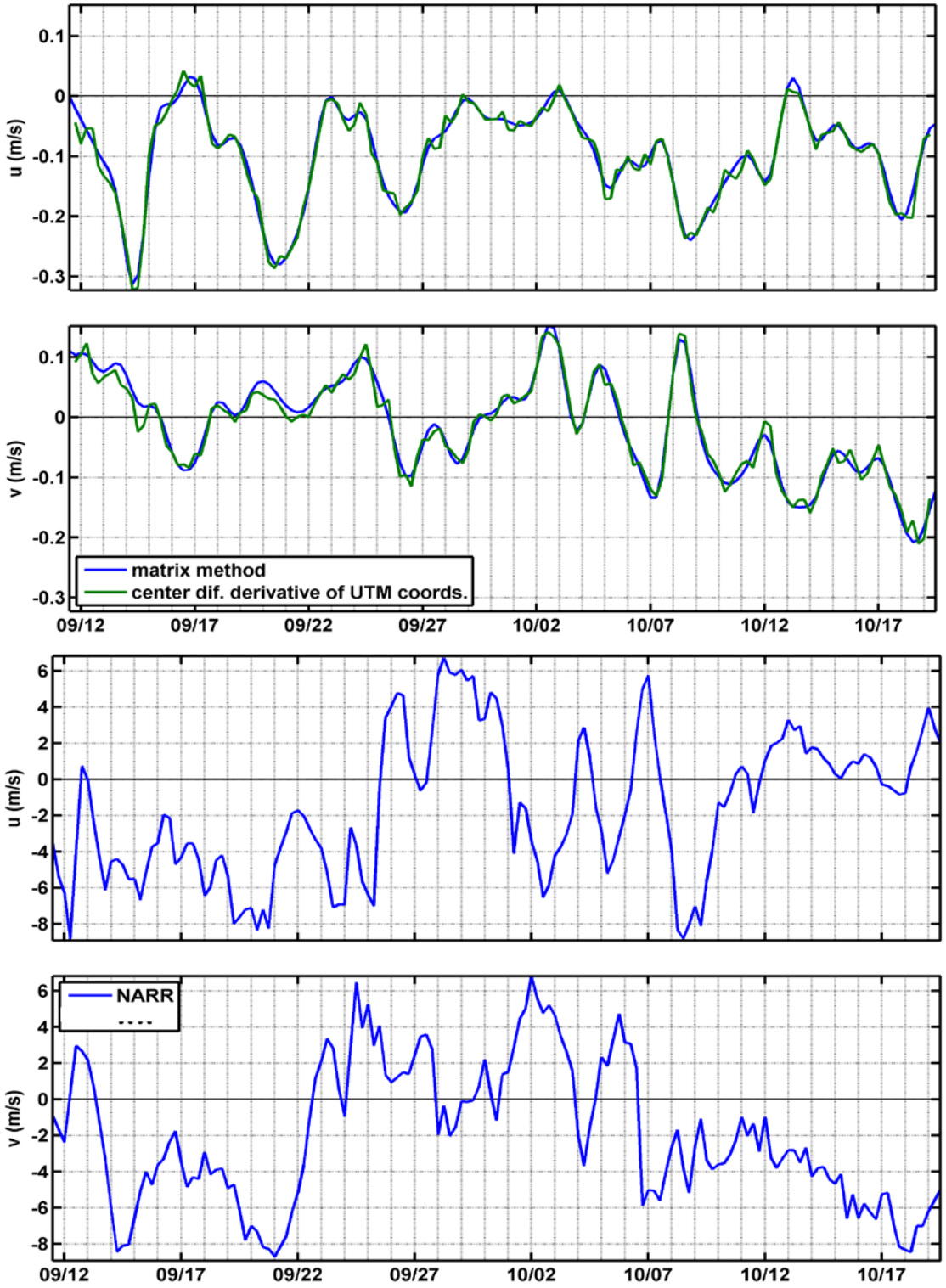

Figure 116. Mean zonal (top) and meridional (2nd from top) NW Hanna Shoal drifter cluster centroid velocities and zonal (3rd from top) and meridional (bottom) NARR wind velocities evaluated at the location of the centroid through time. For the drifter velocities the blue line is based on the least squares solution and the green line is computed by centered differences of the centroid positions divided by the 6-hour time step.

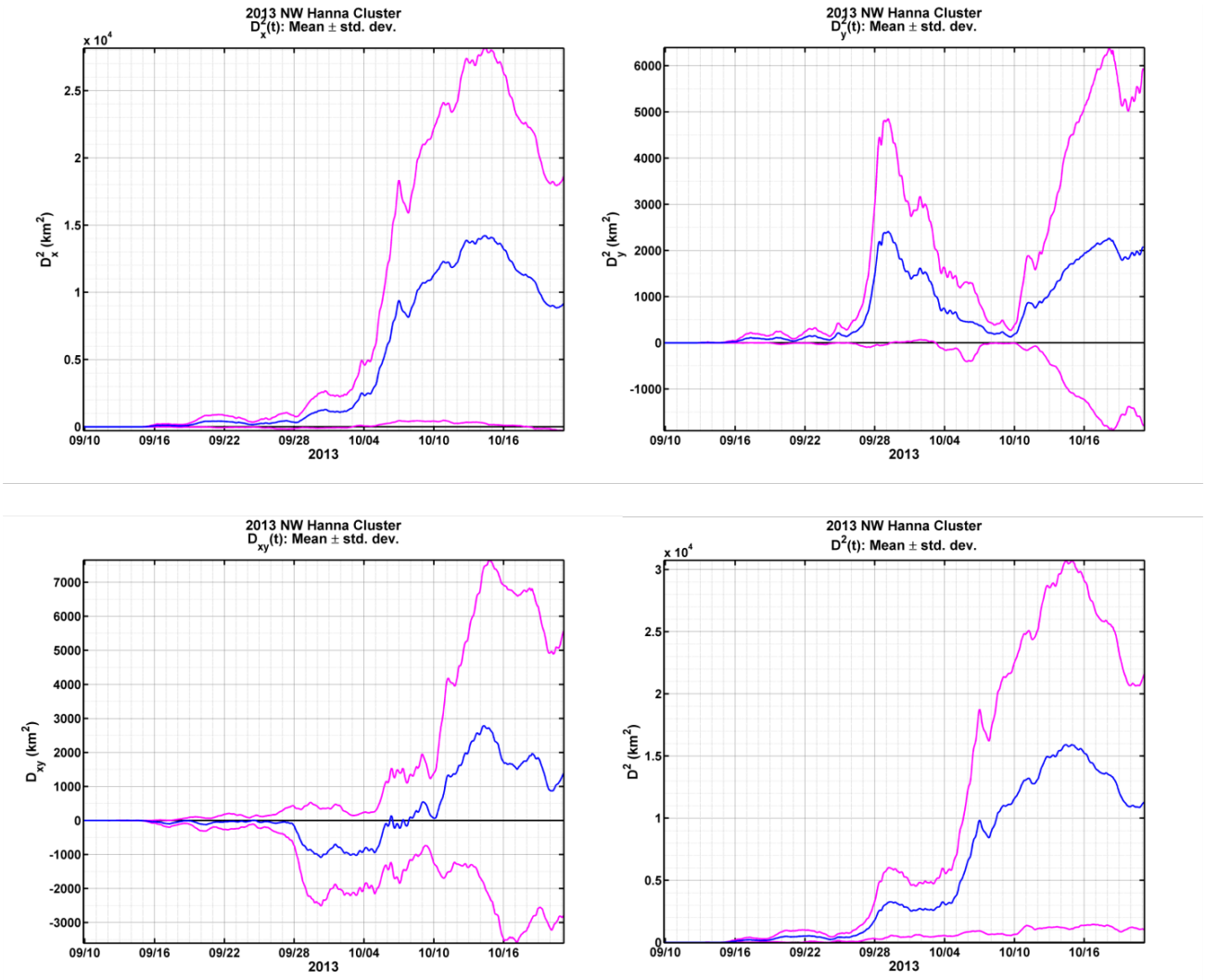

Figure 117. Time series of relative zonal (top left) and meridional (top right) dispersion, the cross-correlation in relative dispersion (bottom left), and the relative dispersion (bottom right) for the NW Hanna drifter cluster.

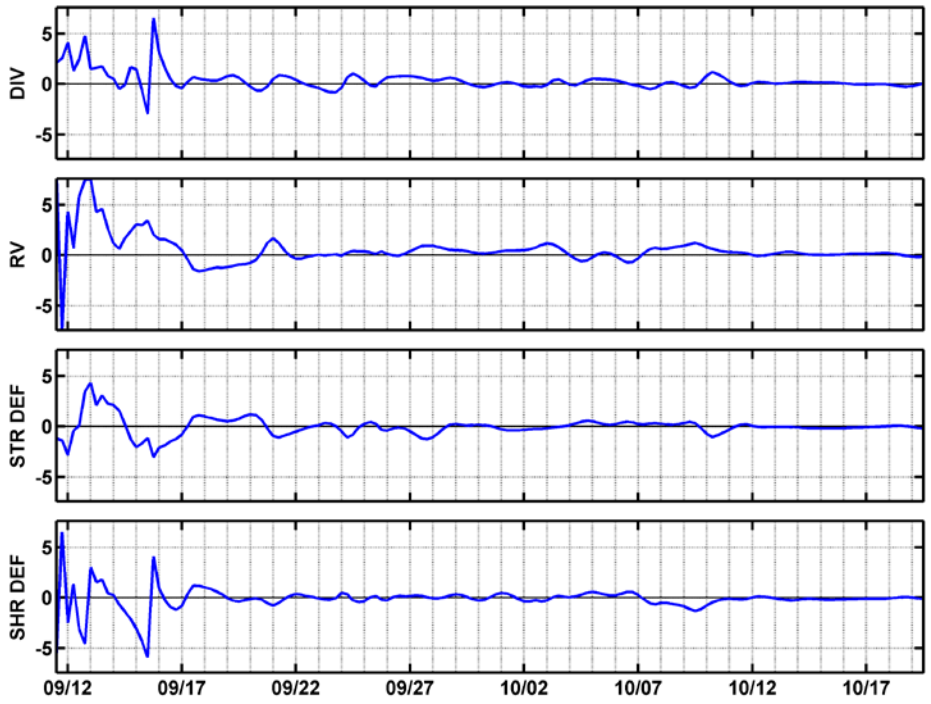

Figure 118. Time series of the horizontal divergence (top), relative vorticity (2nd from top), stretching deformation (3rd from top), and shearing deformation (bottom) for the NW Hanna drifter cluster. Units are 10^{-5} s^{-1}.

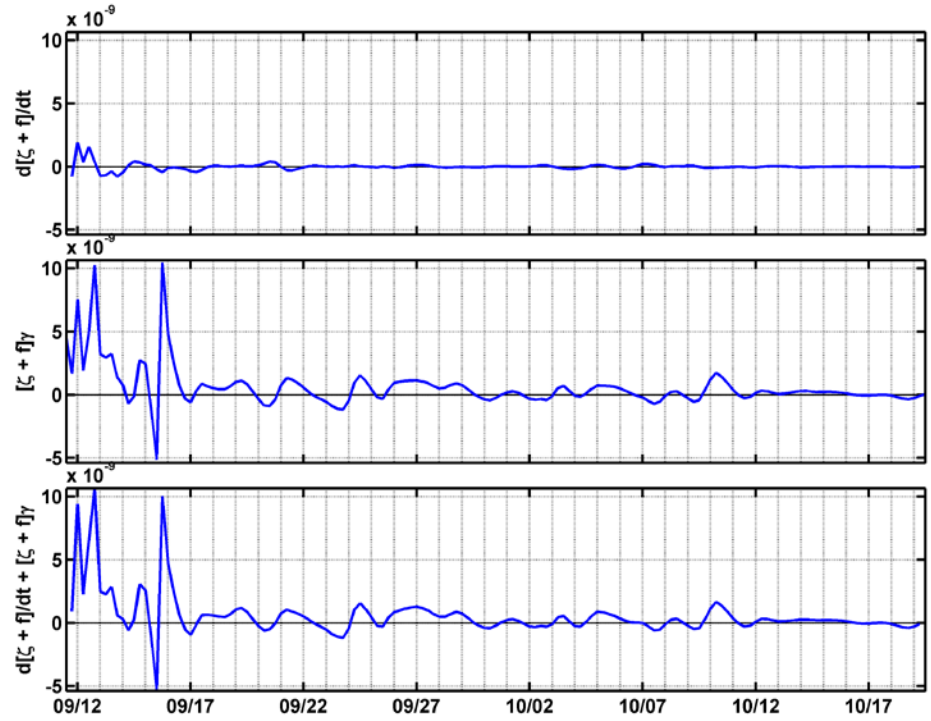

Figure 119. Time series of the terms comprising the absolute vorticity balance for the NW Hanna Shoal drifter cluster. Units are s^{-2}.

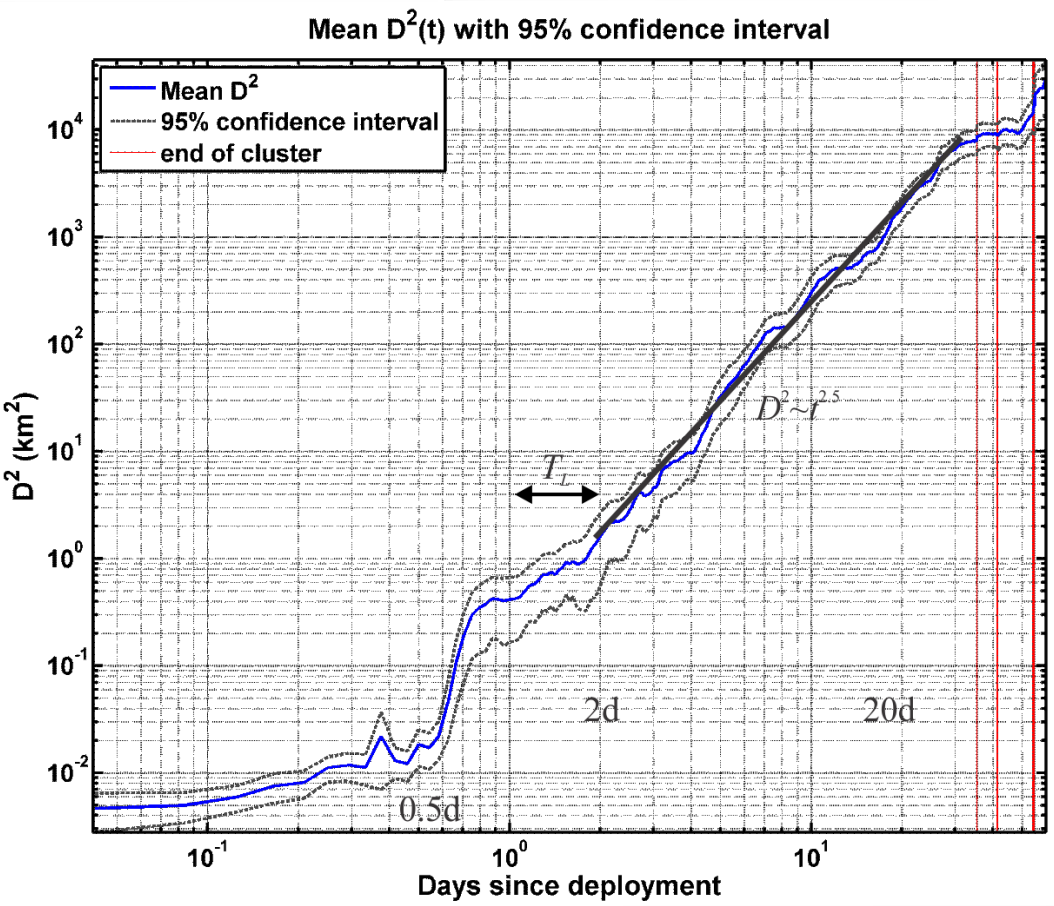

Figure 120. Log-log plot of the total relative dispersion based on the average of the five clusters deployed in 2012 and 2013. The dashed black lines denote the 95% confidence interval around the mean value (blue curve). The black straight line is a subjective fit to the data between 2 and 40 days. The Lagrangian time scale (T_L) is between 1 and 2 days for these clusters.

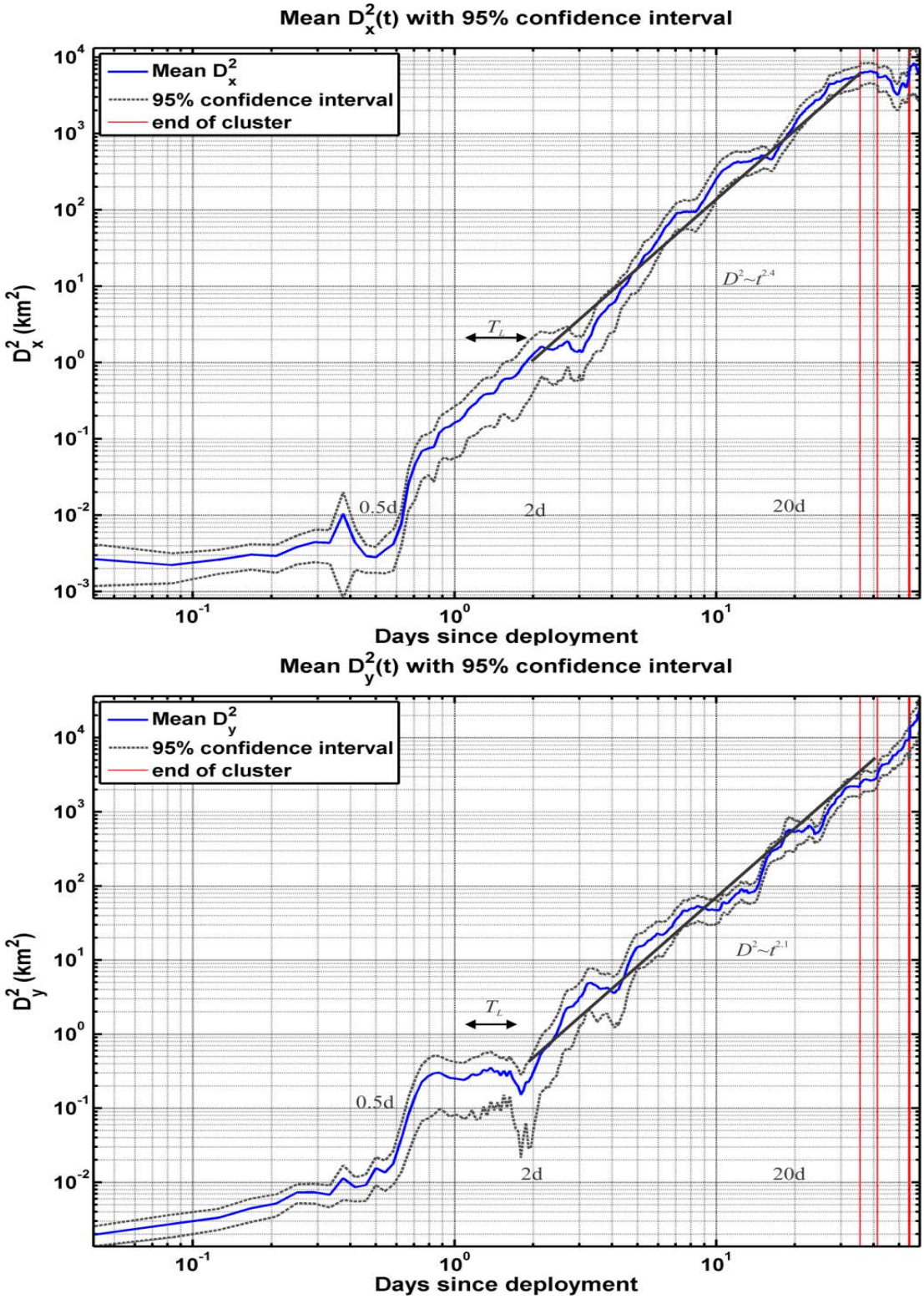

Figure 121. Log-log plots of the relative zonal (top) and meridional (bottom) dispersion based on the average of the five clusters deployed in 2012 and 2013. The dashed black lines denote the 95% confidence interval around the mean value (blue curve). The black straight line is an eyeball fit to the data between 2 and 40 days. The Lagrangian time scale (T_L) is between 1 and 2 days for these clusters.

IVf. Wind-Drifter Correlations

We examined the relationship between the winds and the drifters based on simple linear regressions for the 2012 and 2013 deployments. We anticipated that the regressions might vary spatially and with drifter type. Consequently, for 2012 we fit the regression to each drifter type in six different spatial domains (**Figure 122**):

a) Alaska Coastal domain that encompasses the region within 40 km of the northwest coast of Alaska and south of Barrow Canyon,
b) Barrow Canyon including the mouth of the canyon and all points within 40 km of the coast of Alaska,
c) Continental Slope of both the Beaufort and Chukchi Seas, including all positions between the 80 and 2200 m isobaths,
d) Canada Basin, which includes all locations seaward of the 2200 m isobath,
e) Chukchi Shelf including all points seaward of the Alaska Coastal and Barrow Canyon domains and south of the 80 m isobath, and
f) Beaufort Shelf, between the Beaufort Sea coast and the 80 m isobath.

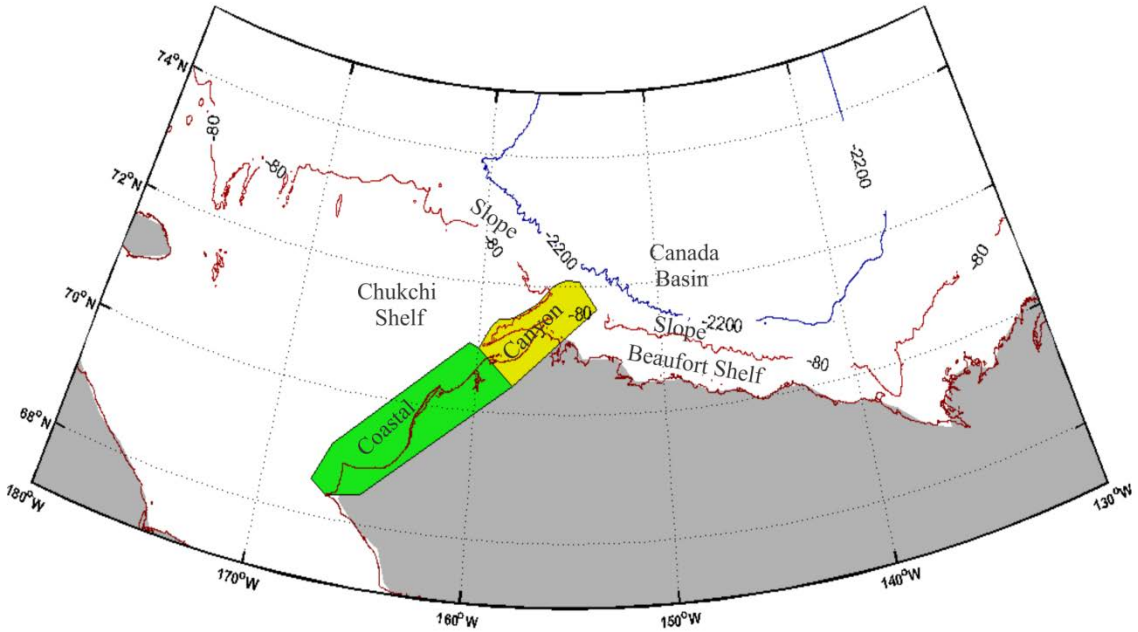

Figure 122. Definition map of the domain locations for the wind-drifter regressions.

The regressions did not include any velocity values from drifters that were incorporated in sea ice. The fits are of the form:

$$u_d = aU_w + bV_w + c \quad \text{and} \quad v_d = dU_w + eV_w + f$$

The variables u_d and v_d are the zonal and meridional velocity components of the drifters in cm s^{-1} and U_w and V_w are the corresponding wind components in m s^{-1}. The coefficients *a, b, e,* and *d* have units of cm m^{-1} and the intercepts, *c* and *f*, have units of cm s^{-1}. Similar fits were made using the wind stress components, with the wind stresses computed based on *Large and Pond* (1981). We only present the results using the wind velocity components since these generally resulted in (slightly) better fits and may be more desirable to use in an operational setting. The results for 2012 are summarized in **Tables 1 – 6** and those for 2013 are in **Table 7**. There are several caveats associated with the results. First, different types of drifters were in the different domains at various times. Hence, the regressions were not all based on the same ambient conditions in terms of winds and stratification. Second, there are different sample sizes involved in constructing the regressions (e.g., there were insufficient iSphere samples from the Canada Basin domain upon which to construct a regression). Third, some domains (e.g., the Chukchi Shelf, Barrow Canyon) include spatially varying stratification and/or fronts associated with ice meltwaters. The drifter responses to wind are expected to vary between these regions. We have made no attempt at this stage to address this issue, but emphasize that these differences will degrade the regression results, since the (implicit) assumption of a constant parameter system is almost certainly violated. Nevertheless, most of the regressions are significant at the 95% confidence level, although the strength of the regression varies widely across domains and drifter types. **Figures 114 – 131** are scatterplots of the drifter velocity components versus the wind velocity components for 2012. For brevity, the scatterplots for 2013 are not included.

Several general features emerge from these calculations. First, the best wind-current regressions are for the iSpheres with most of the R^2 values exceeding 0.5, and in many cases, ~0.6 or larger. However, the winds explained only ~20% of the variance in the iSphere velocities for the continental slope domain. The MS drifters have lower R^2 values compared to the iSpheres. The most useful regressions are for the Coastal and Beaufort Shelf domains, where the R^2 values exceed 0.5. In the Chukchi Shelf domain, the R^2 values are 0.3 to 0.4. However, the variance explained by the wind-current regressions nearly doubles if the calculations are confined to the September – October period (3rd row, **Table 3**). This result may reflect bias in drifter locations because the fall tended to be south of the frontal systems for the most part. In contrast, the drifters deployed in August were likely within the frontal systems. **Figure 132** shows a comparison between wind and drifter velocity components for MS-9 (released in mid-August in the Statoil study area) and MS-8-2 (released in early September in the Burger study area). These time series are similar to others in the same deployment. Visual inspection clearly shows the difference in wind response between the two drifters. Note that the range and variability in wind speeds is similar in both cases so the winds cannot be the cause of the differential response observed. The SVP drifters have the smallest R^2 values overall. In general, less than 25% of the velocity signals in the SVP drifters are explained by the wind. The sole exception is the zonal velocity component on the Beaufort Shelf, for which the winds explain 42% of the variance. The

comparatively poor regression results in the shelfbreak domain for the MS and SVP drifters must, in part, be to eddies and meanders in the current field here.

As seen from the regression coefficients and the figures, the zonal (meridional) current component is more closely related to its corresponding wind component than to the orthogonal wind component. The regression intercepts are also of interest. In the Alaska Coastal domain these suggest that the flow in the absence of any wind forcing is nominally eastward at between 14 cm s^{-1} (iSpheres), 13 cm s^{-1} (MS) and 11 cm s^{-1} (SVP). Similarly, these intercepts for the Chukchi Shelf domain range between 6 and 8 cm s^{-1}. These values are consistent with forcing in the absence of wind by the mean pressure gradient between the Bering Sea and Arctic over most of the central shelf in which these drifters sampled.

The regression results allow us to determine the variation with drifter type in speed and the angle of rotation between the wind and the drifter. For the Chukchi Shelf domain, the iSphere drifter speeds are ~4% of the wind speed and they deviate to the right from the wind direction by 4^o. The MS drifters move at 2% of the wind speed and are deflected ~30^o to the right of the wind. The SVPs move at 1% of the wind speed and are deflected to the right by 57^o. The latter two values are not inconsistent with Ekman's theory when applied to a stratified ocean. We note that in 2013 many of the SVP drifters were deployed in stratified waters in which a strong pycnocline was at ~10 – 15 m depth. In such regions we expect that the Ekman layer is effectively limited to the pycnocline depth, so that there should be a large vertical gradient in wind shear between the surface and 10 m depth. Our results bear this out in the aggregate for the Chukchi Shelf domain.

A general conclusion from these results is that there is no single wind-current regression that can be used with confidence for operational purposes. Our results suggest that these regressions are likely variable in time and space. This suggestion is supported by the results from 2013 for which we computed the regressions for the Pt. Lay and Hanna Shoal clusters separately and results are summarized for each cluster in **Table 7**. WaveWatch winds were used for all clusters except the NW Hanna Shoal cluster. For that cluster regressions were performed using the NARR winds, since the WaveWatch product does not extend beyond the Russian-US convention line. Again, all winds products were interpolated through time to produce an estimate at each of the drifter positions along their trajectory.

Several results emerge from these analyses. For the Pt. Lay clusters the winds account for nearly twice as much of the variance in the zonal velocity component as they do for the meridional velocity. This difference is most likely tied to the northward excursion of these drifters in the Central Channel where the ambient currents are often northward regardless of the wind direction (*Weingartner et al.,* 2005; *Weingartner et al.,* 2013a). The zero-wind intercepts for the Pt. Lay drifters indicate that in the absence of wind the drifters would move to the north-northeast on average; a result consistent with notions of the mean flow over the eastern Chukchi Shelf in the absence of wind-forcing. The slopes for the wind regressions for both Pt. Lay drifters are not

statistically different from one another nor are these slopes statistically different from all of the MS drifters within the Chukchi Shelf domain. The Pt. Lay slopes are, however, significantly different from the slopes for the September – October 2012 MS drifters (compare row 3, Table 3 with rows 1 and 2 of Table 7).

The regression results for the NE Hanna Shoal drifters are similar to those for the Chukchi Shelf domain (**Table 7**) with respect to the fraction of variance explained by the winds. However, the regression coefficients are statistically different from one another. These differences may be a consequence of differences in stratification between the two years or in the deployment locations. The intercepts differ significantly between the NE Hanna Shoal drifters and those from the Chukchi Shelf domain in 2012. For the former, these intercepts yield a mean drift to the southwest, whereas for the latter the mean drift is toward the east-northeast. Finally, we note the extremely poor regression results for the NW Hanna Shoal cluster. These are markedly different from any of the other drifters released in either 2012 or 2013. The reasons for the poor relationship with the winds are unclear, but we suggest the following. First, many of the drifter trajectories stagnated in Herald Canyon. Here the mean flow is often northbound on the east side of this canyon, but there is a large cross-canyon velocity shear associated with a front that extends along the canyon (*Pickart et al.,* 2010). If this background velocity structure existed when the drifters were in Herald Canyon, the response to the winds would differ in accordance with their location within the background velocity field. To investigate this possibility, we reran the regressions after splitting the analyses into two parts; before and after 5 October, with the trajectories after this date largely associated with the Herald Valley region. The regressions are statistically dissimilar to one another. There is, however, no substantial improvement in terms of the total amount of variance explained between the two regressions. We note also that during the first half of the record, the drifters moved westward along the northern Chukchi shelfbreak along about the 100 m isobath. Here they may be entrapped in the southern limb of the Beaufort Gyre and/or interacting with meltwater fronts associated with the ice-edge so that simple wind-current relationships are masked by other dynamics.

Table 1. Regression summary for the Alaska Coastal domain. The numbers in parentheses represent ± the 95% confidence limits on the regression coefficients.

Drifter	$u_d = aU_w + bV_w + c$			R^2	$v_d = dU_w + eV_w + f$			R^2
	A	*b*	*c*		*d*	*e*	*f*	
iSphere	3.5 (3.0, 4.0)	3.3 (2.9, 3.6)	13.5 (11.4, 15.4)	0.52	0.5 (0.2, 0.8)	4.8 (4.6, 5.0)	0.4 (-0.9, 1.7)	0.81
MS (1-m)	3.4 (3.0, 3.8)	3.0 (2.7, 3.3)	12.3 (10.4, 14.4)	0.56	0.5 (0.3, 0.8)	3.8 (3.6, 4.0)	0.7 (-0.6, 1.9)	0.69
SVP (10-m)	1.4 (0.9, 1.9)	2.2 (1.5, 3.0)	10.9 (7.5, 14.4)	0.26	0.4 (0.2, 0.6)	1.5 (1.1,1.8)	1.2 (-0.4, 2.8)	0.29

Table 2. Regression summary for the Barrow Canyon domain. The numbers in parentheses represent ± the 95% confidence limits on the regression coefficients.

Drifter	$u_d = aU_w + bV_w + c$			R^2	$v_d = dU_w + eV_w + f$			R^2
	A	*b*	*c*		*d*	*e*	*f*	
iSphere	7.5 (6.8, 8.1)	6.0 (5.4, 6.6)	-2.6 (-6.0, 0.8)	0.63	1.4 (1.0, 1.8)	4.3 (3.9, 4.6)	0.1 (-1.9, 2.1)	0.55
MS (1-m)	2.4 (2.1, 2.8)	2.0 (1.6, 2.3)	13.5 (11.8,15.1)	0.23	-0.7 (-0.9, -0.6)	1.6 (1.4, 1.8)	6.2 (5.3, 7.0)	0.16
SVP (10-m)	0.1 (-0.2, 0.5)	1.9 (1.5, 2.2)	10.7 (9,12.4)	0.08	-0.4 (-0.6, -0.3)	0.8 (0.6,1.0)	4.5 (3.7, 5.3)	0.06

Table 3. Regression summary for the Chukchi Shelf domain. The numbers in parentheses represent ± the 95% confidence limits on the regression coefficients.

Drifter	$u_d = aU_w + bV_w + c$			R^2	$v_d = dU_w + eV_w + f$			R^2
	A	*b*	*c*		*d*	*e*	*f*	
iSphere	3.8 (3.7, 3.9)	0.8 (0.7, 0.9)	7.8 (3.8, 11.5)	0.67	-0.6 (-0.8, -0.5)	4.1 (4.0, 4.2)	0.0 (-3.1, 3.2)	0.77
MS (1-m) All months	1.8 (1.7, 1.9)	1.4 (1.3, 1.5)	6.1 (5.6, 6.7)	0.38	-0.5 (-0.6, -0.4)	1.7 (1.6, 1.8)	0.3 (-0.2, 0.7)	0.3
MS (1-m) Sept.-Oct.	3.5 (3.3,3.8)	1.5 (1.3,1.7)	13.8 (12.6,14.9)	0.56	-0.02 (-0.18,0.14)	3.7 (3.5,3.8)	5.2 (4.3,6.0)	0.67
SVP (10-m)	0.9 (0.8, 1.0)	1.1 (1.0, 1.2)	6.0 (5.6, 6.6)	0.26	-0.3 (-0.3, -0.2)	0.2 (0.2, 0.3)	-2.9 (-3.2, -2.6)	0.03

Table 4. Regression summary for the Beaufort Shelf domain. The numbers in parentheses represent ± the 95% confidence limits on the regression coefficients.

Drifter	$u_d = aU_w + bV_w + c$			R^2	$v_d = dU_w + eV_w + f$			R^2
	a	*b*	*c*		*d*	*e*	*f*	
iSphere	3.3 (2.7, 4.0)	1.8 (1.3, 2.3)	7.7 (3.8, 11.5)	0.77	-1.1 (-1.6, -0.6)	3.1 (2.7, 3.5)	0.0 (-3.1, 3.2)	0.69
MS (1-m)	2.9 (2.5, 3.4)	1.5 (1.1, 1.9)	7.6 (5.4, 9.9)	0.55	-1.1 (-1.4, -0.9)	2.2 (1.9, 2.4)	-1.1 (-2.5, 0.4)	0.52
SVP (10-m)	2.5 (2.1, 2.9)	0.4 (0.0, 0.8)	-2.8 (-5.3, -0.3)	0.42	-0.9 (-1.1, -0.6)	0.1 (-0.1, 0.4)	1.0 (-0.5, 2.5)	0.16

Table 5. Regression summary for the Continental Slope domain. The numbers in parentheses represent the ± 95% confidence limits on the regression coefficients.

Drifter	$u_d = aU_w + bV_w + c$			R^2	$v_d = dU_w + eV_w + f$			R^2
	a	*b*	*c*		*d*	*e*	*f*	
iSphere	3.4 (3.0, 3.8)	0.8 (0.2, 1.3)	-11.8 (-14.0, -9.6)	0.44	-0.8 (-1.0, -0.6)	3.4 (3.1, 3.7)	4.5 (3.3, 5.7)	0.59
MS (1-m)	0.4 (0.2, 0.6)	1.8 (1.6, 2.2)	-3.6 (-4.8, -2.3)	0.11	-1.2 (-1.4, -1.0)	0.8 (0.6, 1.1)	3.4 (2.3, 4.5)	0.12
SVP (10-m)	2.4 (2.0, 2.9)	-0.9 (-1.4, -0.3)	0.2 (-2.4, 2.5)	0.23	-1.6 (-1.9, -1.3)	1.1 (0.6, 1.6)	4.8 (2.8, 6.9)	0.17

Table 6. Regression summary for the Canada Basin domain. The numbers in parentheses represent the ± 95% confidence limits on the regression coefficients. There were insufficient iSphere values to perform this regression.

Drifter	$u_d = aU_w + bV_w + c$			R^2	$v_d = dU_w + eV_w + f$			R^2
	a	*b*	*c*		*d*	*e*	*f*	
iSphere	-	-	-	-	-	-	-	-
MS (1-m)	1.0 (0.7, 1.2)	1.7 (1.3, 2.2)	-4.0 (-5.8, -2.3)	0.19	-1.4 (-1.7, -1.2)	1.6 (1.7, 2.0)	5.3 (3.8, 6.9)	0.23
SVP (10-m)	1.8 (1.2, 2.3)	0.1 (-0.7, 0.9)	0.2 (-2.4, 2.5)	0.22	-0.9 (-1.4, -0.4)	0.9 (0.3, 1.6)	9.2 (6.0, 12.3)	0.14

Table 7. Regression summary for the Pt. Lay Inshore and Offshore, and NE and NW Hanna Shoal clusters. The numbers in parentheses represent ± the 95% confidence limits on the regression coefficients.

Drifter	$u_d = aU_w + bV_w + c$			R^2	$v_d = dU_w + eV_w + f$			R^2
	a	*b*	*c*		*d*	*e*	*f*	
Pt. Lay Inshore	1.8 (1.7, 1.9)	1.3 (1.2, 1.4)	2.4 (1.9, 2.9)	0.61	-0.5 (-0.6, -.5)	1.96 (1.9, 2.0)	6.0 (5.5, 6.5)	0.43
Pt. Lay Offshore	1.7 (1.6, 1.8)	1.5 (1.4, 1.6)	4.1 (3.7, 4.6)	0.65	-0.3 (-0.4,-0.2)	1.45 (1.3, 1.5)	6.8 (6.4, 7.2)	0.31
NE Hanna Shoal	1.0 (0.9, 1.1)	2.2 (1.5, 3.0)	-0.8 (-1.3,-0.2)	0.41	-0.8 (-0.9,-0.7)	0.97 (0.9,1.1)	-1.9 (-2.5,-1.4)	0.29
NE Hanna Shoal 1st	0.7 (0.6, 0.8)	1.0 (0.9, 1.1)	-1.5 (-2.1, -0.9)	0.44	-0.6 (-0.7, -0.5)	0.6 (0.5, 0.7)	0.3 (-0.3, 0.8)	0.14
NE Hanna Shoal 2nd	1.4 (1.2, 1.5)	1.0 (0.9, 1.2)	1.4 (0.2, 2.7)	0.35	-1.0 (-1.2, -0.9)	0.9 (0.7, 1.0)	-5 (-6.4,-3.8)	0.30
NW Hanna Shoal	0.4 (0.3, 0.6)	0.7 (0.6, 0.9)	-7.8 (-8.2,-6.8)	0.09	-1.3 (-2.3,-1.1)	0.9 (-1.4, -1.2)	0.9 (0.8, 1.1)	0.28
NW Hanna Shoal 1st	0.09 (-0.1, 0.2)	1.0 (0.9, 1.2)	-7.5 (-8.3, -6.7)	0.16	-0.9 (-1.0,-0.8)	0.6 (0.4, 0.7)	0.8 (0.1, 1.4)	0.16
NW Hanna Shoal 2nd	1 (0.8, 1.3)	0.2 (-0.1, 0.5)	-10.1 (-11.6, -8.6)	0.07	-1.5 (-1.8, -4.3)	0.7 (0.4, 1.0)	-5.7 (-7.2, -4.3)	0.24

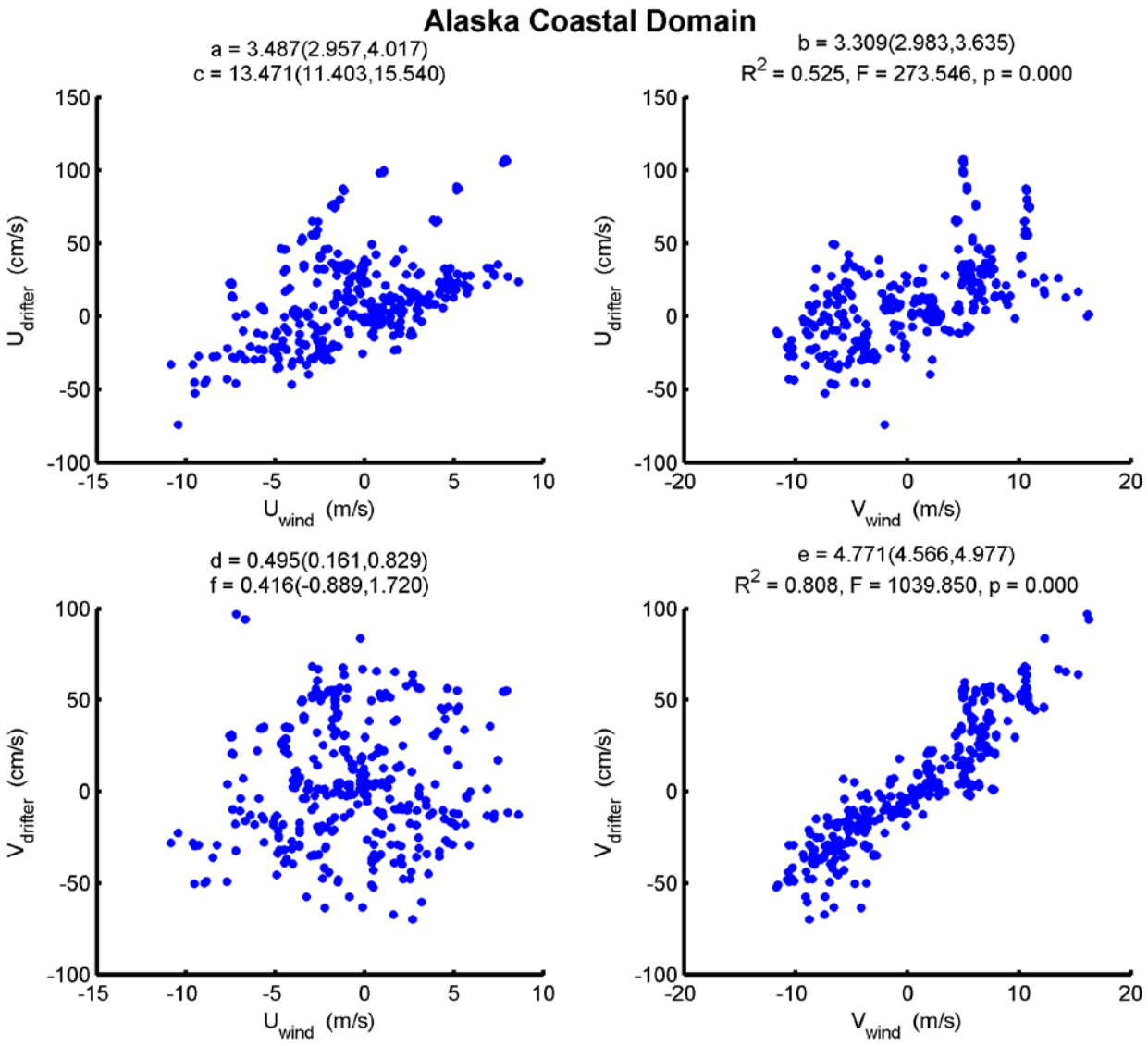

Figure 123. Scatterplots and regression statistics for the iSphere drifters in the Coastal domain. Top row: zonal drifter velocity component versus zonal (left) and meridional (right) wind components. Bottom row: meridional drifter velocity component versus zonal (left) and meridional (right) wind components.

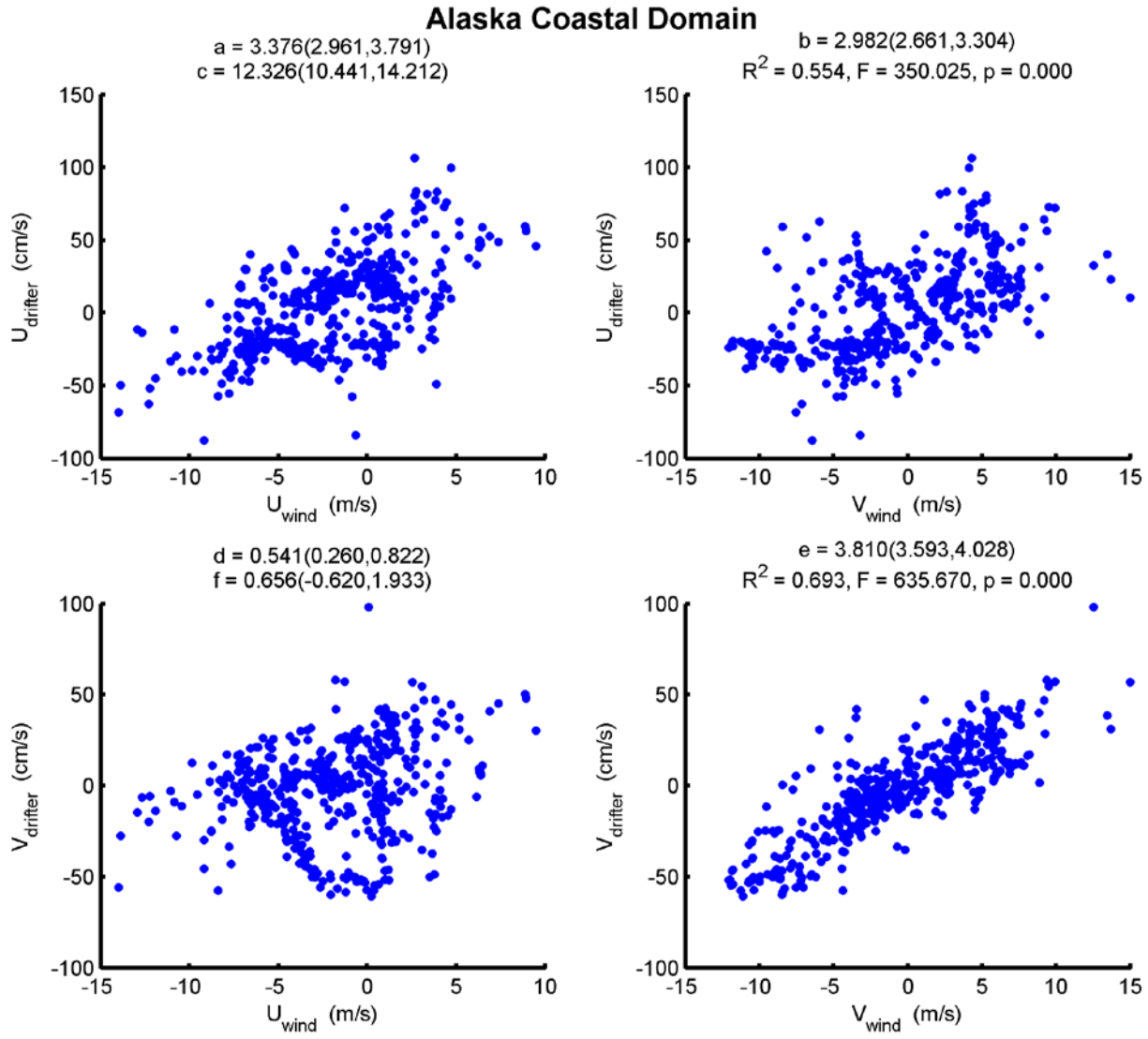

Figure 124. Scatterplots and regression statistics for the MS drifters in the Coastal domain. Top row: zonal drifter velocity component versus zonal (left) and meridional (right) wind components. Bottom row: meridional drifter velocity component versus zonal (left) and meridional (right) wind components.

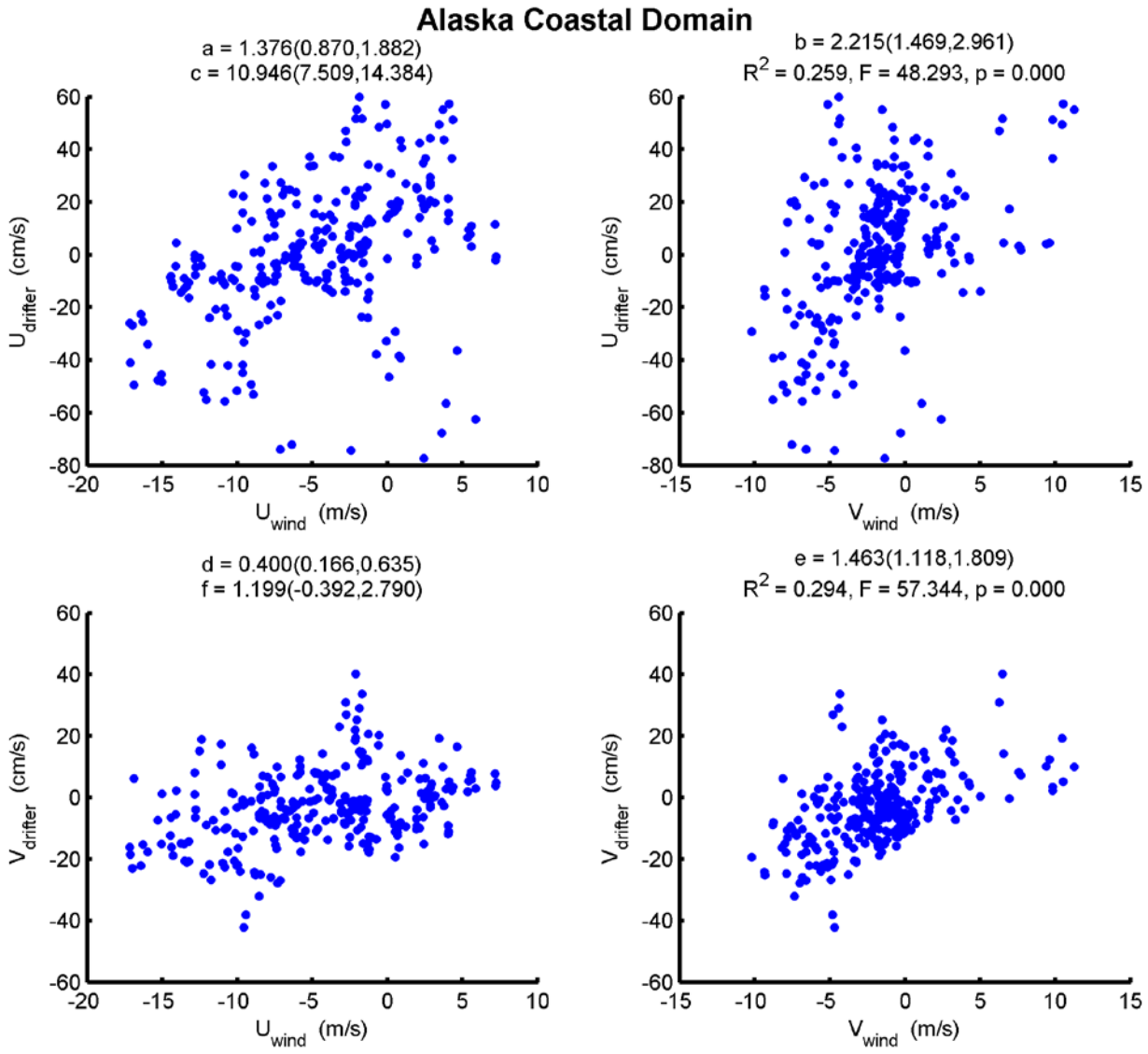

Figure 125. Scatterplots and regression statistics for the SVP drifters in the Coastal domain. Top row: zonal drifter velocity component versus zonal (left) and meridional (right) wind components. Bottom row: meridional drifter velocity component versus zonal (left) and meridional (right) wind components.

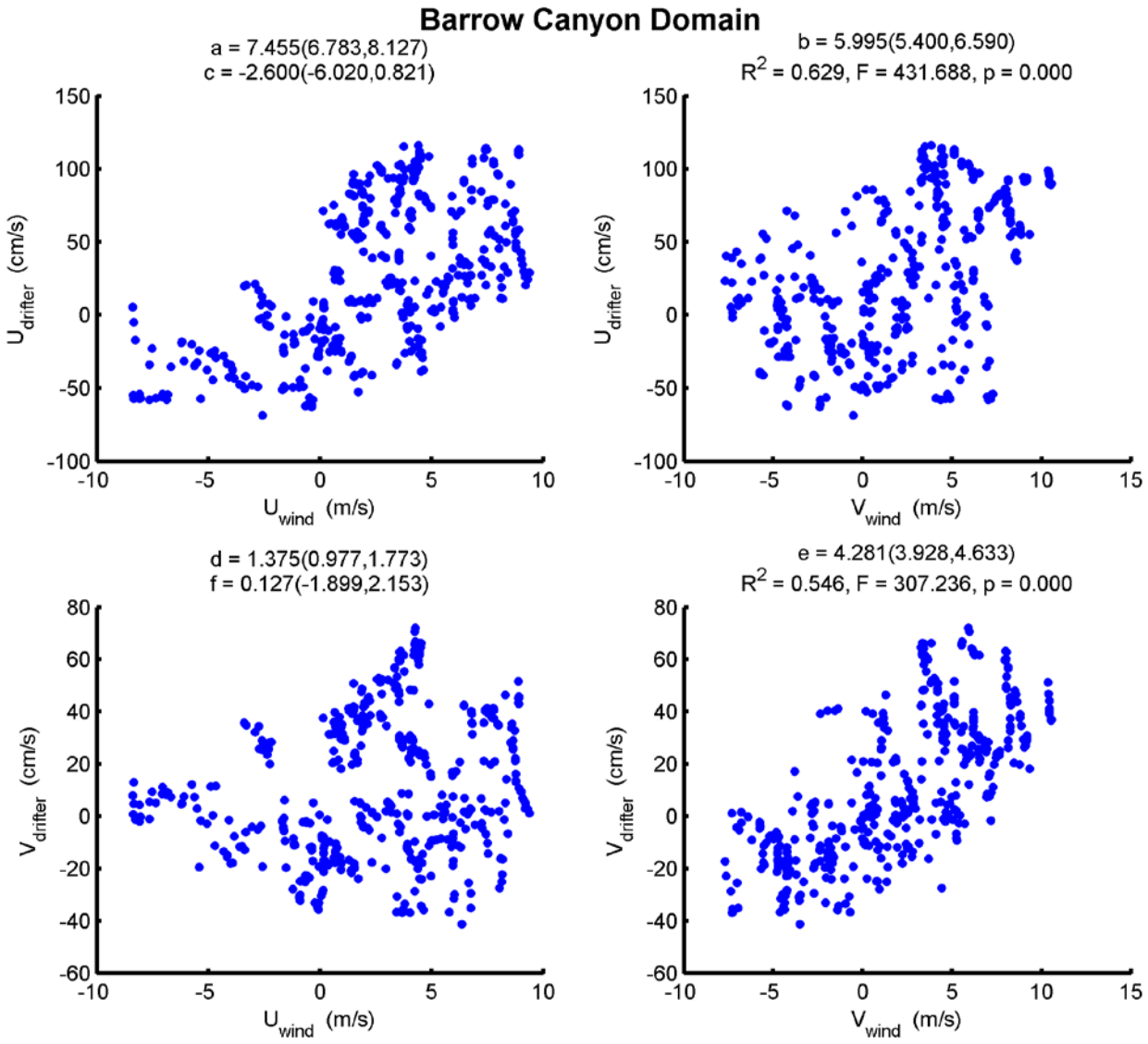

Figure 126. Scatterplots and regression statistics for the iSphere drifters in the Barrow Canyon domain. Top row: zonal drifter velocity component versus zonal (left) and meridional (right) wind components. Bottom row: meridional drifter velocity component versus zonal (left) and meridional (right) wind components.

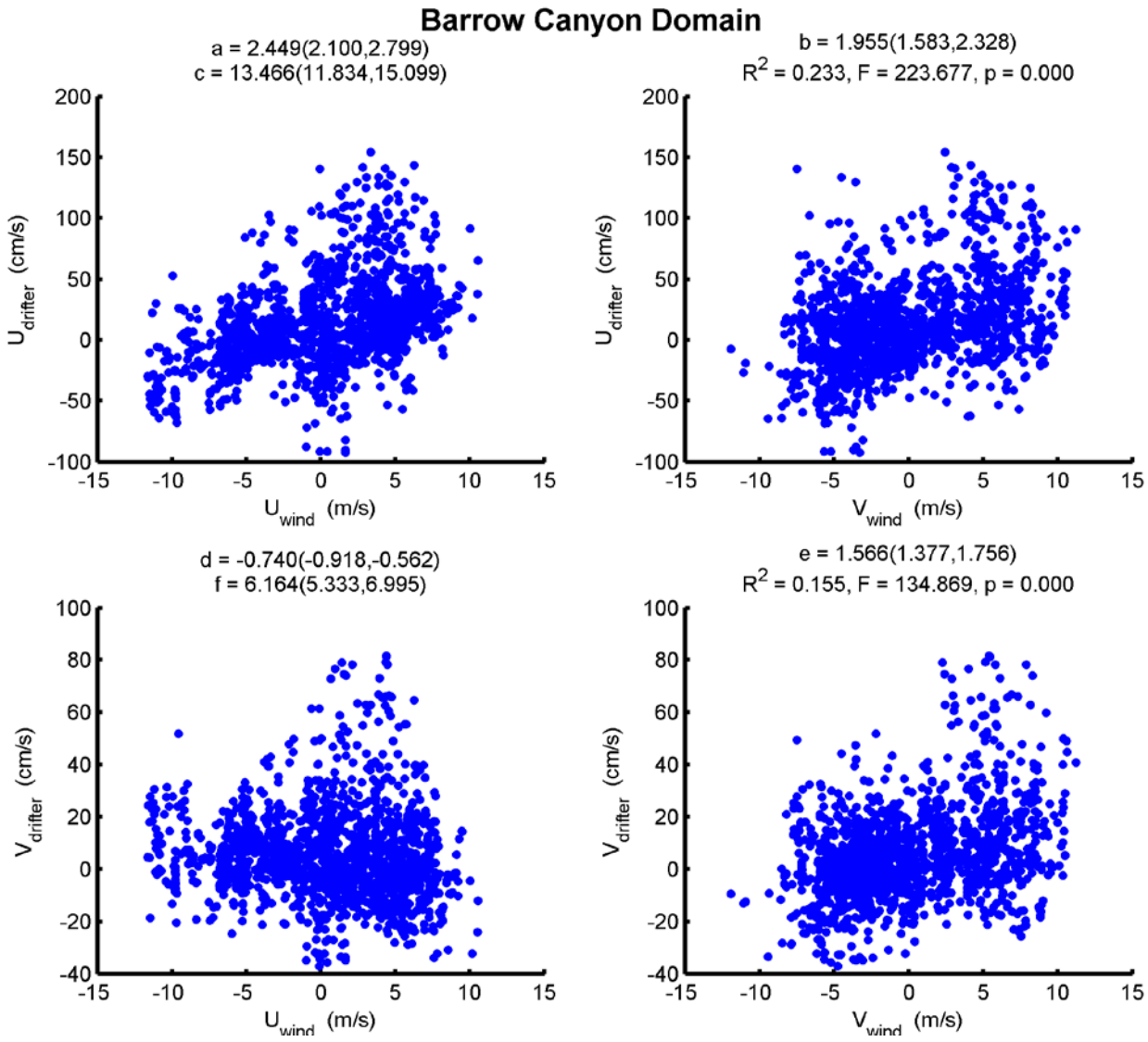

Figure 127. Scatterplots and regression statistics for the MS drifters in the Barrow Canyon domain. Top row: zonal drifter velocity component versus zonal (left) and meridional (right) wind components. Bottom row: meridional drifter velocity component versus zonal (left) and meridional (right) wind components.

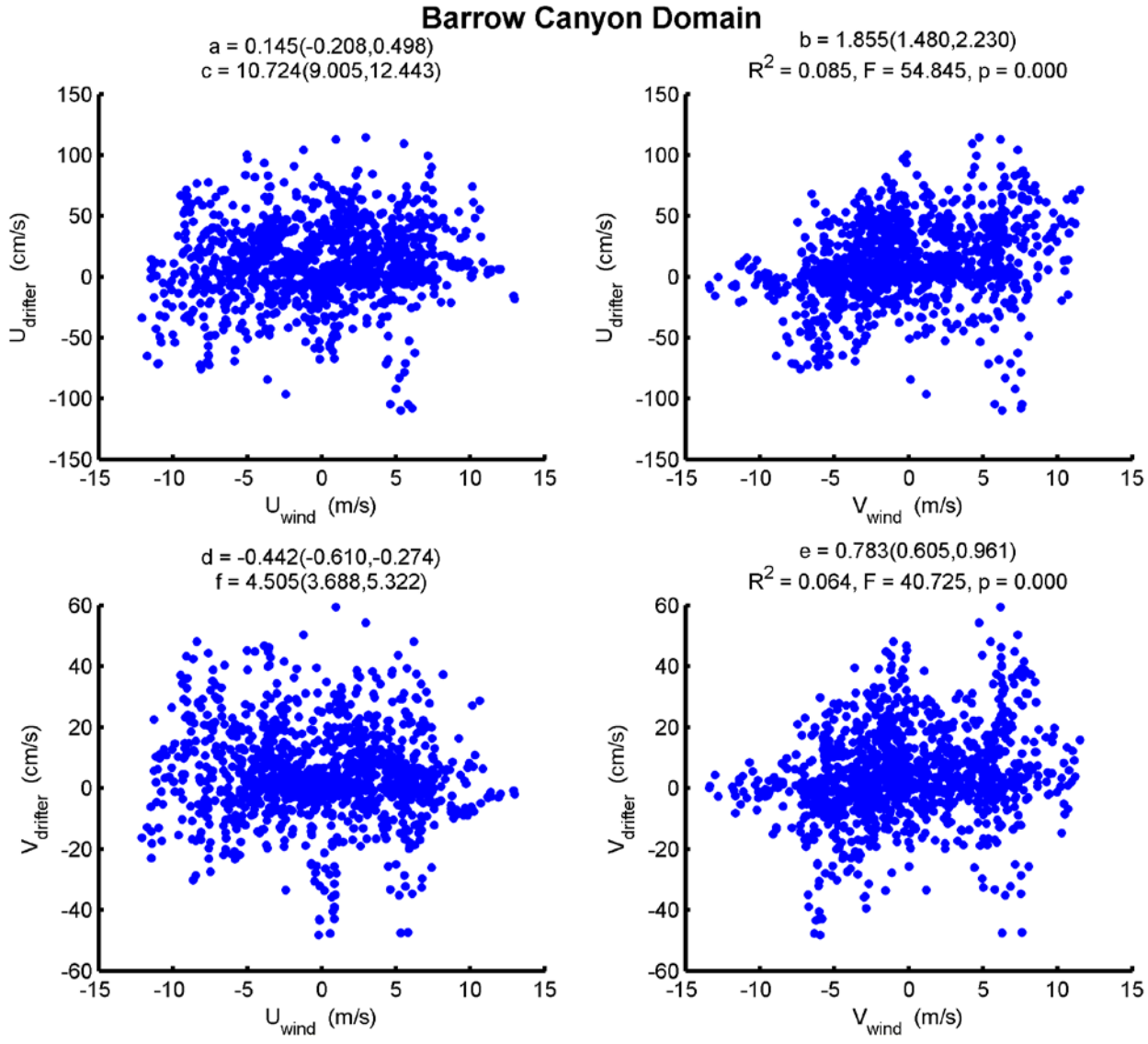

Figure 128. Scatterplots and regression statistics for the SVP drifters in the Barrow Canyon domain. Top row: zonal drifter velocity component versus zonal (left) and meridional (right) wind components. Bottom row: meridional drifter velocity component versus zonal (left) and meridional (right) wind components.

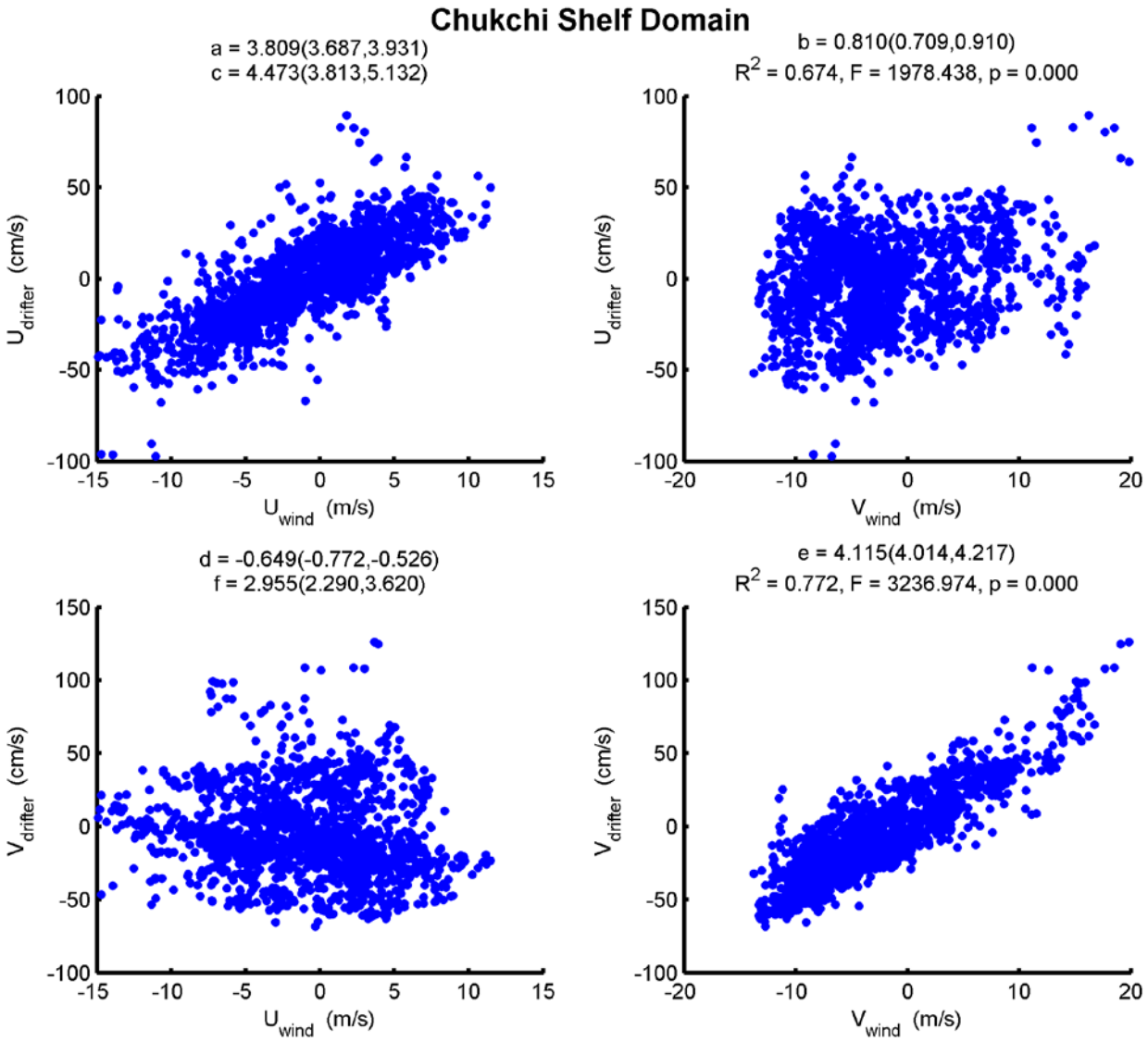

Figure 129. Scatterplots and regression statistics for the iSphere drifters in the Chukchi Shelf domain. Top row: zonal drifter velocity component versus zonal (left) and meridional (right) wind components. Bottom row: meridional drifter velocity component versus zonal (left) and meridional (right) wind components.

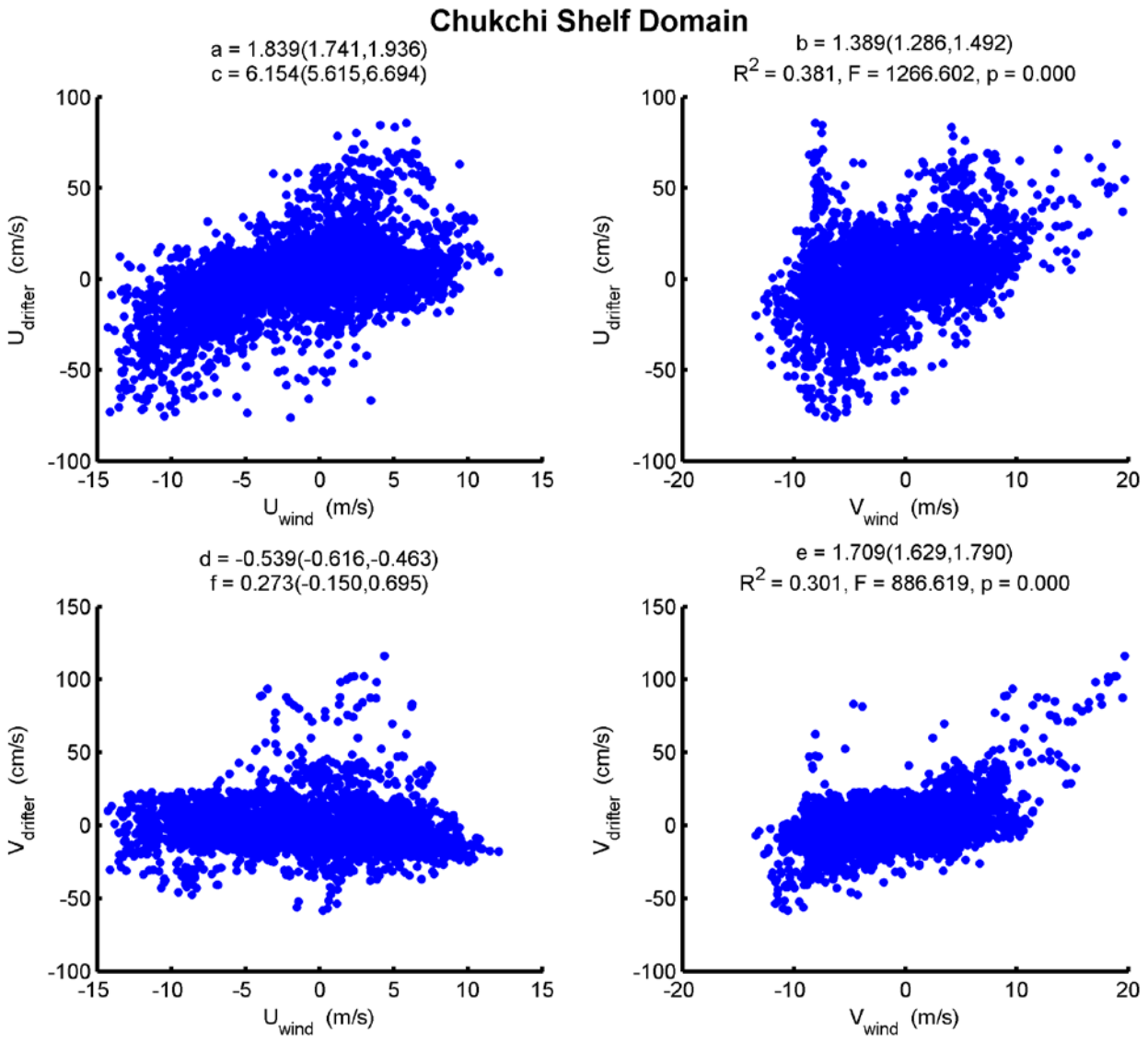

Figure 130. Scatterplots and regression statistics for the MS drifters in the Chukchi Shelf Domain. Top row: zonal drifter velocity component versus zonal (left) and meridional (right) wind components. Bottom row: meridional drifter velocity component versus zonal (left) and meridional (right) wind components.

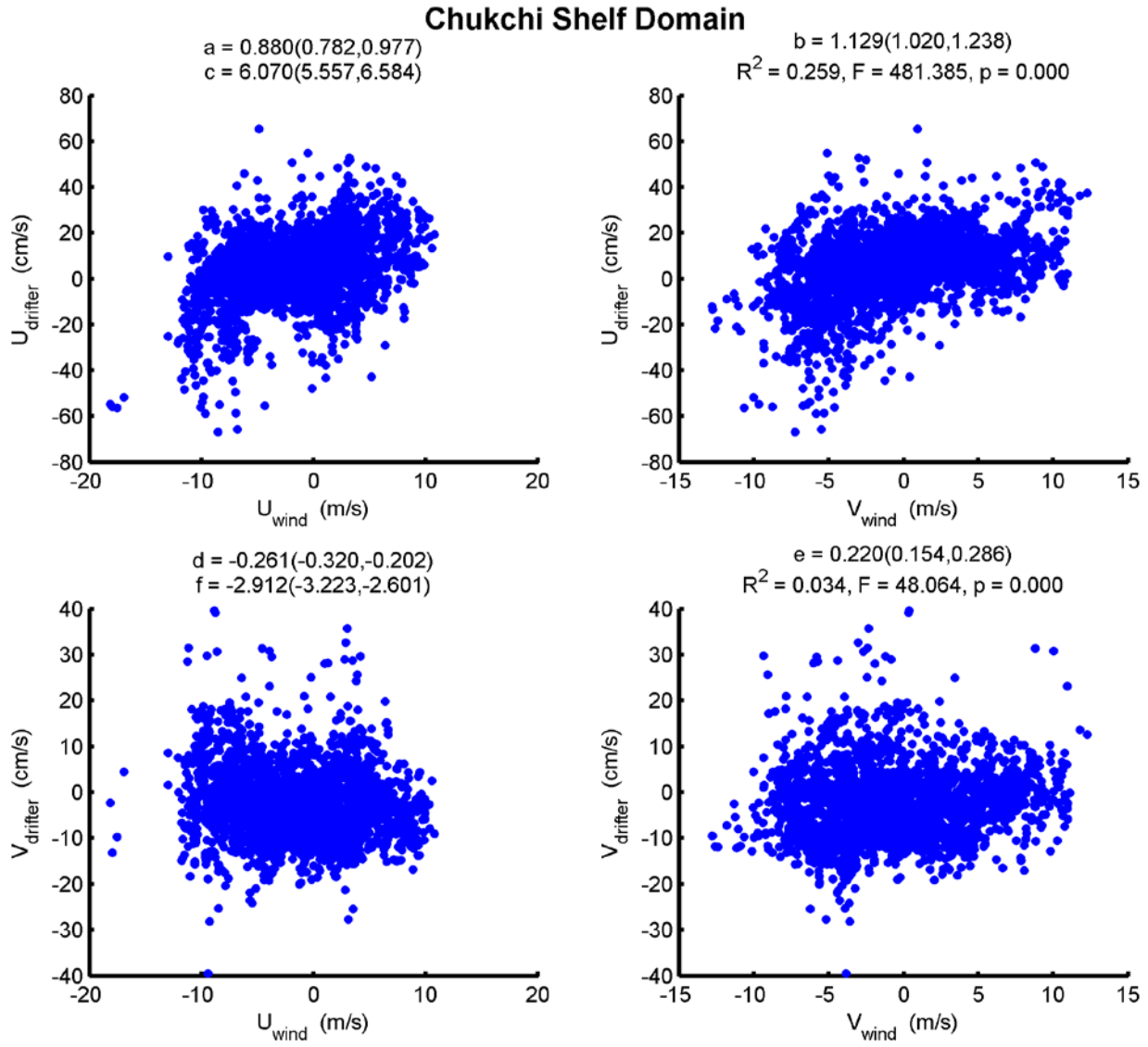

Figure 131. Scatterplots and regression statistics for the SVP drifters in the Chukchi Shelf domain. Top row: zonal drifter velocity component versus zonal (left) and meridional (right) wind components. Bottom row: meridional drifter velocity component versus zonal (left) and meridional (right) wind components.

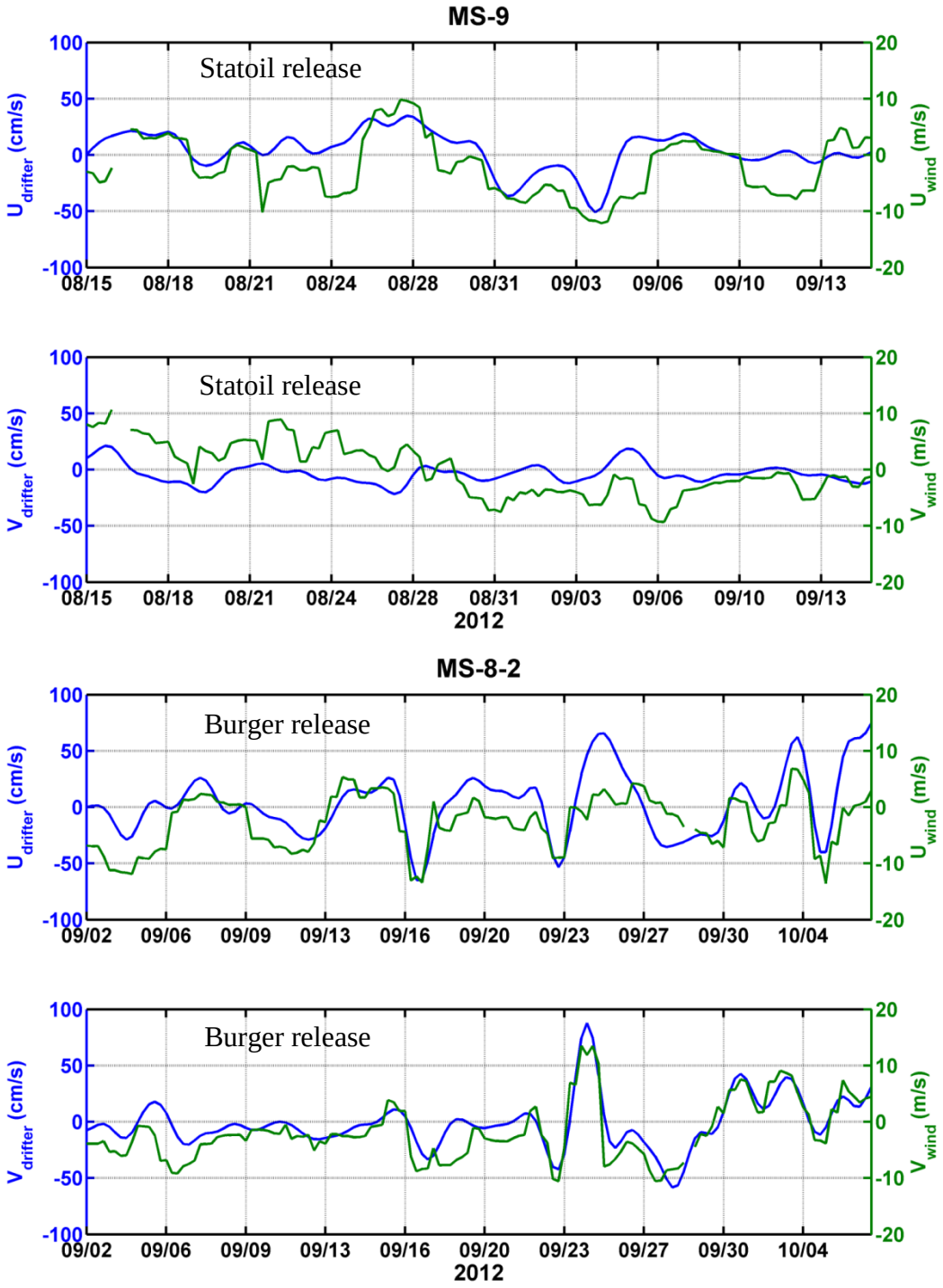

Figure 132. Wind-current comparisons between MS-9 (released in Statoil in mid-August; top two panels) and MS-8-2 (released in Burger in early September; bottom two panels).

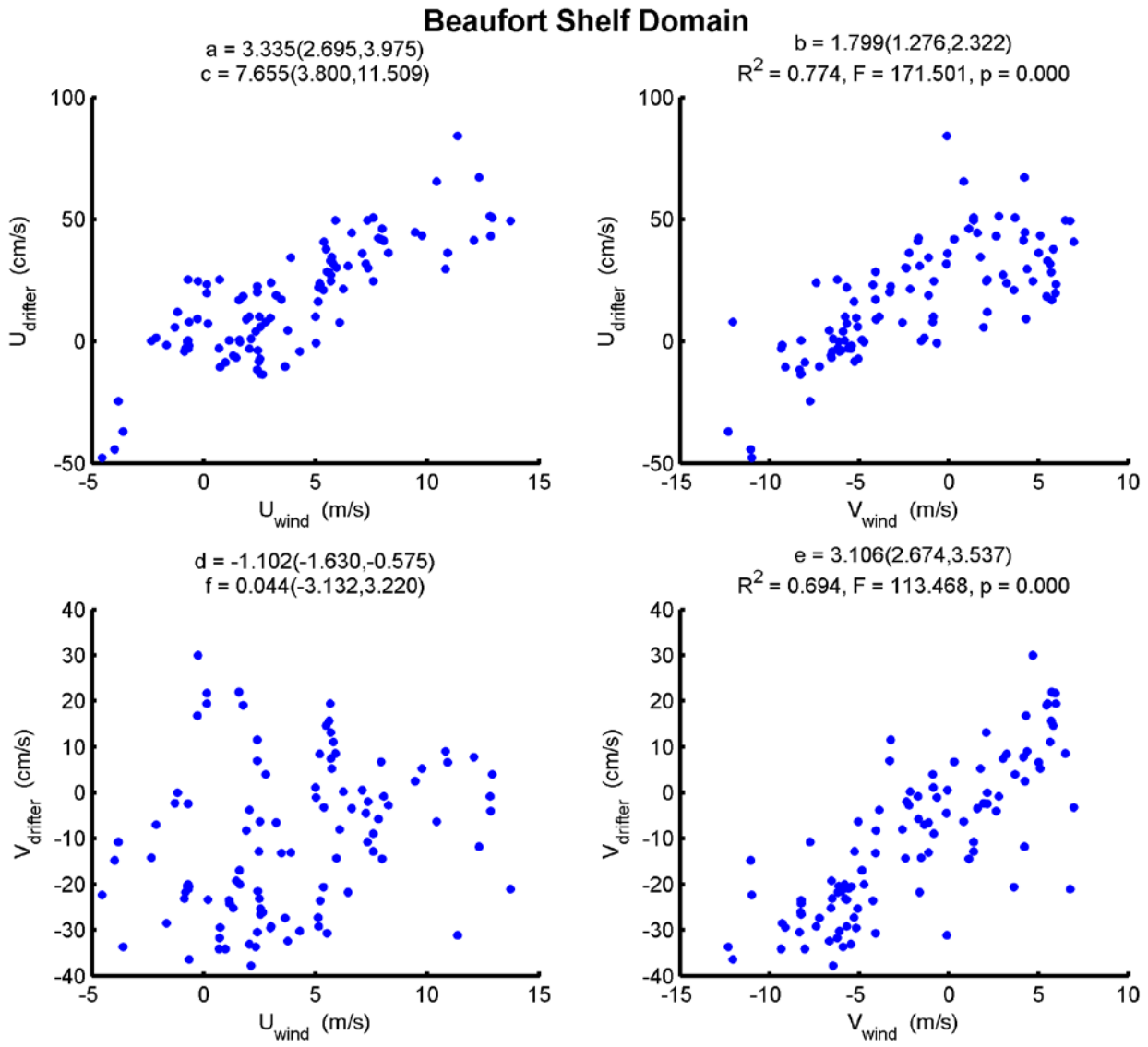

Figure 133. Scatterplots and regression statistics for the iSphere drifters in the Beaufort Shelf domain. Top row: zonal drifter velocity component versus zonal (left) and meridional (right) wind components. Bottom row: meridional drifter velocity component versus zonal (left) and meridional (right) wind components.

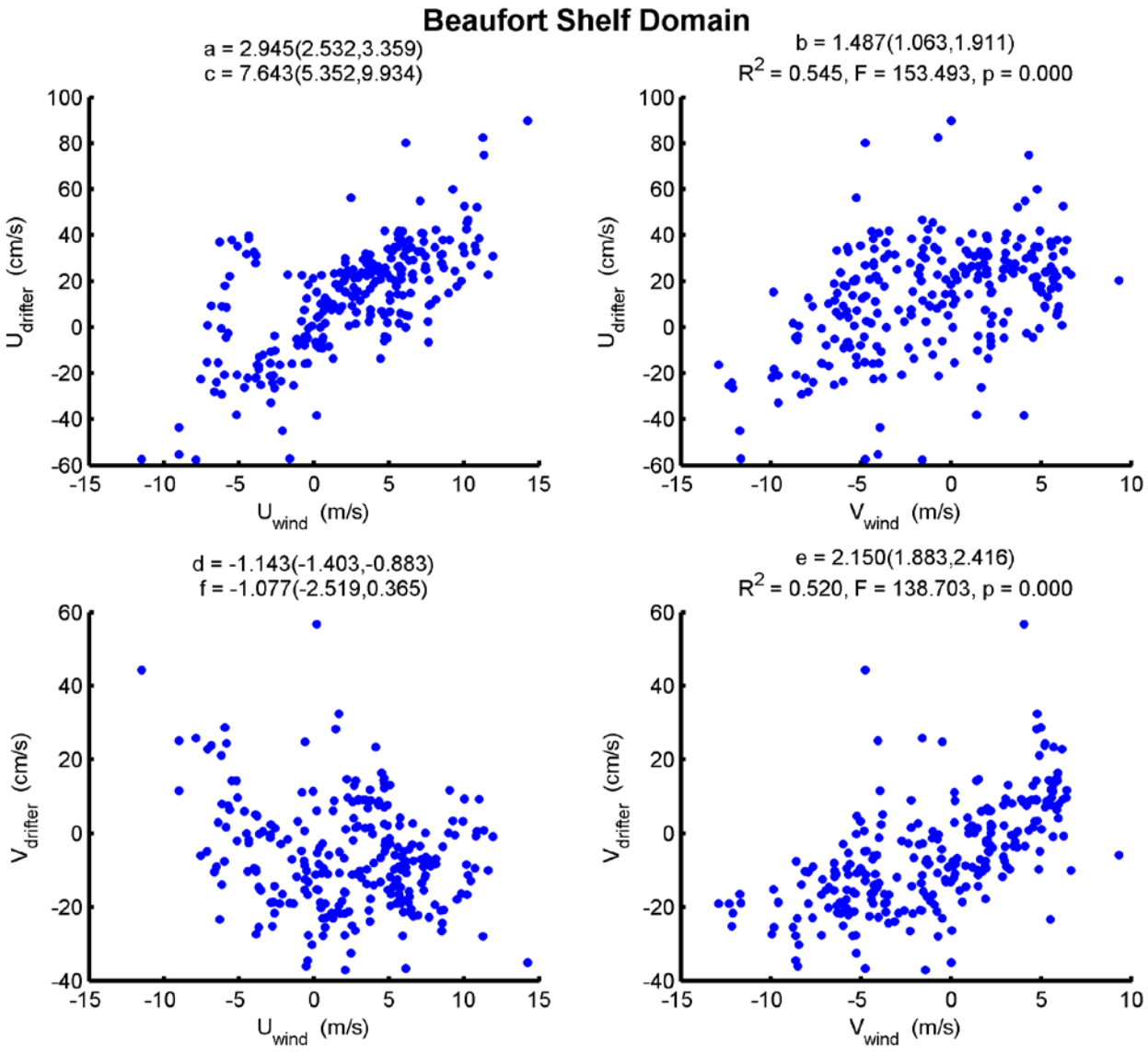

Figure 134. Scatterplots and regression statistics for the MS drifters in the Beaufort Shelf domain. Top row: zonal drifter velocity component versus zonal (left) and meridional (right) wind components. Bottom row: meridional drifter velocity component versus zonal (left) and meridional (right) wind components.

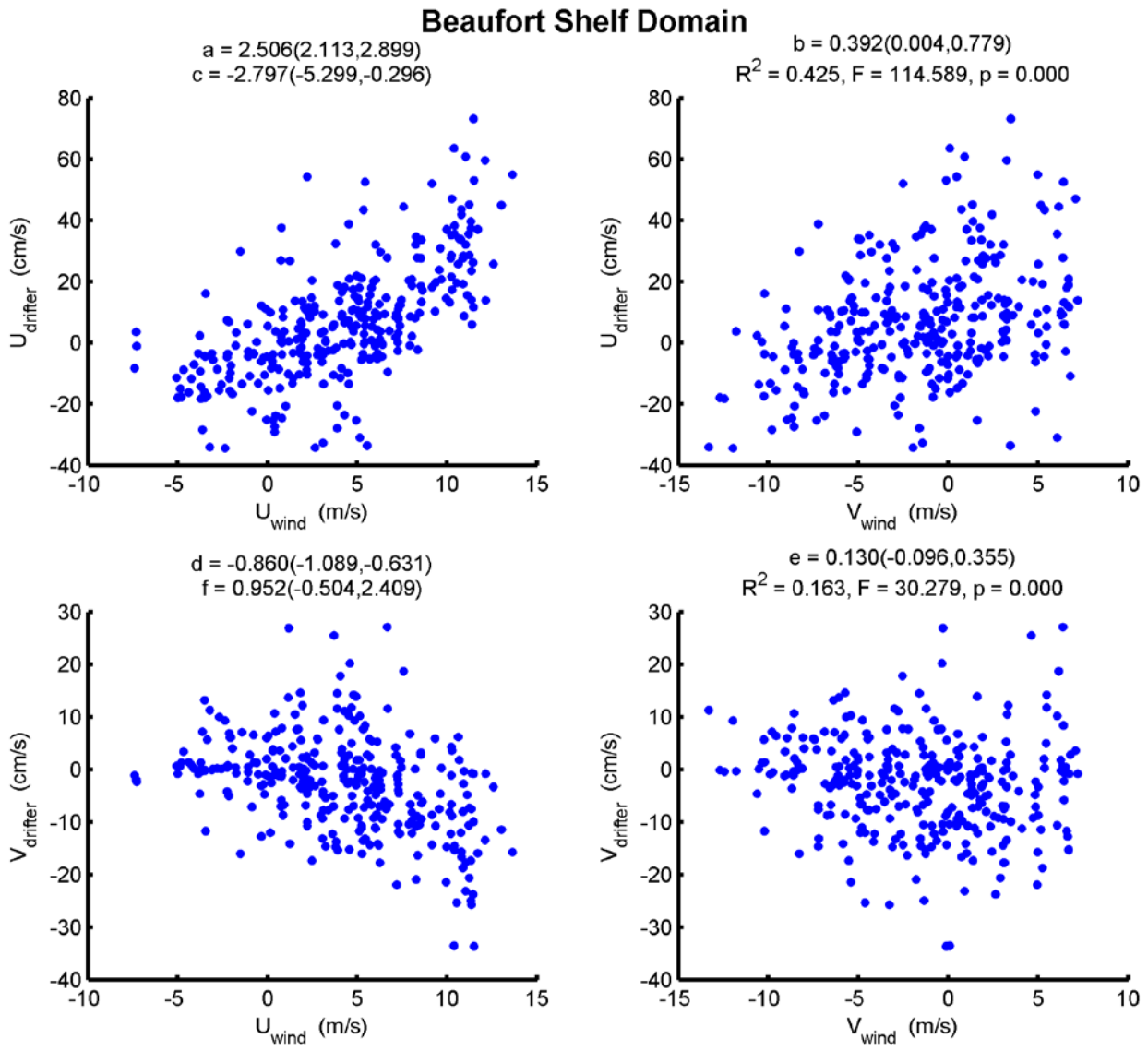

Figure 135. Scatterplots and regression statistics for the SVP drifters in the Beaufort Shelf domain. Top row: zonal drifter velocity component versus zonal (left) and meridional (right) wind components. Bottom row: meridional drifter velocity component versus zonal (left) and meridional (right) wind components.

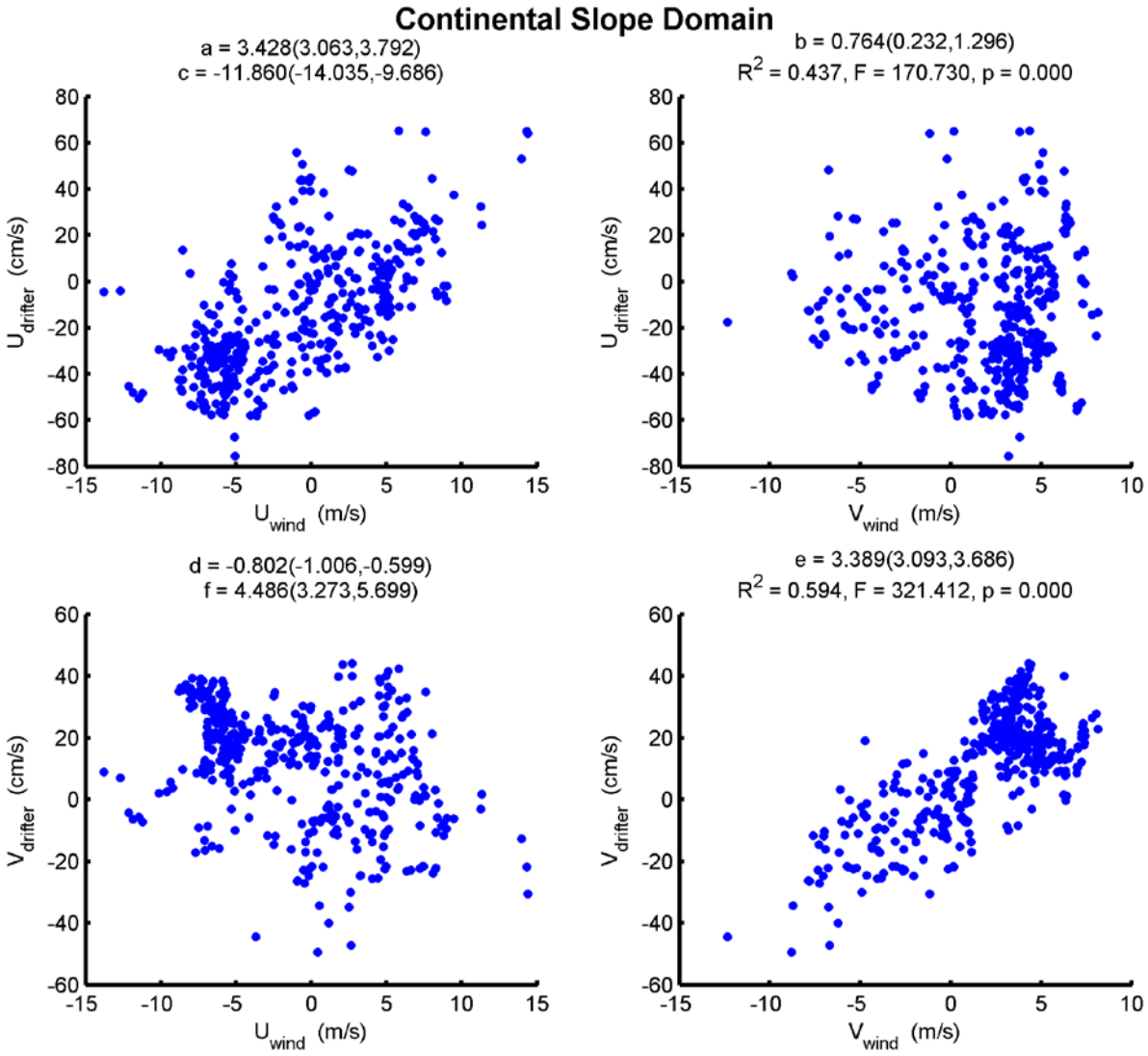

Figure 136. Scatterplots and regression statistics for the iSphere drifters in the Continental Slope domain. Top row: zonal drifter velocity component versus zonal (left) and meridional (right) wind components. Bottom row: meridional drifter velocity component versus zonal (left) and meridional (right) wind components.

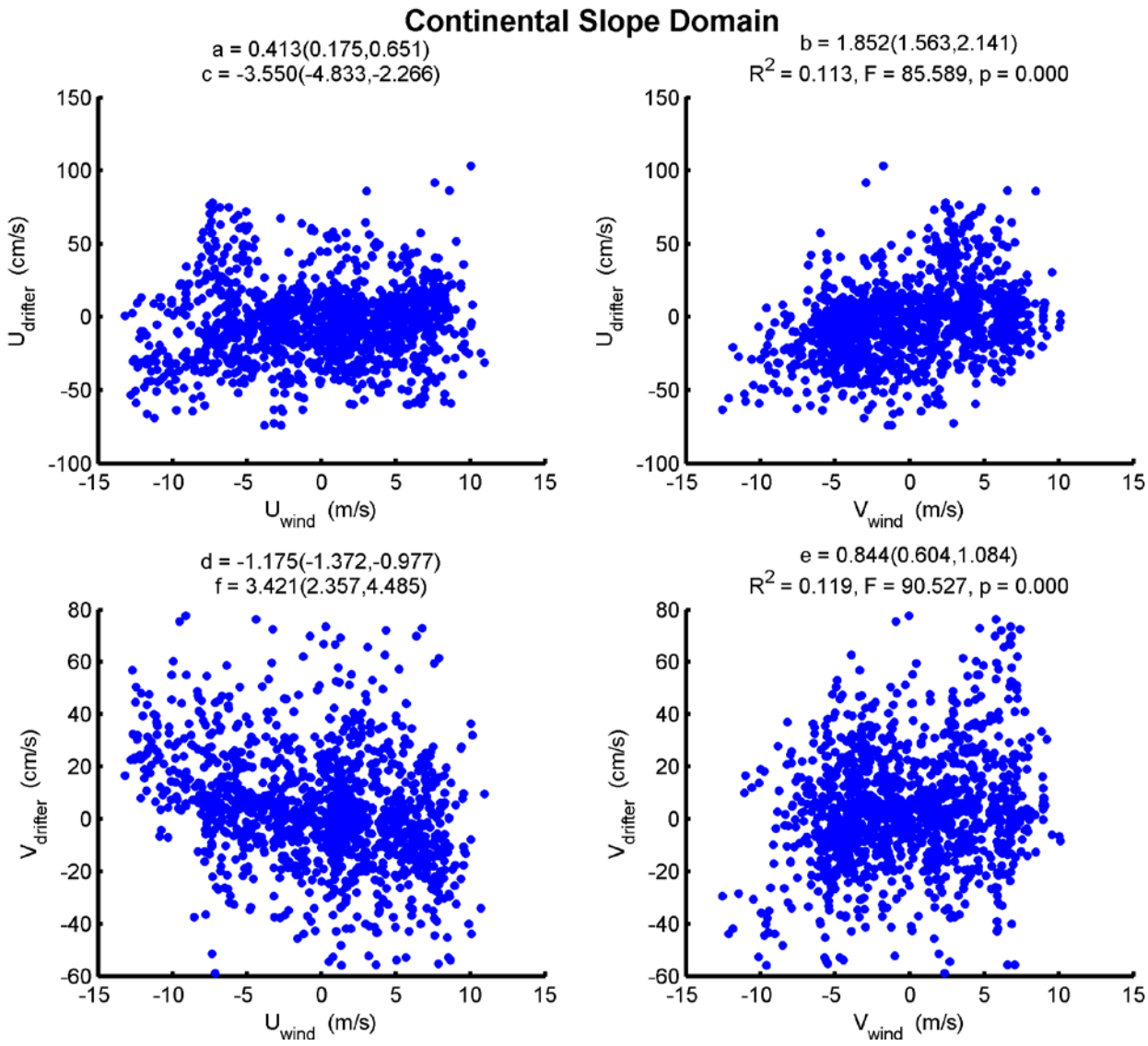

Figure 137. Scatterplots and regression statistics for the MS drifters in the Continental Slope domain. Top row: zonal drifter velocity component versus zonal (left) and meridional (right) wind components. Bottom row: meridional drifter velocity component versus zonal (left) and meridional (right) wind components.

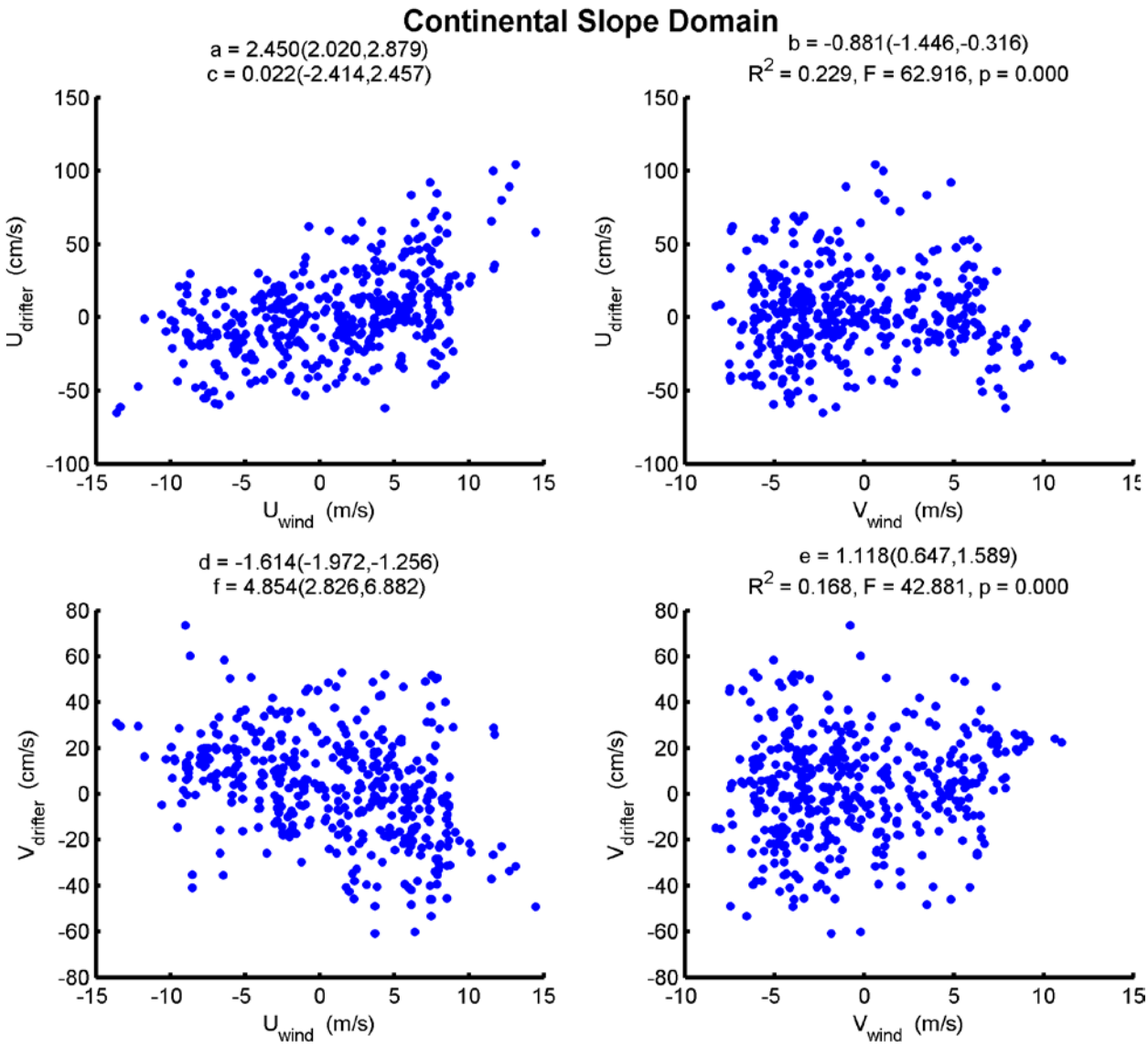

Figure 138. Scatterplots and regression statistics for the SVP drifters in the Continental Slope domain. Top row: zonal drifter velocity component versus zonal (left) and meridional (right) wind components. Bottom row: meridional drifter velocity component versus zonal (left) and meridional (right) wind components.

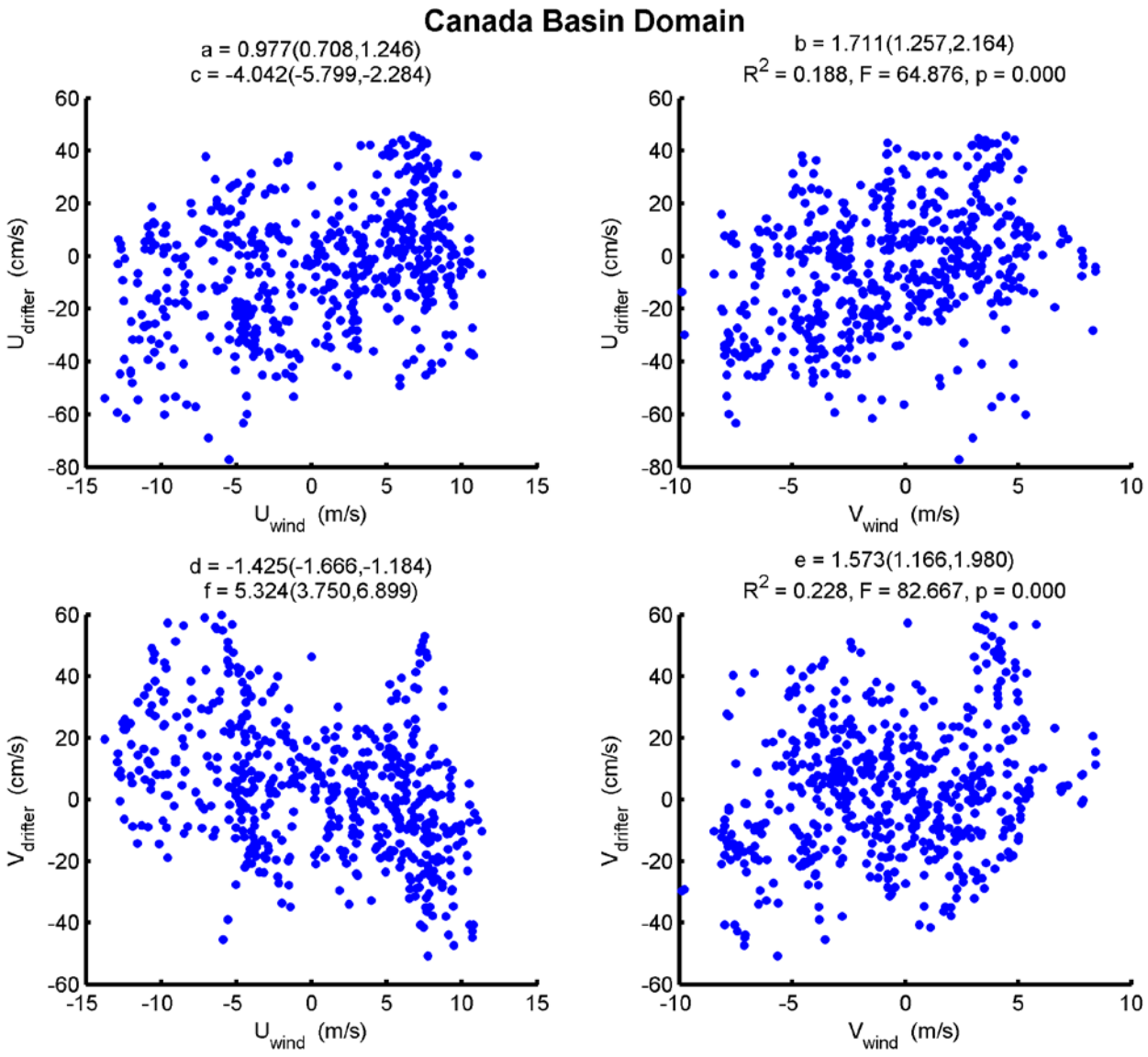

Figure 139. Scatterplots and regression statistics for the MS drifters in the Canada Basin domain. Top row: zonal drifter velocity component versus zonal (left) and meridional (right) wind components. Bottom row: meridional drifter velocity component versus zonal (left) and meridional (right) wind components.

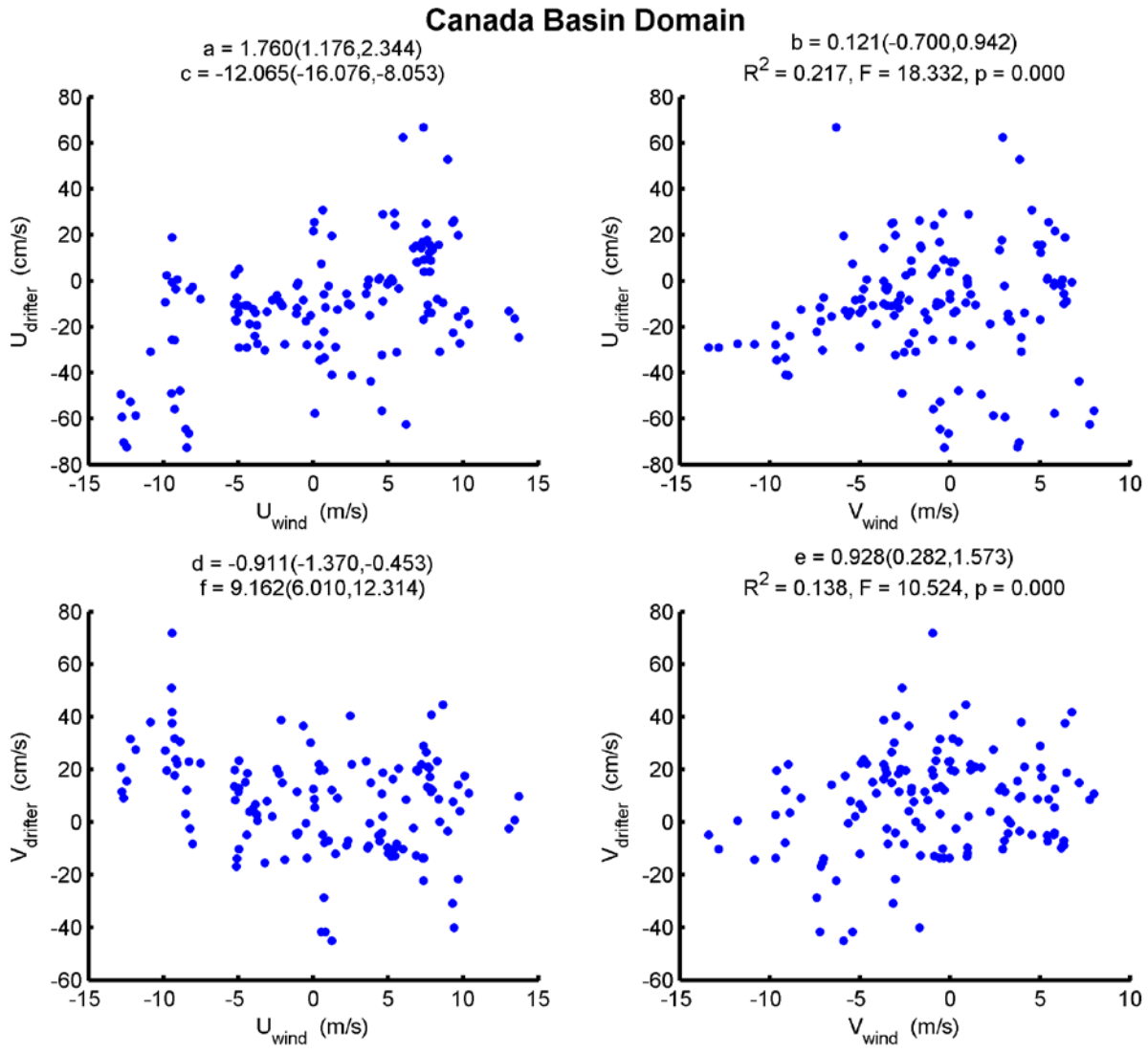

Figure 140. Scatterplots and regression statistics for the SVP drifters in the Canada Basin domain. Top row: zonal drifter velocity component versus zonal (left) and meridional (right) wind components. Bottom row: meridional drifter velocity component versus zonal (left) and meridional (right) wind components.

We conclude this section with a comparison between drifter velocities and those obtained from moorings and/or the HF radar. **Figure 141** consists of the comparison between drifters passing within 15 km of the acoustic doppler current profiler (ADCP) on mooring BC2 (in Barrow Canyon) in September and October 2012. The zonal velocities are in good agreement with the slope not significantly different from 1 and the ADCP explaining about 66% of the variance in the drifter velocities. The intercept indicates that there is no significant bias, but the confidence limits on this statistic are broad. The fit is poorer between the meridional velocity components where the ADCP explains only 38% of the variance in the drifter meridional velocity. These differences may be due to the rather large horizontal shears typically present in the canyon (*Weingartner et al.*, 2013a). **Figure 142** compares the "hourly" HFR U and V components for the period of the Burger cluster in September – October 2012.

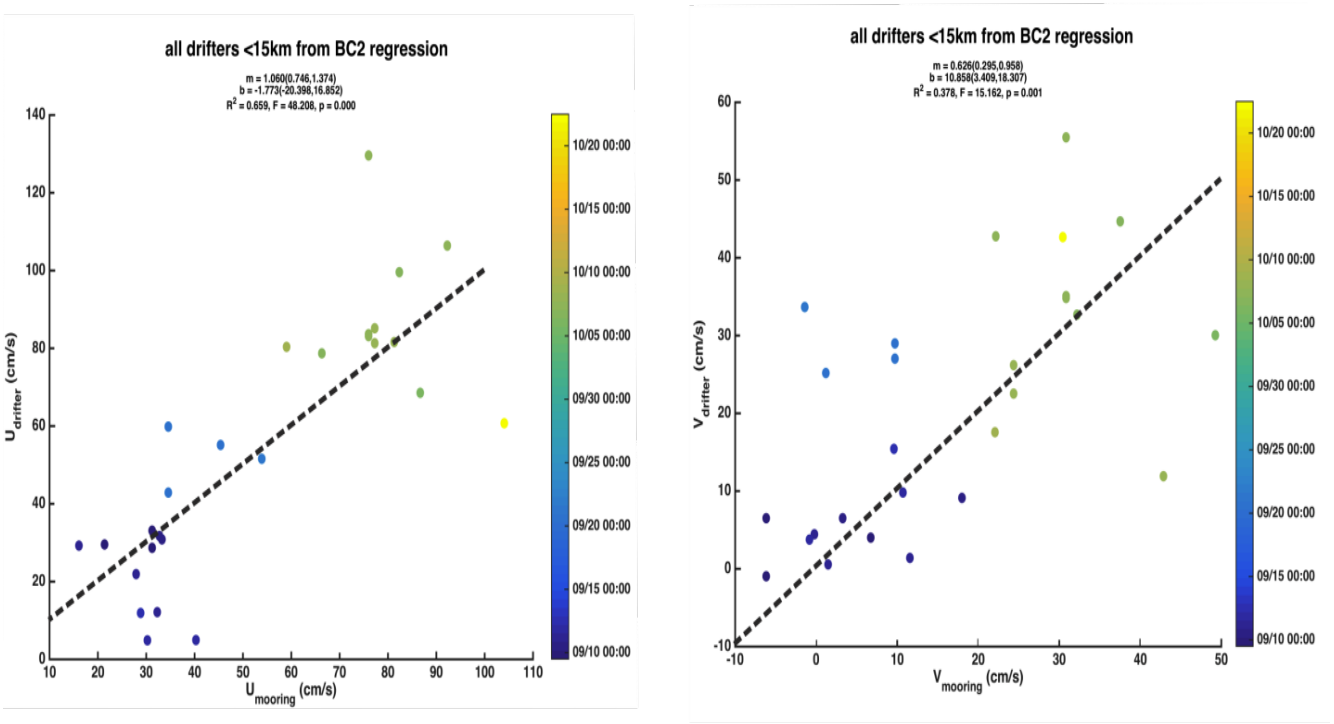

Figure 141. Scatterplots of zonal (U; left) and meridional (V; left) velocities between drifters and mooring BC2 in Barrow Canyon.

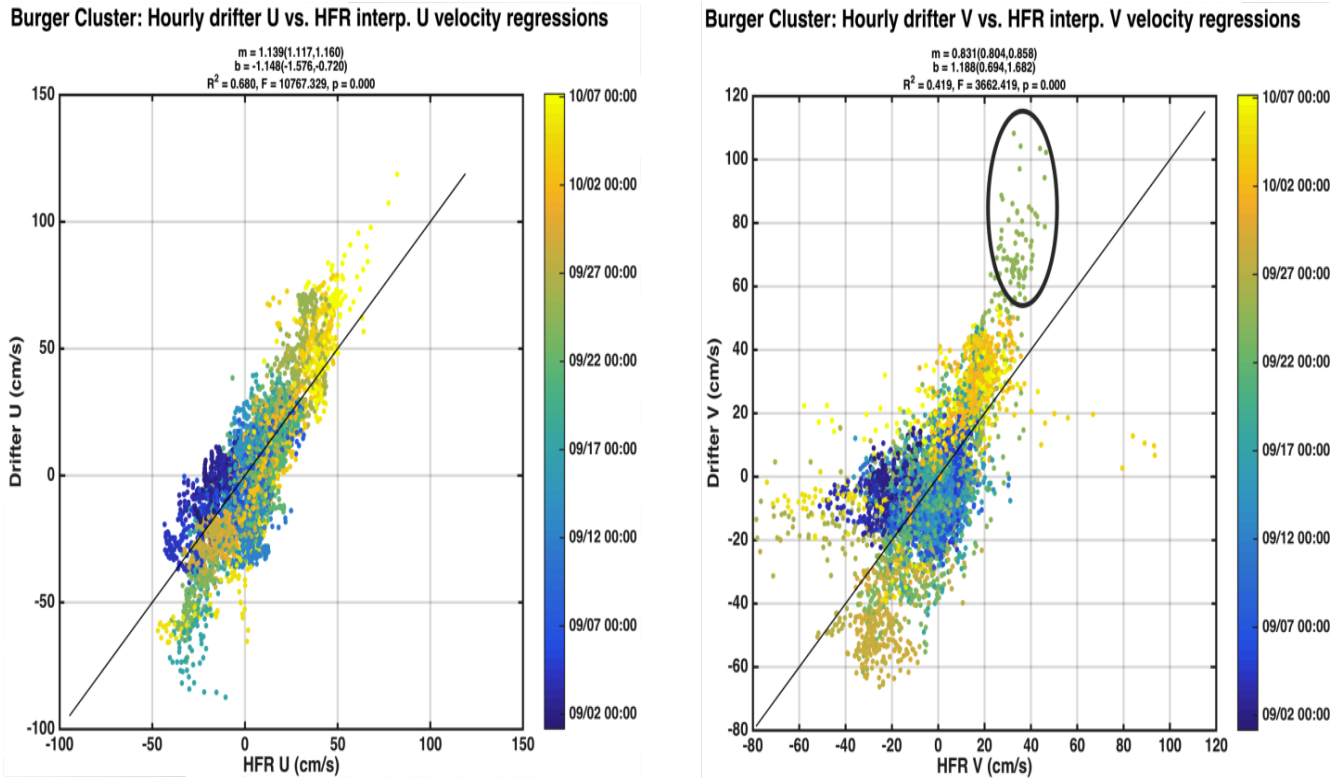

Figure 142. Scatterplots of zonal (U; left) and meridional (V; left) velocities between drifters and the high-frequency radar for the Burger drifter cluster of September and October 2012. The ellipse around the points in the left hand panel describes points in poor agreement on and about 24 September.

The results are good overall, with the U-regressions explaining ~70% of the variance and those for V explaining ~42% of the variance. There are several reasons for the differences between the drifters and the HFR. First, the drifters sample hourly and the velocity is computed at a point. The HFR "hourly" values are actually smoothed estimates made over three-hour intervals. The regressions improve if we filter both the drifter velocities and the HFR data sets with a 35-hour cutoff filter (the r^2 for U and V improve to 80 and 50%, respectively). Each HFR velocity is also interpolated to the position of the drifter at the location of the drifter using at least three surrounding HFR velocities. We have included all points in the HFR radar mask that met our acceptance criteria, including those at the edge of the mask that may be uncertain. In particular, the V velocities disagree noticeably on 24 September (indicated by the ellipse in the figure). At that time, the drifters were all on the southwest edge of the HFR domain and velocity estimates there are relatively poor.

V. Conclusions

The drifter trajectories deployed in this program resulted in an unprecedented Lagrangian perspective of the near surface circulation of the Chukchi and Beaufort Seas and their adjoining shelfbreaks. This achievement was accomplished by drifter deployments made in a variety of different areas of the Chukchi Sea Shelf during the open water periods in 2011 – 2013. The results reflect differences in winds, sea ice, hydrography, bathymetry of the shelf and shelfbreak, and the spatially different dynamical regimes that the drifters moved across. These include the Chukchi Sea Shelf, the inner shelf (water depths <20 m) of the Chukchi Sea, Barrow Canyon, the Chukchi-Beaufort shelfbreak and continental slopes, the Beaufort Shelf, and the Canada Basin. Our results were also subject to interannual variations in winds, sea-ice distribution, and hydrographic conditions.

Winds between August and November in each deployment year were primarily from the northeast, which favor coastal upwelling along the Chukchi Sea coast. There was, however, considerable interannual variability on both seasonal and synoptic timescales. In particular, northeasterly winds were dominant from August through October in 2011 and 2013 when, compared to 2012, there was relatively little synoptic variability. In November of 2011 and 2013, the wind regime included nearly equal frequencies of southerly and northerly winds and was much more variable than in previous months. In contrast, the winds in 2012 were from southerly quadrants in August and through much of October, but northeasterly in September. While there was considerable directional variability in the winds in November of 2012, the wind speeds were generally <5 m s^{-1} and much weaker than the same period in 2011 and 2013.

The ice cover also differed amongst these years. In 2011, the shelf was virtually ice free by mid-August and remained so until early November, when ice started forming along the northwest coast of Alaska. In 2012 and 2013, sea ice extended along 71°N between the Central Channel and the coast until mid-August and then retreated and remained over Hanna Shoal into mid-

September of 2012 and early September of 2013. Sea ice advanced more rapidly compared to 2011 in both of these years. In 2012, the shelf north of 68.5°N was covered with ice by mid-November, whereas in 2013 ice advanced as far south as 71°N by this date.

These differences in ice extent were reflected in the hydrography. In 2011, there was virtually no MW detected on the northeastern shelf and WW was confined to the region around the southeastern and eastern sides of Hanna Shoal. Throughout the rest of the area warmer, and moderately saline BSW occurred. In particular, west of Hanna Shoal weakly stratified BSW was present in the Central Channel. In 2013, the Central Channel waters were the warmest observed over the northeastern shelf. These warmer waters reflect the northward flow typical within the Channel, which serves as an important conduit for waters flowing northward from Bering Strait. In both 2012 and 2013, MW was prevalent north of about 71.5°N throughout August and September and WW extended across much of the northeastern shelf. These differences in water mass distribution profoundly affected the shelf stratification and frontal formation. North of ~71.5°N, the shelf was heavily stratified and a prominent upper ocean front straddled this latitude in both 2012 and 2013. Not surprisingly, these fronts were also approximately aligned with the August ice-edge in both years. In 2011, no surface fronts were evident and the stratification was much weaker overall. With respect to the shallow-drogued drifters used in this project, the stratification affects the efficacy by which the wind's momentum is mixed into the water column. Under the strongly stratified conditions associated with regions where MW overlies WW, the pycnocline is confined to the upper 10 – 15 m and strong vertical shears are expected. Under the more weakly stratified conditions found elsewhere (or at other times) on the shelf, the vertical shear should be weaker. Consequently, we expected to find greater divergence between drifters drogued at different depths where the stratification is strong.

The hydrographic data from 2013 indicated that much of the nearshore hydrographic structure was consistent with the upwelling-favorable winds that prevailed over the northeast Chukchi Sea in August and September of that year. These winds resulted in the offshore displacement of relatively warm and fresh ACW above colder, denser WW. Some of this dense water appeared to have been upwelling within at least 20 km of the coast.

Drifters deployed near the coast under upwelling-favorable winds moved quite differently from those deployed under non-upwelling conditions. In this regard, the drifters deployed in 2013 in the Northeast Chukchi Sea were substantially different from those deployed in August of 2012 under southwesterly winds. In that year, nearly all of the drifters deployed on the shelf and nearshore exited the shelf through Barrow Canyon. In 2013, the Wainwright and Pt. Lay drifters were all deployed under upwelling-favorable winds that exceeded 6 m s^{-1} from the northeast. All of these drifters moved westward and offshore.

It is of some surprise that the year-to-year differences in water properties and ice cover do not appear to depend heavily on the regional winds. For example, we might have expected that the

persistent northeasterly winds in August and September of 2011 would have delayed the arrival of BSW into the area and perhaps delayed the retreat of ice. Similarly, these winds might have been expected to promote the southward advection of both MW and WW. Clearly this did not occur. One might expect also that the southerly winds of August 2012 would have promoted northward advection of BSW into the area and yet the northward extent of this water mass was far less than in August 2011. One possible reason for these interannual differences in shelf properties may have been due to changes in the mass and heat transports in Bering Strait. For example, in 2011, the northward mass and heat transports through the Strait were anomalously high (*Woodgate et al*., 2012; *Danielson et al.,* 2014) and equivalent to that of 2007, which was also a year of very low ice concentrations on the Chukchi Sea Shelf. In contrast the transport in 2012 was almost half that of 2011. One key difference between these years was that the sea surface height difference between the Aleutian Basin in the Bering Sea and the Chukchi Sea Shelf was much greater in 2011 than in the latter years (*Danielson et al., 2014*). This implies that the pressure gradient that forces flow northward through the Strait and over the Chukchi Shelf was stronger in 2011 than in either 2012 or 2013. These transports subsequently decreased markedly in 2012 and 2013. Consequently, the pressure field over the Chukchi Sea Shelf was different among these years. Interannual changes in this pressure field will also affect the magnitude of the wind-forced flow field.

The amount of ice remaining over Hanna Shoal in the summer and fall may be partially a function of advection of sea ice into this region from December through April time frame prior to the open water season. If heavily deformed ice is advected onto and grounded over the Shoal, it may provide the basis for additional ice aggregation and deformation throughout winter. Indeed, there was grounded ice atop Hanna Shoal in both the winters of 2012 and 2013, with this ice persisting through summer (Dr. A. Mahoney, UAF, personal communication, January 2015). An extensive volume of grounded and melting ice over the Shoal can serve as a reservoir for MW that is then distributed over the shelf by winds and/or instabilities generated along the MW/BSW front. As a point of emphasis, the summers of 2011 and 2012 stand out as two of the three lowest years in terms of Arctic-wide sea ice extent (the other summer being 2007) since the dawn of the satellite sea ice record in 1979. Hence, the ice conditions over the northeastern Chukchi Shelf in summer appear to be largely a local phenomenon. The hydrographic conditions in this region are thus a function of local processes (fronts, winds, and the bathymetry with respect to trapping ice and MW) and remote (in both time and space) processes that affect heat, salt, and ice transports.

The prominent frontal structures present in 2012 and 2013 are prone to baroclinic instabilities that give rise to mesoscale meanders and eddies as mentioned previously. We have run a simple model (*Lu et al.,* submitted) that supports our contention that these mesoscale features were operating in 2012 and 2013. This is indicated by **Figure 143**, which shows the model results stemming from two simple manifestations of the frontal and stratification structure of the region. These examples are based on the Rutgers Ocean Modeling System (ROMS) configured on an *f*-plane for a 150 km x 150 km channel, with a constant depth of 50 m. The meridional (*y*) walls

are impermeable, the zonal (x) boundaries are periodic, the horizontal and vertical resolutions are 500 m and 1 m, respectively, and the integration time step is 1 min. Bottom friction is quadratic with a drag coefficient of C_D = 5 x 10^{-4} m s^{-1}. The vertical diffusivity is 5 x 10^{-6} m^2 s^{-1} and the horizontal diffusivity was set to minimal values to suppress numerical noise. We conducted two experiments that differed only with respect to their initial density (ρ) distribution (**Figure 143f**). Model 1 (M1) initially has a strongly stratified 2-layer structure confined to the northern half (y > 75 km) of the domain. This includes a front separating MW in the upper 20 m and WW in the lower 30 m from a 50 m deep layer of unstratified BSW in the southern half of the channel (km 0 – 75). The MW properties are θ = 0 °C, S = 28, and ρ = 1022.5 kg m^{-3}. BSW properties are θ = 5°C and S = 30 and, ρ = 1024 kg m^{-3}, while the properties of the WW are θ = 0 °C, S = 33 and ρ = 1026.5 kg m^{-3}. The water properties in Model 2 (M2) are identical to those in M1, but the spatial structure differs in having a 2-layer structure that consists of WW extending across the entire width of the channel. MW occupies the upper 20 m over the northern half of the channel and BSW occupies the upper 20 m over the southern half.

Both models were run for 30 days. Unstable frontal waves, meanders, and dipole eddies develop after a few days, but for brevity we show only plan views of the temperature and velocity fields at the surface and 20 m for M1 (**Figures 143a, b**) and M2 (**Figures 143d, e**). These fields are shown also at 38 m for M1 (**Figure 143c**) but not for M2 where motions are extremely feeble and temperatures remain constant. The plots are from Day 25, before eddies reach the channel walls. Both models produce cyclonic and anticyclonic eddies with horizontal length-scales of 5–20 km and azimuthal velocities of 0.05–0.25 m s^{-1}. For M1, the eddy signatures extend throughout the water column, and the horizontal velocities are strongly sheared throughout the water column. In contrast, the eddy motions for M2 are confined to depths above the WW. The M1 eddies generally have higher velocities than those of M2 and there is considerable velocity shear over the water column. In both models, cyclonic eddies carry MW southward into the region initially occupied by BSW, while cyclonic and anti-cyclonic eddies transport BSW northward beneath the front and in the pycnocline. In M1, the eddies transport WW southward across the front into the region initially occupied by BSW. The model also indicates that there are large horizontal velocity gradients especially around the frontal regions. These large gradients are reflected in the relatively large magnitudes of the deformation tensor noted in the Burger (**Figure 98**) and the Pt. Lay Inshore (**Figure 106**) clusters.

Vertical cross-channel sections of temperature and salinity for M1 (**Figures 144a, b**) and M2 (**Figures 144c, d**) were made on Day 25 along km 84 (indicated by the dashed line in Figure 3f). The sections show a series of warm intrusions (associated with the eddies and filaments of **Figure 144**) penetrating laterally along the pycnocline between MW and WW. In approximate agreement with the observations, the intrusions vary in thickness from 5 – 25 m and in width from ~5 to ~20 km.

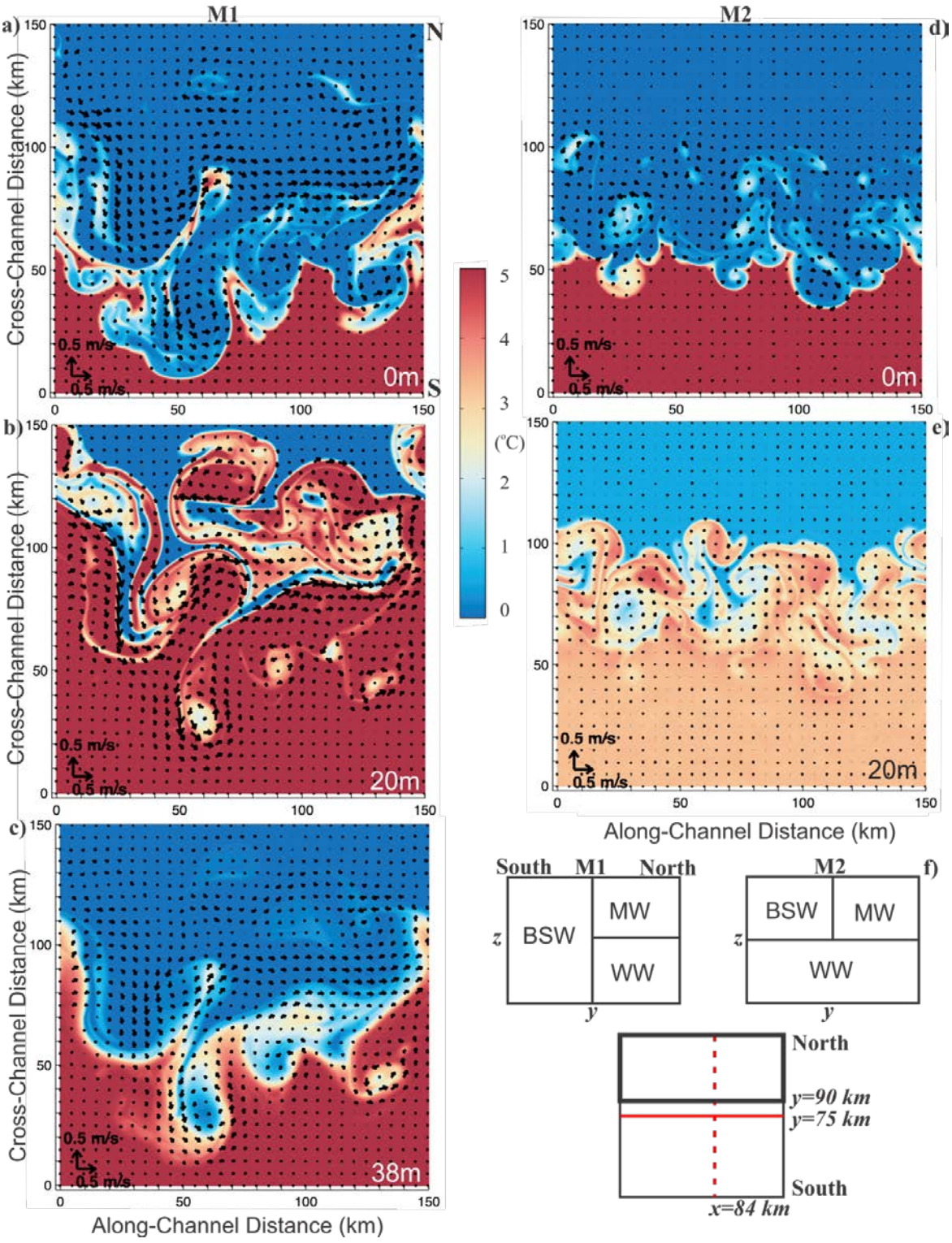

Figure 143. Plan views of temperature and velocity vectors for the M1 (143 a-c) and M2 (143d-e) on Day 25 at the depths indicated. Figure 143f shows the initial stratification conditions for M1 and M2. The initial location of the front is at y = 75 km (red line) and the location of the model cross-sections depicted in **Figures 144a–d** is at x = 84 km (dashed red line).

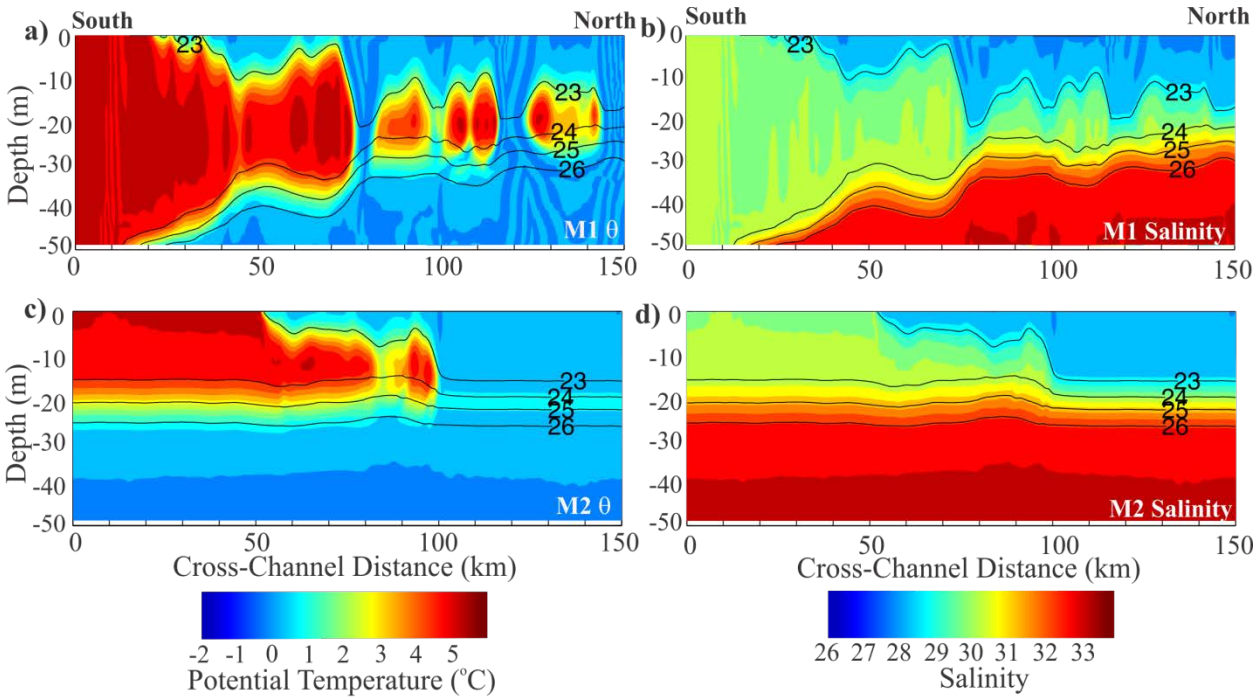

Figure 144. Cross-channel sections of temperature and salinity, overlain with σ_θ contours, at along-channel distance km 84 from M1 (a and b) and M2 (c and d) on Day 25.

Recall that the wind-drifter correlations of Section *IVf* showed that the various drifter types used in the study behaved differently from one another. There were also regional differences in the correlations amongst the same drifter types. For example, the iSpheres were largely controlled by the surface winds. On the Chukchi and Beaufort Shelves, the local winds accounted for ~70% of the iSphere velocity variance. Within Barrow Canyon and over the continental slope, the winds accounted for from 50 – 60% of the iSphere velocity variance. In contrast, for the MS (1-m drogued) drifters the winds accounted for 35% to 60% of the velocity variance on the Chukchi and Beaufort shelves, whereas for the SVP drifters the winds accounted for ~30% of the velocity variance on the Beaufort Shelf and within the shallow (<30 m depth) Alaska Coastal domain of the Chukchi Sea. Over deeper portions of the Chukchi Shelf, the winds account for 35% and 13% of the velocity variances for the MS and SVP drifters, respectively. These differences imply that other forces are operating on the flow fields that propel the drifters.

A number of processes affect these in addition to the stratification and mesoscale motions associated with fronts discussed previously. Our review of the hydrography clearly indicated that there are large spatial gradients in stratification over the shelf and that the stratification can vary seasonally as well as from year-to-year. There are, in addition, time-varying background geostrophic flows established by wind-driven convergences and divergences. *Weingartner* et al. (2013a) found that the sub-inertial flow is largely geostrophic and that the *instantaneous winds were not significant contributors to the local, vertically-averaged momentum balance*. Instead, the geostrophic flow varies in time due to sea level slopes over the Chukchi Sea Shelf that are

generated by wind-driven convergences and divergences as well as the mean background flow described with respect to **Figure 1**. The magnitude and the direction of the sea-level slopes (and associated geostrophic flows) vary with wind speed, direction and the bathymetry. The sea-level slopes across and along Barrow Canyon and the Central Channel differ from, and, in general, are greater than those over more gently sloping regions of the shelf. The differences in the wind-current correlations in Barrow Canyon compared to other regions of the shelf are clearly a manifestation of bathymetric influences on the background circulation. In addition, we noted that the Pt. Lay drifters and some of the NE Hanna Shoal drifters often drifted northward in the Central Channel even when winds were blowing to the south. The northward drift in the Channel is consistent with prior observations, which indicate the flow here is often northward even when northerly winds prevail (*Weingartner et al*., 2005b; *Weingartner et al.,* 2013a). In addition to the shelf-wide winds, *Weingartner et al*. (2013b) and *Danielson et al.* (2014) found that the sub-inertial flow (and sea level slopes) within Barrow Canyon and the Alaskan Coastal domains (and to a lesser extent the Chukchi Shelf domain) is affected by remotely forced barotropic continental shelf waves propagating northward from the southern Chukchi and/or Bering seas along the west coast of Alaska. Although these are trapped waves, with an e-folding cross-shore decay scale proportion to ~140 km (the barotropic Rossby radius of deformation) some of the wave energy may be scattered by coastline protrusions such as at Pt. Hope and/or Cape Lisburne) onto the central shelf. (An assessment of these hypothesized processes would require more complete numerical model experiments.) These waves are almost certainly operating over the Beaufort Sea Shelf as well. Over continental slope, the drifters also respond to sub-inertial, quasi-geostrophic motions associated with barotropic and baroclinic shelf waves that propagate along the shelfbreak and barotropic fluctuations in the Beaufort gyre.

The bathymetry also appears to influence drifter trajectories elsewhere. For example, many of the drogued drifters expelled from Barrow Canyon proceeded either to the west or to the east along the shelfbreak. These trajectories reflect the steeply sloping shelfbreak that influence the width and speed of shelfbreak jets (*Pickart,* 2004; *Nikolopoulos et al*., 2009). These jets can become unstable and shed both cyclonic and anticyclonic eddies (*Spall et al.*, 2008; *Watanabe*, 2011; *Von Appen and Pickart*, 2012). Indeed several of the drifter trajectories clearly revealed the presence of these eddies, which carried the drifters across the continental slope and into the basin. Recall that the wind-current correlations for drifters in the Canada Basin were generally among the weakest found in our data. Although to some extent, these poor results are due to the small sample size, the eddy motions arise due to dynamics unrelated directly to the winds and so contribute to the weak correlation.

Another bathymetric influence on the drifter trajectories appears to occur at the mouth of Barrow Canyon. Recall that for the most part, the drogued drifters moved rapidly through the canyon. Once at the mouth, the trajectories tended to bifurcate with some dispersing to the east and others to the west (cf. **Figures 46 – 52**). The mouth of the canyon may, in fact, be an effective dispersal agent. In general the along-canyon flow is horizontally sheared (*Pickart et al.,* 2005;

Weingartner et al., 2013a) which may lead to the formation of eddies and/or meanders that propagate out of the canyon (*D'Asaro*, 1988). The along-shelf bathymetric changes associated with the canyon indentation, and the abrupt change in shelf-width between the Chukchi and Beaufort Seas' mouth, may lend this area to shelf-wave scattering (*Yankovsky and Chapman*, 1995). An additional mechanism that could enhance dispersal here may be related to the collision of the down-canyon currents with the nearly zonal flows along the shelfbreak.

One of the project goals was to determine if the surface (upper 1 m) and near-surface (10 –15 m) circulation field diverges and differs from the sub-surface circulation as captured by current meter measurements by *Weingartner et al*. (2005b) and *Weingartner et al*. (2013a). We cannot provide an unequivocal conclusion on this point. Clearly the eastward drift of the MS and SVP drifters in August from the central Chukchi Shelf toward the coast and Barrow Canyon is similar to what has been inferred from sub-surface current meter measurements for this portion of the shelf. Similarly, the 2011 drifters that moved northward in the Central Channel were also consistent with sub-surface current measurements for this region. On the other hand, the MS and SVP drifters deployed to the southeast of Hanna Shoal executed trajectories in areas where there were no prior sub-surface current measurements so such comparisons cannot be made at this time. Moreover, these deployments were made in heavily stratified waters in which we cannot assume that the upper ocean and sub-surface waters are moving uniformly. Indeed, *Weingartner et al.*, (2013b) suggested that this area may have substantial velocity shear throughout the water column.

The results obtained from deployments of clusters of drifters are useful in understanding and quantifying particle dispersion (be this dissolved or suspended materials, pollutants, or planktonic organisms). The results presented here, albeit limited by the relatively small number of clusters (five clusters of ~10 drifters each, deployed in 2012 and 2013) used in the estimates, serve as a beginning climatology on the relative dispersion characteristics of the Chukchi Shelf. Moreover, the drifters released in the northeast Chukchi Sea generally remain on this shelf for ~30 days before either moving out onto the slope via Barrow Canyon (as in 2012) or westward and southward (as in 2013). This reflects the rapid advective time scales of the shelf circulation in late summer and fall. The results imply that we may be able to attain relative dispersion estimates only over a brief time period (<40 days), which is relatively short compared to other studies (*Swenson and Niiler, 1996; LaCasce and Ohlmann, 2003*). Although tentative, the results suggest a Lagrangian decorrelation time scale of ~2 days, after which the total relative dispersion grows as a power law according to $(\text{time})^{2.5}$. Our results indicate that relative dispersion is anisotropic, with the zonal relative diffusivity being twice as large as the meridional diffusivity. These findings will be strengthened statistically based on the results from the 2014 drifter deployments that involved ~70 more drifters on the Chukchi Sea Shelf. Once obtained, these results can be compared with dispersion estimates from oil spill trajectory models and serve as an important point for evaluating the accuracy of these models. The dispersion results can inform improved design of oil spill mitigation procedures by offering estimates of how fast a patch may

spread from a point source. We emphasize that the dispersion characteristics we are developing likely only apply to the ice-free season because the scales of the processes that give rise to dispersion during the ice-free season may be quite different when sea ice is present. Clustered deployments of drifters on the ice surface may be helpful in understanding the characteristics of the near surface dispersion in the presence of ice.

Our results are based on a relatively few drifter observations in any one dynamical domain. For example, the Chukchi Shelf domain has the largest number of observations, amounting to about 2000 drifter days. However, the drifters released on the northeast Chukchi Sea Shelf thus far generally remain in this area for less than 30 days before moving out onto the slope via Barrow Canyon (as in 2012) or westward and southward (as in 2013). This reflects the rapid advective time scales of the shelf circulation in late summer and fall. We expect greater statistical confidence in the results presented here as data become available from subsequent drifter deployments. In this regard, BOEM deployed ~30 MS drifters in summer 2014 in the Burger area and the North Slope Borough-Shell Baseline Studies program deployed ~104 drifters in 2014 in the Coastal domain of the Chukchi Sea and on the Beaufort Sea Shelf. Each of the 2014 deployments included clusters of 10 – 26 drifters and should inform better estimates of the dispersion characteristics for these regions.

When viewed in aggregate, the drifter trajectories indicate the multiplicity of potential pathways by which waters from the Northeast Chukchi Sea may spread. Drifters ranged as far to the east as the Mackenzie Shelf and as far to the west as to the shelf north of Wrangel Island and Herald Valley. Several also drifted northward over the Northwind Ridge between 75 and 76°N, while others drifted southward to the Chukotkan Peninsula. Most of these excursions took place within 3 – 4 months of deployment, which is a testament to the advectively vigorous nature of this shelf and its adjacent areas. The results imply that the residence time of surface waters on this shelf is no more than a few months at least.

VI. Future Recommendations with Respect to Drifter Studies

1. As stated previously, the surface circulation and dispersion characteristics discussed in this study are unlikely to apply to the drift of ice and so a fundamental question arises as to how the ice drift and dispersion differs from the open water measurements. At present the Coastal Marine Institute is conducting a study of using inexpensive prototype ice drifters that can easily by deployed by snow machine and/or helicopter. Assuming that these work as designed, we suggest that clustered deployments using these drifters be undertaken. Deployments should be made on both the landfast ice and in the pack ice. Given the large interannual variability in this region, consideration should be given to making multi-year deployments as these will contribute to the understanding of variability on this time scale and toward building a dispersion climatology.

2. We were unable to satisfactorily determine if there is divergence between the surface (1-m depth) and subsurface (10-m) depth motion, although our contention is that this occurs in the heavily stratified MW/WW areas and in the frontal regions separating BSW from MW. Drifter deployments in such regions are recommended, but these should be conducted in conjunction with process studies that include high resolution CTD sampling (such as afforded by the Acrobat). A process study devoted to understanding frontal dynamics and subduction would be well-served by having a drifter component. Given that this exercise well involve shipboard sampling, it may be possible to design the study so that the drifters can be recovered and re-used during the study.
3. Ledyard Bay appears to be critical habitat for a number of organisms including those important to subsistence hunters. The circulation characteristics of this region have not been addressed to date. A limited drifter study would provide useful information in this area. Such a study would be inexpensive insofar as the residents of Pt. Lay frequently hunt and fish in this region throughout the summer. This program has demonstrated the numerous advantages to be had by involving local communities in drifter deployments. A Ledyard Bay study would conceivably consist of multiple clustered deployments throughout summer and, if possible, ice drifters in winter.
4. There may be interest on the part of the Northwest Arctic Borough in conducting drifter studies, similar to those undertaken here, which would expand deployments into the Bering Strait, southern Chukchi Sea, and Kotzebue area. Data from such studies would provide useful information on transit times from the southern to the northern Chukchi Sea and enhance the development of a dispersion climatology for the Chukchi Sea Shelf.

VII. Acknowledgements

This study was supported under cooperative agreement M11AC00001 through the Coastal Marine Institute of the University of Alaska Fairbanks in partnership with BOEM. Additional support was provided by the North Slope Borough-Shell Baseline Studies Program. Support for the drifters and deployment logistics was provided through BOEM cooperative agreement M12AC00008. We thank the crews of the Norseman II and USCG icebreaker Healy for assistance with the deployments and we are grateful to the North Slope Borough Baseline Studies Program for their support of the analyses, which added greatly to the value of the results presented herein.

VIII. Project Presentations

Weingartner, T., S. Danielson, P. Winsor, and E. Dobbins, Satellite-tracked drifter measurements in the Northeast Chukchi Sea. CMI Annual Review, November 2012, Fairbanks, AK.

Irvine, C., K. Martini, L. DeSousa, P. Winsor, E. L. Dobbins, S. Danielson, and T. Weingartner, Satellite-tracked drifter measurements in the Chukchi and Beaufort Seas. Alaska Marine Science Symposium, January 2014, Anchorage, AK.

Winsor, P., T. Weingartner, T., H. Statscewich, R. Potter, E. Dobbins, K. Martini, and S. Danielson, High-Resolution Observations of Hydrography and Circulation of the Chukchi Sea. Alaska Marine Science Symposium, January 2013, Anchorage, AK.

DeSousa, L., T. Weingartner, P. Winsor, S. Danielson, E. Dobbins, and C. Irvine, Interannual Variability in Surface Circulation in the Chukchi and Beaufort Seas: Satellite-tracked Drifter Measurements. Alaska Marine Science Symposium, January 2015, Anchorage, AK.

In addition, informal presentations that included some of these data were made to the oil industry and to residents of the communities of Barrow, Pt. Lay, Wainwright, Nuiqsuit, and Kaktovik by Dr. Weingartner as part of his membership on the NSBW-Shell Baseline Studies Program.

IX. References

Aagaard, K., T. J. Weingartner, S.L. Danielson, R.A. Woodgate, G. C. Johnson, and T. E. Whitledge (2006), Some controls on flow and salinity in Bering Strait. *Geophysical Research Letters*, 33, L19602, doi:10.1029/2006GL026612.

Brower, Jr., W. A., R. G. Baldwin, C. N. Williams, Jr., J. L. Wise, and L. D. Leslie (1988), *Climatic atlas of the outer continental shelf waters and coastal regions of Alaska, Vol. III Chukchi-Beaufort Sea*. Arctic Environmental Information and Data Center, University of Alaska, Anchorage, AK. 497 pp.

Coachman, L. K., K. Aagaard, and R.B. Tripp (1975), *Bering Strait: The Regional Physical Oceanography*, 172 pp., University of Washington Press, Seattle, Washington.

Danielson, S., K. Aagaard, T. Weingartner, S. Martin, P. Winsor, G. Gawarkiewicz, and D. Quadfasel (2006), The St. Lawrence polynya and the Bering Shelf circulation: New observations and a model comparison. *Journal of Geophysical Research, 111*, doi:10.1029/2005JC003268.

Danielson, S., T. Weingartner, K. Hedstrom, K. Aagaard, R. Woodgate, E. Curchitser, and P. Stabeno (2014), Ekman transport, continental shelf waves, and variations of the Pacific-Arctic sea surface height gradient: Coupled wind-forced controls of the Bering-Chukchi Shelf circulation and the Bering Strait throughflow. *Progress in Oceanography*, 125, 40–61.

D'Asaro, E. A. (1988), Generation of submesoscale vortices: A new Mechanism. *Journal of Geophysical Research*, 93, 6685–6693.

Davis, R. E. (1985), Drifter observations of coastal surface currents during CODE: The method and descriptive view. *Journal of Geophysical Research*, 90, 4741–4755.

Davis, R. E. (1991), Observing the General-Circulation with Floats. *Deep-Sea Research Part A-Oceanographic Research Papers*, 38: S531–S571. 10.1016/S0198-0149(12)80023-9.

LaCasce, J. H. (2008), Statistics from Lagrangian observations. *Progress in Oceanography*, 77, 1–29.

LaCasce, J. H., and C. Ohlmann (2003), Relative dispersion at the surface of the Gulf of Mexico. *Journal of Marine Research*, 61, 285–312.

Large, W. G., and S. Pond (1981), Open ocean momentum flux measurements in moderate to strong winds. *Journal of Physical Oceanography*, 11, 324–481.

Lu, K., T. Weingartner, S. Danielson, P. Winsor, E. Dobbins, K. Martini, and H. Statscewich. Lateral mixing across ice meltwater fronts of the Chukchi Sea Shelf. submitted to *Geophysical Research Letters.*

Mesinger, F., and 19 Co-authors (2006), North American regional re-analysis. *Bulletin of the American Meteorological Society*, 87, 343–360.

Nikolopoulos, A., R. S. Pickart, P.S. Fratantoni, K. Shimada, D. J. Torres, and E. P. Jones (2009), The western Arctic boundary current at 152°W: Structure, variability, and transport. *Deep-Sea Research II*, 56, 1164–1181.

Okubo, A., and C. C. Ebbesmeyer (1976), Determination of vorticity, divergence, and deformation rates from analysis of drogue observations. *Deep-Sea Research*, 23, 349–352.

Pickart, R. S. (2004), Shelfbreak circulation in the Alaskan Beaufort Sea: Mean structure and variability. *Journal of Geophysical Research*, 109(C4), C04024 10.1029/2003JC001912.

Pickart, R. S., L. J. Pratt, D. J. Torres, T. E. Whitledge, A. Y. Proshutinsky, K. Aagaard, T. A. Agnew, G. W. K. Moore, and H. J. Dail (2010), Evolution and dynamics of the flow through Herald Canyon in the Western Chukchi Sea. *Deep-Sea Research II*, 57**,** 5–26. doi:10.1016/j.dsr2.2009.08.002.

Pickart, R. S., T. Weingartner, L. J. Pratt, S. Zimmermann, and D. J. Torres (2005), Flow of winter-transformed Pacific water into the western Arctic. *Deep-Sea Research, Pt. II*, 52, 3175–3198.

Shimada, K., T. Kamoshida, M. Itoh, S. Nishino, E. Carmack, F. McLaughlin, S. Zimmermann, and A. Proshutinsky (2006), Pacific Ocean inflow: Influence on catastrophic reduction of sea ice cover in the Arctic Ocean. *Geophysical Research Letters,* 33(8): doi:10.1029 2005GL025624L08605.

Shroyer, E., and A. J. Plueddemann (2011), Wind-driven modification of the Alaskan Coastal Current. *Journal of Geophysical Research*, 116, C03031,doi:10.1029JC007650.

Spall, M. A. (2007), Circulation and water mass transformation in a model of the Chukchi Sea. *Journal of Geophysical Research*, 112, C05025,doi:10.1029/2005JC002264.

Spall, M., R. S. Pickart, P. Fratantoni, and A. Plueddemann (2008), Western Arctic shelfbreak eddies: Formation and transport. *Journal of Physical Oceanography*, 38, 1644–1668.

Springer, A. M., and C. P. McRoy (1993), The paradox of pelagic food webs in the northern Bering Sea-III: Patterns of primary production. *Continental Shelf Research*, 13, 575–599.

Swenson, M. S., and P. P Niiler (1996), Statistical analysis of the surface circulation of the California Current. *Journal of Geophysical Research*, 101, 22631–22645.

Von Appen, W-J, and R. S. Pickart (2012), Two configurations of the Western Arctic shelfbreak current in summer. *Journal of Physical Oceanography*, 42, 329–351.

Walsh, J. J., C. P. McRoy, L. K. Coachman, J. J. Goering, J. J. Nihoul, T. E. Whitledge, T. H. Blackburn, P. L. Parker, C. D. Wirick, P. G. Shuert, J. M. Grebmeier, A. M. Springer, R. D. Tripp, D. A. Hansell, S. Djenedi, E. Deleersnijder, K. Henriksen, B. A. Lund, P. Andersen, F. E. Müller-Karger, and K. Dean (1989), Carbon and nitrogen cycling within the Bering/Chukchi seas: Source regions for organic matter affecting AOU demands of the Arctic Ocean. *Progress in Oceanography*, 22, 277–359.

Watanabe, E. (2011), Beaufort shelfbreak eddies and shelf-basin exchange of Pacific summer water in the western Arctic Ocean detected by satellite and modeling analyses. *Journal of Geophysical Research*, 116, C08034, doi:10.1029/2010JC006259.

Weingartner, T., E. Dobbins, S. Danielson, R. Potter, H. Statscewich, and P. Winsor (2013a), Hydrographic variability over the northeastern Chukchi Sea Shelf in summer–fall 2008–2010. *Continental Shelf Research*. http://dx.doi.org/10.1016/j.csr.2013.03.012.

Weingartner, T., P. Winsor, R. Potter, H. Statscewich, and E. Dobbins (2013b), Application of high frequency radar to potential hydrocarbon development areas in the Northeast Chukchi Sea: *Final Report,. BOEM Contract No: M09AC15207*, 165 pp.

Weingartner, T., S. Danielson, and T. C. Royer (2005a), Freshwater variability and predictability in the Alaska Coastal Current. *Deep-Sea Research*, 52, 169–192.

Weingartner, T., K. Aagaard, R. Woodgate, S. Danielson, Y. Sasaki, and D. Cavalieri (2005b), Circulation on the North Central Chukchi Sea Shelf. *Deep-Sea Research, Pt. II*, 52, 3150–3174, doi:10.1016/j.dsr2.2005.10.015.

Weingartner, T. , S. Danielson, Y. Sasaki, V. Pavlov, and M. Kulakov (1999), The Siberian Coastal Current: A wind and buoyancy-forced Arctic Coastal Current. *Journal of Geophysical Research*, 104, 29697–29713.

Weingartner, T.**,** D. Cavalieri, K. Aagaard, and Y. Sasaki (1998), Circulation, dense water formation and outflow on the northeast Chukchi Sea Shelf. *Journal of Geophysical Research,* 103, 7647–7662.

Winsor, P., and D. C. Chapman (2004), Pathways of Pacific Water across the Chukchi Sea: A numerical model study. *Journal of Geophysical Research,* 109, C03002, doi: 1029/2003JC001962.

Woodgate, R. A., T. Weingartner, and R. Lindsay (2012), Observed increases in oceanic fluxes from the Pacific to the Arctic from 2001 to 2011 and their impacts on the Arctic. *Geophysical Research Letters*, 39, L24603, doi:10.1029/2012GL054092.

Woodgate, R. A., K. Aagaard, and T. Weingartner (2006), Interannual changes in the Bering Strait fluxes of volume, heat and freshwater between 1991 and 2004. *Geophysical Research Letters*, 33, L15609, 10.1029/2006GL026931

Woodgate, R. A., K. Aagaard, and T. Weingartner (2005b), A Year in the Physical Oceanography of the Chukchi Sea: moored measurements from autumn 1990–91. *Deep-Sea Res., Pt II,* 52, 3116–3149.

Woodgate, R. A., K. Aagaard, and T. Weingartner (2005a), Monthly temperature, salinity, transport variability for the Bering Strait throughflow. *Geophysical Research Letters*, 32, L04601, doi:10.1029/2004GL021880.

Woodgate, R. A., T. Weingartner, and R. Lindsay (2012), Observed increases in Bering Strait oceanic fluxes from the Pacific to the Arctic from 2001 to 2011 and their impacts on the Arctic Ocean water column. *Geophysical Research Letters*, 39, L24603, doi:10.1029/2012GL054092.

Yankovsky, A. E., and D. C. Chapman, 1995, Generation of mesoscale flows over the shelf and slope by shelf wave scattering in the presence of a stable, sheared mean current. *Journal of Geophysical Research,* 100**,** 6725–6742.

Zhang, X., J. Zhang, J. Kreiger, M. Shulski, F. Liu, S. Stegall, W. Tao, J. You, W. Baule, and B. Potter (2013), Beaufort and Chukchi Seas mesoscale meteorology modeling study. *Final Report, BOEM OCS Study 2013–0119*, 204 pp.

The Department of the Interior Mission

As the Nation's principal conservation agency, the Department of the Interior has responsibility for most of our nationally owned public lands and natural resources. This includes fostering the sound use of our land and water resources, protecting our fish, wildlife and biological diversity; preserving the environmental and cultural values of our national parks and historical places; and providing for the enjoyment of life through outdoor recreation. The Department assesses our energy and mineral resources and works to ensure that their development is in the best interests of all our people by encouraging stewardship and citizen participation in their care. The Department also has a major responsibility for American Indian reservation communities and for people who live in island communities.

The Bureau of Ocean Energy Management

The Bureau of Ocean Energy Management (BOEM) works to manage the exploration and development of the nation's offshore resources in a way that appropriately balances economic development, energy independence, and environmental protection through oil and gas leases, renewable energy development and environmental reviews and studies.